Study on Low-cost Alternatives for Synthesising Powder Metallurgy Titanium and Titanium Alloys

A thesis submitted in fulfilment

of the requirements for the degree

of

Doctor of Philosophy in Materials Process Engineering

at

The University of Waikato

by

Stiliana (Stella) Rousseva Raynova

THE UNIVERSITY OF
WAIKATO
Te Whare Wānanga o Waikato

2017

To my family:

With deep respect and love to my mother, who thought me the importance of education.

With my deepest and infinite love to my children Peter and Venny, who give me a joy and a purpose of life.

With great appreciation and love to my partner John who makes me to feel special.

Abstract

The aim of this work was to carry out research about cost effective ways for synthesising powder metallurgy Ti and Ti alloys. This was done: using low cost Ti powders produced by the hydrogenation dehydrogenation (HDH) method; using induction heating, instead of the more traditionally used electrically heated vacuum furnace, for sintering and in the thermomechanical processing of powders; using low cost alloying elements such as Fe and stainless steel powders and investigating the possibility of using low amounts of alloying elements.

The first main stream investigation in this work focussed on a study of induction sintering of Ti and pre-alloyed Ti6Al4V powders. This initial work included the following investigations: the effect of powder compact density on induction heating rates, the levels of porosity and the tensile properties of sintered samples; and the effect of induction sintering process parameters, such as temperature and time on the sintered densities, porosity distribution, microstructure, tensile properties and fracture characteristics of Ti and pre-alloyed Ti6Al4V powders.

The second main study was on the application of induction sintering for consolidating pre-alloyed Ti6Al4V powders by thermomechanical processing via open die forging. The aim was to reduce processing time by eliminating the need for lengthy vacuum sintering and additional reheating required before final processing. The effect of the induction sintering parameters on the deformation behaviour, microstructure, mechanical properties and fracture behaviour were studied. Furthermore, the effect of a recrystallization annealing heat treatment on the tensile properties and microstructure was also analysed.

The third study was focused on the development of low cost powder metallurgy Ti alloys with mechanical properties similar to those of the most commonly used wrought Ti6Al4V alloy. To achieve this aim an approach using Ti HDH powder with a high oxygen content of 0.25wt% was used along with low cost alloying elements such as Fe and stainless steel powders. The maximum alloying element content was limited to 5% and a blended elemental approach for making the alloys was employed. Induction sintering and vacuum sintering prior to thermomechanical processing by open die forging and extrusion were used for consolidation. The alloy compositions studied were Ti3Al2V, Ti5Fe with two different particle sizes of Fe powder and Ti5SS (addition of 316 stainless steel powder). A blended elemental Ti6Al4V alloy was also studied for comparison.

The relationship between microstructure, mechanical properties and fracture behaviour was studied. The effect of recrystallization annealing after forging and extrusion was investigated for some of the alloys on its effect on microstructure and tensile properties.

The results showed that induction sintering significantly reduces the sintering time. Induction sintering for four to ten minutes produces Ti and Ti alloy with closed porosity structures as well as densities and mechanical properties comparable with those found in vacuum sintered Ti based material.

The use of induction sintering in direct open die forging of prealloyed Ti6Al4V powders with a high oxygen content of 0.5wt% resulted in material with a solid structure and tensile properties, such as YS and UTS, significantly higher than those given by wrought Ti6Al4V alloy. The ductility was affected by the high oxygen content and was generally lower than that of the wrought material. Thermomechanical processing of the low cost alloys Ti5Fe, Ti5SS and Ti3Al2V with oxygen contents between 0.33wt% and 0.45wt% resulted in material with an excellent combination of tensile strength and ductility, comparable to the values found in wrought Ti6Al4V alloy. A post forging or extrusion recrystallization annealing heat treatment played a significant role in producing microstructures with fine α+β lamellae, which was a controlling factor for achieving good ductility in Ti alloys with a high oxygen content.

Acknowledgements

Table of Contents

List of Figures

List of Tables

List of Abbreviations:

ASTM- American society for testing and materials

BE- blended elemental

CP- cold pressed

CPC- cold powder compaction

DSC- differential scanning calorimetry

EDS- energy dispersive spectrum

ε- elongation to fracture

GA- gas atomized

HDH- hydride de-hydride

HIP- hot isostatic pressing

HT- heat treatment

IS- induction sintering

LOM- light optical microscope

M_s- martensitic transformation

MIM- metal injection moulding

ODF- open die forging

PA- pre alloyed

PCE- powder compact extrusion

PM- powder metallurgy

PREP- plasma rotating electrode process

RA- recrystallization annealing

SEM- scanning electron microscope

SS- stainless steel

ST- solution treatment

T- temperature

t- time

UTS- ultimate tensile strength

VS- vacuum sintering

WPC- warm powder compaction

XRD- X-ray diffraction

YS- yield strength

Chapter 1

Introduction and Literature Review

1.1 Introduction

Titanium and titanium alloys have many favourable properties such as high strength to weight ratio, good ductility and fracture toughness, high corrosion resistance, good high temperature properties and good biocompatibility with human tissues, making them very important engineering materials for many applications in aerospace, chemical engineering, automotive, biomedical and other industries. The use of titanium and titanium alloys is restricted by the high manufacturing cost. In the traditional ingot manufacturing technologies like casting and forging from ingot, the high cost derives from the manufacturing waste and expensive machining. The powder metallurgy (PM) approach has the advantage to process powders into net or near-net shapes, which eliminates or minimizes the need for post machining and consequently minimizes the material waste. PM is suitable for mass production of small parts with complex shapes, where the material waste could be even greater if traditional manufacturing methods such as machining from ingot material are used. Even though powder metallurgy has many advantages, the cost of the metal powders, particularly those of Ti is still high. Ti is the ninth most abundant element and fourth most abundant structural metal and Ti ore is widely available. To make titanium products more viable and used in everyday applications such as family automobiles, outdoor devices and home appliances, the overall production cost needs to be reduced. The current worldwide research is focused in several areas, such as reducing the production costs of Ti by improving or developing new extraction technologies. The research work on Ti powder metallurgy is focused on: reducing the cost of powder production; developing cost effective powder alloys; new technologies for powder consolidation or optimisation of the existing ones.

The aim of this research is to develop a cost effective method of consolidation of Ti and Ti alloy powder which achieves mechanical properties comparable to those of the most widely used wrought Ti and Ti6Al4V alloy. The studied consolidation

methods are sintering and open die forging (ODF). Some research work on powder compact extrusion (PCE) was also done. The approach is: (1) to develop a new technology for powder sintering, by using induction heating instead of the traditional sintering in electric vacuum furnaces; (2) optimization of the powder compact forging process by eliminating one of the processing steps, the most appropriate being removal of the need to reheat the as-sintered powder compact. This goal was achieved by forging directly after sintering by using induction heating instead of the commonly used vacuum sintering; (3) developing new low cost Ti powder alloys by reducing the amount of alloying elements (introducing the powder metallurgical Ti3Al2V alloy), or using low cost alloying elements such as elemental Fe powders or Fe based alloy powder for substitution of traditionally used Al and β-phase stabilising elements such as V.

Induction sintering (IS) of pure Ti- and pre-alloyed (PA) Ti6Al4V alloy powders and ODF of PA Ti6Al4V powders were extensively studied. Some of the experimental equipment and the experimental set up for the IS and the ODF was in house designed and made. The effect of process parameters such as induction sintering and forging temperature, holding time etc. on the physical, mechanical and microstructure properties were investigated. Powder compact extrusion (PCE) was also studied, mainly for comparison with ODF. The conventional vacuum sintering of blended elemental (BE) Ti6Al4V, Ti3Al2V and Ti-Fe based alloy powder compacts was also studied for comparison. Two types of Ti alloy powders were used- pre-alloyed (PA) powders and blended elemental (BE) powders. Four different Ti alloys were area of interest- Ti6Al4V, Ti3Al2V, Ti5Fe and Ti5SS (Ti3Fe1Cr0.6Ni0.2Mo). Ti6Al4V alloy was studied because this is the most popular alloy used in the titanium industry. The other three alloy compositions Ti3Al2V, Ti5Fe and Ti5SS were studied as a cost effective alternative of Ti powder metallurgy alloys and the aim was to achieve properties comparable to those of Ti6Al4V wrought alloy. For a base material, Ti powders, produced by hydrogenation dehydrogenation method (HDH), were used. Even though having comparatively higher oxygen content, HDH Ti powders were chosen over the gas atomized (GA) Ti powders for two reasons: the lower cost of the HDH powders; and their irregular powder particle morphology, which is favourable in the powder compacting stage of the consolidation process.

This PhD thesis consists of six chapters. Chapter 1 presents a literature review of the theoretical fundamentals of the powder metallurgy, introduction to titanium and titanium alloys, introduction to each of the studied powder consolidation methods, followed by a review of previously done research work related to each method. The experimental procedures are described in Chapter 2. Chapter 3 to Chapter 5 are dedicated to the results and discussion on each research subject as follow: (1) induction sintering of pure Ti and PA Ti6Al4V powders; (2) open die forging of prealloyed Ti6Al4V powders; (3) development of low cost titanium alloys- Ti3Al2V and Ti-Fe based alloys using blended elemental powder approach and consolidation by induction sintering, vacuum sintering, open die compact forging and powder compact extrusion. Finally, Chapter 6 presents the conclusions and recommendation for future work.

1.2 Literature Review

1.2.1 Powder metallurgy

1.2.1.1 Brief history and development

Powder metallurgy has been called a lost art. Sintering of metal powders was entirely forgotten for many centuries and was revived again in Europe at the end of 18th century. The essential features of the art of PM are the production of powder and its consolidation into a solid form by the application of pressure and heat at a temperature below the melting point of the major constituents. Early mankind learned by chance that particles of metal could be joined together by hammering, resulting in a solid metallic structure [1]. The very first records of using of powder metallurgy principles originates from 3000BC when ancient Egyptians, Indians and Africans discovered a way of producing iron sponge for making tools. In this early process, iron oxide was heated in a charcoal and crushed shell fire, which was intensified by air blasts from below to reduce the oxide to a spongy metallic iron. The resulting hot sponge iron was then hammered to weld the particles together. Final shapes were obtained by simple forging procedures. Although the product often contained large amounts of non-metallic impurities, some remarkably solid and sound structures were discovered. 18th centuries later the powder metallurgical routes were rediscovered again for manufacturing platinum laboratory apparatus and also coins were fabricated from

copper, silver and lead powders. The major turning point for the use of powder metallurgy in the modern days is owed to Coolidge [1], who developed a durable filament, for the Edison light bulb, made from tungsten powder. Around the same decade (1930), cemented carbides, porous bearings and electrical contacts were developed by powder metallurgical approach. By 1940s, powder technique was involved in the fabrication of hard metals, insulators, ferroalloys, refractory metals [2]. Many qualities contribute for the success of the PM. The Venn diagram shown in Figure 1.1 illustrates three of the main reasons for the success: cost, properties and captivity of the PM methods.
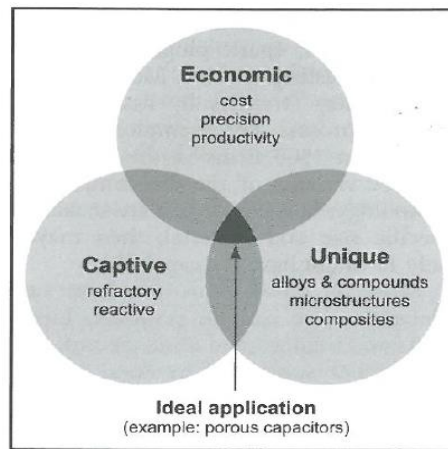
Figure 1.1 Powder metallurgy Venn- diagram [2].

First are the many applications which rely on the low cost production of complex parts. Components for the automotive industry represent good examples of this area and their production is a large PM activity. Justification for using a PM approach is the unique properties or microstructure. Some examples include porous filters, oxide dispersion strengthened alloys, cermets and cemented carbides, metal ceramics such as titanium- hydroxyapatite for artificial bones and hard cutting tools. Fabrication of these materials and products is difficult or impossible by any other technique. The third circle shown on the Venn-diagram corresponds to captive applications. These are the materials which are quite difficult to process by any other techniques. Ideal examples are the reactive and refractory metals where casting techniques are not practical. Another group of materials are the amorphous or glassy metals. Low temperature processing is desirable to avoid microstructural damage associated with using elevated temperatures. PM techniques are also attractive because they are solid state

methods. Often, elements from all three categories exist in practical PM applications. The major growth and expansion will most likely come from further combinations of these three elements in the Venn diagram in forming unique, low cost, high quality products. The ideal example for the success of the PM is the large scale production of porous capacitors, made of tantalum or barium titanate, for electronic circuits reaching over hundreds of millions parts per day.

1.2.1.2 Principles

Powder metallurgy is a technology for manufacturing of near-net or net shape products by combining the features of shape making technology for powder compaction with subsequent densification or consolidation processes to get the final material and design properties. To choose the most appropriate PM approach the following six considerations must be considered: the size of the product; the complexity of the shape of the product; dimensional tolerance; raw materials (powder shape, size, purity); the desired properties; quantity and cost. Table 1.1 gives a comparison of the relationship between all of these six factors for different powder processing methods and shows the advantages and disadvantages of each of the powder processing techniques [3].

Table 1.1 Comparison of different powder processing methods [3].

Characteristics	Conventional sintering	Metal Injection Moulding	Hot Isostatic Pressing	Powder Forging
Size	Good	Fair	Excellent	Good
Shape complexity	Good	Excellent	Very good	Good
Density	Fair	Very good	Excellent	Excellent
Dimensional tolerance	Excellent	Good	Poor	Very good
Production rate	Excellent	Good	Poor	Excellent
Cost	Excellent	Good	Poor	Very good

The use of PM products is expanding continuously in a broad range of applications and PM techniques are in a stage of continuous development. Powder metallurgy parts can be broadly separated into three categories: those in which the PM approach allows a lower-cost component to be produced; an intermediate category of cost-effective/high-performance parts; and those parts for which a PM

approach leads to enhanced mechanical properties [4]. The first approach generally results in a product with lower mechanical properties than obtained in the wrought product. The third approach is normally a higher-cost approach. Many PM parts are now used in a variety of industries, including automobiles, household appliances, yard and garden equipment, computers, fabrication industry equipment, and orthodontic devices. Automotive parts continue to be the leading application. In middle 1990s a typical U.S. automobile contained about 14 kg of parts made by PM, with an increase up to 23kg by year 2000 (Figure 1.2) [4]. The growth was due to increased use of PM components in engines, transmissions, brakes, airbags, and other complex parts.
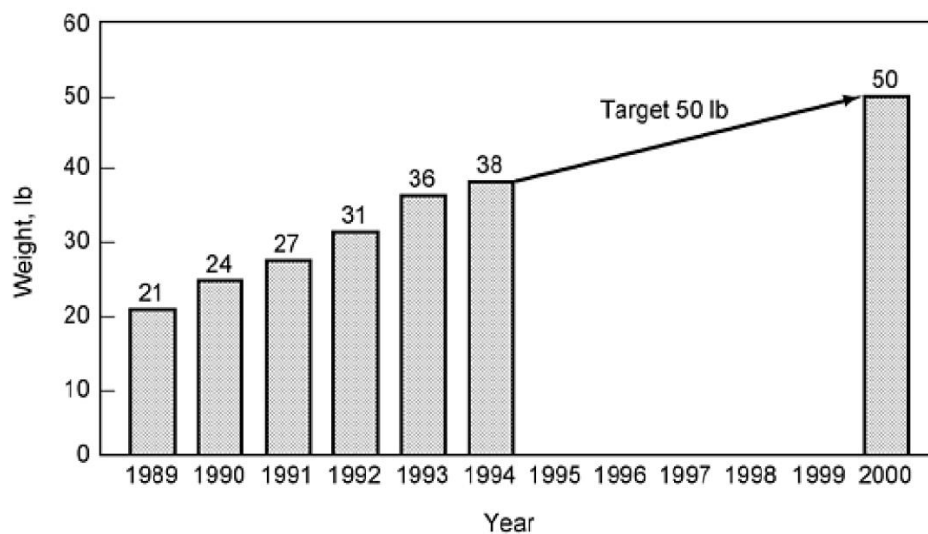
Figure 1.2 Growth of powder metallurgy in Ford automobiles [4].

1.2.2 Titanium and titanium alloys

Titanium was first discovered by Gregor in England in 1791. It was later named Titanium in 1795 by Klapproth in Germany after the Titans of Greek mythology [2]. The production of high purity titanium proved to be difficult, because of the strong tendency of this metal to react with oxygen and nitrogen. Because of that, it was not used until 1938, when a commercially attractive process for production of pure Ti was developed by W.J. Kroll in Luxemburg. This process involves the reduction of titanium tetrachloride with magnesium in an inert-gas atmosphere. The resulting titanium is called "titanium sponge" because of the porous and spongy appearance. The commercial interest in titanium and its alloys is because of the relatively low density of this metal (between those of aluminium and iron)

6

in combination with a high yield strength (especially in the 200-450°C temperature range), and its excellent corrosion resistance. With properties like these, titanium is ideal for many applications. However, because of the high production cost Ti and its alloys are used primarily in two areas: for corrosion resistance [5-7] in the chemical industry and in areas where weight-saving and high strength are predominant, such as in aircraft and aerospace applications [8-10]. In the last decades the interest for using titanium in automotive applications has increased [11-13]. Another area of interest for use of titanium is in medical applications in both surgical tools and implants, due to the corrosion resistance and the biocompatibility [14-17].

1.2.2.1 Characteristics of titanium and titanium alloys.

Titanium undergoes an allotropic phase transformation at 882.5°C, changing from a closed-packed hexagonal crystal structure (α phase) below, to a body-centered cubic crystal structure (β phase) above this temperature [18] (Figure 1.3).
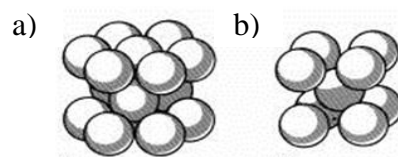
Figure 1.3 Crystal structure of Ti a) α phase- hexagonal close packed and b) β phase- cubic body centred [18].

The exact transformation temperature is influenced by interstitial and substitution elements and therefore depends on the purity of the metal. The intrinsic anisotropic behaviour of the hexagonal crystal structure of the α- phase has important consequences for the elastic and plastic deformation behaviour of titanium and its alloys. The alloying elements added to titanium are categorised as α or β phase stabilizers on the basis of their effects on the α/β transformation temperature [19]. The substitutional element Al and the interstitials O, N and C are strong α-phase stabilizers. The α/β transus temperature increases with increasing solute content of these elements (Figure 1.4a). The β-stabilizing elements, which lower the α/β transus temperature are distinguished into β-isomorphous, such as V, Mo and Nb, (Figure 1.4b) and β-eutectoid, such as Mn, Fe, Cr, Co, Ni, Si and H (Figure 1.4c). In addition, there are other elements, for

example Zr and Sn, which are neutral or slightly decrease the α/β transition temperature (Figure 1.4d) [19].
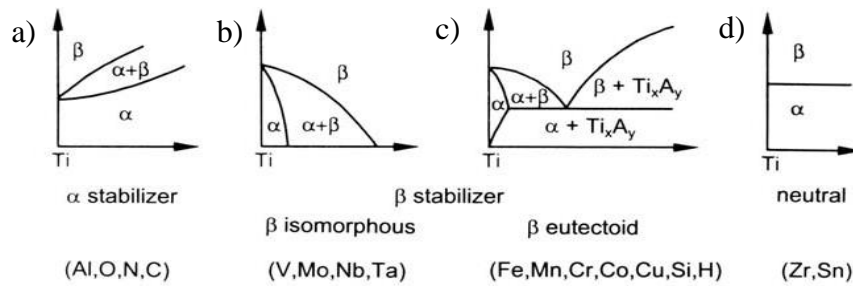
Figure 1.4 Effect of alloying additions on equilibrium phase diagrams of Ti-alloys (schematically) a) α-phase stabilisers, b) β-phase stabilisers (isomorphous), c)) β-phase stabilisers (eutectoid), and d) neutral [19].

The phase relationship in Ti alloy systems is represented easily in a phase diagram for binary systems (Figure 1.4). When more than two elements are present it is difficult to show the quantative relationships. Pseudo binary phase diagrams are a useful way of showing behaviour especially on a comparative basis [18]. Figure 1.5 shows compositions of some Ti alloys marked on the pseudo binary β-isomorphous phase diagram called a road map. The x-axis represents the concentration of the β phase stabilizing elements.
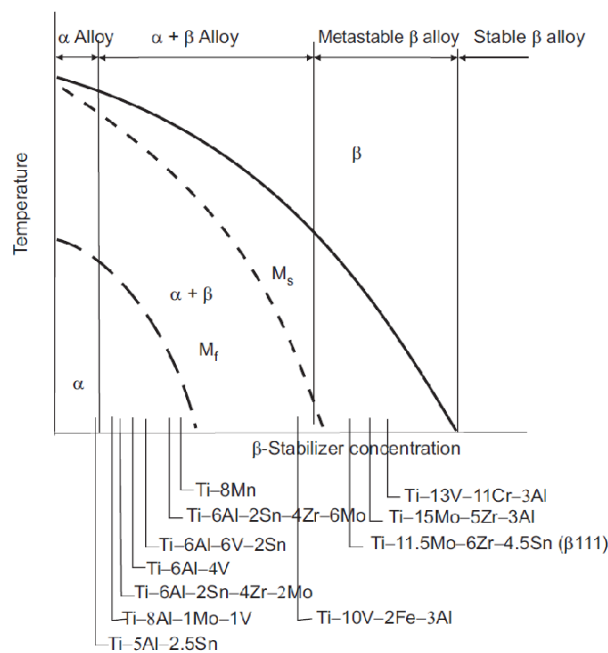
Figure 1.5 Example of Ti alloy compositions related to the pseudo binary β-isomorphous phase diagram [18].

8

Commercial titanium alloys are classified conventionally in four different categories as α, near α, α+β, and β alloys according to their equilibrium composition, which varies with the types and concentrations of alloy elements. This is shown in a schematical pseudo binary β-isomorphous phase diagram in Figure 1.5 [18]. Commercially pure titanium with various amounts of interstitial oxygen and alloys with α- phase stabilizers (Al, Sn) are classified as α alloys. The majority of the commercial alloys belongs to the α+β alloys. These alloys contain, in addition to α stabilizing element, also β stabilizing elements such as V, Mo, Nb or Cr. These elements decrease the α/β transformation temperature and increase the width of the α+β phase field proportional to their total amount. They also lower the temperature where the β phase starts to transform by the martensitic process (Ms-temperature). With a further increase in β stabilizing elements, the β phase can be retained at room temperature even during slow, air cooling [18]. In typical commercial titanium alloys with intermediate amounts of alloying elements, a sufficiently slow enough cooling rate from the single β phase field into the α+β field, allows the β phase to decompose by nucleation of α at the β grain boundaries. Subsequently there is diffusion controlled growth into the retained β phase. The resulting microstructure consists of colonies of parallel α-plates which are separated by plates of the retained β-phase. The α-plates within a colony have the same crystallographic orientation. An example of such a microstructure which is known as "lamellar", "basket weave" or "Widmanstätten" structure is shown in Figure 1.6 [18].
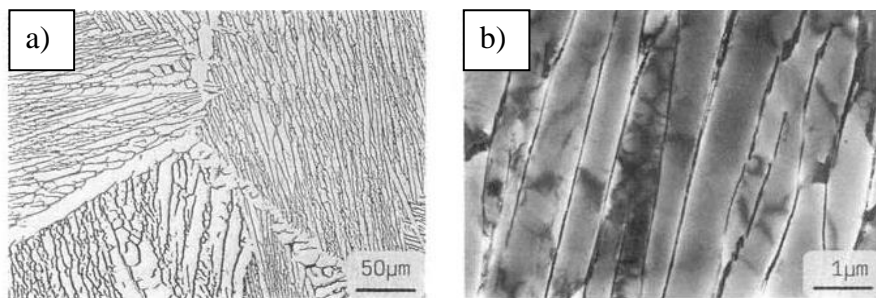
Figure 1.6 Basketweave α+β microstructure in Ti alloy observed by a) light optical microscope and b) transmission electron microscope [18].

The microstructure of titanium alloys is an essential characteristic for achieving the required mechanical properties. In titanium alloys, the microstructure is often described by the α/β phase distribution. The shape, size and ratio of α and β

phases dictate to a large extent the mechanical properties. To achieve the necessary microstructure after metal processing a heat treatment is often used. Titanium and titanium alloys are heat treated in order to reduce residual stresses developed during fabrication (i.e. stress relieving); produce an optimum combination of ductility, machinability, and dimensional and structural stability (annealing); increase strength (solution treating and aging); optimize particular properties such as fracture toughness, fatigue strength, and high-temperature creep strength [20].

The response of titanium alloys to heat treatment depends on the alloy composition. The α, near α and α-β alloys with a low solute content are usually heat treated by annealing: most commonly a mill anneal, recrystallization or beta annealing [20]. Figure 1.7 shows the response of commercial purity Ti to different types of heat treatment: annealing at 700˚C, showing equi-axed grains of α- phase (Figure 1.7 a); quenched from the β-phase field showing martensitic α- phase (Figure 1.7 b); air cooled from the β-phase field showing large Widmanstätten plates of the α- phase (Figure 1.7 c). For comparison of the effect of the alloying elements on microstructure, a near α-alloy IMI 685 (Ti-6Al-5Zr-0.5Mo-0.25Si) air cooled from the β phase field is shown in Fig. 1.7d). This shows a fine basket weave configuration of Widmanstätten plates of α phase outlined with small amounts of β phase [19].
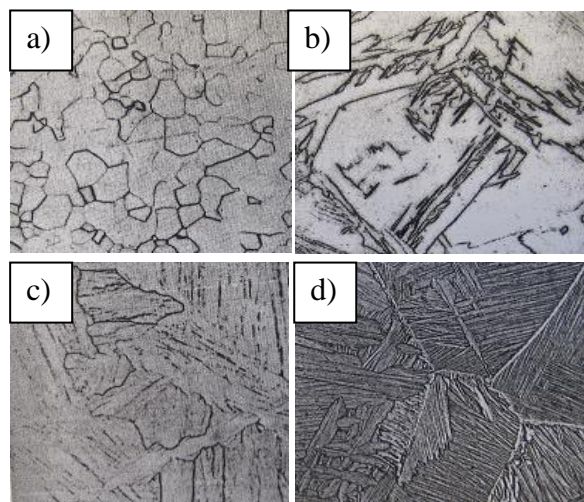
Figure 1.7 Microstructure of commercial purity Ti after: a) annealing at 700˚C (x100), b) quenched from β phase field (x100), c) air cooled from β phase field (x150), and d) near α-alloy IMI 685 air cooled from β phase field (x75) [19].

Figures 1.8 [21] and 1.9 [22] show respectively a schematic and optical micrographs of the microstructural development in Ti6Al4V alloy after heat treatment at three different temperatures i.e. in the β-phase field; in the α-β phase region, above the temperature for martensitic transformation (M_s); and in the α-β phase region below the M_s.
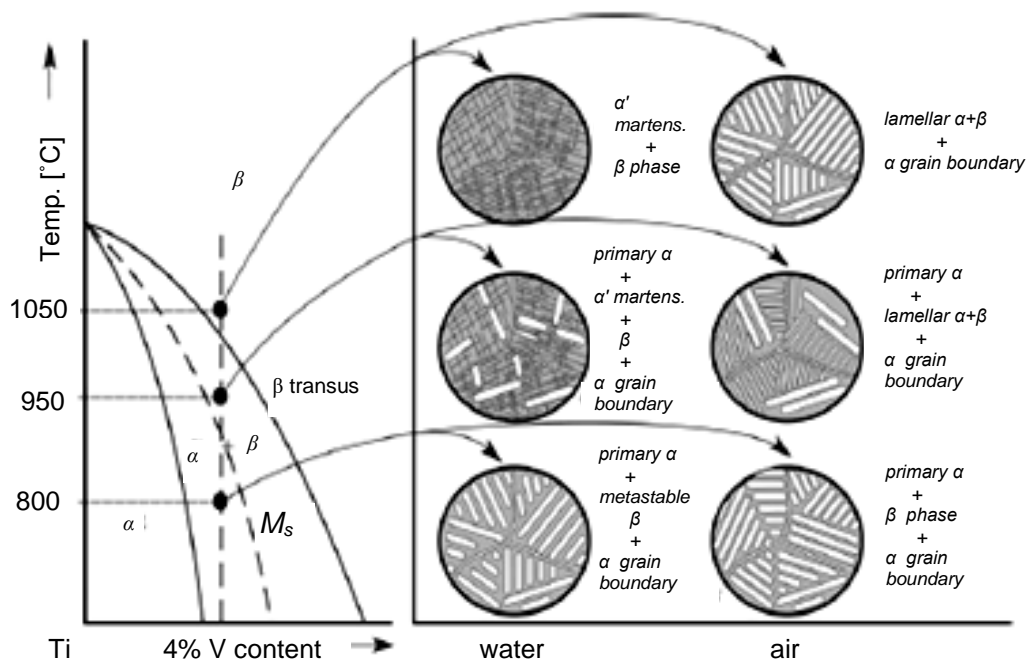
Figure 1.8 Microstructure development of Ti6Al4V cast alloy after heat treatment at different temperatures and subsequent cooling with different rates [21].

The heating was followed by cooling at different rates using water, air or furnace cooling. Water quenching from temperatures above M_s leads to the formation of an α′ martensitic structure in which the volume fraction of martensite is reduced with decreasing temperature (Figure 1.8 and Figure 1.9a) and b). After air and furnace cooling, only primary α- and β- phases are present in all annealed alloys. Cooling from lower temperatures, below M_s, produces structures with large amounts of finer α- phase outlined with β- phase. A similar tendency of α-β phase distribution is found in other research on heat treatment of cast and wrought Ti6Al4V alloy [23-26].
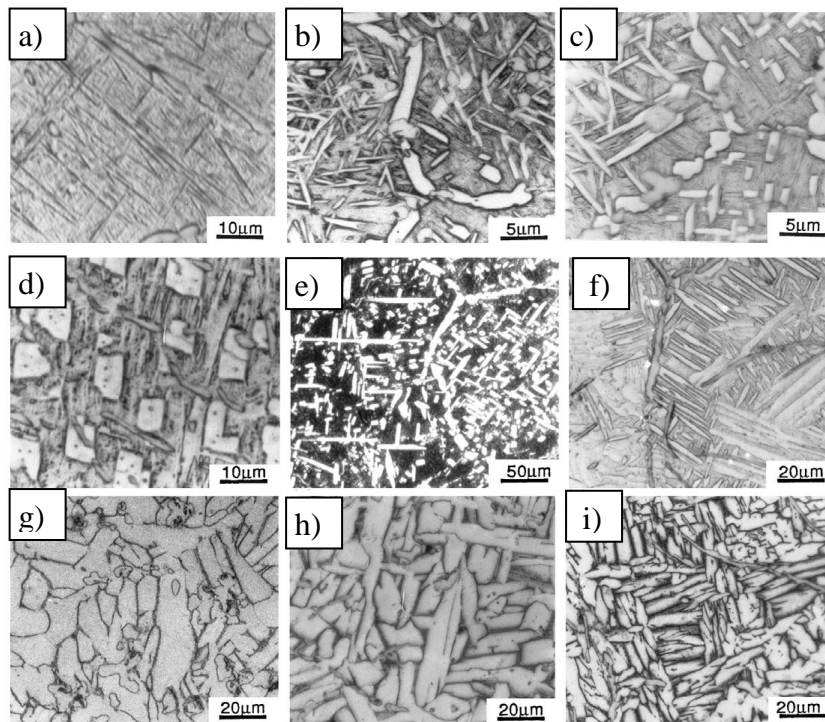
Figure 1.9 Microstructures of cast Ti6Al4V alloy annealed at different conditions, a), d) and g) 1100˚C, b), e) and h) 950˚C, c), f) and i) 900˚C; and cooled accordingly by water quenching, air cooling and furnace cooling [22].

Mechanical properties such as hardness, tensile strength and ductility are largely influenced by the heat treatment conditions [22-28]. Tensile strength changes in a similar manner to hardness with increasing annealing temperature, as seen in Figure 1.10 [22].
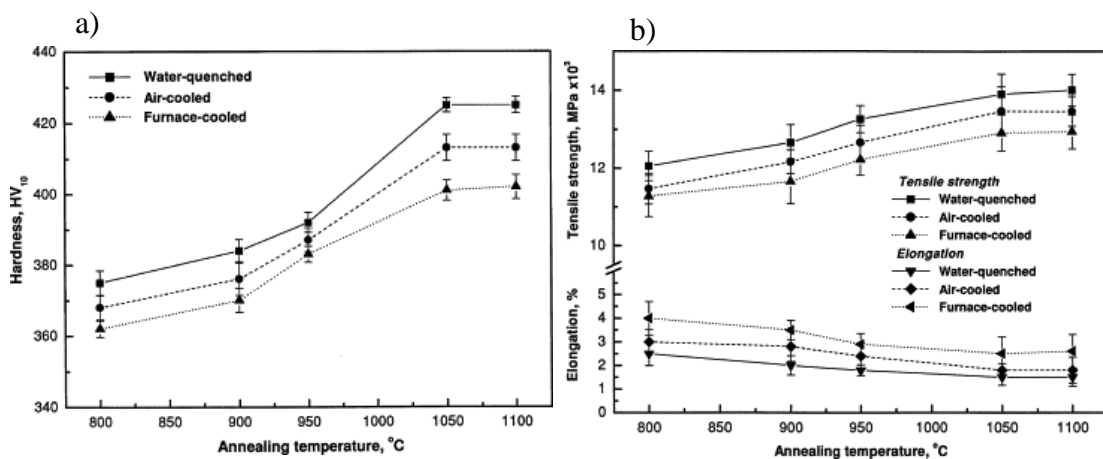
Figure 1.10 The effect of different annealing temperatures and cooling rates on the a) hardness and b) tensile strength of Ti6Al4V cast alloy [22].

12

Hardness and tensile strength increase with increasing annealing temperature and this is highest after water quenching. Furnace cooling gives the lowest values of hardness and tensile strength. Conversely, elongation to fracture decreases with both increased annealing temperature and cooling rate. The highest values of hardness and tensile strength accompanied with very low ductility are obtained when the martensitic α′ phase is produced upon water quenching from temperatures above Ms.

1.2.2.2 Powder metallurgy of Ti

As mentioned previously titanium and titanium alloys are key advanced materials for improved performance in aerospace and terrestrial systems. However, the more widespread use of titanium and its alloys is limited by their high cost compared with competing materials such as steel and aluminium alloys [29]. This has led to various investigations to find ways of lowering the cost of titanium production by researching and developing new processes for Ti extraction and processing. One of the leading ways for achieving cost reduction is by employing powder metallurgy and utilising the potential to produce near net shapes. The cost of fabricating various cast and mill products is shown in Figure 1.11, which shows the greatly increased cost of producing these compared with the cost of the ore, extraction processes and production of the titanium sponge [29-31].
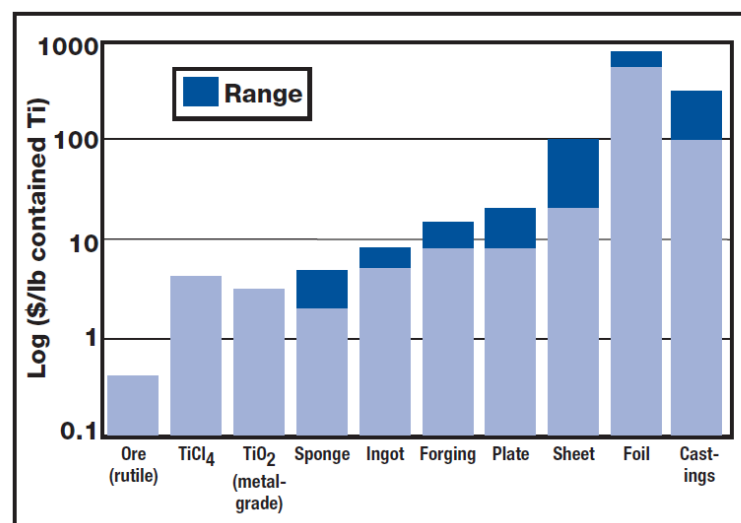
Figure 1.11 Cost of titanium at various stages of component fabrication [29].

To produce a final component from an ingot by milling, involves in some cases up to 70% material waste. The post machining after casting also doubles the cost of the final product [29] (Figure 1.12).
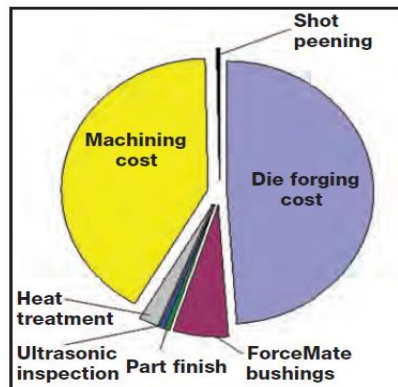
Figure 1.12 Manufacturing cost of side-of-body chord for Boeing 787 [29].

So, the drive for developing powder metallurgical processing of titanium and titanium alloys is to reduce the cost while maintaining mechanical properties at a level equivalent to those obtained by ingot metallurgy [32]. There are several well-known processes for producing titanium and titanium alloy powders. Currently, chemical reduction, hydrogenation dehydrogenation (HDH), gas atomization (GA), plasma- rotating electrode process (PREP) are mainly used for commercial production [33, 34]. GA and PREP powders have high purity and are commercially available. The disadvantage is their high production cost [29], which makes them suitable only for higher end applications. Another disadvantage of alloyed GA and PREP powders is that they have low compactability due to their spherical morphology. The elemental Ti HDH powders on the other hand are low cost, have excellent compactability, low chlorine contamination and are commercially available. The oxygen content of elemental HDH powders is higher than that of GA powders. In PM of titanium alloys two ways of preparing the alloy powders can be used: blended elemental (BE) and pre-alloyed (PA) [35]. The advantage of the PA approach is that the mechanical properties of the final products are equivalent to those of ingot metallurgy. The challenges with them are associated with availability, cost and powder compactability [36-38]. When the BE approach is used, more attention is needed on process parameters such as sufficient mixing, longer sintering for complete inter-diffusion of the alloying elements into the titanium matrix. Caution

14

is also needed to prevent the formation of intermetallic compounds during sintering, because they are normally brittle at room temperature and therefore lower the mechanical properties [35, 39]. A big advantage of the BE approach is the lower cost of the starting powders, as well the additional freedom with alloy compositions especially during the research and development stage.

An additional challenge in titanium powder metallurgy is the high affinity of titanium with atmospheric gases. The effect of the impurity level of the most common interstitials (oxygen, nitrogen and carbon) on the tensile strength and ductility of pure Ti is shown on Figure 1.13 [40], where the strength increases but the ductility decreases with the content of interstitials.
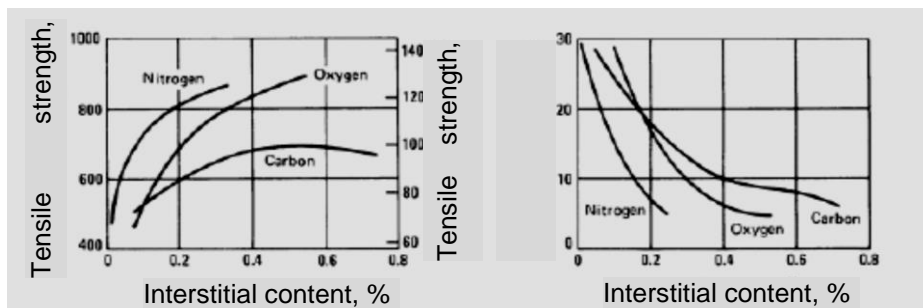
Figure 1.13 Effect of the interstitial element content on the strength and ductility of Ti [40].

The most traditional PM methods used for titanium and its alloys are press and sinter [41-45], hot isostatic pressing (HIP) [46-48] or isothermal forging [49]. Along with the newer technologies for powder consolidation such as metal injection moulding (MIM) [50-53] and selective laser sintering (SLS) [54], innovations in the sintering practice is also area of research. Press and sinter is considered as practical way for consolidation. The disadvantage of the traditional vacuum sintering (VS) is the length of the process due to the design and the method of heating in the electric furnaces. So, the effort in the current research is using alternative heating sources, where the aim is to increase the heating rates and reduce the sintering time. Using electromagnetic waves or microwaves (MWs) is one alternative. Some materials can interact with MWs, converting the electromagnetic energy into heat within the material. The process of heating is rapid with reduced energy consumption and enhanced sintering [55, 56]. The process is called microwave sintering (MWS). Another alternative is spark plasma

sintering (SPS). SPS is a sintering technic utilizing uniaxial force and a pulsed direct current under low atmospheric pressure to perform high speed powder consolidation [57]. This direct way of heating allows very high heating and cooling rates, enhanced densification and fully dense products. The combination of sintering and further forging or powder compact extrusion have become other areas of interest more recently [58-62]. Conductive materials can be also heated using direct-current heating or induction heating. Induction heating is widely used in metal casting industry. Similarly, to MWS and SPS, induction heating allows very fast heating rates and for sure has a potential to be used in sintering of metal powders.

1.2.3 Induction Sintering

In powder metallurgy practice, sintering is used for consolidating metal powders into fully solid or porous products. Sintering is a thermal treatment of pre-compacted powder particles to achieve bonding between particles into a coherent, predominantly solid structure. The thermal process is at temperatures lower than the melting point of the material where densification occurs via mass transport or diffusion at atomic level [63]. The resulting structures have strength and other engineering properties comparable to the corresponding wrought and cast material compositions. In conventional sintering batch or continuous furnaces are commonly used for sintering of pre-shaped powder compacts. The process is long and economically inefficient, considering the slow heating rates and the long sintering times. The increased demand for more efficient powder metallurgy production and from economic aspects, an improvement in sintering practice is required. Several novel techniques have been explored to increase and intensify the heat penetration beyond traditional limits. Conductive materials can be subject to direct-current heating or induction heating [63]. Studies to investigate the possibility of using induction heating for sintering of metal powders originate from the 1980s. In induction sintering, a powder compact is surrounded by an induction coil which carries an alternating current. The current in the induction coil creates a magnetic field that in turn induces eddy currents in the metal powder compact, assuming electrical conductivity. The main attraction is the rapid heating. Heat transfer for induction heating could be 3000 times better than that from radiant heating. Figure 1.14 gives an example of heating rates that could be

achieved when induction heating is used [64]. Another advantage is the possibility of achieving higher sintering temperatures. A traditional belt type sintering furnace has a temperature limitation and their strength and life is restricted at higher temperature.
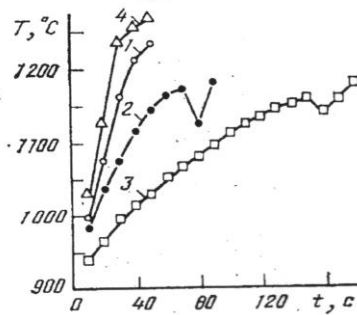
Figure 1.14 Time- temperature curves of high frequency induction heating with power capacity 1- 20kW, 2-30kW, 3- 40kW and 4- 50kW [64].

In 1990 Pfaffmann and Templeton [65] reported on the metallurgical and technological advantages of sintering iron alloy powders for automotive components at high temperature using induction sintering. The authors stated that, the metallurgical advantages were increased diffusion, resulting in faster elimination of prior grain boundaries and their inherent grain boundary oxides, faster pore spheroidization, a possibility of alloying with high melting point elements and alloying with low cost elements such as chromium and manganese. The reason is that the oxides of these elements can only be reduced at high temperatures. This results in improved impact and fatigue properties. The authors also stated the technological advantages of using induction sintering are: (1) easy to automate; (2) an induction system is simple and compact, consisting only of an induction coil and a powder unit; (3) higher temperatures; (4) less floor space; (5) lower cost operation and higher yield rates; (6) increased net pieces per hour, coming from the higher heating rates and shorter sintering time; (7) significant reduction of the volume of the protective gas required because of the compact volume of the inductor; (8) minimizing the amount of part scrap from system failure, considering the simplicity of the system. Research on the use of induction heating for sintering has been mainly concerned with applications for sintering metal based alloy powders or for hard metal powders. Bulatova [66] studied the heating kinetics of iron based alloy ring parts using a high frequency alternating

17

magnetic field. The model presented in this study helps with an understanding of the electromagnetic nature of a powder metallurgy part, showing that induction heating depends on changes in the magnetic and electrical properties of the circuit produced from contacting powder granules. Two different voltages (52V and 63V) were used for sintering. Three stages of thermo-kinetics (I, II and III) were defined and they were common for both methods 52V and 63V (Figure 1.15). Toward the end of Stage I a reduced heating rate is observed. The average temperature, reached at the end of Stage I, differs insignificantly but the heating times are significantly different. The character of the I(t) curve also changes in the different portions. A decrease in the heating rate is accompanied with an increase in the current which means a decrease in the inductive resistance of the material.
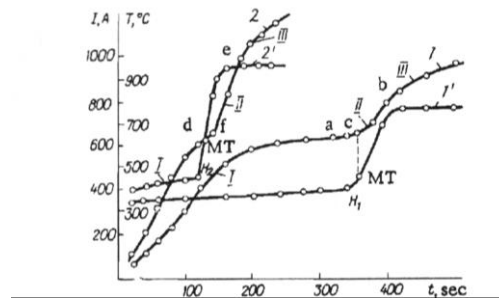
Figure 1.15 Changes in average temperature T(t) and effective current I(t) during induction heating of a powder metallurgy ring part with voltages 52V (1,1 ′) and 63V (2,2′), where 1 is $T_1(t)$, 1′ is $I_2(t)$, 2 is $T_2(t)$ and 2 ′ is $I_2(t)$; I, II and III are the stages of the thermo-kinetic process [66].

Changes in inductive resistance occur because of the transformation of the microstructure in the granulated powder material and it is explained by the model shown in Figure 1.16.

a)
1- powder particles
2- oxide film
3- conductive bridge

b)
1- powder clusters
2- metallic contact
3- high resistance bridge
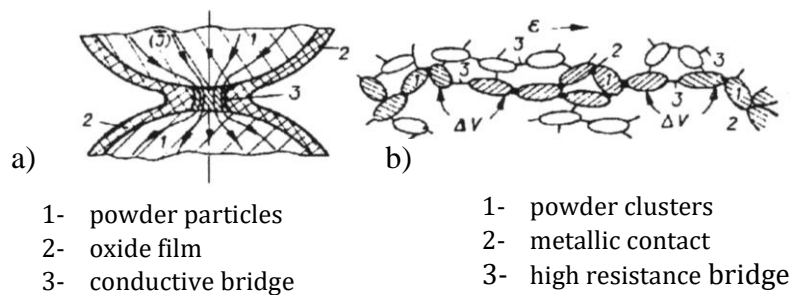
Figure 1.16 Model of contact between a) two powder particles, and b) the schematic model of the material including clusters of powders [66].

18

The surface of the powder particles receiving the mechanical forces consists of contact spots with metallic conductivity, areas of non-metallic contacts (oxide film) playing the role of insulator (having high electrical resistance). These films cause low electrical conductivity at the start of induction heating. With increasing temperature to several hundred degrees Celsius, thermal diffusion of the atoms stimulated by the high frequency electrical field leads to the formation of conductive bridges between the powder particles. However, the cohesive forces of these bridges are low. For iron powders, when the temperature increases to 500°C, there is increased diffusional transfer of the metal to the bridges. The oxide film starts failing because of its lower coefficient of thermal expansion. As a result, the density of the contact spots increases. This correspond to stage II in Figure 1.15 where the I(t) curve significantly changes to an almost vertical line showing the decrease in electrical resistance. Conta [67] reported similar findings for the reduced heating rate at the beginning of the induction heating process. He named this stage an incubation period and describes it as a very poor coupling between the material and the heating coil. Consequently, most of the induction energy is dissipated in the cooling water flowing in the induction coil. An explanation of the incubation mechanism hypothesis is related to surface chemistry principles. It is thought that a thin layer of adsorbed gases lying on the surface of the powder metal particles may act as a partial insulator between particles. If these gases are driven out from the particle surface by heating at lower temperatures, the particles may come into more close contact and therefore the conductivity of the compact increases. It was found that if the powder preform is first heated to 400°F (240°C) for a short time, no incubation period is observed during subsequent induction heating (Figure 1.17).
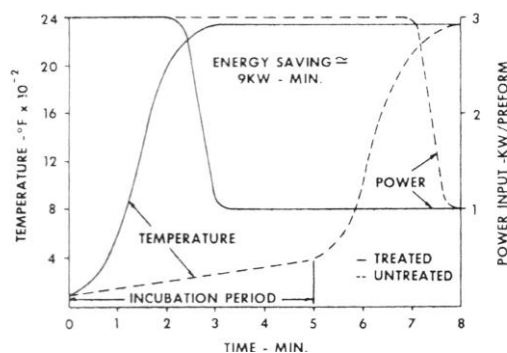
Figure 1.17 Typical temperature and power profiles during induction sintering of preheated (treated) and not preheated (untreated) 300g iron powder preforms [67].

Another way of reducing, but not eliminating the incubation period is to increase the density of the powder preform (Figure 1.18).
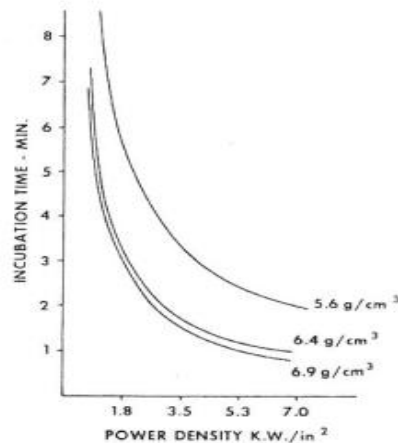
Figure 1.18 Effect of powder compact density and power density input on the incubation time [67].

Studies on the effect of induction sintering on the mechanical properties of iron based powder materials and comparison with the conventional furnace sintering were mostly found in the literature. Nikishov et al. [68] studied the microstructure and properties of two iron alloys sintered using conventional heating and induction heating. The sintering conditions and the related mechanical properties such as hardness and tensile strength are shown in Table 1.2. The improved tensile properties were related to the microstructure properties, where induction heated materials had more uniform alloying element distribution and the carbide powders when compared to specimens sintered by conventional electric heating.

Table 1.2 Mechanical properties of powder metallurgy alloys sintered by conventional furnace and induction heating [68].

Powder composition	Sintering process	HRB	Tensile strength, MPa	Elongation, %
Fe- 2%C, 3%Cr, 2%Cu	Furnace, 1140°C, 2h	80-90	> 450	5.4-6.5
Fe-1.6%C, 2.7%Cr,1.7%Cu	Induction, 1260°C, 2min	80-95	>500	6.4-8.2
Fe- 0.7%C, 3.5%CrC	Furnace, 1200°C, 2h	90-105	>750	7.3-10.6
Fe- 0.6%C, 3.5%CrC	Induction, 1280°C, 2min	32	>850	17.5-23.0

Using three point bending Cavdar et al. [69] made a comparative study of the rupture strength of Fe with 3wt% Cu alloy samples sintered by conventional heating and induction heating using the same temperature of 1120˚C (Table 1.3).

Table 1.3 Three point bending test results of Fe-3wt% Cu alloy samples sintered by conventional and induction sintering [69].

Sintering time and sintering environment	Maximum stress, MPa	Elongation to fracture, %
Conventional sintering at 1120°C		
30 min, atmospheric environment	285.6	2.8
30 min, argon environment	375.2	3.1
Induction sintering at 1120°C		
1 min, atmospheric environment	93.6	1.2
2 min, atmospheric environment	236.6	3.3
3 min, atmospheric environment	318.2	3.1
Pre-sintering at 500°C for 10min followed by Induction sintering at 1120°C		
1 min, atmospheric environment	310.6	2.6
2 min, atmospheric environment	335.2	4.6
3 min, atmospheric environment	348.3	4.1

Increasing the holding time at the sintering temperature clearly improved the maximum stress and the elongation to fracture of the tested samples, achieving comparable to the properties of conventional sintering. The pre-sintering at 500˚C for 10min has a positive effect on the tensile strength and elongation to fracture. Salak et al. [70] also compared conventional and induction sintering of Fe based alloy powders using a range of sintering temperatures and sintering times. The sintering conditions of conventionally sintered samples used for comparison were 1120˚C for 1hour. Two types of Fe-Mn-C alloy powders were used: gas atomized and Hometag powders. The induction sintered samples prepared with gas atomized powders did not achieve a tensile strength comparable with that for conventionally sintered specimens, even after sintering for 10min at 1300˚C. The Hometag powder responded well on induction sintering. Table1.4 presents the induction sintering conditions for the Hometag powders and the mechanical properties achieved in each condition. Good values of strength and hardness were

achieved at high sintering temperatures of 1300˚C for only 1 to 3 min. At a lower sintering temperature of 1200˚C, a sintering time of 10 min was needed to achieve comparable strength and hardness.

Table 1.4 Properties of Fe-Mn-C induction sintered samples prepared with Hometag powders [70].

Sintering conditions		Density g/cm³	Tensile strength MPa	Hardness HV 20
Temp. C°	Time min			
1100	1	6.58	294	133
	3	6.58	359	151
	10	6.63	465	166
1200	1	6.60	413	158
	3	6.61	542	165
	10	6.65	650	156
1300	1	6.62	565	157
	3	6.63	589	157
	10	6.75	600	156

Another comparative study by Krumphold et al. [71] reported improved tensile strength of iron and iron-nickel alloy samples when induction sintering temperatures of 1200°C and 1300°C were used (Figure 1.19).
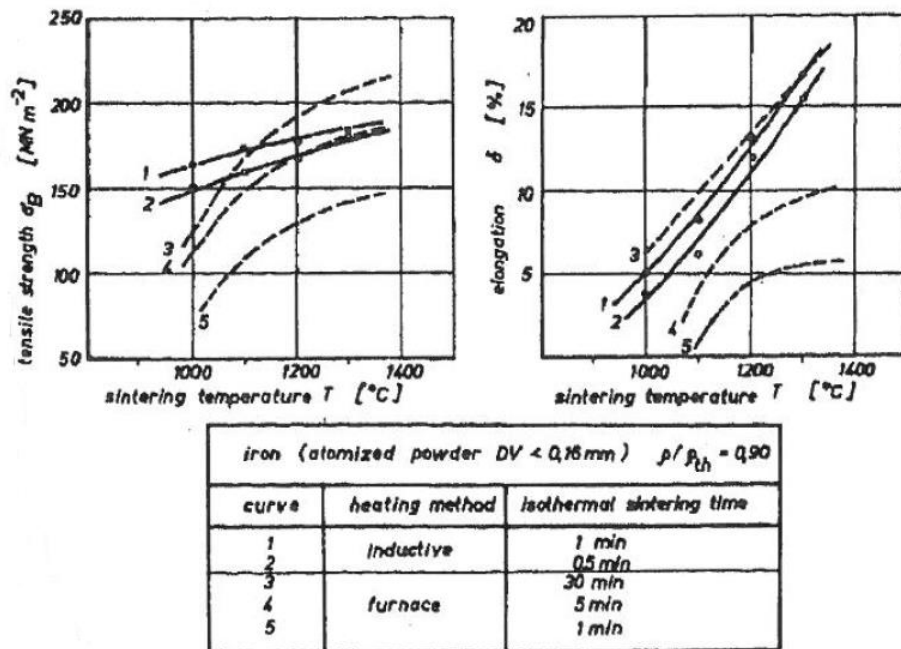
Figure 1.19 Tensile properties of PM iron based alloy after induction sintering and furnace sintering [71].

The powder compacts were sintered by induction and furnace heating at similar temperature-time conditions. Sintering times of 1 and 5 min at temperatures up to 1300˚C in a conventional furnace were not enough to achieve good strength and ductility, while induction sintering at 1200˚C and 1300˚C for only 0.5 min and 1 min achieved strength and ductility similar to the properties achieved by furnace sintering at 1300˚C for 30min. The economy was increased by using induction sintering as the specific energy input was reduced by 50% and the throughput was doubled.

Krumphold et al. and Hermel et al. have also studied induction sintering of hard metals where the authors proposed this method as a future technique for consolidation of WC-Co [71] and WC-TiC-Co powders [72] respectively. Short time induction sintering of hard metals is characterised by sintering time of 2 to 8 min at temperatures of 1450˚C to 1600˚C and heating periods within 5 and 15min. The parts produced by the short time induction sintering showed the same or in some cases improved wear behaviour as the standard furnace sintered samples. Figure 1.20 shows the properties of K10 hard metal (WC-6%Co) samples sintered by induction sintering and furnace sintering.
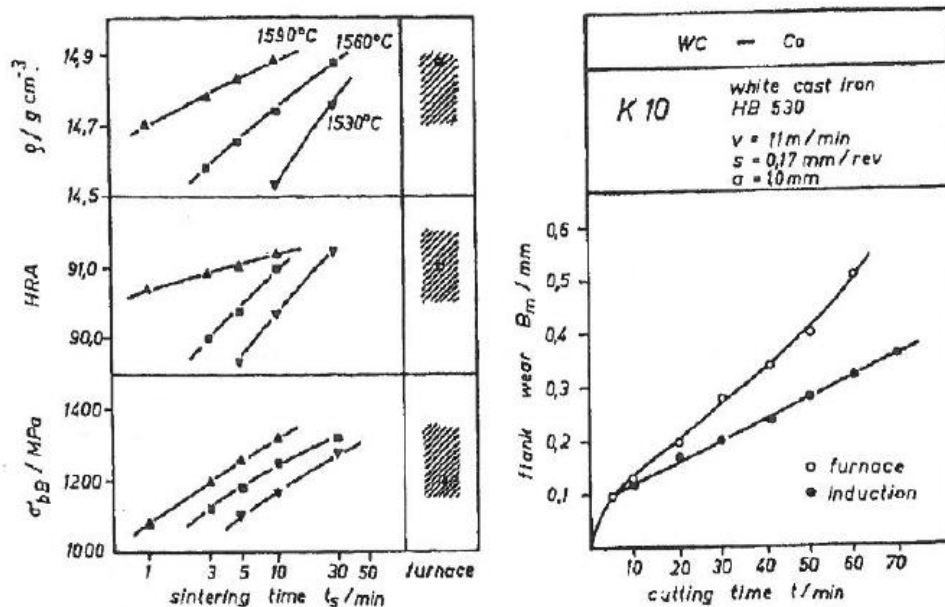
Figure 1.20 Density, mechanical properties and wear behaviour of WC-Co [71].

The same authors also reported that, two induction sintering facilities were developed and built in Germany with an installed generator power of 20 kW and

65 kW for research and production. The equipment, designed to treat 5 and 10 kg/h respectively, showed the beneficial effect of short time sintering on the quality of the material.

Induction sintering has also been used for consolidation of TiB_2-WB_2 powders, where the samples achieved relative density of 91% after induction heating at 1940˚C for 10 min [73].

The most recent research which investigated the use of induction heating for consolidation of Ti and Ti alloys was carried out by Bolzoni et al. [74]. The process was called induction hot pressing. Small amount of 15g of each Ti alloy powders were directly poured into a graphite die heated up to 1100˚C to 1300˚C using induction heating. The process was performed in a vacuum chamber. The pressure was applied after the temperature reached the required value. The authors stated that using induction heating instead of conventional resistance heating shortened the consolidation process significantly. The heating rate of induction hot pressing was 50˚C /min compared to 10˚C/min in a conventional furnace, with a 15min holding time. Also, the cooling time was significantly faster. The whole processing time from heating to cooling took approximately 40min compared to 6h when a conventional hot pressing method was used. Hot pressed density between 97% to close to 100%, depending upon temperature, material and the powder production method were achieved (Figure 1.21).
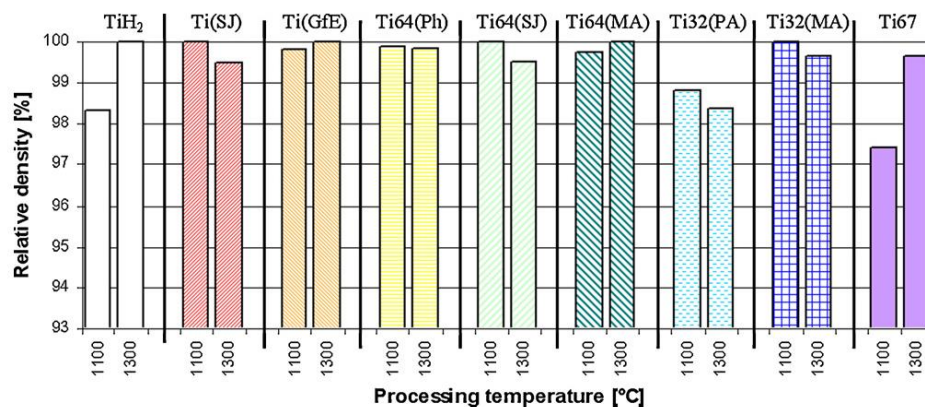
Figure 1.21 Relative density results of the sintered materials processed by inductive hot-pressing at two temperatures [74].

Bolzoni et al. [74] also investigated the oxygen contamination during induction hot pressing (Figure 1.22). The chemical analysis revealed that some oxygen pick-up occurred. Because of their larger surface area, powders with a smaller particle

size, are more sensitive to oxygen pick up. When the average powder particle size was over 75 microns the oxygen pick up varied between 0 and 0.1wt%.
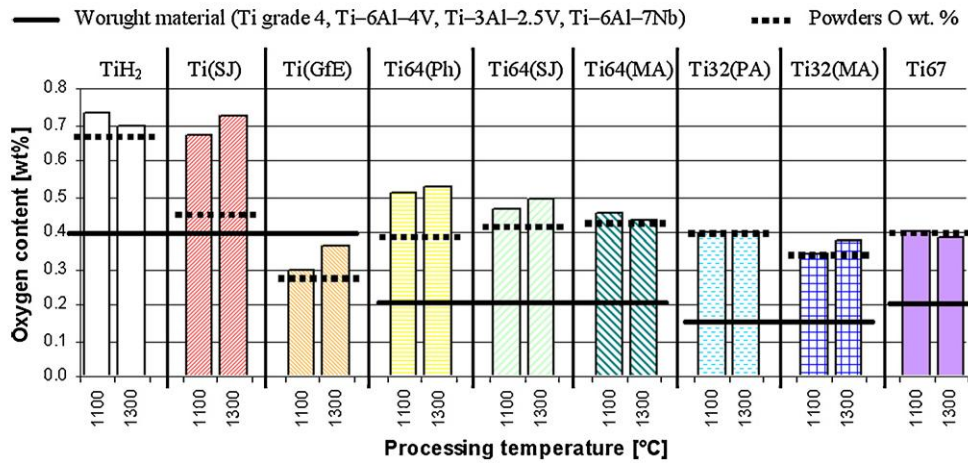
Figure 1.22 Oxygen content of the samples processed by hot-pressing compared with both the content of the starting powders and that of wrought materials [74].

In studies carried out by Jia et al. [75, 76] on the induction sintering of pure Ti HDH and HDH and GA Ti6Al4V powders, only one induction sintering condition was considered i.e. heating to a temperature of 1350°C and holding for 3 min. The results for sintered density and tensile strength are given in Table 1.5 and Figure 1.23.

Table 1.5 Relative densities of induction sintered pure Ti- HDH, Ti6Al4V-GA and Ti6Al4V- HDH powder compacts [76].

	Ti- HDH	Ti6Al4V-HDH	Ti6Al4V-GA
Relative IS density, %	91.0	80.8	85.8
Densification parameter, %	7.2	15	11.3
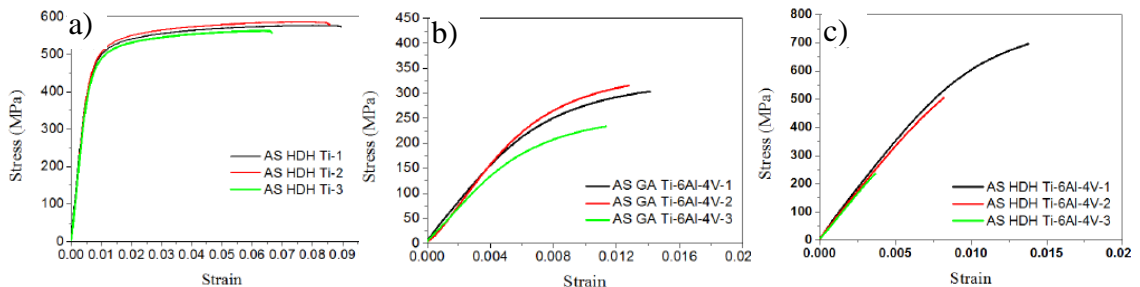
Figure 1.23 Stress-strain curves of specimens cut from as-sintered compacts: (a) HDH Ti, relative density of 91%; (b) GA Ti-6Al-4V, relative density of 85.8%; (c) HDH Ti-6Al-4V, relative density of 80.8% [76].

After 3 min induction sintering, all of the powder compacts had significantly increased density. An observation made in this research is that the lower the initial compact density the higher the densification factor of the induction sintered samples. Ti HDH increased its relative density from 83.8% to 91%, and achieved a tensile strength up to 575 MPa and an elongation to fracture of 6.6%-8.9%. For HDH-Ti6Al4V and GA-Ti6Al4V the respective density increases were 11.3% and 15%. However, because of the lower final induction sintered density these samples showed low tensile strength and poor elongation to fracture.

From the literature, previous work on the sintering of metallic powders using induction heating is limited. Most of the research originates from the 1980's and it is mainly concerned with iron and iron alloy powders. Induction sintering of titanium and titanium alloy powders is a more recent area of research and therefore there is only limited information available on the effects of processing parameters on mechanical properties. From the literature it is evident that induction sintering has the advantages of shorter processing times, simple equipment set up and improved mechanical properties (in the case of iron powder metallurgy) compared with conventional vacuum sintering. It is not yet clear if the use of induction sintering for consolidating titanium and titanium alloy powders will achieve comparable or enhanced properties compared with those obtained using conventional vacuum sintering. More research on the effect of induction sintering process parameters such as temperature and holding time on microstructure and mechanical properties is required.

1.2.4 Powder Compact Forging

The powder compact forging (PCF) process is a rapid densification of pre-sintered powder preforms by a single or a multiple forging force. The main characteristic of the process is the production of net or near net shaped products with very high, or close to full density, suitable for high performance applications. The powder forging process (Figure 1.24) is performed in three steps with the first two steps similar to the standard PM processing [77]. The powders are compacted into a preform using a die and most commonly uniaxial pressure. The mass, density, and shape of the preform are controlled closely to ensure consistency in the characteristics of the final forged component. The preform is then sintered in a

controlled atmosphere furnace. The sintered preform is then reheated, placed in the forging die, and forged to the required final shape and full density.
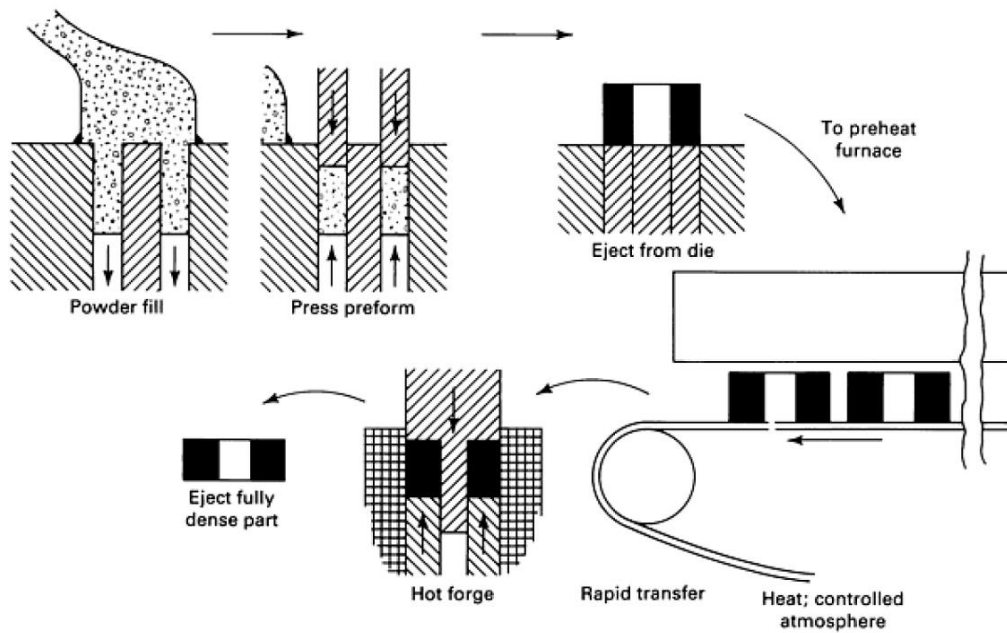
Figure 1.24 The powder forging process [77].

The tooling shape is designed to be close to that of the finished part with material flow controlled to fill the cavity completely.

The PCF process can be differentiated into two categories: powder repressing and powder forging or upsetting (Figure 1.25) [78].
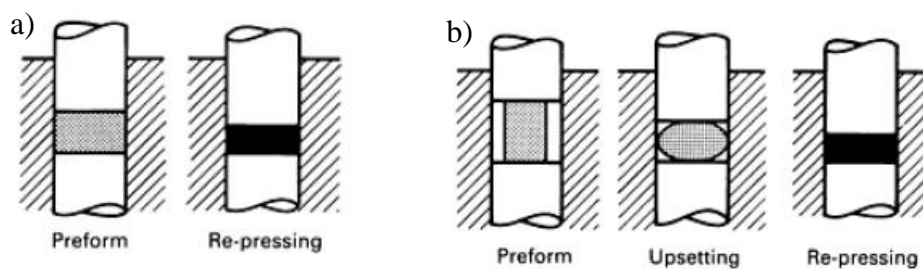
Figure 1.25 Schematic of PCF a) repress and b) upset forging [78].

Powder repressing has a limited amount of powder flow, which occurs in the pressing direction. The final part matches the shape of the preform. Powder upset forging has significant powder flow in both forging and lateral directions. The high powder flow results in parts with good mechanical properties, but the process has problems with high die wear. In the case of repressing, more complex shapes

can be formed with a lower degree of die wear although mechanical properties are lower.

 Another differentiation in forging is based on the type of the die used: a trap die (Figure 1.25) or an impression die (Figure 1.26) [78].
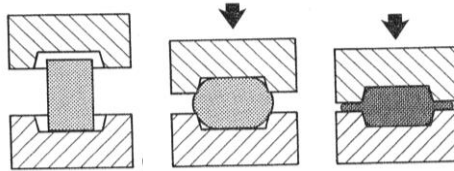
Figure 1.26 Schematic of impression die forging [78].

Impression die forging practice (Figure 1.26) uses moving die halves. The die also has a flash gutter to accommodate excessive material. The flash represents the major material loss, which is mainly associated with conventional forging where the preforms are wrought or cast billets. Therefore, the key to successful powder forging depends on the powder preform, since the amount of material used and the compact shape can be closely tailored to eliminate materials loss.

Nonetheless, during forging the material flow should allow complete filling the die cavity resulting in fully dense material. During PCF porous preforms experience large plastic deformation due to the extensive unconstrained directional and lateral flow. Pore collapse occurs rapidly resulting in flattening and elongation of pores in the lateral direction. The stress state around the particle is a combination of a normal and shear stress (Figure1.27) [79].
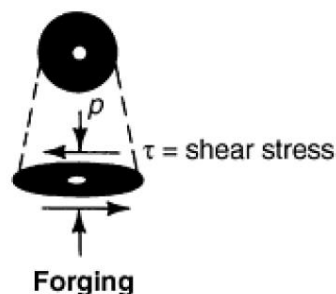
Figure 1.27 Stress state around a powder particle during powder compact forging [79].

The shear stress component causes the disintegration of any oxide or contamination on a powder particle surface, which leads to the formation of clean powder contact surfaces, resulting in a very strong metallurgical bond. The strong metallurgical bond and the overall high density of a part results in enhanced mechanical properties such as fracture toughness, impact strength and fatigue strength [80].

1.2.4.1 Applications of powder compact forging

Powder forging for mass-produced structural parts was developed to meet performance requirements beyond that available from conventionally pressed and sintered powder parts. Currently, powder forged parts are produced mainly using iron based alloys for applications in the automotive industry. One of the most popular automotive parts produced by PCF is a connecting rod [77]. Powder forged connecting rods are now used in at least 13 engines among major U.S. automakers and are also used in some European and Japanese engines. The connecting rods are typically forged from Fe-Cu-C powders to a minimum density of 7.84 g/cm^3. At this density level they have an ultimate tensile strength of 760 MPa (110 ksi), a yield strength of 550 MPa. A powder forged connecting rod eliminates the surface defects inherent in conventional forging, has a uniform microstructure, dimensional consistency and superior machinability. James Dale [62] has reported a much improved fatigue stress using powder forging of HS150 and HS160 (Fe-Cu-C-Mn) alloys compared with traditionally wrought C-70 (Fe-Mn-C). The main reason for using powder forging is a 58% reduction in the manufacturing cost compared with conventional processing by machining a forged part blank [81]. The cost saving was derived from up to 60% in material saving, a lower machining cost and lower total energy use.

Figure 1.28 shows the most common auto parts produced by forging of various steel powders [77]. Powder forging has also been used for specialty materials, such as tungsten, molybdenum, and beryllium. Since these materials cannot be cast easily, powder forging is the best option for processing fully dense net shapes.
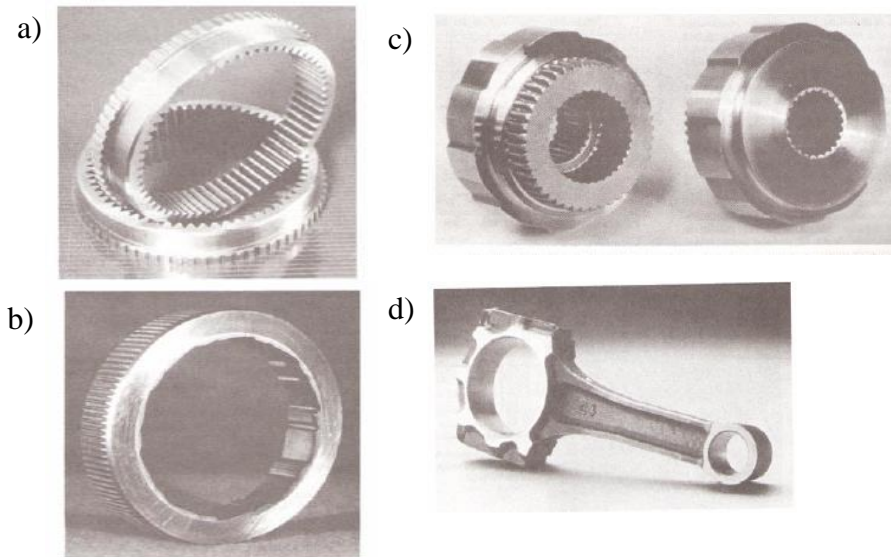
Figure 1.28 Car parts produced by powder compact forging a) converter clutch, b) ring gear, c) inner cam/race and d) connecting rod [77].

Powder forging concepts are also emerging for the fabrication of ceramic parts. With the recent development of superplastic ceramic materials, forming of complex shapes from simple ceramic preforms has been developed for high temperature bearing and seal applications [78].

1.2.4.2 Research approach to powder compact forging

The most common research approach to metal powder forging involves cold compaction of powders into shaped preforms which are then sintered. Sintering is usually for 30 min to 120 min in a high temperature vacuum or protective atmosphere furnace followed by direct forging or reheating and forging using a variety of forging dies and pressing equipment. PCF of BE or PA Fe alloy powders has been widely researched [62, 82-84]. Das et.al. [83] used a BE approach for hot forging of different Fe-P-Cr alloy compositions. The powders were encapsulated prior to sintering and forging as shown in Figure 1.29.
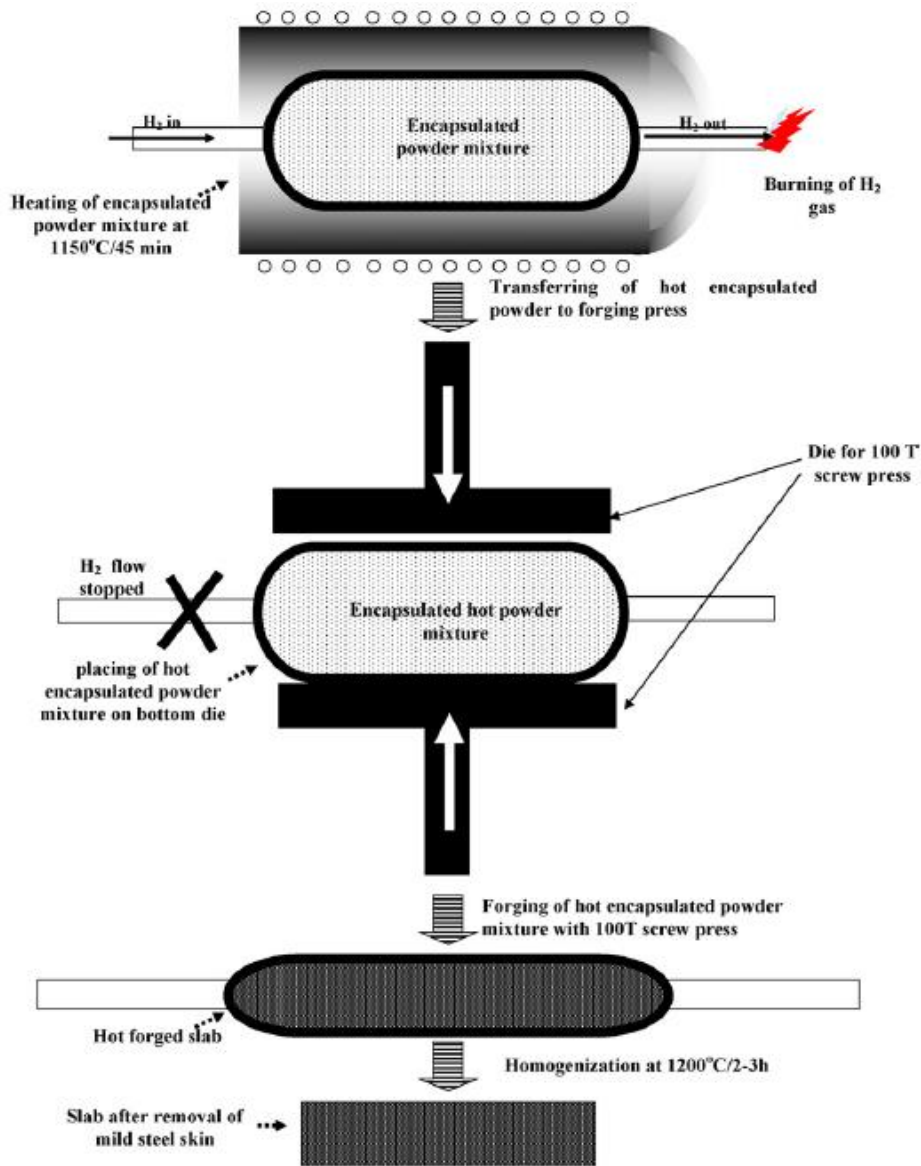
Figure 1.29 Schematic diagram illustrating hot forging of Fe-P-Cr powders [83].

Chandramouli et al.[82] and Shanmugasundaram et al. [84] used different PCF approaches for Fe-C and Fe-Cr-Ni-Mo BE alloy powders. The powders were cold compacted into cylindrical samples, coated with a ceramic based coating and sintered at 1000°C or 1100˚C for 120 min in a muffle furnace, without a protective atmosphere. Immediately after sintering the compacts were hot upset forged. In the first study, the effect of the amount carbon addition and the effect of the flow rate on the densification were studied. The maximum forged density achieved in this study was below 96% of the theoretical density. The second study [84] focused on the tensile and impact behaviour of the as forged specimens. It was reported that the tensile properties of sintered and forged Fe-C-Ni-Mo-Cr

steels are comparable to those of conventionally processed wrought alloy steels with similar composition.

Patents on powder forging are also available in the literature [85-87]. Work [85] focusses on a design of apparatus for fabricating hollow parts made from high strength materials such as superalloys and titanium alloys. Work [86] focusses on a method for consolidating iron alloy powders by powder compaction, conventional sintering and closed die forging. The advantages claimed in this patent are the production of complex shaped powder forgings which are flash/free or have only a minimum amount of flash, cost effective manufacturing and minimized contact time with the tooling, which increases the tool life. Work [87] is a patent for forging of titanium-based material for producing engine valves. Ti HDH powders, Al-40V master alloy powders and in some cases TiB_2 powders were premixed, pressed into cylindrically shaped green compacts and sintered in a high vacuum at 1300˚C for 4h. The sintered preforms were reheated and upset forged with an upset ratio of 60%. The samples without the addition of hard particles achieved yield strength of 880MPa and elongation to fracture of 12%. TiB_2 additions refined the grain size after sintering and lead to increase in the yield strength, but caused a reduction in ductility.

1.2.4.3 Powder compact forging of Ti and its alloys

In the powder forging practice of iron alloys, a cold powder compact is coated with a ceramic based or graphite coating prior to sintering. A graphite coating can have two purposes (i) to reduce oxidation during heating and to provide added lubrication during forging; (ii) to carburise a preform during heating, which may eliminate any additional surface heat treatment steps [78]. This technique may not be suitable when Ti and Ti alloy powders are used. During high temperature sintering, graphite reacts with Ti to form TiC. TiC is highly detrimental to the ductility of Ti and Ti alloys. Ti is also highly reactive with oxygen and nitrogen at temperatures over 500˚C. For this reason, sintering and even fast heating needs to be done in a protective atmosphere.

Another consideration is that the deformation characteristics of all classes of titanium alloys are highly sensitive to temperature. This effect is illustrated in Figure 1.30 [88].
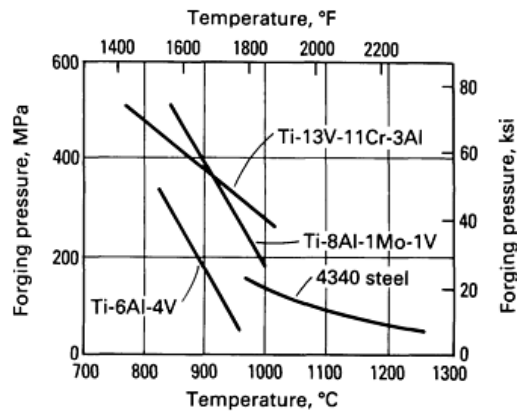
Figure 1.30 Effect of temperature on forging pressure for three titanium alloys and 4340 (Fe-Ni-Cr-Mn) alloy steel [88].

For each one of the titanium alloys, the forging pressure increases dramatically with relatively small changes in metal temperature. For Ti6Al4V alloy the forging pressure increases threefold with a 100°C decrease in temperature. Therefore, it is important to minimize temperature losses when transferring heated samples to the forging equipment and to minimize contact time with the much cooler forging dies.

Several techniques have been used for compacting and sintering Ti alloy powders prior to forging. Guo et al. [89] used cold isostatic pressing (CIP) for compacting HDH Ti-1023 (Ti-10V-2Fe-3Al) alloy powders followed by vacuum sintering for 3h at 1300°C. Qiu et al. [90] used the same approach to compact and sinter Ti-1.5Fe-2.25Mo blended powders. As-sintered powder compacts were then used for forging a connecting rod. In other studies [91, 92], powders were put into a stainless steel container which was evacuated and degassed at 500°C and then hermetically sealed under vacuum. The canned powders were heated to 900°C for 0.5h in a muffle furnace for subsequent forging. After sintering, the relative density of the canned and sintered samples was between 93.5% and 95%.

Qiu et al. [90, 93] studied the hot compression deformation behaviour of Ti-1.5Fe-2.25Mo alloy and the manufacture of a connecting rod by powder compact forging. An examination of different sections of the as-forged connecting rod was carried out to see the effect of differences in effective strain on the microstructure and the effect of this on mechanical properties in different sections [90]. This work showed that there is a close relationship between the microstructure, the effective strain and the cooling rate. The α/β phase morphology and distribution varied throughout the different parts and thicknesses of the connecting rod. In the

33

thick areas, such as the crank pin end and the fork part the microstructure was lamellar α+β [90]. The α+β lamellae were coarser at the centre and finer towards the surface due to the difference in cooling rates. The effective strain in the surface region was comparatively low and did not have any effect on the microstructure. The faster cooling in the thin areas resulted in an acicular martensitic structure. The areas with higher deformation resulted in deformed β phase grain boundaries and the formation of a fine equiaxed α-phase instead of one with a lamellar shape [90]. The tensile strengths of the different parts of the connecting rod were similar, except for the piston pin (Table 1.6) [90]. The lowest ductility in the shank region is attributed to the acicular martensite caused by the enhanced cooling rates during forging.

Table 1.6 Mechanical properties of powder compact forged Ti-1.5Fe-2.25Mo (wt%) alloy connecting rod [90].

Part	YS, MPa	UTS, MPa	Elongation, %
Crank pin end	837	863	13.0
Fork	844	871	12.1
Shank	825	853	4.5
Piston pin end	806	847	15.1

Smarsly and Bunk[94, 95] studied the microstructure and mechanical properties of Ti6Al4V powder compacts processed by combined die forging with three different deformation ratios (A_0/A): 0.62; 0.30 and 0.23. The lower deformation ratio resulted in a material with a relative density of 96.2% and insufficient powder particle bonding as revealed by fractography of a sample after a three-point bending test. An increase in the amount of deformation led to fully dense material. Observations of the fracture surface and microstructure of these samples did not indicate any residual porosity. The authors derived the following conclusions from this study: (a) the degree of shear deformation is the most significant parameter which influences the amount of porosity, the microstructure and the texture of the combined forged powder material and (b) post deformation annealing is necessary for full recrystallization of the deformed structure and formation of a homogeneous fine equiaxed structure. In another study [92] the focus was on a comparison of die forging and HIP processing on the tensile properties of Ti6Al4V powder compacts. These were then compared with tensile

properties specified in the ASTM international standards. The powders were canned, heated at 900°C for 30min and forged. Subsequently, a post heat treatment at a temperature of 925°C with a 30min hold time was done. Compared to the HIP-ed samples prepared with identical powders, the forged material showed a refined and more homogeneous microstructure and increased tensile strength and ductility (Figure 1.31).
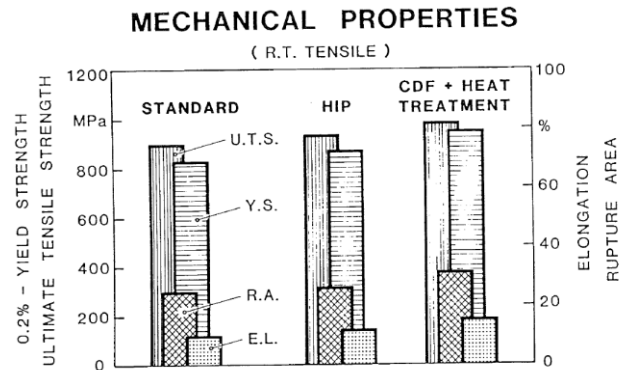
Figure 1.31 Comparison of tensile strength and ductility of combined die forging and HIP Ti6Al4V powder material [92].

Another comparative study was done by Guo et al. [89], where cold isostatic pressing (CIP), sintering and forging were used to consolidate Ti-10V-2Fe-3Al alloy HDH powders with an oxygen content of 0.26wt%. The microstructure microstructural evolution during the different processing steps was studied (Figure 1.32). The relative density of the sintered and the forged samples was 93.5% and 99.6% respectively. The coarse α-lamellar microstructure caused by the prolonged sintering (Figure 1.32 a) was refined after heat treatment. The finer precipitated α-lamellas are well aligned and formed a typical Widmanstäten structure (Figure 1.32 b). Isothermal forging with speed 0.5mm/sec, from the β-region at 950˚C (Figure 1.32 c) and from 780˚C (Figure 1.32 d), caused break up of α phase grain boundary and refinement of the α-lamellas. After forging from 950˚C with a pneumatic hammer, the microstructure showed that the grain boundary α-phase had completely disappeared and the intra-crystalline α phase was more dispersed and finer, forming a typical equiaxed α phase structure (Figure1.32e). For comparison, the authors of this study showed the

microstructure of a bar of the same alloy produced by traditional casting and forging (Figure 1.32 f).
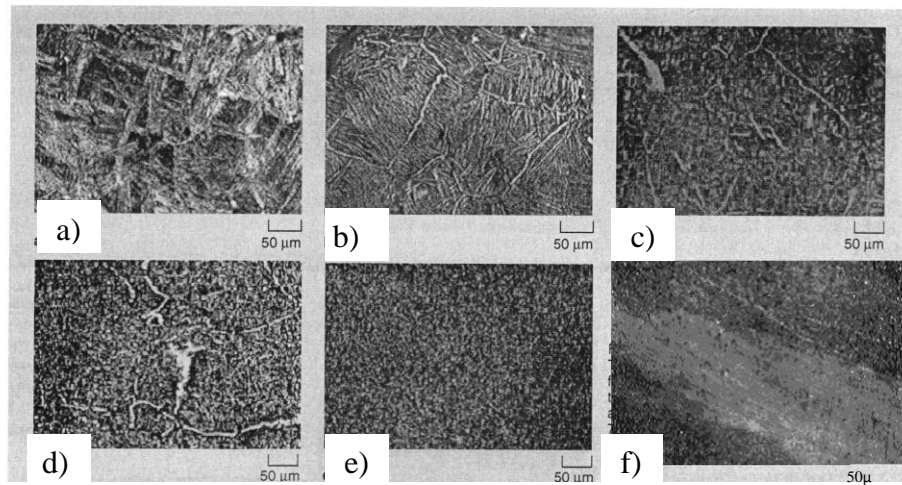
Figure 1.32 The microstructure evolution of Ti-10V-2Fe-3Al powder alloy a) as sintered; b) sintered and heat treated; c) isothermally forged at 950˚C and heat treated; d) isothermally forged at 780˚C and heat treated; e) open die forged and heat treated, and f) Ti-10V-2Fe-3Al wrought alloy [89].

Notably, the microstructure of the PM Ti10V2Fe3Al alloy was fully homogeneous and improved mechanical properties were obtained in the forged material (Table 1.7) due to refinement of the microstructural features.

Table 1.7 Tensile properties of the Ti-10V-2Fe-3Al alloy manufactured by different methods [89].

Powder consolidation condition	YS, MPa	UTS, MPa	Elongation, %
CIP, Sinter, Solution treatment + aging (STA)	1090	1160	2.0
CIP, Sinter, Forged, STA	1260	1290	19.0
BE Pressed and Sintered, HIP, STA	1233	1268	9.0
BE Pressed and Sintered	854	930	9.0
PREP HIP, STA	1213	1310	9.0
PREP HIP, Forged, STA	1286	1386	7.0
Cast	1129	1177	4.0
Wrought	1157	1210	10.0

Nadakuduru et al. and Zhang et al. [96, 97] studied the tensile properties of forged Ti and Ti6Al4V powder compact, where the starting powders had different morphology and different oxygen content. The powder forging conditions were similar for all samples. The powders were compacted into cylindrical shapes, sintered at temperatures up to 1200˚C using induction heating and then open die forged. A summary of the tensile results is given in Table 1.8.

Table 1.8 Tensile properties of Ti and Ti6Al4V powder open die forged plates [96, 97].

Powder characteristics:	Yield strength, MPa	Maximum strength,	Elongation, %
HDH Ti, <75µm, 0.35wt% O_2	≈700	≈780	≈10
HDH Ti6Al4V,<75µm,0.83wt% O_2	no yield	≈500	no strain
GATi6Al4, <75µm, 0.27wt% O_2	≈970	≈1120	≈12

The tensile strength was clearly influenced by the oxygen content, which confirms the sensitivity of titanium to oxygen. The samples prepared with powders containing 0.83wt% oxygen had a very low strength of only 500MPa with no ductility. The samples prepared with powders containing 0.27wt% oxygen had excellent strength of 1120MPa and an elongation to fracture of 12%. Zhang et al. [97] suggested that the absence of yielding in the Ti6Al4V HDH alloy was because the inter-particle boundaries were still present and full diffusion bonding was not achieved. Jia et al. [75, 76] studied the effect of powder characteristics and sintering time on the tensile properties of impression die forged Ti and Ti6Al4V powder compacts. The aim was to produce a rocker arm part for an internal combustion engine. Table 1.9 is a summary of the mechanical properties obtained in this study [76]. The PCF samples showed significantly higher strength but lower ductility compared to ingot material due to the higher oxygen content of the starting powders. Compared with no sintering at all, using induction sintering with a 5min holding time significantly increased the ductility of a Ti HDH sample without affecting the value of UTS. The ductility of this sample is close to that of Grade 1 Ti and exceeds the ductility of a Grade 4 Ti ingot. The improved mechanical properties of the pure Ti PCF samples was attributed to the finer grain size as a result of the short 5 min induction sintering.

Table 1.9 Tensile properties of Ti and Ti6Al4V alloy rocker arm samples made by PCF, using HDH and GA powders compared to ingot material [76].

Sample	Oxygen content, %	YS, MPa	UTS, MPa	Elongation, %
As forged HDH Ti- 1	0.41	661	769	12.0
As forged HDH Ti-2	0.42	638	789	22.4
As forged GA Ti	0.12	462	563	19.5
Grade 1 Ti ingot	≤0.18	170	240	24.0
Grade 4 Ti ingot	≤0.40	480	550	15.0
As forged HDH Ti6Al4V	0.52	1161	1292	6.2
As forged GA Ti6Al4V	0.14	955	1063	9.3
Ti6Al4V ingot	0.08-0.20	800-1100	900-1200	13-16

This study also stated that the HDH powders have better response to deformation on forging compare to GA powder due to the irregular shape of the HDH powders. Irregularly shaped powder favours powder particle interlocking which reduces the effect of powder particle flow leading to increased shear stress in the powder particles which improves consolidation.

Jia et al. [75] also studied PCF of Ti6Al4V alloy powders made by BE or mechanical alloying (MA) of pure Ti and Al40V master alloy powders. It was found that complete dissolution of the Al60V40 master alloy particles was achieved after holding for 10min at 1350°C using induction heating, leading to the formation of an α/β dual phase lamellar microstructure and full densification. Samples prepared using the BE approach achieved YS of 1139MPa, UTS of 1242MPa and elongation to fracture of 4.3%. On the other hand, samples prepared by mechanical alloying had poor mechanical properties. Although no detailed explanation was provided for the low mechanical properties.

1.2.5 Powder compact extrusion of powder metallurgy Ti6Al4V alloy

Recently, research on thermomechanical processing of BE HDH Ti6Al4V by powder compact extrusion (PCE) was done by Yang et. al [98-100] and Singh et. al [101, 102] where three different pre-consolidation methods such as IS, VS and hot pressing were used prior extrusion. The effect of IS time [100], pre-

consolidation method and oxygen content [101], amount of plastic deformation [99] and post heat treatment [98] on the microstructure and mechanical properties were studied. The study on the effect of IS time at temperature of 1300°C showed that sintering time of 2 to 10min prior extrusion resulted in structures with high YS and UTS and the ductility increased with increase of the sintering time and microstructure became more homogeneous [99]. The extruded Ti6Al4V alloy with oxygen content of 0.4wt% showed YS and UTS in the range between 1200MPa and 1400MPa [98] significantly higher compared to those of the wrought alloy (Figure 1.33). The elongation to fracture is the most variable property. Reported values are between 4% and 11% and are highly dependent on the IS time, microstructure deformation ratio and post heat treatment.
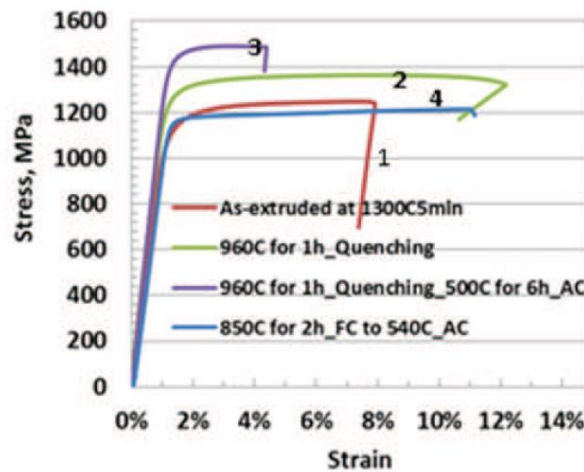
Figure 1.33 Tensile stress-strain curves of extruded powder metallurgy Ti6Al4V alloy in as-extruded and various heat treated conditions [98].

Study [101] shows that oxygen content has a strong influence on the tensile properties. Increase in oxygen from 0.32wt% to 0.5wt% led to increase of YS from 920MPa to 1070MPa and UTS from 1100MPa to 1170MPa but the elongation to fracture decreased from 11% to 2% (Figure 1.34).
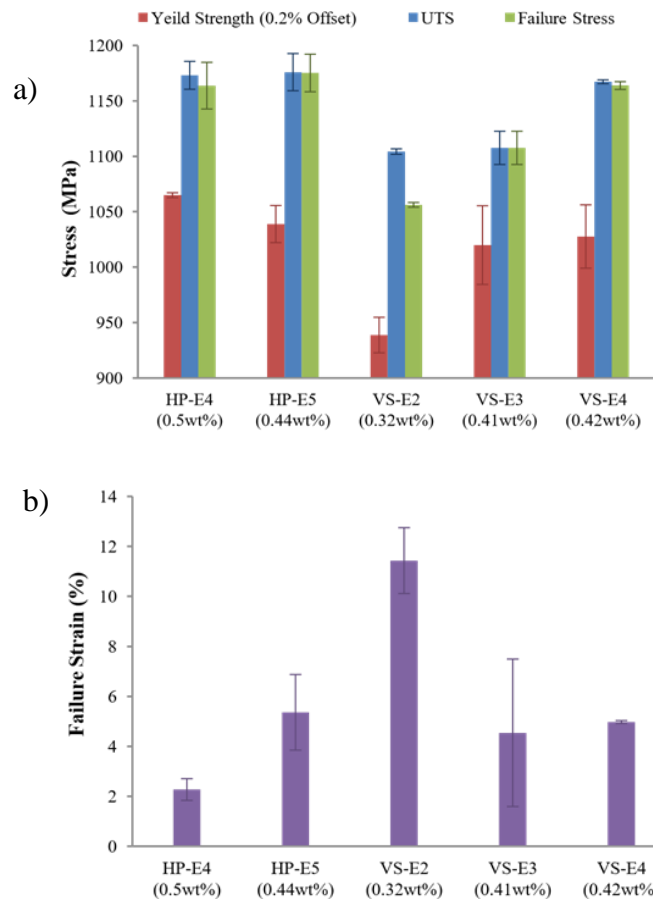
Figure 1.34 Effect of oxygen content on the a) YS and UTS and b) elongation to fracture of PM Ti6Al4V alloy made by powder compact extrusion [99].

Similarly, increase in the oxygen content leads to decreases in the fracture toughness of extruded Ti6Al4V bar [102].

In summary, TMP by powder compact forging (PCF) and powder compact extrusion (PCE) are an effective way for achieving near net-shape consolidation of metal powders and has a potential for enhanced mechanical properties compared to those in material made using ingot metallurgy and other PM technologies. The use of induction sintering instead of the traditional vacuum sintering prior to forging is a newly developed technique. It is attractive for two reasons: firstly, it is economical since it eliminates the need for reheating a sintered billet and secondly, it allows consolidation to occur after significantly shorter sintering times. The results presented to date in the literature have shown that induction sintering can achieve enhanced mechanical properties due to a finer microstructure. Processing parameters such as TMP temperature and induction sintering time play a crucial role in determining the achievable level of

40

mechanical properties. There has been only a limited amount of research on PCF using induction heating and because this processing method looks promising for economical production of titanium and titanium alloys, further extensive studies on the effect of the pre-forging parameters such as temperature and holding time on physical and mechanical properties are required.

1.2.6 Low cost powder metallurgy Ti alloys

Powder metallurgy offers a possibility of alloying with elements which are normally not possible or difficult to use in casting. A blended elemental approach in the development of new Ti alloys is very convenient since it allows metal powders to be mixed in different elemental ratios to those commercially available. Currently, the use of Ti and Ti alloys is mostly in aerospace applications and there are just a few Ti alloys which are commercially available in the market for other applications. For Ti to become more widely used, the price of the final product needs to be reduced. In aerospace applications, where the price is not a primary concern, expensive good quality GA powders are used to achieve acceptable mechanical properties. For everyday products such as family automobiles, sport and leisure products, where minimising the cost is essential, another approach needs to be used [11, 12, 103]. Current Ti research is focused on different ways of reducing production costs. There is an interest in researching new methods of powder production or modifying the existing ones, developing new powder consolidation technologies [30, 104] and developing new low cost Ti alloys [105-107]. The approaches used in the development of new low cost titanium alloys consider using low-priced Ti powders such a HDH powders; a blended elemental approach for making alloys rather than using pre-alloyed powders; substituting more expensive alloying elements with cheaper and readily available alloying elements. Recent research on Ti HDH powders has shown that with appropriate processing, powder with higher than normally acceptable levels of oxygen can give consolidated material with better than expected mechanical properties in particular YS and UTS [108].

1.2.6.1 Ti-Fe based powder metallurgy alloys

In the latest research on developing low cost alloys attention has been given to alloying Ti with elemental iron [105, 109-113]. In the casting industry Fe is not

41

commonly used as an alloying element in Ti because of the segregation of Fe during melting, due to its relatively higher density. Since powder metallurgy does not involve heating up to melting point, Fe segregation during processing is no longer an issue. A blended elemental approach gives a uniform distribution of Fe powder particles within the base Ti powders. Fe is a desirable element for alloying because is readily available and inexpensive. Fe is particularly good for alloying with Ti because it is a strong β stabilizing element [114]. Fe is also attractive because of its high diffusivity in Ti, as shown in Table 1.10 [114] and this should be favourable for improved sinterability. There are a few considerations when alloying Ti with Fe. Eutectic liquid formation should be avoided when heating over 1085˚C as indicated in the Ti-Fe phase diagram [115] because it results in formation of TiFe intermetallic compound which leads to embrittlement of the Ti-Fe based alloys. Of particular interest is also the corrosion resistance of Ti-Fe based alloys as Fe has noticeably poor corrosion resistance. However, there are no studies about the corrosion resistance of Ti-Fe based alloys available in the literature.

Table 1.10 Average diffusivity of Fe in Ti, as compared to other alloying elements, at different sintering temperatures [114].

Temperature	Al$(x10^{-13}m^2s^{-1})$	V$(x10^{-13}m^2s^{-1})$	Mo$(x10^{-13}m^2s^{-1})$	Cr$(x10^{-13}m^2s^{-1})$	Fe$(x10^{-13}m^2s^{-1})$
1250˚C	≈12.5±75	14±0.1	3.25±1.25	≈40	≈300
1020˚C	1±0.2	1.25±0.25	0.33±0.15	≈4	≈30

In the literature, four different aspects of the use of Fe as a potential alloying element for PM Ti alloys have been studied: adding Fe to an existing alloy composition to improve sinterability [107, 114, 116, 117]; replacing V with Fe in Ti6Al4V alloy for biocompatibility [106, 118, 119]; the development of Ti-Fe alloys with various amounts of pure elemental Fe powders with different size and morphologies [105, 110-113, 120, 121] and Ti-Fe alloys with small amount of other additives such as Sn, TiC etc. [120, 122-124]. The most common processing route used for developing PM Ti-Fe alloys has been by pressing and sintering. The powder mixes were blended, compacted by cold pressing and consolidated by vacuum sintering. In some cases a heat treatment was applied to modify the microstructure and mechanical properties. The main areas of study have been on

the diffusion of alloying elements, homogenisation, microstructural evolution and the effect of all of the above factors on sintered density and mechanical properties. In order for any newly developed or modified PM Ti alloys with Fe additions to be suitable candidates for industrial applications, their level of mechanical properties should be acceptable and comparable with those obtained in wrought alloys such as Ti6Al4V.

Fujita et al. [117] and Carman et al. [114] have reported that modification of standard Ti-Al-Mo-Cr and Ti-6Al4V alloy with Fe additions resulted in better sinterability and good hot workability.

Fujita et al. [117] studied the diffraction peaks, after sintering at temperatures between 700˚C and 1200˚C, from one Fe containing alloy compared to the standard Ti6Al4V. It was reported that, after sintering at 700˚C and 800˚C, diffusion of the alloying elements had not started in either of the alloys. After sintering at 900˚C the position of the α-phase peaks from Ti6Al4V corresponded to that for pure Ti, while peaks from the Ti-Fe alloy where shifted to the right and a peak corresponding to the β-phase had appeared. This means that the formation of the alloy in the sample containing Fe had already started at 900˚C. After sintering above 1000˚C and up to 1200˚C the peaks for the Fe containing alloy remained in the same position, while those for Ti6Al4V gradually shifted to the right as the sintering temperature increased. From this observation the authors concluded that the Fe containing alloy has better sinterability than Ti6Al4V (Figure 1.35).
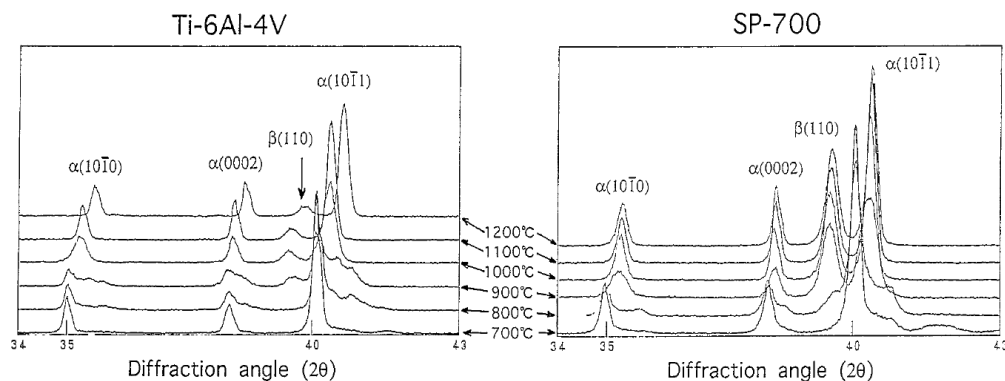
Figure 1.35 XRD profiles of Ti6Al4V and SP-700 (Ti-4.5A1-3V-2Mo-2Fe) alloys sintered at different temperatures [117].

43

Studies on the effect of replacing vanadium with iron in PM Ti alloys have been done for two reasons, to reduce the cost of the alloy and to improve its biocompatibility. Considering the latter, vanadium is toxic to human body tissue. Moreover, it has been found that replacing V with Fe improves sinterability and in some cases gives improved mechanical properties (Table 1.11) [117].

Table 1.11 Tensile properties of sintered Ti-6A1-4V and SP-700 (Ti-4.5Al-3V-2Fe-2Mo) [117].

Alloy	Titanium powder	Relative density, %	YS, MPa	UTS, MPa	Elongation, %
Ti-4.5Al-3V-2Fe-2Mo	GA	99.8	922	1010	20
		98.5	902	1000	8
	HDH	99.6	890	998	20
		98.5	902	1000	14
Ti-6Al-4V	GA	99.6	843	941	18
		97.5	804	912	8
	HDH	99.6	809	926	19
		97.7	833	954	12

Siqueira et al. [119] have researched the microstructural evolution of vacuum sintered Ti-5Al-2.5Fe alloy, which was developed to replace Ti6Al4V alloy because V toxicity. Two approaches were used to make the alloy: by using elemental Fe and Al powders or an intermetallic Al/Fe compound. When elemental Fe and Al powders were used, the dissolution of Fe particles started at temperatures close to 900°C (Figure 1.36 a).
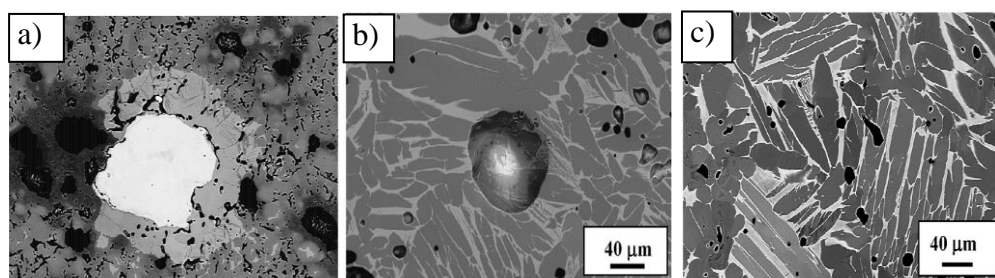
Figure 1.36 Microstructure of BE Ti-5Al-2.5Fe alloy vacuum sintered at a) 900°C, b) 1200°C) using elemental powders, and c) 1200°C using Al-Fe master alloy powders [119].

With increasing sintering temperature, the dissolution of Fe particles continued with consequential formation of the two-phase (α+β) structure. Fe particles were fully dissolved after sintering at 1200°C for 2h and the microstructure became

plate-like α outlined by β. Large Kirkendall pores were observed in the microstructure as a result of the fast diffusion of Fe towards the Ti matrix (Fig. 1.36 b). When Al-Fe master alloy powders were used the dissolution started at 900°C and was complete between 1000˚C and 1100˚C. A Widmanstätten α+β structure was predominant at 1200˚ (Figure 1.36c), with finer α platelets and much smaller pores. A new α-β alloy Ti-6Al-1.7Fe-0.1Si (Ti-62S) was developed by Hagiwara et al. to replace Ti-6Al4V alloy for use in automobile parts [106]. Ti HDH powder was blended with Al-14Fe-0.83Si-35Ti master alloy powder in an appropriate ratio, vacuum sintered, followed by heat treatment and hot isostatic pressing (HIP). For comparison, similar processing was done for PM Ti-6Al-4V alloy. The newly developed Ti-62S alloy showed much higher YS of 1117MPa and UTS of 1156MPa compared to 862MPa and 951MPa for Ti-6Al-4V. Nevertheless, the 8% elongation for the Ti-62S alloy was lower than 15% typically found in Ti-6Al-4V.

Another approach to alloying Ti with iron is to use pure Fe without any other alloying additions. This is purely an attempt to make a low cost Ti alloy. In 2008 the work performed by Esteban et al. [105] attracted the attention of the Metal Powder Report journal which published an article "Low- cost Ti alloys? Iron may hold the answer". Esteban et al. also published an article about the properties of a low cost alloy Ti-7Fe [110], incorporating Ti HDH powder. Two types of pure iron powders with different powder particle sizes and two types of master alloy (316 stainless steel and Fe-25Ti) powders were used. The consolidation was done in two steps: cold pressing followed by vacuum sintering at temperatures between 900˚C and 1400˚C. The summarised results of this study are shown in Figure 1.37 and Figure 1.38. The maximum density was in the sample alloyed with carbonyl iron and attributed to the larger specific surface area of the carbonyl powder particles (smaller powder particle size) causing more diffusion before reaching the eutectic temperature. On the other hand, the alloy made with the larger powder particle size (below 100micron) contained larger pores, a lower sintered density and a liquid phase formed during heating at temperatures above the eutectic transformation temperature. The alloy made with carbonyl iron had the highest tensile strength and elongation to fracture (Figure 1.38)
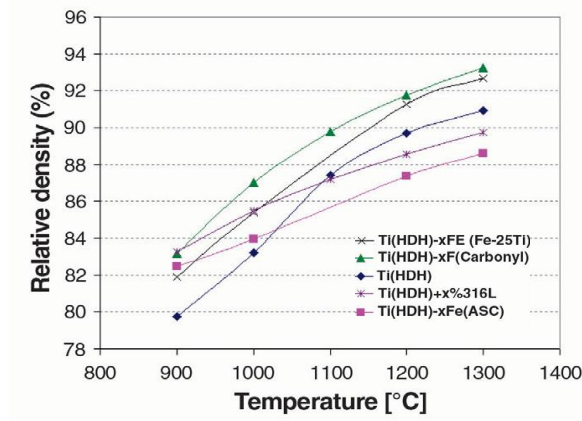
Figure 1.37 Relative sintered density of Ti and Ti-Fe based alloys using different sintering temperatures [105].
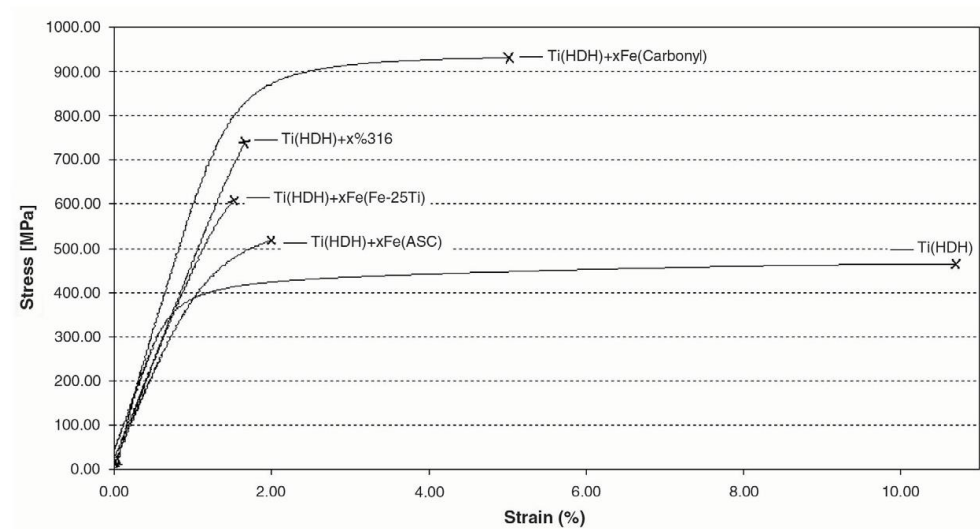
Figure 1.38 Examples of stress-strain curves of pure Ti and Ti-Fe based alloys [105].

Esteban et al. [111] published further research on the influence of the Fe content and powder particle size on the mechanical properties of Ti-xFe based alloys. The powder particle size of the powders used in this study is given in Table 1.12.

Table 1.12 Characteristics of the starting powders of Ti-xFe alloys [111].

	Powders	Oxygen content, wt%	Nitrogen content, wt%	Purity, %	Mean particle size, μm
Ti-base powder	Ti HDH	0.343	0.098	99.6	48
Fe additions	Fe ASC10029	0.094	0.003	99.9	38
	Fe carbonyl	0.244	0.007	99.5	3

46

Alloys with two different types of Fe powders and four different iron contents were made by blending followed by cold pressing and vacuum sintering at three different temperatures 1100˚C, 1200˚C and 1300˚C. The results for the sintered density and tensile properties are shown in Figure 1.39 and Figure 1.40 respectively.
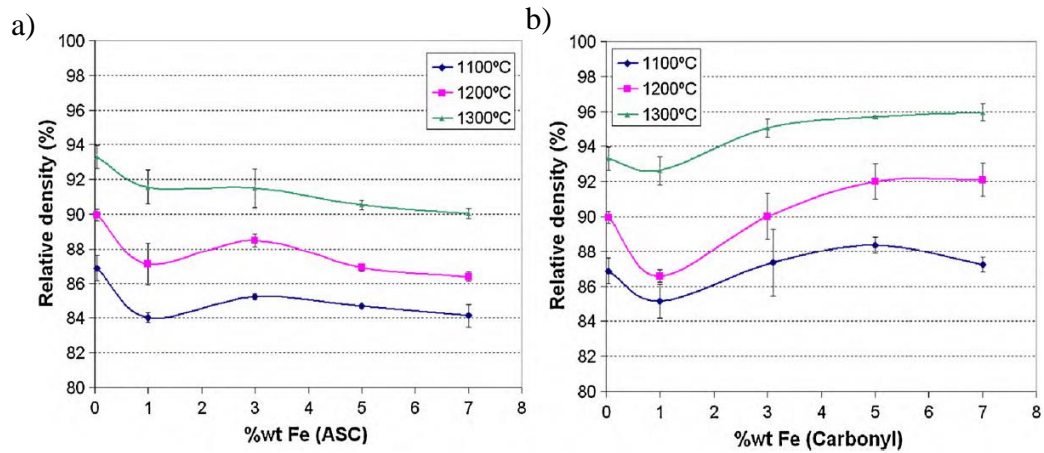
Figure 1.39 Relative density of Ti-xFe alloy samples sintered at different temperatures: a) samples made with Fe (ASC) powders and b) with Fe (Carbonyl) powders [111].
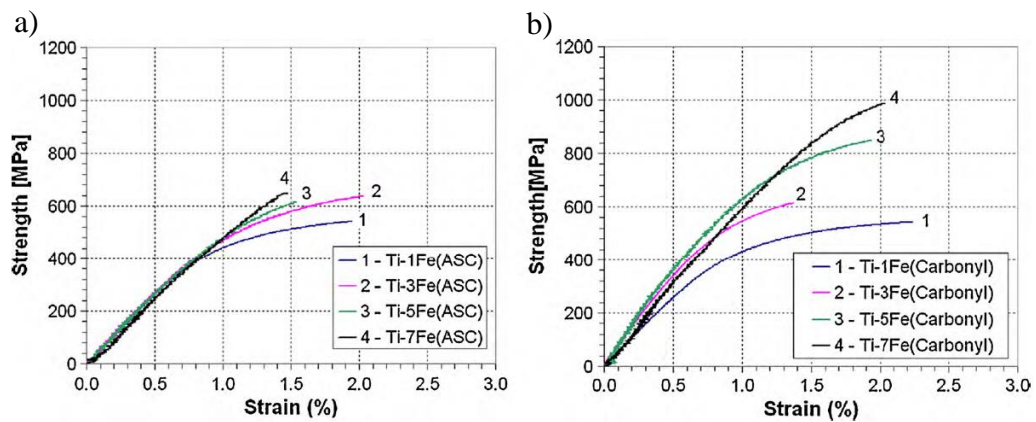
Figure 1.40 Engineering stress-strain curves of selected Ti-xFe vacuum sintered samples: a) samples made with Fe (ASC) powders and b) with Fe (Carbonyl) powders [111].

The major finding from this study was that the sinterability depends on the type of Fe powders used, in particular their particle size, which in this study was the most significant variable (Table 1.12). In all cases the density increased with increased sintering temperature (Figure 1.39). The influence of the Fe content on the sinterability varies with the powders used. Increased Fe content, when using ASC

powder, led to lower sintered density values. This result was related to the relatively larger Fe particles, which left larger pores due to faster diffusion. The larger pores were not able to close during sintering [110]. Fe atoms diffuse much faster into Ti particles than Ti atoms into Fe particles. The diffusion coefficient of Fe is more than two orders of magnitude higher than that of Ti [112]. In contrast when finer carbonyl iron powders were used, the relative density increased with increasing iron content (Figure 1.39 b). The mechanical properties were also found to be dependant of the type of powder used, especially for those alloys with a higher Fe concentration (Figure 1.40).

Wei et al. [121] had similar results when fine spherical iron particles (below 20 microns) were used. They studied the expansion- contraction behaviour of pure Ti and Ti-5Fe powder compacts during heating. From the results of this study (Figure 1.41), it was concluded that densification was initiated of 950°C.

a)

b)
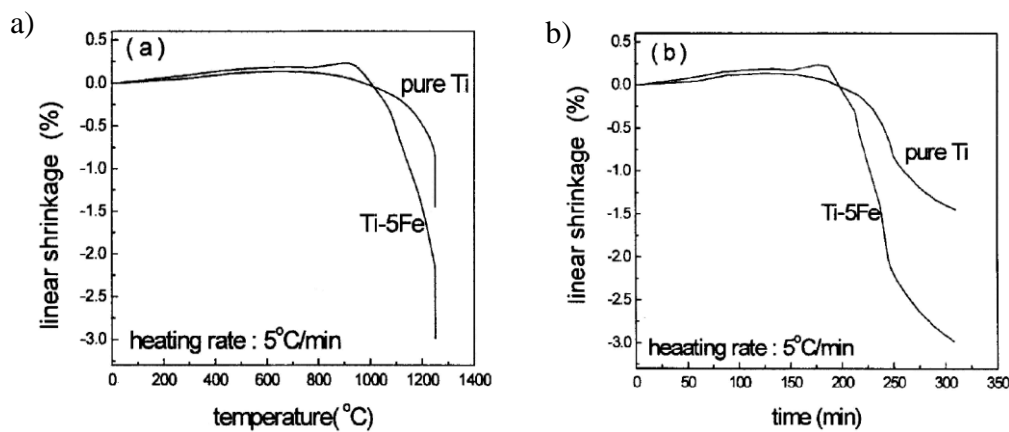
Figure 1.41 Expansion- contraction behaviour of a) pure Ti and b) Ti-5Fe compact heated to 1250°C and held for 60 min [121].

From 950°C to 1080°C, below the first eutectic temperature (1085°C), iron quickly diffuses into the Ti matrix. The formation and growth of sintering necks also starts in this temperature range. Above 1080°C, diffusion, homogenisation and densification took place in the single β-phase. Most of the sintering shrinkage was achieved between 950°C and 1250°C and the mean shrinkage rate of Ti-5Fe was about three times that of pure Ti.

O'Flynn and Corbin [113] tried to solve the porosity problem associated with sintering Ti-Fe alloys. The pore formation is a result of either the fast solid state diffusion of Fe below the eutectic point, or the formation of an Fe rich liquid

48

phase above 1085°C. Similar to Esteban et al. [111], the effect of the Fe powder particle size on pore formation, densification and homogenisation was studied. This study pointed to a possible solution for preventing melting and the exothermic reaction at the eutectic point by introducing a soak or hold period to the sintering profile below the eutectic temperature. Figure 1.42 shows the DSC curves of different holding times at 1050°C.
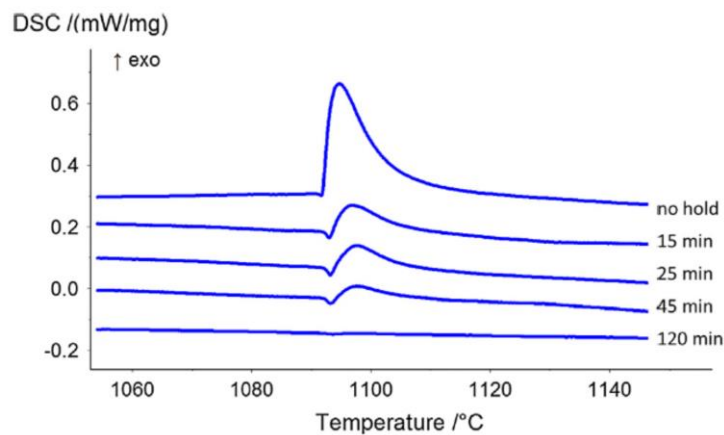
Figure 1.42 Comparison of exothermic peaks measured by DSC after sintering of Ti-2.5Fe alloy at 1050°C with different holding times [113].

The sequence of the curves shows that with increasing holding time the reaction peak slowly decreases and completely disappears after holding for 2h. This means that, during the holding time the iron particles slowly disappeared, without forming a liquid phase at the eutectic temperature. However, the holding time did not eliminate the pores in the samples prepared with coarse Fe powders. When fine Fe particles were used the porosity appearance and the pore size were much improved and a DSC study showed that there was no exothermic peak at the eutectic temperature.

In addition to densification, it is also important to achieve a uniform distribution or homogenisation of the alloying elements during the sintering process. This insures a uniform microstructure and optimum mechanical properties. O'Flynn and Corbin [113] indicated that the use of fine Fe particles results in a more uniform microstructure when similar sintering conditions were used (Figure 1.43). No large scale, isolated regions of retained β were found. These two microstructures show features of homogenised Ti-Fe alloy compositions.
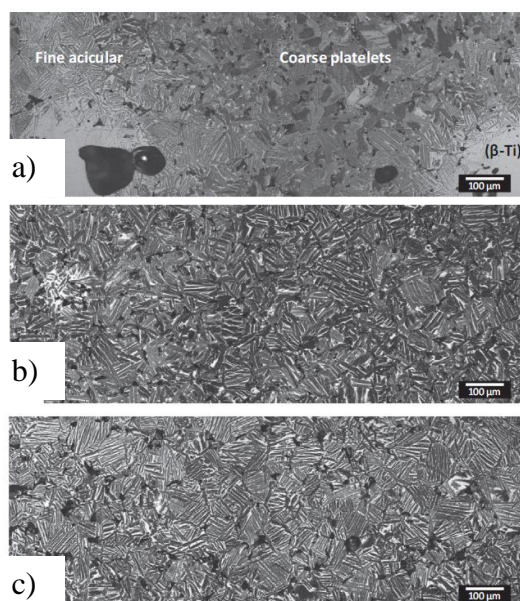
Figure 1.43 Microstructure of Ti-2.5Fe DSC samples heated to 1200˚C and cooled with 20˚C/min with a) coarse, b) medium and c) fine Fe particles [113].

A further study on homogenisation [113] showed that with enough holding time at the sintering temperature the homogenisation in all samples was complete. For the coarse Fe powders 30 to 60 min at 1200˚C was necessary to complete homogenisation while for the finer Fe powders the homogenisation was complete during the heat up to 1200°C without a need for holding at the sintering temperature.

Bor-Yuan et al. [125] studied the effect of cooling rate after sintering on the microstructure and mechanical properties of Ti-Fe alloys with various Fe compositions. The study suggested two cooling profiles after sintering Ti-7Fe at 1150˚C for 2h, for good tensile properties comparable to those of wrought Ti6Al4V alloy (Table 1.13).

Table 1.13 Tensile properties of PM Ti-7Fe alloy as result of different cooling processes after sintering [125].

Cooling condition	A	D	E	F
Tensile strength, MPa	916 ± 21	976 ± 24	818 ± 27	825 ± 25
Elongation, %	13 ± 2	12 ± 2	12 ± 2	13 ± 1
Hardness, HRC	27 ± 1	31 ± 1	25 ± 1	23 ± 2

Note: A-furnace cooling + fan cooling; D- furnace cooling to 740˚C + 24h hold+ fan cooling; E- furnace cooling to 640˚C + 24h hold+ fan cooling; F- furnace cooling to 540C + 24h hold+ fan cooling.

Using furnace cooling followed by fan cooling led to a tensile strength of 916MPa and 13% elongation. With isothermal holding at 740˚C for 24h prior to fan cooling the tensile strength increased further to 976MPa while the elongation decreased only slightly to 12%. The authors studied the effect of 4 cooling rates on the amount of the retained β phase (Figure 1.44). The results suggested that to obtain more β phase and consequently better mechanical properties, isothermal holding in the α+β region near the β transus is preferred.

Process	α (vol.%)	β (vol.%)
(a) Process A	72	28
(b) Process D	35	65
(c) Process E	65	35
(d) Process F	77	23
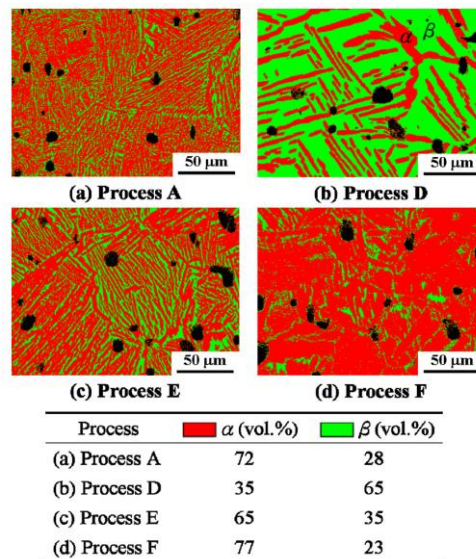
Figure 1.44 EBSD phase mapping showing α and β phase distribution in sintered and subsequently cooled with different rates Ti-7Fe alloy [125].

Bor-Yuan et al. also studied the effect of different Fe additions on tensile properties (Figure 1.45).
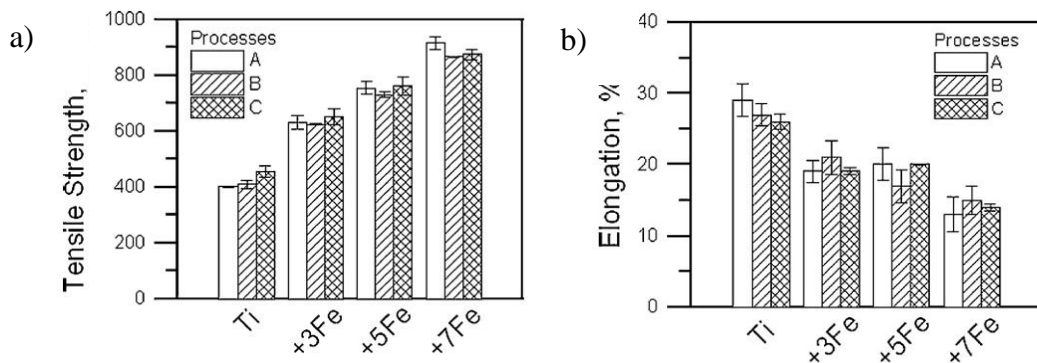
Figure 1.45 Tensile properties of Ti-Fe alloys with various Fe compositions sintered using different cooling rates a) tensile strength and b) elongation to break [125].

As the amount of Fe increased, the tensile strength increased due to a larger solid solution strengthening effect of Fe and the fine lamellar structure achieved as a result. The elongation decreased with increasing Fe content.

Studies of Ti-Fe based alloys were taken further by adding small amounts of other elements or compounds to improve the alloy performance. TiC has been added to Ti-7Fe PM alloy, to improve the mechanical properties [126]. In another study Si was added to Ti-xFe alloy compositions, to improve the mechanical properties and oxidation resistance [37]. Sn was added to Ti-Fe powder alloy in an attempt to develop an ultra-fine eutectic heterogeneous composite to enhance the mechanical properties [124].

Overall, in recent years an interest in the PM of Ti-Fe based alloys has been an area of research for achieving a low cost replacement for Ti6Al4V alloy mainly for biomedical applications. The research has mostly investigated consolidation by cold pressing followed by vacuum sintering. The main conclusions which can be drawn are: (a) in powder metallurgy Fe can be used for alloying with Ti. The diffusion coefficient of Fe in Ti is more than twice that of Ti in Fe, which has a positive effect on the sinterability. However, this can also lead to large pores in vacuum sintered microstructures. To avoid this, attention should be given to selecting the right powder size and using an appropriate sintering profile; (b) if Fe is not fully diffused in the Ti matrix before reaching the eutectic reaction temperature, a liquid TiFe phase can be formed; (c) homogenisation and formation of a fine $\alpha+\beta$ platelet microstructure, with large amounts of retained β is desirable for good mechanical properties, which are comparable to those found in wrought Ti6Al4V alloy.

However, there is almost no research done on the consolidation of Ti-Fe PM alloys using induction sintering, powder compact forging or powder compact extrusion. Results from previous work reported in the literature on vacuum sintering of Ti-Fe alloys will contribute to the research aims of this thesis.

1.2.6.2 Ti3Al2V powder metallurgy alloy

Ti3Al2V alloy is a near α or super α titanium alloy, with intermediate strength between those of pure Ti and Ti6A4V alloy. The wrought Ti3Al2V alloy was originally designed to be used in hydraulic and fuel structures in conventional

aeroplanes [40]. Recently it has been considered in applications for biomedical and dental implants [127]. This alloy has also been considered for manufacturing connecting rods in sport cars [128]. The advantage of Ti3Al2V against Ti6Al4V derives from its improved machinability [128]. Figure 1.46 shows the influence of the aluminium content on the carbide tool life during turning. The carbide tool life when machining Ti3Al2V is three times longer compared to that of Ti6Al4V [128]. The same rule applies for the machining speed.
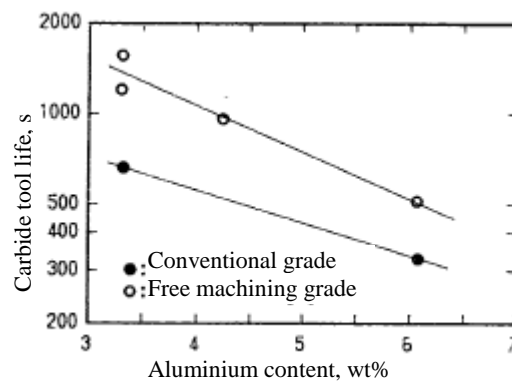
Figure 1.46 Influence of aluminium content on the carbide tool life when turning Ti alloys [128] .

An addition of rare earth elements such as Ru to Ti3Al2V has been investigated for use in the energy industry [129].

However, in general there is little reported work on the powder metallurgy of Ti3Al2V. Bolzoni et al. extensively studied the consolidation of blended elemental Ti3Al2.5V alloy powders by a press and sinter method [130] and vacuum hot pressing [127]. Two ways of obtaining the alloy composition were considered: by mixing pure HDH Ti powders with 60Al40V master alloy powder (referred to by the authors as Ti32-MA method) or mixing HDH Ti6Al4V powders with pure Ti HDH powders (referred to as the Ti32-BE method). The influence of processing parameters on the microstructure, porosity, mechanical properties such as hardness and flexural strength, the oxygen pickup during processing were studied. A comparison of the properties achieved with those found in conventional Ti wrought alloys was also done. Figure 1.47 shows values of the relative density of mechanically alloyed Ti3Al2V-MA and blended elemental Ti3Al2V-BE samples as a function of the sintering conditions.

53
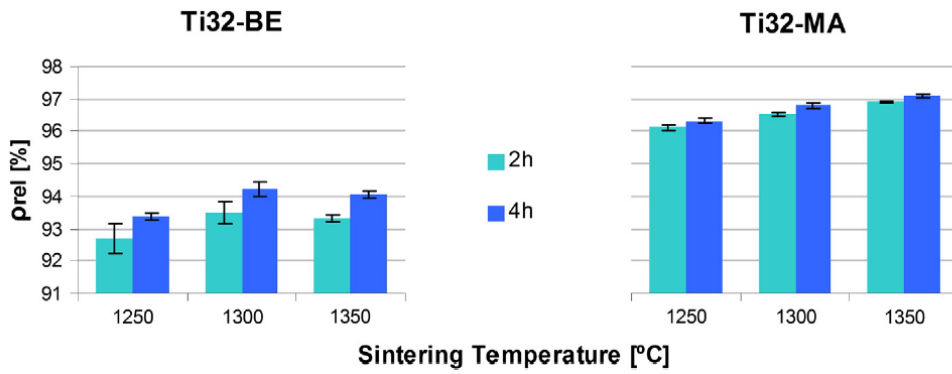
Figure 1.47 Relative density of Ti3Al2V-BE and Ti3Al2V-MA sintered samples as a function of the sintering conditions [130].

The Ti3Al2V-MA samples achieved a much higher sintered density. This is because the starting green densities were 69.0% for the BE powders and 86.6% for the MA powders. This shows the importance of the initial density of the powder compact. Both the increment of sintering temperature and the dwell time led to an increase in the relative sintered density. Because of the slow cooling from temperatures above the β transus, in all cases the microstructure consisted of α grains and α+β lamellae (Figure 1.48) [130].
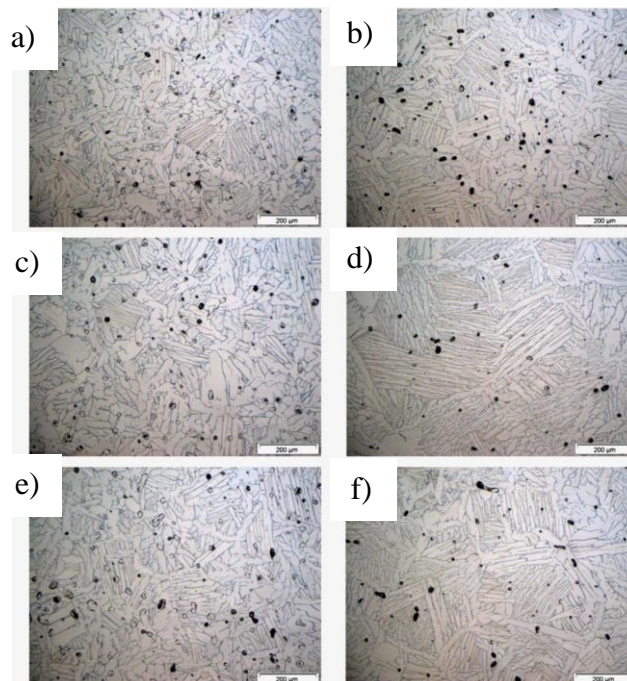
Figure 1.48 Micrographs of Ti3Al2V samples sintered at a) and b) 1250°C for 2h, c) and d) 1350°C for 2h and e) and f) 1250°C for 4h accordingly for alloys made by BE or MA [130].

54

The α-phase lamellae grew with increasing temperature and holding time. This behaviour was more pronounced after longer sintering times. The Ti3Al2V-MA lamellae appeared to be finer, which according to the authors is because of the combined effect of the originally finer Ti3Al2V-BE powders and the greater amount of thermal energy used to homogenise the alloying elements for the Ti3Al2V-MA samples. EDS studies showed a homogeneous distribution of alloying elements and no undissolved alloying element particles after all the temperature-time sintering conditions used. The oxygen pick up was on average up to 0.02wt% for both BE and MA alloys sintered at 1250˚C independently of holding times. Increased oxygen pick up of up to 0.09wt% was observed with increase of the sintering temperature to 1350˚C for both sintering times. Mechanical properties such as hardness and flexural strength were found to be highly dependent of the processing parameters. Hardness increased with temperature and time and reached values similar or higher than that for wrought Ti3Al2V alloy. Flexural stress increased with higher sintering temperature and holding time as a result of the higher sintered density. Conversely higher sintering temperature and dwell time resulted in lower flexural strain, caused by a coarser microstructure and increased amounts of contamination pick up [130].

In a study of vacuum hot pressing of Ti3Al2V-BE and Ti3Al2V-MA, sintering temperatures of 900˚C, 1100˚C and 1300˚C and a dwell time of 30min or 60 min were much lower than those used in the previous study [120]. The parameters used led to no oxygen pick up, except for the Ti3Al2V-MA sample heated to 1300˚C. The relative sintered densities were higher than those achieved by press and sinter. The hot press temperature of 900°C, which is below the β-phase transus, produced a porous and inhomogeneous microstructure with undissolved alloying elements still present in the microstructure. Increasing the hot pressing temperature to 1100˚C improved the appearance of the microstructure which was denser and composed of α grains and α-β lamellae. The lamellae were finer for Ti3Al2V-MA and more concentrated in the areas where the former master alloy particles were. The authors indicated that the samples hot pressed at 1300˚C exhibited a lamellar microstructure typical of a slow cooled wrought Ti3Al2V alloy. The hardness of the hot pressed samples was similar to that of the vacuum sintered samples in the previous study. The hardness and the maximum bending strength of the Ti3Al2V-BE samples were higher compared with those found in

the Ti3Al2V-MA samples. Contrary to the results from press and sinter, using PA Ti6Al4V powder for alloying results in enhanced mechanical properties.

To conclude, the PM Ti3Al2V alloy is not extensively used commercially yet and only a limited amount of research has been done on the powder metallurgy of Ti3Al2V alloy. However, preliminary results indicate that this alloy is promising as a pathway towards a cost effective Ti alloy for applications where slightly lower strength compared with that obtainable in Ti6Al4V is required. Consolidation of BE Ti3Al2V alloy powders by pressing and sintering and hot vacuum pressing have been studied. The processing parameters, such as a temperature over 1300°C, are required to produce dense and homogenous microstructures similar to those found in wrought Ti3Al2V alloy. To date there is only limited data available for flexural strength and hardness and little published data for tensile strength. The research presented in this thesis is an investigation which tests the hypothesis that consolidation of the alloy composition Ti3Al2V by other PM methods such as IS, PCF and PCE is feasible and produces material with acceptable tensile properties.

1.3 Objectives and Hypothesis

1.3.1 An overview of the Literature Review

From the literature review is clear that Ti and its alloys are desirable materials to use in many engineering applications including components and devices used in everyday life. A large constraint preventing a more widespread use of titanium alloys is the high production and manufacturing cost. It is evident from the literature that the application of powder metallurgy for Ti processing points to a way of achieving materials saving and a reduction in cost. Looking at the cost reduction aspects of using powder metallurgy the following observations from this literature review can be made:

(1) In current Ti powder metallurgy processing, vacuum sintering is still the most popular technology used for single step consolidation or in combination with subsequent thermomechanical processing. There are some disadvantages to consolidation using vacuum sintering. The relatively long sintering time results in a coarse microstructure, which adversely affects mechanical properties. To prevent this, addition of microstructural refining elements might be used, which

would further increase processing costs and might also affect mechanical properties, especially ductility. As an alternative to vacuum sintering there are reports in the literature of consolidation using induction sintering (IS). Although reported results for IS look promising, there is only a limited amount of available data, especially on the use of IS in Ti powder metallurgy.

(2) This literature review leads to the conclusion that thermomechanical processing (TMP) of Ti and Ti alloys is an effective way of achieving full consolidation and acceptable strength and ductility. The currently used processing method is prolonged because of a requirement for pre-consolidation of powder compacts using separate and lengthy vacuum sintering. After vacuum sintering, a further reheating of the sintered billet is required before further processing. To increase the efficiency and reduce the cost, a new initial powder consolidation technique is required before the thermomechanical processing.

(3) One of the major aspects of the current research is related to cost reductions in Ti alloy processing using powder metallurgy. Of particular interest is a reduction in the cost of producing PM Ti6Al4V alloy, which is the most popular titanium alloy used in the wrought form and for powder metallurgy processing. In recently published research, an attempt has been made to reduce the cost of PM Ti6Al4V alloy by using HDH Ti powders. Although HDH Ti powders have many advantages such as relatively low cost and irregularly shaped powder particles, they also have high oxygen content. The high oxygen content affects the mechanical properties causing increased yield and tensile strength by up to 300MPa, compared with values in the ASTM standard. Oxygen also lowers ductility, in most cases to values well below ASTM requirements. There are also issues with the hot workability of high oxygen Ti6Al4V alloy because oxygen is an α-phase stabilizer.

1.3.2 Hypothesis

Based on the findings from the literature review, the hypothesis to be tested in this thesis is as follows:

The cost of Ti and Ti alloy processing, whilst retaining fit-for-purpose mechanical properties, can be reduced by using cheaper, higher oxygen content HDH Ti and Ti alloy powders to include induction sintering for powder pre-consolidation, thermo-mechanical processing and the development of alternative cheaper alloys.

1.3.3 Objectives

In order to test the hypothesis, the following investigations will be carried out to examine the feasibility of achieving economic PM processing of Ti and Ti alloys with fit for purpose mechanical properties:

(1) A study on an alternative technology for sintering which uses induction heating to significantly reduce sintering time and consequently refine the microstructure and improve the mechanical properties.

(2) Employment of IS in combination with thermomechanical processing by powder compact open die forging (ODF) and powder compact extrusion (PCE) with the aim of shortening the processing time by eliminating both vacuum sintering and the need for reheating. Short time IS will be followed by direct forging or extrusion.

(3) The development of cost effective PM Ti alloys by:

 a) Using Ti HDH powders to develop low cost alloys with properties similar to or approaching those found in wrought Ti6Al4V alloy.

 b) Investigating the processing and the structure and properties of three alloy compositions: Ti3Al2V, Ti5Fe and Ti5SS (Ti3Fe1Cr0.6Ni0.2Mo).

 c) Employing IS as a single consolidation method or in combination with TMP by forging or extrusion for making these alloys.

1.3.4 The approach

(1) Since studies on IS of Ti and Ti alloys have received little attention in the literature, this research program will begin with an extensive investigation of (a) the effect of the initial green density of a powder compact on the level of consolidation and tensile properties and; (b) the effect of IS temperature and holding time on sintered density, porosity distribution and tensile properties of Ti HDH powders and pre-alloyed Ti6Al4V HDH powders. Later in this work IS will be used together with a blended elemental approach to make Ti alloys.

(2) A single step IS followed by direct forging will be used for consolidation of pre-alloyed Ti6Al4V HDH powders with high oxygen content. Since the success of powder forging is related to the pre-consolidation properties of a powder compact and the forging temperature, the effect of IS temperature and

time on microstructure and mechanical properties will be an area of research interest.

(3) To achieve reduced cost, the Ti alloys to be studied will be made using HDH Ti powder with a maximum of 5wt% of alloying elements. A blended elemental (BE) approach will be used to manufacture the alloys using cheap and readily available Fe and Fe master alloy powders. Five alloy compositions will be studied and their response to sintering and thermomechanical processing compared. The alloy compositions will be Ti6Al4V, Ti3Al2V, two Ti5Fe compositions with different Fe powder characteristics and a Ti5SS (Stainless Steel) alloy. To provide a better understanding of the effect of sintering conditions on microstructure and tensile properties, a comparison will be made between the respective effectiveness of IS and VS when used for pre-consolidation before TMP. Optimised processing conditions deriving from previous research work will be used to achieve the best possible consolidation and mechanical properties.

(4) Investigate the effect of heat treatment of the forged and extruded alloys on the microstructure and tensile properties.

References

1. White, D.G., *Powder Metal Technologies and Applications*, in *ASM Hand Book Vol.7*. 1998, ASM International. p. 10-23.

2. German, R.M., *Introduction*, in *Powder Matallurgy & Particulate Materials Processing*. 2005, Metal Powder Industies Federation. p. 1-9.

3. Sanderow, H.I., *Powder Metallurgy Methods and Design*, in *ASM Handbook Vol.7*. 1998, ASM International. p. 32-34.

4. Froes, S.H., *Advances in Powder Metallurgy Applications*, in *ASM Metals Handbook Vol.7*. 1998, ASM International. p. 43-63.

5. Titanium Metals Corporation. *Corrosion resistance of Titanium*. 2011 11/12/15 11/12/15]; Available from: http://www.parrinst.com/wp-content/uploads/downloads/2011/07/Parr_Titanium-Corrosion-Info.pdf.

6. Hanson, B., *Titanium- corrosion and erosion resistance*, in *The Selection and Use of Titanium: A Design Guide*. 1995, Institute of materials,. p. 645-646.

7. Lalik, S., J. Cebulski, and R. Michalik, *Corrosion resistance of titanium in water solution of hydrochloric acid.* International Scientific Journal, 2007. **28**(6): p. 349-352.

8. Peters, M., et al., *Titanium Alloys for Aerospace Applications*, in *Titanium and Titanium Alloys: Fundamentals and Applications*. 2003, John Wiley & Sons. p. 333-350.

9. Froes, F.H., *Current and emerging opportunities in titanium expanding market.* JOM, 2007. **59**(6): p. 27-30.

10. Boyer, R.R., *An overview on the use of titanium in the aerospace industry.* Materials Science and Engineering: A, 1996. **213**(1–2): p. 103-114.

11. Faller, K. and F.H. Froes, *The use of titanium in family automobiles: Current trends.* JOM, 2001. **53**(4): p. 27-29.

12. Froes, F.H., et al., *Titanium in the family automobile: the cost challenge.* JOM, 2004. **56**(2): p. 40-44.

13. Sachdev, A.K., et al., *Titanium for Automotive Applications: Challenges and Opportunities in Materials and Processing.* JOM, 2012. **64**(5): p. 553-565.

14. Jackson, M.J. and W. Ahmed, *Titanium and Titanium Alloy Applications in Medicine*, in *Surface Engineering Surgical Tools and Medical Devices*, M.J. Jackson, Ahmed, W, Editor. 2007, Springer US. p. 533-576.

15. The Titanium Information Group. *Titanium Alloys in Medical Applications*. 2013 11/12/15]; Available from: http://www.azom.com/article.aspx?ArticleID=1794.

16. Wang, K., *The use of titanium for medical applications in the USA.* Materials Science and Engineering: A, 1996. **213**(1–2): p. 134-137.

17. Rack, H.J. and J.I. Qazi, *Titanium alloys for biomedical applications.* Materials Science and Engineering: C, 2006. **26**(8): p. 1269-1277.

18. Donachie, M.J., *Introduction to selection of Ti alloys*, in *Titanium : A Technical Guide* 2000, ASM International: Materials Park, OH, USA. p. 5-15.

19. Polmear, I.J., *Titanium alloys*, in *Light alloys: metallurgy of the light metals*. 1995, John Wiley & Sons. p. 249-254.

20. Gillbert, R. and R. Shannon, *Heat treating of Titanium and Titanium alloys*, in *ASM Metals Handbook Vol.4*. 1998, ASM International. p. 2043-2060.

21. Pinke, P., M. Reger, and T. Kovacs, *Heat Treatment of the casted Ti6Al4V titanium alloy*, in *12th International Scientific Conference, Bratislava 2004*. 2004. p. 1042-1046.

22. Jovanović, M.T., et al., *The effect of annealing temperatures and cooling rates on microstructure and mechanical properties of investment cast Ti–6Al–4V alloy.* Materials & Design, 2006. **27**(3): p. 192-199.

23. Gil, F.J., et al., *Formation of α-Widmanstätten structure: effects of grain size and cooling rate on the Widmanstätten morphologies and on the mechanical properties in Ti6Al4V alloy.* Journal of Alloys and Compounds, 2001. **329**(1–2): p. 142-152.

24. Lütjering, G., *Influence of processing on microstructure and mechanical properties of (α+β) titanium alloys.* Materials Science and Engineering: A, 1998. **243**(1–2): p. 32-45.

25. Reda, R., A. Nofal, and A. Hussein, *Effect of quinching temperature on the mechanical properties of cast Ti-6Al-4V alloy.* Journal of Metallurgical Engineering (ME) Volume 2 Issue 1, January 2013, 2013. **2**(1): p. 48-54.

26. Žitňanský, M. and L. Čaplovič, *Effect of the thermomechanical treatment on the structure of titanium alloy Ti6Al4V.* Journal of Materials Processing Technology, 2004. **157–158**: p. 643-649.

27. Ding, R., Z.X. Guo, and A. Wilson, *Microstructural evolution of a Ti–6Al–4V alloy during thermomechanical processing.* Materials Science and Engineering: A, 2002. **327**(2): p. 233-245.

28. Filip, R., et al., *The effect of microstructure on the mechanical properties of two-phase titanium alloys.* Journal of Materials Processing Technology, 2003. **133**(1–2): p. 84-89.

29. Froes, F.H., *Titanium Powder Metallurgy: A Review- Part 1.* Advanced Materials and Processes, 2012. **170**(9): p. 16-22.

30. Froes, F.H., *Innovations in titanium technology.* Materials Technology, 2007. **22**(2): p. 101-104.

31. Gungor, M.N., I.M. Ashraf, and F.H. Froes, *Innovations in Titanium Technology: Preface*. TMS Annual Meeting, 2007: p. 9-11.

32. Froes, F. and D. Eylon, *Titanium powder metallurgy- a review*, in *Titanium-net shape technologies*. 1984, The metallurgical society of AIME: Los Angeles, California. p. 1-20.

33. Neikov, O.D., et al., *Production of Ti and Ti Alloy powders*, in *Handbook of none-ferrous metal powders Technologies and Applications*. 2009, Elsevier B.V. p. 314- 323.

34. Antony, L.V. and R.G. Reddy, *Process for production of high purity metal powders*. JOM, 2003. **March 2003**: p. 14-18.

35. Kelto, C., et al., *Titanium powder metallurgy -a perspective*. Journal of Metals, 1980. **32**(8): p. 1-17.

36. Roberts, P.R. and P. Loewenstein, *Titanium alloy powders made by rotating electrode process*. Highway Engineer, 1980(1980): p. 21-35.

37. Laughlin, J., L. Dooley, and J. George, *The hydride process for producing titanium alloy powders*. Highway Engineer, 1980(1980): p. 37-46.

38. Froes, F.H., *Titanium Powder Metallurgy: A Review- Part 2*. Advanced Materials and Processes, 2012. **170**(10): p. 26-29.

39. Andersen, P.J. and P.C. Eloff, *Development of higher performance blended elemental powder metallurgy of Ti alloys*. Highway Engineer, 1980(1980): p. 175-187.

40. Lampan, G., *Wrought titanium and titanium alloys*, in *ASM Matals Handbook Vol.2*. 1990, ASM International. p. 1782-1886.

41. Anokhin, V.M., O.M. Ivasishin, and A.N. Petrunko, *Structure and properties of sintered titanium alloyed with aluminium, molybdenum and oxygen*. Materials Science & Engineering A, 1998. **243**(1-2): p. 269-272.

42. Guden, M., et al., *Compression testing of a sintered Ti6Al4V powder compact for biomedical applications*. Materials Characterization, 2005. **54**(4–5): p. 399-408.

43. Qian, M., *Cold compaction and sintering of titanium and its alloys for near-net-shape or preform fabrication*. International Journal of Powder Metallurgy, 2010. **46**(5): p. 29-44.

44. Robertson, I.M. and G.B. Schaffer, *Review of densification of titanium based powder system in press and sinter processing*. Powder Metallurgy, 2010. **53**(2): p. 146-162.

45. Bosman, H.L. and D.C. Blaine, *Influence of powder particle size destribution on the properties of press and sinter titanium and Ti-6Al-4V preforms*, in *Light Metals conference 2014*. 2014: South Africa. p. 225-230.

46. Eylon, D., et al., *Ftigue crack initiation of titanium alloy powder compact.* Highway Engineer, 1980(1980): p. 93-102.

47. Abouelmagd, G., et al., *Mechanical properties of a TiAL6V4 alloy processed by powder metallurgy.* Advances in Powder Metallurgy, 1991. **6**: p. 347-360.

48. Bolzoni, L., et al., *Modification of sintered titanium alloys by hot isostatic pressing.* Key Engineering Materials, 2012. **520**(2012): p. 63-69.

49. Banik, A., et al., *Advances in titanium isothermal forging.* Journal of Metals, 1984(June 1984): p. 267-278.

50. Ebel, T., *Metal injection moulding of titanium.* Materials Science Forum, 2011. **690**: p. 181-184.

51. Ebel, T., et al., *Metal injection moulding of titanium and titanium-aluminides.* Key Engineering Materials, 2012. **520**: p. 153-160.

52. Froes, F.H., German,R.M, *Cost reduction prime Ti PIM for growth.* Metal Powder Report, 2000. **55**(6): p. 12-14.

53. Froes, F.H., *Advances in titanium metal injection molding.* Powder Metallurgy and Metal Ceramics, 2007. **46**(5-6): p. 303-310.

54. Froes, F. and B. Dutta, *The additive manufacturing (AM) of titanium alloys.* Light metals conference 15th- 17th October 2014, South Africa., 2014: p. 19-26.

55. Imam, M.A., et al., *Processing of titanium and its alloys by microwave energy.* Light metals conference 15th-17th October 2014, South Africa, 2014: p. 11-19.

56. Yoshikawa, N., *Fundamentals and Applications of Microwave Heating of Metals.* Journal of Microwave Power and Electromagnetic Energy, 2010. **44**(1): p. 4-13.

57. Suárez, M., et al. *Challenges and Opportunities for Spark Plasma Sintering: A Key Technology for a new genorations of materials*. 2013 [cited 2017 March]; Available from: http://www.fct-systeme.de/download/20140619125935/2013-InTech-Challenges.pdf.

58. Gabbitas, B., et al., *Cost effective forging of titanium alloy parts and their mechanical properties* Light metals conference, 15-17 October 2014, South Africa, 2014: p. 3-11.

59. Yang, F., et al., *Prepartaion of titanium alloy rods by powder compact extrusion.* Advanced Materials Research, 2014. **1019** p. 241-247.

60. El-Soudani, S.M., et al., *Optimization of Blended-Elemental Powder-Based Titanium Alloy Extrusions for Aerospace Applications.* Metallurgical and Materials Transactions, 2013. **44**(2): p. 899-910.

61. Sun, B., et al., *Fabrication of high-strength Ti materials by in-process solid solution strengthening of oxygen via P/M methods.* Materials Science and Engineering A 2013. **563**(2013): p. 95-100.

62. Dale, J.R., *Connection Rod Evaluation* January 2005: Metal Powder Industries Federation.

63. German, R.M., *Solid-state sintering fundamentals*, in *Sintering Theory and Practice*. 1996, John Wiley & Sons, Inc. p. 95-96.

64. Plehanov, B.G., *Experimental results of sintering velocity of powder metallurgy parts sintered by high frequency induction heating.* Porochkovaia Metallurgia 1992. **12**: p. 96-99.

65. Pfaffmann, G.D. and W.E. Templeton, *Induction high temperature sintering process and equipment.* Advances in Powder Metallurgy, 1990: p. 399-408.

66. Bulatova, L.S., *Kinetics of heating of constructional parts of ferromagnetic powders in induction furnaces.* Soviet Powder Metallurgy and Metal Ceramics, 1988. **27**(7): p. 547-550.

67. Conta, R.L., *A process for improved induction heating of powder metal compacts.* IEEE Transactions on Industry Applications, 1977. **IA-13**(4): p. 330-334.

68. Nikishov, N.A., I.V. Bogolyubova, and N.V. Nikitina, *Effect of methods of heating during sintering on the properties of iron-base powder materials.* Metal Science and Heat Treatment, 1991. **33**(1-2): p. 61-64.

69. Cavdar, U. and E. Atik, *Induction sintering of 3wt% Cu contented iron based powder metal parts.* Modern Applied Science, 2010. **4**(3): p. 63-70.

70. Salak, A., G. Leitner, and W. Hermel, *Properties of induction-sintered Fe-Mn-C and Fe-Mn-Cu-C steel in the sintered and forged states.* Powder Metallurgy International, 1981. **13**(1): p. 21-24.

71. Krumphold, R., W. Hermel, and G. Leitner, *Short-time induction sintering of Fe-based materials and hardmetals.* Sintered Metal-Ceramic Composites. Proceedings of the Third International School on Sintered Materials, 6-9 Dec. 1983, 1984: p. 127-138.

72. Hermel, W., et al., *Short-time induction sintering of hard metals.* Powder Metallurgy, 1983. **26**(4): p. 217-220.

73. Shibuya, M. and M. Ohyanagi, *Effect of nickel boride additive on simultaneous densification and phase decomposition of TiB2-WB2 solid solutions by pressureless sintering using induction heating.* Journal of the European Ceramic Society, 2007. **27**(1): p. 301-306.

74. Bolzoni, L., et al., *Inductive hot-pressing of titanium and titanium alloy powders.* Materials Chemistry and Physics, 2012. **131**(3): p. 672-679.

75. Jia, M., D.L. Zhang, and B. Gabbitas, *Comparisson of blended elemental and mechanical alloyed powder compact forging into Ti-6Al-4V rocker arms.* Key Engineering Materials, 2012. **520**(2012): p. 82-88.

76. Jia, M., *The Effect of Powder Characteristics and Processing Conditions on the Microstructure and Mechanical Properties of Titanium Alloys Made by Powder Forging* 2013, The University of Waikato.

77. James, B.W., M.J. McDermott, and R.A. Powel, *Powder Forging*, in *ASM Metals Hand book Vol. 14*. 2003. p. 409.

78. Bose, A. and W.B. Eisen, *Powder Forging*, in *Hot Consolidation of Powders & Particulates*. 2003, Metal Powder Industries Federation- Technology & Engineering. p. 129-164.

79. Kuhn, H.A., *Forging and Hot pressing*, in *ASM Metals Handbook*. 1991. p. 1489.

80. Zhang, D.L., C.C. Koch, and R.O. Scattergood, *The role of new particle surfaces in synthesizing bulk nanostructured metallic materials by powder metallurgy.* Materials Science and Engineering: A, 2009. **516**(1–2): p. 270-275.

81. Donachie, M.J., *Powder Metallurgy*, in *Titanium- A Technical Guide.* 2000 ASM International. p. 52-53.

82. Chandramouli, R., et al., *Deformation, densification, and corrosion studies of sintered powder metallurgy plain carbon steel preforms.* Materials and Design, 2007. **28**(7): p. 2260-2264.

83. Das, J., et al., *Hardness and tensile properties of Fe–P based alloys made through powder forging technique.* Materials Science and Engineering: A, 2008. **479**(1–2): p. 164-170.

84. Shanmugasundaram, D. and R. Chandramouli, *Tensile and impact behaviour of sinter-forged Cr, Ni and Mo alloyed powder metallurgy steels.* Materials & Design, 2009. **30**: p. 3444-3449.

85. Matheny, P. and P. Buxe, *Powder Forging of Hollow Article* U. Patent, Editor. 1992.

86. Chiesa, A. and D. Lenhart, *Powder Metal Forging and Method and Apparatus of Manufacture*. 2012.

87. Yamaguchi, T., et al., *Process for forging titanium-based material, process for producing engine valve. .* 2003.

88. Kuhlman, G.W., *Forging of Titanium Alloys*, in *ASM Metals Handbook Vol. 14*. 1993, ASM International. p. 269-601.

89. Guo, H., et al., *The powder sintering and Isothermal Forging of Ti-10-2Fe-3Al.* JOM, 2008. **60**(11): p. 47-49.

90. Qiu, J.W., et al., *Microstructures and mechanical properties of titanium alloy connecting rod made by powder forging process.* Materials & Design, 2012. **33**: p. 213-219.

91. Smarsly, W. and W. Bunk, *Microstructure and texture of combined die forged (CDF) prealloyed Ti-6Al-4V powder compacts.* Powder Metallurgy International, 1985. **17**(2): p. 63-67.

92. Smarsly, W. and W. Bunk, *Influence of the cobmined die forging (CDF) of prealloyd Ti-6Al-4V powder on microstructure and mechanical properties* Metal Powder Report, 1986. **41**(10): p. 753-760.

93. Qiu, J.W., et al., *Optimizing the hot-forging process parameters for connecting rods made of PM titanium alloy.* Journal of Materials Science, 2012. **47**(8): p. 3837-3848.

94. Smarsly, W. and W. Bunk, *Microstructure and texture of Combined Die Forging (CDF) Prealloyd Ti-6Al-4V Powder Compacts.* Powder Metallurgy International, 1985. **17**(26): p. 63-67.

95. Smarsly, W. and W. Bunk, *Influence of Combined Die Forging (CDF) of Prealloyd Ti-6Al-4V Powder on Microstructure abd Mechanical Properties.* Metal Powder Report, 1986. **41**(10): p. 753-760.

96. Nadakuduru, V.N., et al., *Mechanical Behaviour of Titanium, Ti-6Al-4V (wt %) Alloy and Ti-47Al-2Cr (at %) Alloy Produced using Powder Compact Forging.* Advanced Materials Research Vol. 275 (2011) 2011. **275**: p. 186-101.

97. Zhang, D., et al., *Consolidation of titanium, and Ti-6Al-4V alloy powders by powder compact forging.* Materials Science Forum, 2009. **618-619**: p. 513-516.

98. Yang, F. and B. Gabbitas, *Effect of heat treatment on microstructures and mechanical properties of a Ti-6Al-4V alloy rod prepared by powder compact extrusion.* International Journal of Modern Physics B, 2015. **29**(10-11): p. 1540004 (7 pp.).

99. Yang, F., et al., *Microstructural evolution during extrusion of a Ti/Al/Al35V65 (Ti-6Al-4V) powder compact and the mechanical properties of the extruded rod.* Materials Science and Engineering A, 2014. **598**: p. 360-367.

100. Yang, F., et al., *Effect of powder compact holding time on the microstructure and properties of Ti-6Al-4V alloy produced by powder compact extrusion of a powder mixture of HDH titanium and Al-V master alloy.* Key Engineering Materials, 2013. **551**: p. 67-72.

101. Singh, A., et al., *Effect of pre-consolidation methods and oxygen on the mechanical properties of as-extruded Ti-6Al-4V alloy rod.* Proceedings of 13th World Conference on Titanium, 16-20 August, 2015, San Diego, California, USA, 2015.

102. Singh, A.P., et al., *Mechanical properties of Ti-6Al-4V rods produced by powder compact extrusion.* 143rd Annual Meeting and Exhibition, TMS 2014, February 16, 2014 - February 20, 2014, 2014: p. 605-612.

103. Froes, F.H., *How to Market Titanium: Lower the Cost.* JOM, 2004. **56**(2): p. 39.

104. Froes, F.H. and M. Ashraf Imam, *Cost affordable developments in titanium technology and applications.* Key Engineering Materials, 2010. **436**: p. 1-11.

105. Esteban, P.G., et al., *Low-cost titanium alloys? Iron may hold the answers.* Metal Powder Report, 2008. **63**(4): p. 24-27.

106. Hagiwara, M., S.J. Kim, and S. Emura, *Blended elemental P/M synthesis of Ti-6Al-1.7Fe-0.1Si alloy with improved high cycle fatigue strength.* Scripta Materialia, 1998. **39**(9): p. 1185-1190.

107. Liu, Y., et al., *Design of powder metallurgy titanium alloys and composites.* Materials Science and Engineering A, 2006. **418**(1-2): p. 25-35.

108. Tamirisakandala, S., et al., *Powder metallurgy Ti-6Al-4V-xB alloys: Processing, microstructure, and properties.* JOM, 2004. **56**(5): p. 60-63.

109. Chen, B.-Y., K.-S. Hwang, and K.-L. Ng, *Effect of cooling process on the α phase formation and mechanical properties of sintered Ti–Fe alloys.* Materials Science and Engineering: A, 2011. **528**(13–14): p. 4556-4563.

110. Esteban, P.G., et al., *PM processing and characterisation of Ti-7Fe low cost titanium alloys.* Powder Metallurgy, 2011. **54**(3): p. 242-252.

111. Esteban, P.G., E.M. Ruiz-Navas, and E. Gordo, *Influence of Fe content and particle size the on the processing and mechanical properties of low-cost Ti-xFe alloys.* Materials Science and Engineering: A 2010. **527**(21-22): p. 5664-5669.

112. Nakajima, H., K. Yusa, and Y. Kondo, *Diffusion of iron in a diluted -Ti-Fe alloy.* Scripta Materialia, 1996. **34**(2): p. 249-53.

113. O'Flynn, J. and S.F. Corbin, *The influence of iron powder size on pore formation, densification and homogenization during blended elemental sintering of Ti–2.5Fe.* Journal of Alloys and Compounds, 2015. **618**: p. 437-448.

114. Carman, A., et al., *Role of alloying elements in microstructure evolution and alloying elements behaviour during sintering of a near- titanium alloy.* Materials Science and Engineering: A, 2011. **528**(3): p. 1686-1693.

115. Murray, L.S., *Binary alloy phase diagrams*, in *ASM Metals Handbook Vol.3.* 1992, ASM International. p. 869-870.

116. Ahmed, M., et al., *The effect of cooling rates on the microstructure and mechanical properties of thermo-mechanically processed Ti-Al-Mo-V-Cr-Fe alloys.* Materials Science and Engineering A, 2013. **576**: p. 167-177.

117. Fujita, T., et al., *Microstructure and properties of titanium alloy produced in the newly developed blended elemental powder metallurgy process.* Materials Science and Engineering A, 1996. **213**: p. 148-153.

118. Hsu, H.-C., et al., *Structure and mechanical properties of as-cast Ti-5Nb-xFe alloys.* Intermetallics, 2014. **47**: p. 11-16.

119. Siqueira, R.P., et al., *Microstructural evolution during sintering of the blended elemental Ti-5Al-2.5Fe alloy.* Journal of Alloys and Compounds, 2009. **476**(1-2): p. 130-137.

120. Bor-Yuan, C. and H. Kuen-Shyang, *Sintered Ti-Fe alloys with in situ synthesized TiC dispersoids.* Materials Science & Engineering A (Structural Materials: Properties, Microstructure and Processing), 2012. **541**: p. 88-97.

121. Wei, W., et al., *Effect of Fe addition on sintering behaviour of titanium powder.* Powder Metallurgy, 2003. **46**(3): p. 246-250.

122. Lee, D.B., et al., *Mechanical and oxidation properties of Ti–xFe–ySi alloys.* Materials Science and Engineering: A, 2002. **328**(1–2): p. 161-168.

123. Qiu, J.W., et al., *Microstructures and mechanical properties of titanium alloy connecting rod made by powder forging process.* Materials & Design, 2012. **33**: p. 213-19.

124. Song, G.A., et al., *Optimization of mechanical properties of Ti-Fe-Sn alloys by controlling heterogeneous eutectic structure.* Intermetallics, 2012. **23**: p. 27-31.

125. Bor-Yuan, C., H. Kuen-Shyang, and K.-L. Ng, *Effect of cooling process on the alpha phase formation and mechanical properties of sintered Ti-Fe alloy.* Materials Science and Engineering A 2011. **528**: p. 4556-4563.

126. Chen, B.-Y. and K.-S. Hwang, *Sintered Ti-Fe alloys with in situ synthesized TiC dispersoids.* Materials Science and Engineering A (Structural Materials: Properties, Microstructure and Processing), 2012. **541**: p. 88-97.

127. Bolzoni, L., E.M. Ruiz-Navas, and E. Gordo, *Influence of vacuum hot-pressing temperature on the microstructure and mechanical properties of Ti-3Al-2.5V alloy obtained by blended elemental and master alloy addition powders.* Materials Chemistry and Physics, 2012. **137**(2): p. 608-616.

128. Kimura, A., et al., *A free machining titanium alloy for connecting rods.* International Congress and Expostition, February 25, 1991 - March 1, 1991, 1991.

129. Schutz, R.W. and H.B. Watkins, *Recent developments in titanium alloy application in the energy industry.* Materials Science and Engineering A, 1998. **243**: p. 305-315.

130. Bolzoni, L., E.M. Ruiz-Navas, and E. Gordo, *Influence of sintering parameters on the properties of powder metallurgy Ti-3Al-2.5V alloy.* Materials Characterization, 2013. **84**: p. 48-57.

Chapter 2

Experimental Method

This chapter describes the characteristics of the materials used in each of the experiments, experimental methodology and the processing parameters for each powder consolidation technique, the equipment used for each of the experiments and the techniques and the equipment used for analytical work.

2.1 Raw Materials

Various metal powders with different characteristics were used for the experiments in this research work. Table 2.1 and Table 2.2 give details about the powder suppliers and powder characteristics such as particles size and composition. The morphology of the powder particles are shown in Figure 2.1. The commercial purity (CP) Ti and the pre-alloyed Ti6Al4V powders were irregularly shaped and produced by the hydrogenated de hydrogenated (HDH) method. Two types of iron powders were used. The iron powder (A-230, annealed) was made by milling electro-refined iron chips. The iron carbonyl powder was prepared by chemical decomposition of purified iron pentacarbonyl. The 316SS powder was made by water atomization.

Table 2.1 Characteristics of the Ti, Ti6Al4V and Al60V40 powders.

Powders	Batch	Supplier	part. size, mesh	Si, wt. %	Fe, wt.%	Cl, wt.%	C, wt.%	O, wt.%	N, wt.%	H, wt.%	Al, wt.%	V wt.%,	Ti, wt.%
Ti	1	Xi'an Lilin Ltd., China	-200	0.02	0.02	0.08	0.02	0.33	0.02	0.04	-	-	Balance
	2	Xi'an Lilin Ltd., China	-200	0.02	0.04	0.04	0.02	0.25	0.03	0.03	-	-	Balance

	3	Goodfellow Ltd., UK	-200	0.01	0.02	0.02	0.01	0.23	0.01	0.02	-	-	Balance
Ti6Al4V	1	Xi'an Lilin Ltd., China	-200	-	-	0.02	0.02	0.30 / 0.78[1]	0.04	0.01	6.03	3.94	Balance
	2	Xi'an Lilin Ltd., China	-200	-	0.05	-	0.02	0.29 / 0.50[1]	0.18	0.04	6.00	3.90	Balance
Al40V	1	Xi'an Lilin Ltd., China	-250	0.11	-	-	0.003	0.24 / 0.61[1]	-	-	Balance	42.24	-

[1]Additional oxygen analyses done in Durkee Testing Laboratories, Inc, US

Table 2. 2 Characteristics of pure Fe powders and 316LSS powders.

Powders	Supplier	Powder particles size, mesh	Cr, wt.%	Ni, wt%	Mo, wt.%	Mn, wt.%	C, wt.%	P, wt.%	S, wt.%	O, wt.%	Fe, wt.%
Fe A-230	Sigma Aldrich Ltd, USA	-100	-	≤ 0.05	-	≤ 0.10	-	≤ 0.03	≤ 0.02	0.46	≥ 99.00
Fe carbonyl	Sigma Aldrich Ltd., USA	-1200	≤ 0.01	≤ 0.05	-	≤ 0.05	-	≤ 0.01	≤ 0.01	0.32	≥ 99.50
316LSS	Xi'an Lilin, China	-400	17.40	13.00	2.40	≤ 2.00	0.02	≤ 0.03	≤ 0.03	0.20	Balance
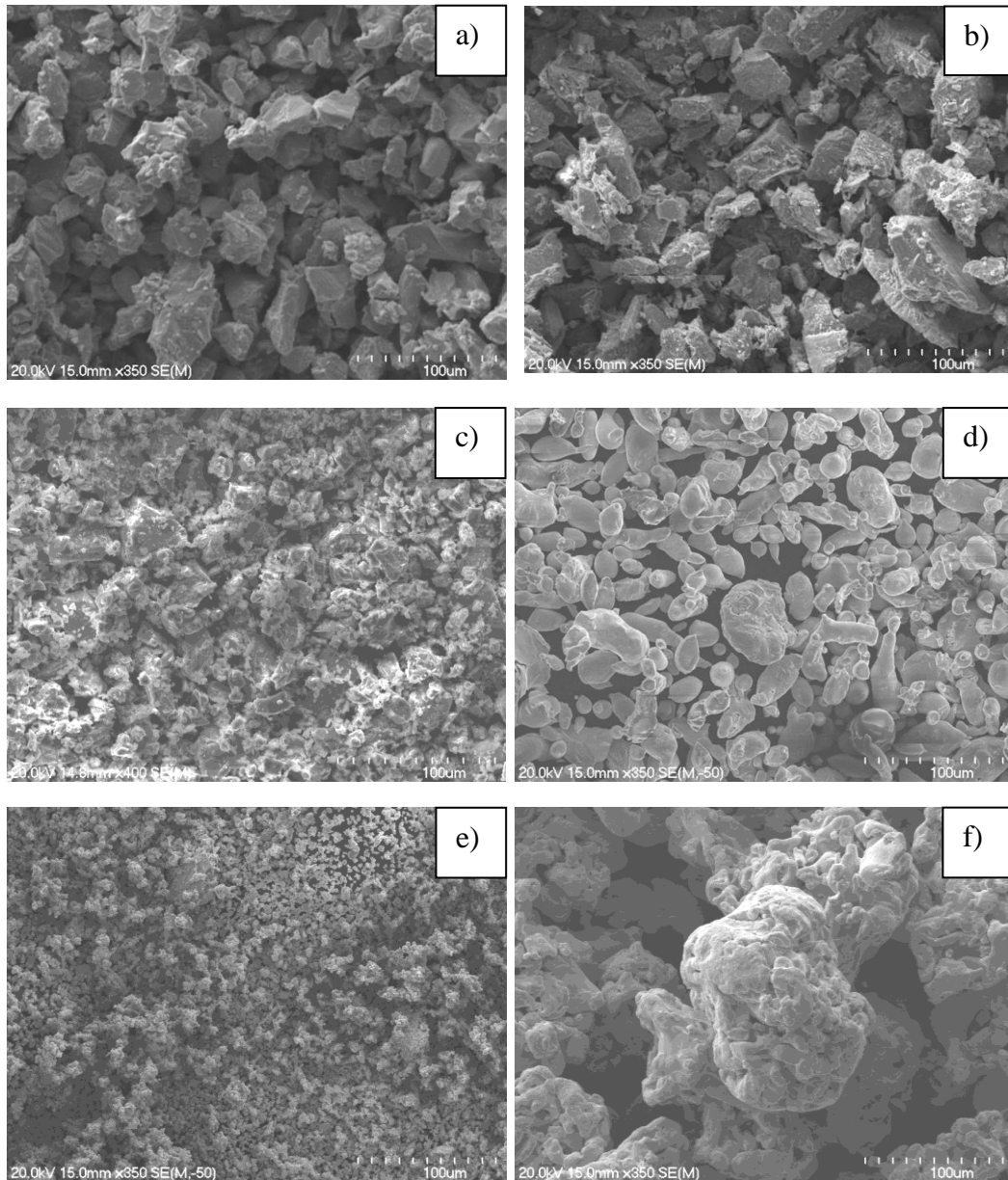
Figure 2.1 SEM image of the powders used a) CP-Ti, b) prealloyed Ti6Al4V, c) master alloy Al40V, d) 316L SS, e) Fe carbonyl and f) Fe A-230.

2.2   Experimental set ups and process parameters

2.2.1 Induction sintering of Ti and PA Ti6Al4V powders

Induction sintering was done in two steps. Firstly, Ti and Ti6Al4V cylindrical billets were made by powder compaction using 130 g of batch 1 Ti and Ti6Al4V powders respectively for each billet. These were then heated using an induction furnace. The characteristics of the powders are given in Table 2.1. The powders were compacted in a 100 ton hydraulic press using a cylindrical die with a diameter of 40 mm (Figure 2.2).

73
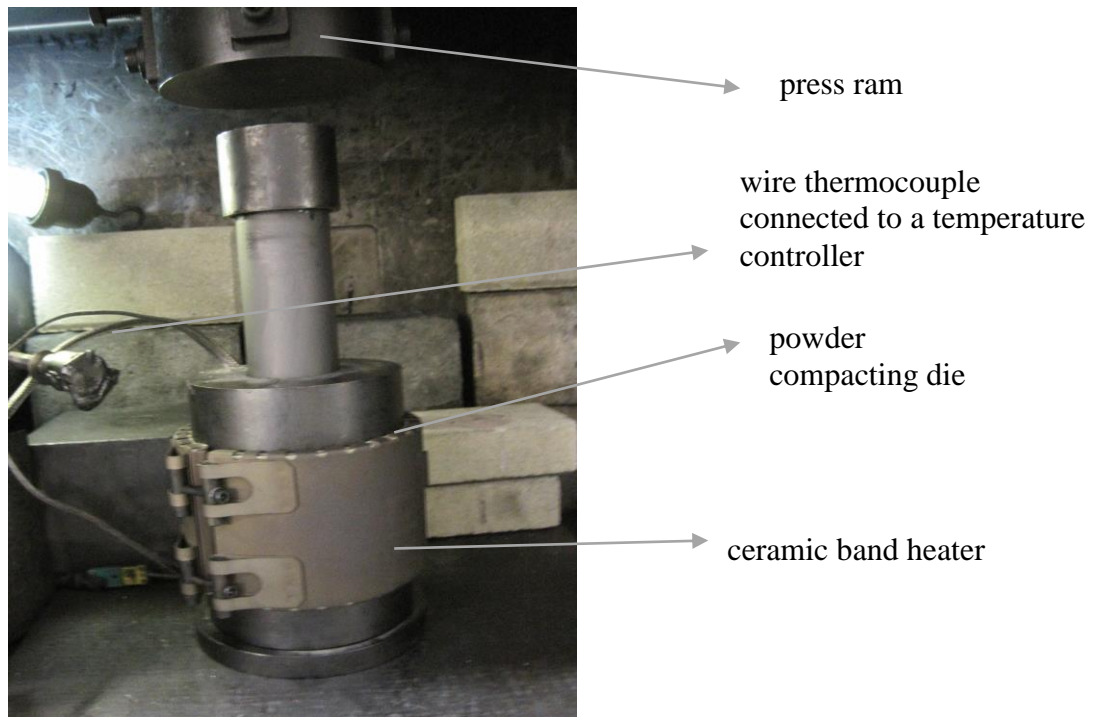
Figure 2.2 Experimental set up for warm powder compaction.

Two different powder compaction conditions were used to manufacture two sets of samples with different green densities. To achieve a lower targeted green density, powder compaction was done at room temperature by applying a uniaxial pressure of 457MPa and 497MPa respectively Ti for Ti-6Al-4V powders. Compacts were held at maximum pressure for 1min. The aim of the second method was to achieve a higher green density. In this case the powder was preheated to 250˚C inside the die prior to pressing while maintaining the same conditions as before. This process is called warm powder compaction (WPC). A ceramic band heater, placed on the outer surface of the compaction die, was used for preheating the powders. The temperature was measured using a K type wire thermocouple inserted into a hole made on the upper surface of the compaction die. The thermocouple was connected to a digital thermometer.

The powder compacts were further consolidated by sintering using induction heating. A schematic of the experiments is shown in Figure 2.3 and the experimental setup is shown in Figure 2.4.
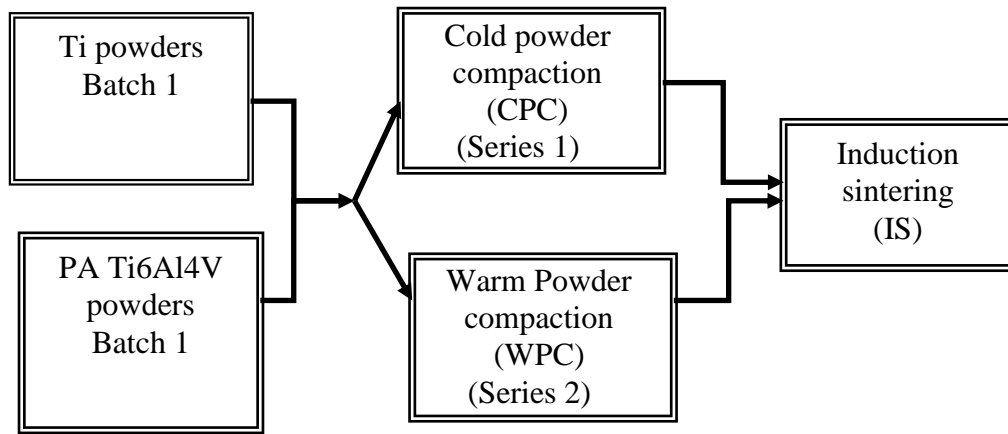
Figure 2.3 Diagram of the experimental method for induction sintering.

Figure 2.4 Experimental setup for induction sintering: a) controlled atmosphere chamber, b) argon bottles, c) oxygen analyser, d) induction coil mounted in a protective atmosphere chamber and e) induction power control unit.

The experimental arrangement consisted of an induction heating control unit, an induction coil mounted in the protective atmosphere chamber, argon bottles, an

oxygen analyser and K type wire thermocouple connected to a digital temperature controller. Before commencing the IS experiments, the chamber was back filled with argon to replace the ambient atmosphere. The oxygen level was measured and kept below 200ppm during IS. This was an essential step to avoid any oxidation of the powder compact during IS. Each powder compact was placed in the induction coil and heated up to a temperature above the α/β phase transformation. The temperature of the heated samples was monitored by a flexible K type thermocouple which was placed in a hole made in the centre top section of each powder compact. The temperature was controlled by adjusting the power level from the control panel of the induction unit. During the holding time the temperature was maintained within 30°C of the target temperature. The same induction sintering parameters were used for both Ti and PA Ti6Al4V powder compacts (Table 2.3).

Table 2.3 Induction sintering conditions.

IS1	IS2	IS3	IS4	IS5	IS6
1200°C no holding	1200°C 4min	1300°C no holding	1300°C 4min	1400°C no holding	1400°C 4min

In order to obtain the induction heating rates, recordings were made of the temperature increase versus time during IS every 50˚C increase in temperature. After completing each IS experiment the sample was removed from the induction coil and left to cool down in the protective atmosphere chamber. The various analyses included measurements of green density, sintered density, the porosity distribution over the cross section of the IS samples, tensile properties and fracture surface analyses. Details of the equipment used and the analytical techniques are described in Section 2.3.

2.2.2 Open Die Forging (ODF) of pre-alloyed (PA) Ti6Al4V powders

The powders used for open die powder compact forging were PA Ti6Al4V powders Batch 2 (described in Table 2.1). Powders were initially warm compacted into 40 mm diameter cylindrical shapes, 35mm high and with an

average relative density of 78%. The warm powder compacting procedure used was similar to that described in Section 2.2.1.

The open die forging (ODF) was done in a controlled atmosphere hydraulic press chamber used for the IS experiments described above. The process flow is described schematically in Figure 2.5.
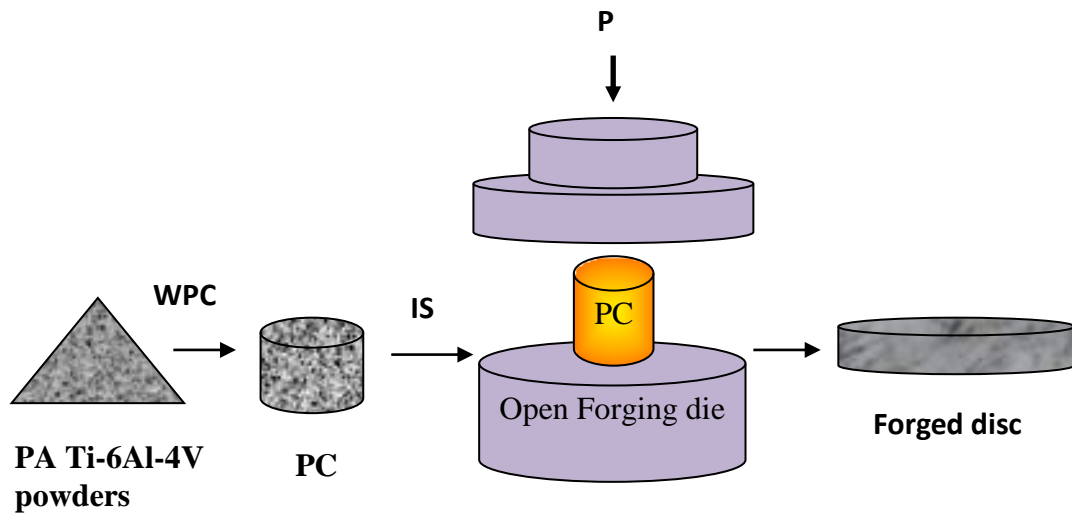
Figure 2.5 Diagram of the open die forging process.

Powder compacts were first induction sintered using different time temperature conditions. Immediately after induction sintering each sample was transferred to an open forging die and forged into a disc using the maximum load of 100 ton. The working surfaces of the forging dies were cold spray coated with TiAl(O)/Al$_2$O$_3$ composite powders [1]. The process parameters for induction sintering are shown in Table 2.4. The forged discs were analysed to determine the porosity distribution, tensile properties, α/ β phase distribution, fracture surface features and the amount of impurity pickup during thermo-mechanical processing.

Table 2.4 Open die forging conditions.

Forging condition	F1	F2	F3	F4	F5	F6	F7	F8	F9	F10
Temperature, °C	1000	1000	1100	1100	1200	1200	1300	1300	1400	1400
Sintering time, min	0	4	0	4	0	4	0	4	0	4

Two of the forged discs were selected for a recrystallization annealing heat treatment. The recrystallization annealing parameters used were selected from the ASM Metals Handbook [2] and the parameters are given in Figure 2.6. Heat treatment was carried out in a ceramic tube furnace using argon as a protective atmosphere.
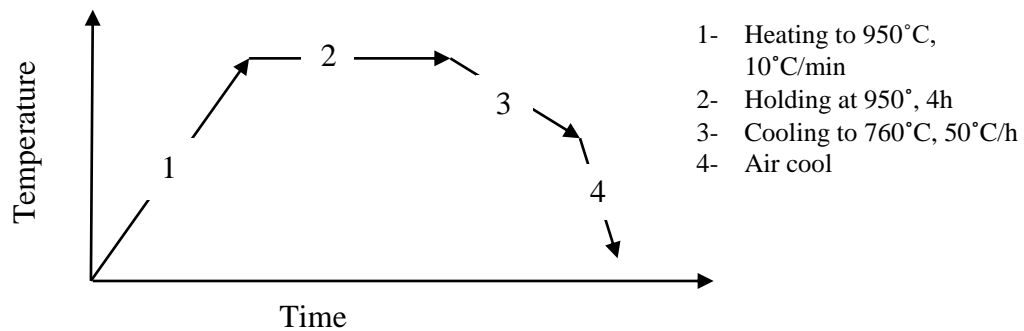
Figure 2.6 Parameters for recrystallization annealing of the Ti6Al4V as forged discs.

2.2.3   Consolidation of Ti based alloys using blended elemental approach

Four types of low cost Ti alloy powders were prepared, Ti6Al4V, Ti3Al2V, Ti5Fe and Ti5SS alloys using a blended elemental (BE) approach. Ti HDH powders Batch 2 and Batch 3 (Table 2.1) were used as a base material. For preparation of Ti6Al4V and Ti3Al2V BE powder alloys, the pure Ti powders were mixed with an appropriate ratio of 60Al40V master alloy powders (Table 2.1). For preparation of Ti5Fe and Ti5SS BE powder alloys, the pure Ti powders were mixed in an appropriate ratio with pure Fe powders and 316LSS (stainless steel) powders respectively (Table 2.2). The powder mixtures were placed in a container with stainless steel (SS) balls with a weight ratio of powders to SS balls of 1 to 2 and blended for 24h using a roller mixer. The speed of the roller mixer was kept at 200 rpm. After mixing, the powders were compacted into billets using warm powder compaction. The parameters for the warm powder compacting were similar for all BE alloy powders and are given in Table 2.5. The powder compact billets were further consolidated by vacuum sintering (VS), induction sintering (IS), open die forging (ODF) and powder compact extrusion (PCE). The

processing conditions for the different type of consolidation are listed in Table 2.6
and a schematic diagram for powder consolidation is given in Figure 2.7.

Table 2. 5 Warm powder compaction pressing conditions.

Amount of powders	Compacting die diameter	Powder temperature	Pressure applied	Time at pressure
150g	40mm	250˚C	750MPa	8min

Table 2.6 Process parameters for the consolidation of BE Ti alloy powder compacts by vacuum sintering, induction sintering, open die forging and powder compact extrusion.

powders	Consolidation method	Process parameters		
		Temperature/ Time profile	Environment:	Powder compact coating
Ti6Al4V/ Ti3Al2V	IS	1000˚C 8min→1200˚C 2min	argon	N/A
	IS→F	1000˚C 8min→ 1200˚C 2min→F	argon	N/A
	IS→E	1000˚C 8min→ 1200˚C 2min →1300˚C→E	argon	colloidal graphite
	VS	1000˚C 2h→ 1300 2h	vacuum	N/A
	VS→F	1200˚C → F	air	colloidal graphite
	VS→E	1300˚C → E	argon	colloidal graphite
Ti5Fe-carbonyl/ Ti5FeA-230/ Ti5SS	IS	1000˚C 8min→1150˚C 2min	argon	N/A
	IS→F	1000˚C 8min→ 1150˚C 2min →1100˚C→F	argon	N/A
	IS→E	1000˚C 8min→1150˚C 2min→ E	argon	colloidal graphite
	VS	1000˚C 2h→ 1250 2h	vacuum	N/A
	VS→F	1100˚C → F	air	colloidal graphite
	VS→ E	1150˚C→ E	argon	colloidal graphite

The WPC was done in air. The IS and the ODF and PCE associated with IS were
done in a protective argon atmosphere and the experimental set up used for these
experiments is described in Section 2.2.1 (Figure 2.4). Vacuum sintering was
done using a high vacuum sintering furnace at a vacuum of $2x10^{-2}$Pa. ODF and
PCE associated with VS were done in an ambient and argon protective

environment respectively. The reduction ratio for extrusion was 3.3/1. The diameter of the extruded bars was 12mm. The open die forging was done to full deformation where 100ton force was applied.

```
                    ┌─────────────────────┐
                    │   Powders mixing    │
                    │    and blending     │
                    └─────────────────────┘
                              │
                              ▼
                    ┌─────────────────────┐
                    │ Warm powder compacting│
                    │     (6 samples)      │
                    └─────────────────────┘
                       ╱              ╲
                      ╱                ╲
        ┌─────────────────────┐   ┌─────────────────────┐
        │ Induction Sintering │   │  Vacuum Sintering   │
        │    (3 samples)      │   │    (3 samples)      │
        └─────────────────────┘   └─────────────────────┘
           ╱          ╲              ╱          ╲
  ┌──────────┐ ┌──────────────┐ ┌──────────┐ ┌──────────────┐
  │ Open die │ │Powder compact│ │ Open die │ │Powder compact│
  │ forging  │ │  extrusion   │ │ forging  │ │  extrusion   │
  │(1sample) │ │  (1sample)   │ │(1sample) │ │  (1sample)   │
  └──────────┘ └──────────────┘ └──────────┘ └──────────────┘
```
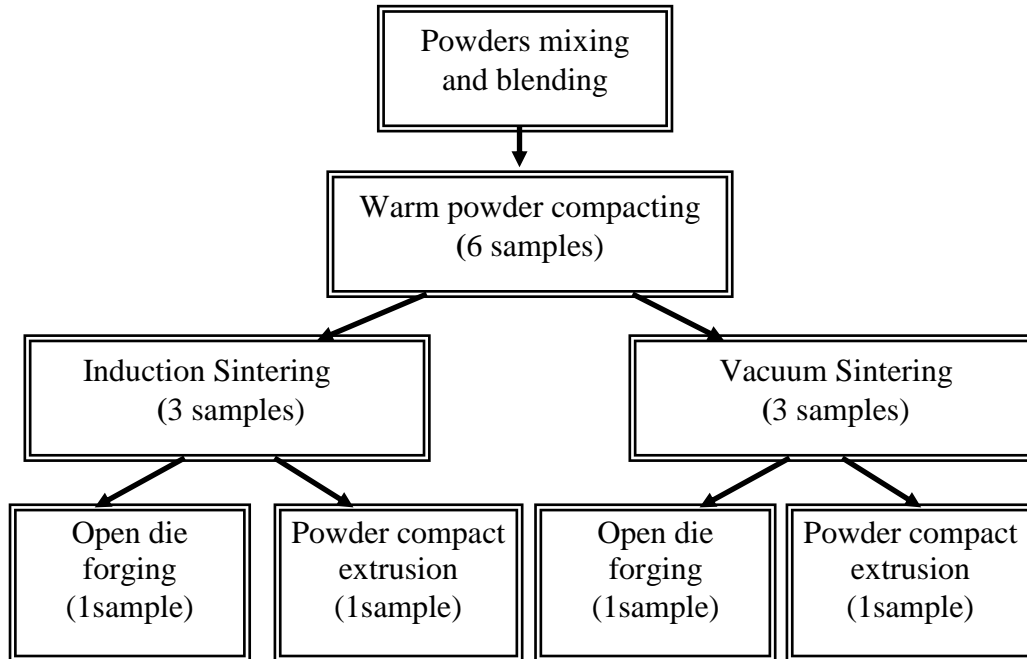
Figure 2.7 Diagram of the experimental method for consolidation of BE Ti based alloy powders.

2.3 Equipment used

2.3.1 Dies

A variety of dies were used in the experimental work. These included a 40 mm diameter cylindrical powder compaction die, a forging die and a 12 mm diameter extrusion die (Figure 2.8). All the dies were in-house designed and made of H13 tool steel. The extrusion die was manufactured by Pilling and Leggett Engineering Co. Ltd., Hamilton. The die heat treatment was done by Heat treatment Ltd, Auckland.
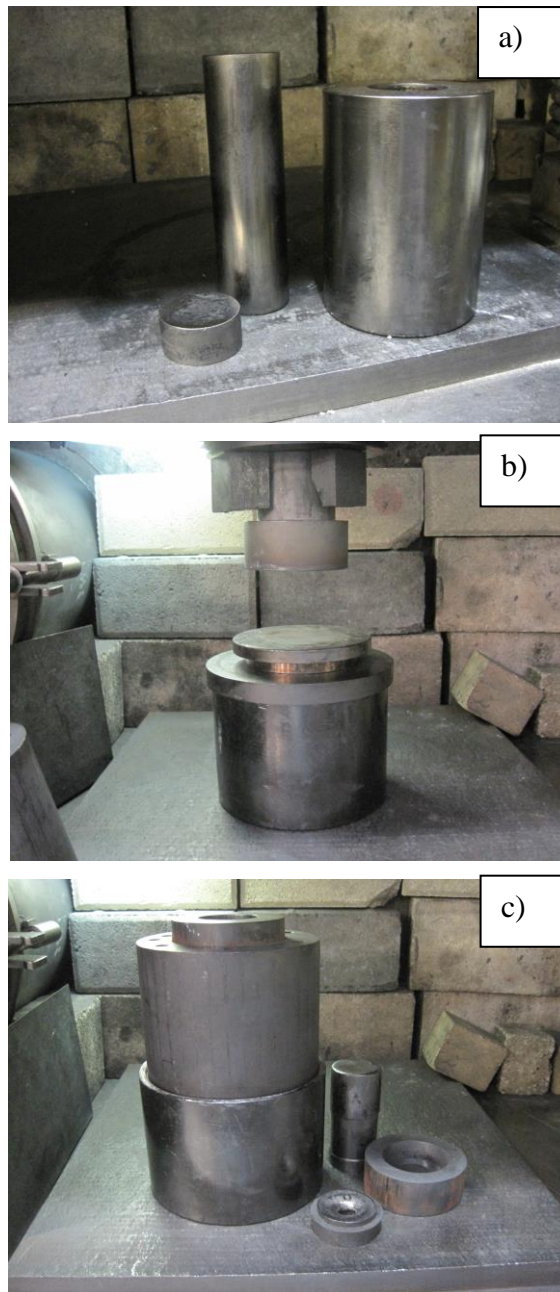
Figure 2.8 Photos of: a) powder compaction die, b) open forging die and c) powder compact extrusion die.

2.3.2 Heating equipment and temperature control

The ceramic band heaters used for warm powder compaction and the extrusion experiments were designed and manufactured by Hislop and Barley Ltd., Auckland. The heaters were attached to the outer cylindrical surface of the powder compaction or extrusion die. The ceramic band heaters can be seen as the part of the experimental equipment in Figure 2.2.

An Inductotherm Powertrack 15-96 induction heating furnace with medium frequency and a power capability of 15 kW was used for the IS experiments and

the pre-sintering or preheating of samples for the ODF and PCE experiments. The induction sintering coil was in-house designed and made and the power unit and induction coil can be respectively seen in Figure 2. 4d) and Figure 2.4e).

A high vacuum furnace ACME 30kW, $2x10^{-3}$ Pa, was used for the vacuum sintering experiments or for consolidation of the samples prior to some of the ODF and PCE experiments (Figure 2. 9)

Figure 2.9 High vacuum furnace used for vacuum sintering.

A controlled atmosphere horizontal tube furnace was used for the heat treatment experiments (Figure 2.10) using argon as a controlled atmosphere gas. The air was first evacuated using a vacuum pump and then the tube chamber was back filled with argon. This purging was done at least 3 times before starting each of the heat treatment experiments.

Figure 2.10 Horizontal tube furnace used for heat treatment.

A K-type thermocouple wire connected to a digital temperature control unit Shinko GW44217 was used for temperature measurement and control during the warm powder compacting and the induction sintering or induction reheating (Figure 2.11).

Figure 2.11 Thermocouple wire connected to a temperature controller.

2.3.3 Powder compaction and forging press

A hydraulic press HRB-1010 with a capacity of 3kW and 100ton was used for powder compaction, ODF and PCE (Figure 2.12).

Figure 2.12 100 ton hydraulic press.

2.3.4 Other equipment

A controlled atmosphere glove box chamber (Figure 2.4 a) was used for all IS and some of the ODF and PCE experiments. The chamber, made of 316SS steel, was

designed in-house and manufactured by Stainless Design Ltd., Hamilton. The chamber has a transparent cover with 4 glove ports and gloves to facilitate handling the samples during experiments. An induction coil is also mounted in the side wall of the chamber. It is also equipped with a system of hoses connected to argon bottles, a <u>small vacuum pump</u> and an <u>oxygen analyser</u> Rapidox (Figure 2.4c).

<u>An electro discharge machine (EDM)</u> with a digital control Jiangsu Zhongxing was used for cutting the tensile test samples and the samples for metallography and oxygen analyses (Figure 2.13).

Figure 2.13 EDM cutting machine with a digital control.

2.4 Test methods and analyses

2.4.1 Density

The green density of the powder compacts made by cold or warm powder compaction was determined by calculation based on the following equation:

$$\rho_{gs} = m/V, \text{ g/cm}^3 \qquad (2.1)$$

where :
  ρ_{gs} - calculated density of the green sample, g/cm^3
  m - weight of the green sample, g
  V- volume of the green sample, cm^3

The weight of each sample was determined using a digital laboratory balance with a maximum capacity of 3kg and accuracy of 0.1g. The volume of the cylindrical powder compacts was calculated from the measurements of the diameter and the height of each sample, taken with a digital calliper.
The relative density was calculated by the following equation:

$$\rho_{relative} = (\rho_{gs}/\rho_o) \times 100, \% \qquad (2.2)$$

where, ρ_o is the full or the theoretical density of the material.

The theoretical density of Ti6Al4V and Ti3Al2V was taken from the literature. The theoretical density of Ti5Fe and Ti5SS alloys was calculated based on the theoretical full densities of the alloy constituents and their stoichiometric ratios (Table. 2.7)

Table 2.7 Theoretical densities of the materials used.

Pure metal/ Alloy	Theoretical Density, g/cm^3	Obtained by:
Ti	4.51	Reference [3]
Fe	7.87	
316SS	7.93	
Ti3Al2V	4.48	
Ti6Al4V	4.46	
Ti5Fe	4.67	Calculation
Ti5SS	4.68	

The density of the induction sintered (IS) and vacuum sintered samples (VS) was measured by Archimedes' method which is described in the ASTM standard B962-14 [4]. The set up for measuring the weight of the sintered samples in air and in water is shown on Figure 2.14.
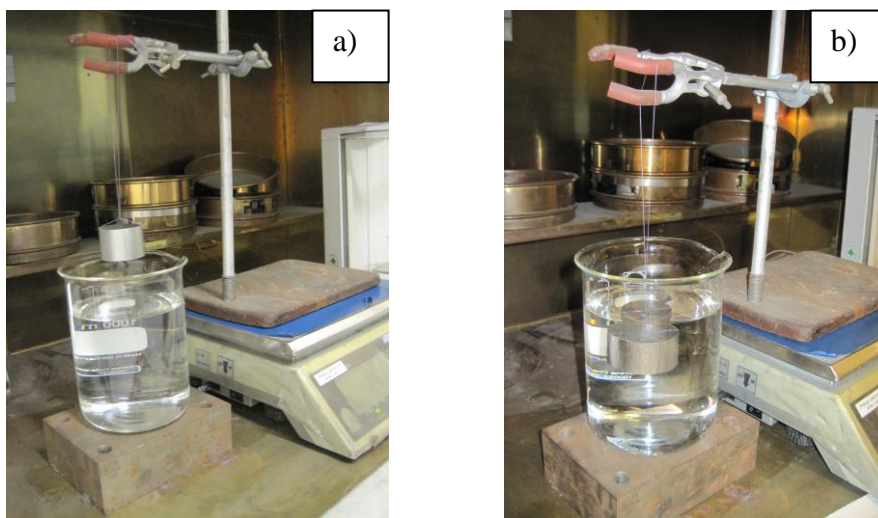
Figure 2.14 Set up for obtaining the density of the sintered samples by Archimedes' principle: the weight measurement in a) air and b) water.

The equation used was:

$$\rho_{sint} = m_o \, \rho_w \, (m_o - m_1) \qquad\qquad (2.3)$$

m_o - weight of the sintered sample in air

m_1 - weight of the sintered sample in water

ρ_w - density of the water

ρ_{sint} – sintered density

The room temperature density of water at the temperature when the test was completed was taken from the ASTM standard [4]. For supporting the specimen a textile string with a diameter below 0.025mm was used and the weight of the string was in the range of 0.022g and 0.025g. According to the ASTMS standard [4], a specimen support with this specification used for a sample weighing over 100g, can be ignored.

2.4.2   Tensile test

Tensile properties such as yield strength (YS), ultimate tensile strength (UTS) and elongation to fracture of the samples consolidated by IS, VS, ODF and PCE were measured. Tensile test samples with a shape and dimensions shown in Figure 2.15 were cut from each sample.
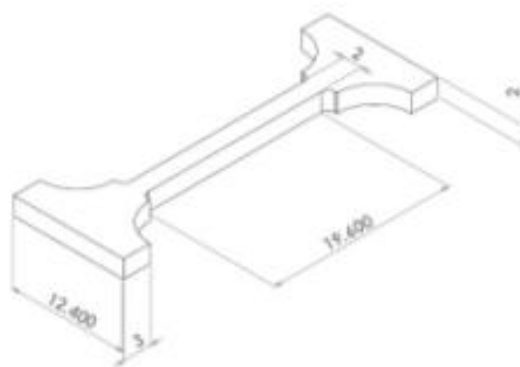
Figure 2.15 Drawing and dimensions (mm) of a tensile test piece.

An EDM cutting machine was used for cutting after which each sample was ground to remove the surface roughness caused by the cutting. A Dremel 3000 electric hand grinder with a SiC grinding wheel was used on the side surfaces. A

metallographic grinding machine with 320 and 600 grit SiC paper was used for the flat surfaces. Tensile testing was carried out at room temperature using an Instron 33R4204 universal testing machine with a load cell of 5 kN and a cross head speed of 0.1mm/min. The calculated strain rate was $8.33 \times 10^{-5} sec^{-1}$. An extensometer with a gauge length of 10 mm was used to record the elongation during tensile testing.

2.4.3 Microstructure analysis

For metallographic analysis, Olympus BX60 light optical microscope (LOM) equipped with a digital camera and Hitachi S4700 scanning electron microscope (SEM) equipped with energy dispersive spectrum (EDS) analyser were used. Samples from the consolidated materials were: cut using an electro discharge machine (EDM); mounted in resin; and metallographically ground and polished. The samples described in Chapters 3 and 4 were prepared using manual metallographic polisher- Struers RotoPol-21. Each sample was first ground using 120, 320, 600, 1200, 2000 and 4000 grit SiC papers to produce flat surfaces. Further, to eliminate the fine surface scratches, the samples were polished using alumina dispersion with a particle size of 0.3 μm. The metallography samples described in Chapters 5 were ground and polished using Struers Tegramin-25 semi- automatic metallographic polisher. For grinding 600 grit SiC paper was used followed by polishing with a 9μm diamond suspension and final polishing with a colloidal silica suspension OP-S.

To reveal the grain size and α/β phase distribution, polished samples were etched with Kroll reagent: 3% HF, 10 % HNO_3 in distilled water. The etched samples were then observed by LOM or SEM.

Fractography on broken tensile test samples was done using SEM.

2.4.4 Oxygen analysis

Oxygen analysis of some of the starting powders, sintered, forged and extruded samples were done by an inert gas infusion method using LECO equipment. The oxygen analysis were done at the Durkee Testing Laboratory, USA.

Reference

1.   Salman, A., et al., *Characterization of Ti(Al,O)-Al2O3 Composite Powders and Thermally Sprayed Coatings.* Advanced Engineering Research, 2007. **29-30**: p. 135-138.
2.   Gilbert, R., *Heat Treating of Titanium and Titanium Alloys* in *ASM Metals Handbook*. 1991. p. 2043- 2047.
3.   Murray, G.T. and T.A. Lograsso, *Pure Metals*, in *ASM Handbook Vol. 2*, A. International, Editor. p. 2923-3216.
4.   ASTM, *Standard test methods for density of compacted or sintered PM products using Archimeded principle*. ASTM International: US. p. 1-7.

Chapter 3

Induction Sintering of Ti and prealloyed Ti6Al4V powders

3.1 Introduction

Induction heating has many advantages as a heating source and it is widely used in conventional hot metal working technologies such as casting, forging, extrusion and surface heat treatment. There has been only limited use of induction heating in powder metallurgy, even though its use in the powder metallurgy of titanium may be beneficial. In particular, there is a cost reduction which derives mainly from a simple processing setup and a shorter heating time. The faster heating rates and considerably shorter sintering time lead to a much shorter exposure of powder compacts to high temperatures. This may be beneficial for minimizing the amount of oxygen pick up during processing which is always an issue in the powder metallurgical processing of titanium. This chapter focuses on studies which investigate the possibility of using induction heating for consolidation of titanium and Ti6Al4V alloy powders. Both the Ti and prealloyed (PA) Ti6Al4V powders used in this work were produced by the hydrogenation- dehydrogenation (HDH) method, which gives irregularly shaped powder particles which are below 75 microns in size. The oxygen content of the as-received powders was 0.33wt% and 0.80wt% respectively for the Ti and Ti6Al4V powders. The following aspects were considered: (1) the effect of powder composition and the green density of the powder compacts on the induction heating rates; (2) the effect of green density and induction sintering conditions on the density and porosity of the sintered samples; (3) the effect of induction sintering conditions on the tensile properties and the fracture behaviour; (4) the degree of oxygen pick up during induction sintering of pure Ti powders ; (5) factors affecting the tensile properties and (6) a comparison of the results with those from other sintering methods.

3.2 The effect of powder composition and powder compact density on the induction heating rates

For each of the Ti and Ti6Al4V powders used, two series of powder compacts were prepared: Series 1, with a lower powder compact (green) density and Series 2 with a higher powder compact (green) density. The compacting pressure for Series 2 was kept similar to that used for Series 1, but the powder was preheated to 250˚C before applying the compacting pressure. The relative density of the powder compacts was obtained by calculation using the relationship between mass and volume for each compact (Table 3.1 and Table 3.2).

Table 3.1 Relative density of Ti Series 1and Series 2 powder compacts.

Ti-Series 1	Relative green density,%	Average green density, %	Ti-Series 2	Relative green density,%	Average green density, %
Ti-1-1	71.98		Ti-2-1	84.86	
Ti-1-2	72.73		Ti-2-2	85.28	
Ti-1-3	72.53	72.23	Ti-2-3	84.71	85.02
Ti-1-4	71.97	± 0.27	Ti-2-4	85.07	± 0.75
Ti-1-5	72.01		Ti-2-5	85.85	

Table 3. 2 Relative density of Ti6Al4V Series 1 and Series 2 powder compacts.

Ti6Al4V-Series 1	Relative green density,%	Average green density, %	Ti6Al4V-Series 2	Relative green density,%	Average green density, %
Ti64-1-1	61.40		Ti64-2-1	68.90	
Ti64-1-2	61.70		Ti64-2-2	69.60	
Ti64-1-3	59.86	60.65	Ti64-2-3	67.50	69.04
Ti64-1-4	59.33	± 1.10	Ti64-2-4	68.30	± 1.30
Ti64-1-5	60.01		Ti64-2-5	70.16	
Ti64-1-6	61.60		Ti64-2-6	69.78	

The increase in the density of Series 2 powder compacts is related to the reduction of the yield strength (YS) of the powders with increasing temperature[1]. The lower powder compact (green) density of the Ti6Al4V samples compared with that of the pure Ti samples is because of the higher yield strength of Ti6Al4V. Six temperature/time conditions were used for the induction sintering experiments. The same conditions were used for both Series 1 and Series 2 Ti and Ti6Al4V samples (Table 3.3). The power input on the induction heating control unit was kept 10V constant for all experiments.

Table 3.3 Induction sintering conditions.

Condition	IS1	IS2	IS3	IS4	IS5	IS6
Temperature, °C	1200	1200	1300	1300	1400	1400
Holding time, min	no hold	4	no hold	4	no hold	4

Induction heating rates were obtained for most of the experiments by recording the heating time in the relation to the temperature increase. The temperature/time curves for all recorded experiments are shown in Figure 3.1 and the calculated average heating rates are shown in Table 3.4. The average heating rates were calculated by obtaining the ratio of the final temperature and the corresponding heating time. It should be mentioned that the heating rates obtained in this study are valid only for the mass of the samples studied which was 130g. It was found that the heating rates varied depending on the composition of the powders and the powder compact density. The heating rates may vary with the sample mass. The average heating rates varied between 5. 1°C/s and 11.6°C/s (Table 3.4), depending on the green density of the powder compact and the powder composition. There was some noticeable difference found in the heating curves for Ti6Al4V samples.
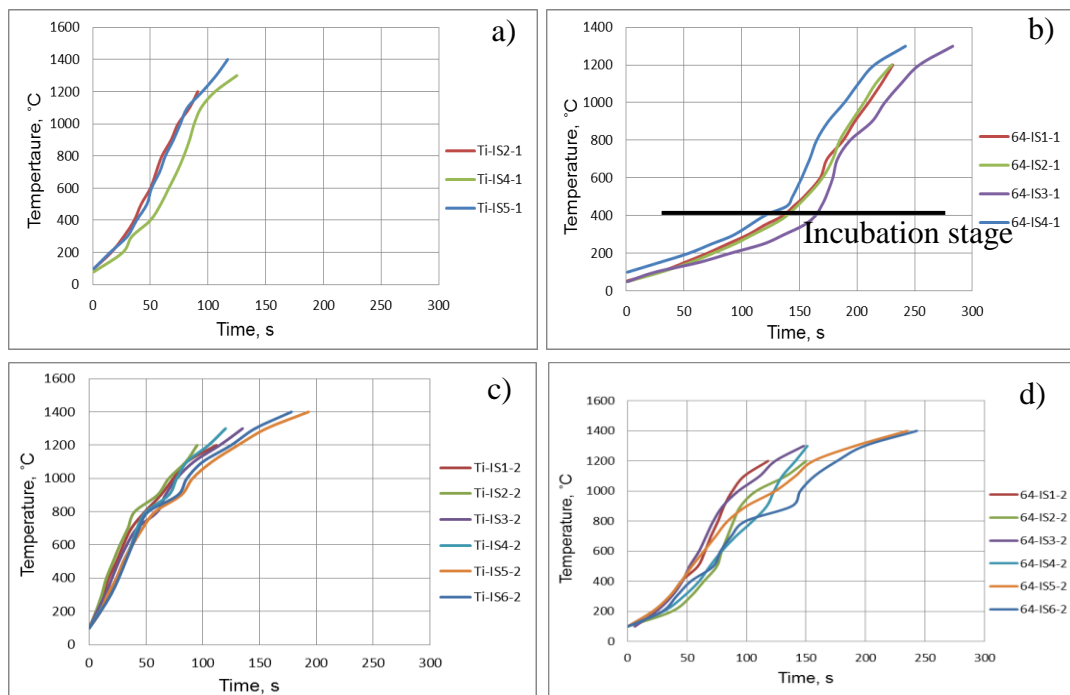
Figure 3.1 Time/temperature curves during induction sintering of a) Ti and b) Ti6Al4V powder compacts- Series 1 and Ti(c) and Ti6Al4V (d) powder compacts- Series 2.

Table 3.4 Calculated average heating rates during induction sintering of Ti and Ti6Al4V powder compacts, ˚C/s.

Series 1-Calculated heating rates, ˚C/s											
Ti						Ti6Al4V					
IS1	IS2	IS3	IS4	IS5	IS6	IS1	IS2	IS3	IS4	IS5	IS6
x	12.6	x	10.4	12.0	x	5.2	5.2	4.6	5.3	x	x
Average heating rate: 11.6±1.1˚C/sec						Average heating rate: 5.1± 0.4˚C/sec					
Series 2- Calculated heating rates, ˚C/s											
Ti						Ti6Al4V					
IS1	IS2	IS3	IS4	IS5	IS6	IS1	IS2	IS3	IS4	IS5	IS6
10.7	12.6	9.6	10.8	7.3	7.9	9.6	8.0	7.8	8.6	5.9	5.8
Average heating rate: 9.8 ± 2.7˚ C/s						Average heating rate: 7.6 ± 2.1˚ C/s					

For Series 1 there were two distinct stages: a slower heating rate of approximately 3˚C/s up to around 400˚C, followed by an increase in the heating rate to approximately 10˚C/s (Figure 3.1b). This observation is similar to that reported by other researchers (Figure 1.5 and Figure 1.7 in the literature review) [2, 3], where the authors defined the period of slower heating as an incubation period. The slower heating rate was attributed to the poor coupling between the induction coil and the powder compact as a result of the air trapped between the powder particles. The air may act as an insulator and decrease the conductivity of the material. The authors of the research study [3] suggested that preheating of the powder compact prior to induction sintering or increasing the compact density helps to minimise the amount of trapped air. The difference in the green densities found in this study supports this finding, because the incubation period during heating was significantly shorter in the Ti64-Series 2 (Figure 3.1 d) samples with a higher starting density, compared to that for Ti64-Series1 (Figure 3.1 b). Figure 3.2 and Figure 3.3 show typical heating curves for powder compacts with a similar composition but different green densities. The average heating rates of the Ti powder compacts with different green densities were similar during heating to 1300˚C (Figure 3.2). However, in the initial heating stage and up to 800˚C the compacted sample with a higher density (Series 2) heated up at a significantly faster rate. At a temperature of 800˚C the calculated heating rate of a Ti- Series 2 sample was 17.7˚C/s, compared with 10.0˚C/s for a Ti-Series 1 sample.
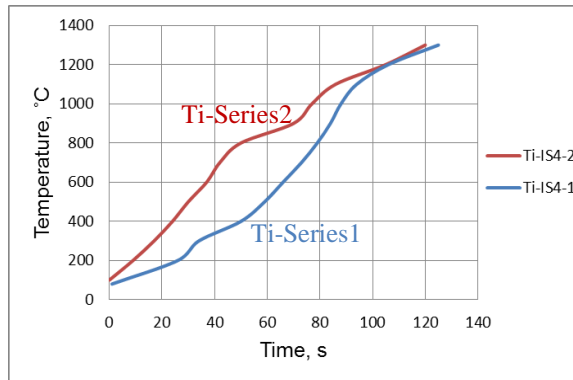
Figure 3. 2 Induction heating curves of powder compacts from Ti- Series 1 with relative density of 69% and Ti-Series 2 with relative density 85%.
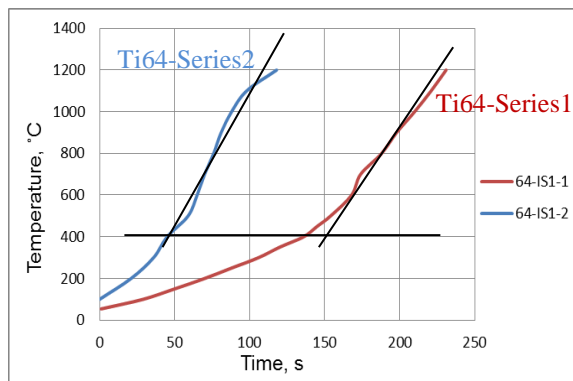
Figure 3.3 Induction heating curves of powder compacts from Ti64- Series 1 with relative density of 60% and Ti64-Series 2 with relative density 69%.

For Ti6Al4V powder compacts, the difference in the compact density had a critical influence on the heating rates (Figure 3.3). The incubation stage was much more prolonged for the powder compact with a lower relative density of 60%. Up to 400˚C the heating rate of these samples was almost three times slower compared to the Series 2 sample with a green density of 69%. After the incubation stage, the slopes of the heating curves for both samples are almost parallel.
It was also observed that it was not only the compact density which affected the heating rates but also the powder composition (Figure 3.4). It can be seen that in spite of the similar compact density of both samples, it took 110 second to heat up a Ti powder compact to 1400˚C, while for a Ti6Al4V specimen the heating time was almost doubled (240 seconds). A possible reason for the difference in the heating rate may be the lower thermal conductivity of the Ti6Al4V alloy powders compared with that of the Ti powders. The conductivity of Ti ASTM grades is 3.4 -4.1% IACS (International Annealed Copper Standard), compared to 1.1% IACS for Ti6Al4V alloy [4].

93
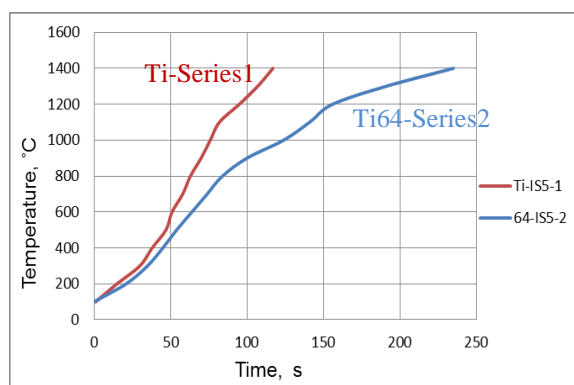
Figure 3.4 Induction heating curves of powder compacts from Ti- Series 1 with relative density of 71% and Ti64-Series 2 with relative density 69%.

Another possible reason may be the difference in the oxygen impurity content in the two powders. The Ti powders contained 0.33wt% oxygen, while the Ti6Al4V powders used in this work contained 0.80wt% oxygen. The oxygen impurity in the metal powders exists mostly as an oxide film covering the surface of the metal powder particles and these acts as an insulator with a similar effect to that of air trapped in the powder compact. Considering that the oxide layer on Ti6Al4V powder particles is much thicker than that on Ti particles, it would take longer to break down during heating. This reduces the overall conductivity of the powder compact during induction heating and slows down the heating process. Summarising the results from this section, there were three factors affecting the heating rate: the green density of the powder compacts, the composition of the powders and the oxygen content of the powders. The green density determines the amount of air trapped between the powder particles. The composition of the Ti-based powders affects the thermal conductivity. The thickness of the oxide layer surrounding each powder particle acts as an insulator and causes a reduction in the overall conductivity of the powder compact. To minimize the insulation effect and optimize the heating rate the important factor to be controlled is the green compact density. The results of this study show that green compact density should be at least 70%. It is also better to use powders with lower oxygen content, but this is not always economical and viable.

3.3 Induction sintering of Ti powder compacts

3.3.1 Effect of powder compact density and induction sintered conditions on the sintered densities

Induction sintered samples kept their integrity during induction heating with the exception of one sample. Sample Ti-IS6 from Series 1 partially melted while heating up to 1400˚C. A possible reason could be overheating due to poor temperature control. Images of some of the induction sintered Ti compacts are shown on Figure 3.5.
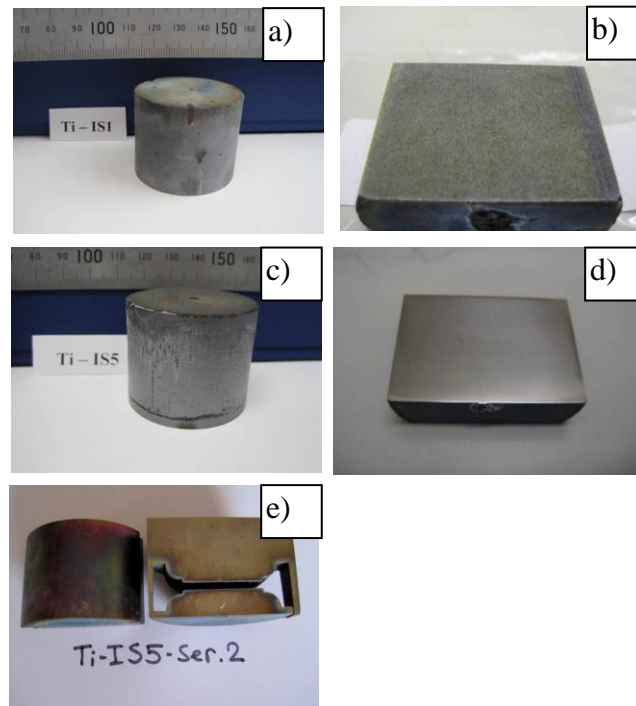
Figure 3.5 Images of induction sintered samples: Ti- Series 1 sample induction sintered at a) and b) 1200˚C, c) and d) 1400˚C, respectively without holding and 4 min holding; and e) Ti- Series 2 sample induction sintered at 1400°C without holding.

No major surface defects were observed. In some of the samples from Series 1 (samples IS2 and IS5), there were small surface cracks along the bottom section, but no cracks were observed in the samples with higher green density (Series 2). No microcracks were observed over the cross sections of any of the sintered samples.

The density increase in the Ti powder compacts as a result of IS is shown in Figure 3.6. The horizontal black lines indicate the average initial green densities

of the powder compacts. Each graph has two sections, one for the IS condition without holding at temperature and the other showing the effect of holding at maximum temperature for 4 min. Each section represents the influence of the IS temperature on the sintered density.
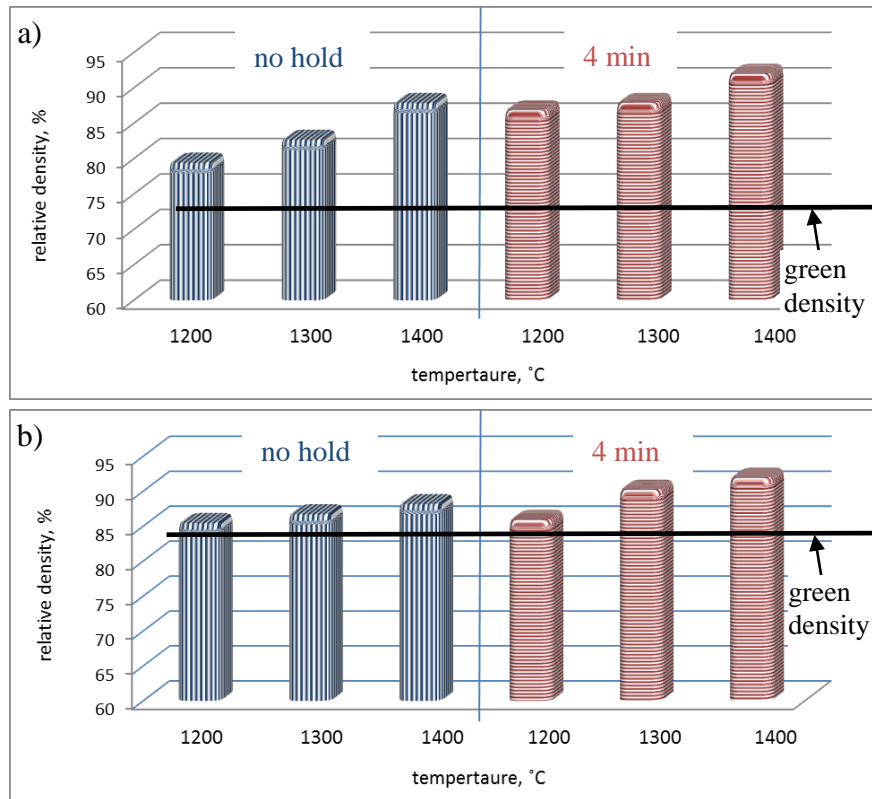
Figure 3.6 Relative densities of Ti powder compacts after induction sintering at different time-temperature conditions a) Ti- Series 1 and b) Ti- Series 2 samples.

The density increase was more evident for Series 1 samples with a lower powder compact density (Figure 3.6 a). These samples increased their density by 7.4% to 19.8%, while the samples from Series 2 increased their density by only 0.5 to 6.5% (Figure 3.6 b). The effect of the green density was fairly evident when the induction sintering was done without holding at the sintering temperature. Considering that the difference in the green densities of the two series was 12%, after sintering at 1200°C without hold at this temperature, the difference in densities dropped to 6%. Further drop of 4% and 0.3% difference was noted with increase of the sintering temperature to 1300°C and 1400°C respectively. When a 4 min holding time was included in the sintering process, the difference in the sintered densities in respect to the sintering temperature was very small, approximately 1%, with sintered densities being higher for Series 2 samples.

For Series 2 samples sintered without hold at sintering temperature, the temperature increase did not have significant effect on the densities. The density increased up to only 3%, having values of 85.4%, 86.6% and 88.1% respectively for sintering at 1200˚C, 1300˚C and 1400˚C. Introducing holding time of 4min at lower temperature of 1200˚C did not lead to major improve of the density, showing that the rate of the Ti self-diffusion was very slow at this temperature. Nevertheless, 4 min holding time at higher temperatures had more significant effect on the sintered densities, showing increase of 4.8% with increase of the temperature to 1300˚C, and further 1.8% after sintering at 1400˚C, reaching values of 90.2% and 91.8% respectively.

The reason for a greater increase in sintered density of the samples with a lower initial powder compact density can be explained by the sintering theory [5]. Sintering by itself is unbalanced process. In the initial stage of sintering, diffusion between the closely packed particles results in the formation of number of necks between the powder particles. The formation of necks is unbalanced because of the inhomogeneous packing of the powder particles. Formation of necks also leads to formation of new grain boundaries. The new grain boundaries energies are different depending on their crystallographic orientation. The unbalanced surface energies and inhomogeneous formation of necks generate torques in response to which the particles rotate or twist. In the powder compacts with lower density there are more gaps between the particles and these have more space for greater rotation and repacking, hence there is a bigger potential for a density increase during the initial stage of sintering.

3.3.2 Effect of the powder compact density and the induction sintered conditions on the porosity

Cross-sections of sintered samples were studied to observe the porosity distribution. Figure 3.**7** shows optical metallographic mapping of the cross section of two induction sintered samples from Series 1. The images show an uneven distribution of pores with more pores observed near the surface of the samples. In a sample sintered at 1300˚C without holding at the sintering temperature some of the inner regions look denser than other areas (Figure 3.7 a). A sample sintered at the same temperature but given a 4min hold at the sintering temperature appeared to be denser with a more even pore distribution in the inner region (Figure 3.7 b).

The greater spacing between the powder particles in samples with a lower green density led to preferential powder rearrangement. As a result some areas in the sintered samples have more porosity than others. The uneven distribution of pores was reduced by increasing the IS temperature and the holding time, but there were still a lot of pores remaining around the edges of the sintered samples.

Regions with less pores   Regions with more pores
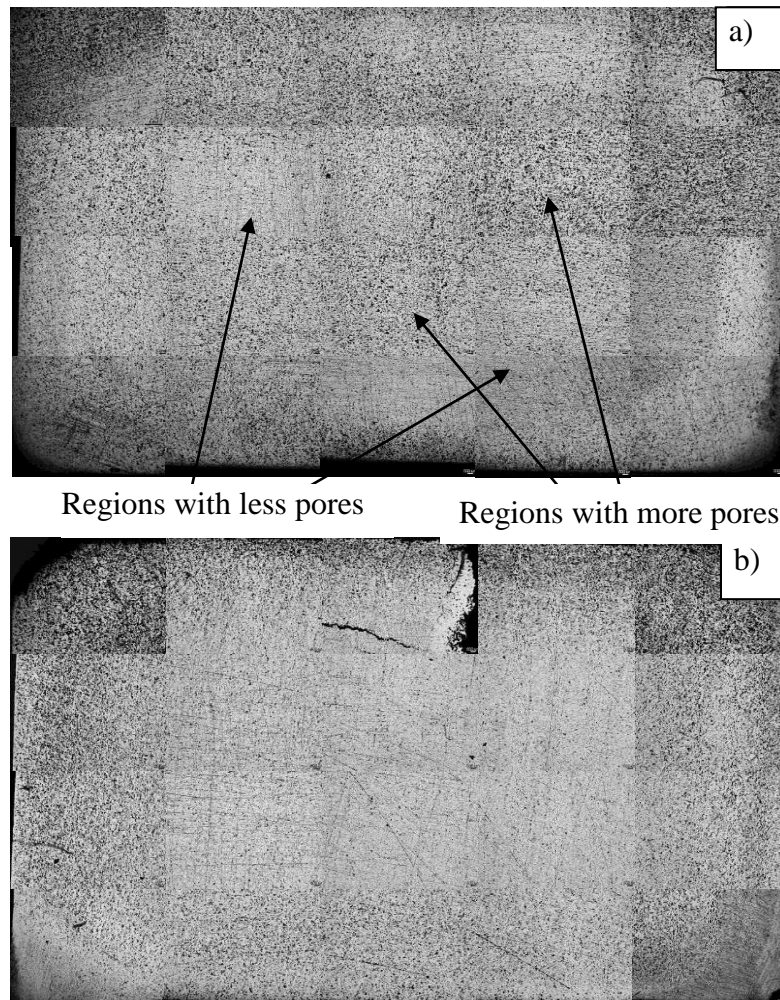
Figure 3.7 Porosity distribution in the cross section of Series 1 samples induction sintered at a) 1300˚C with no holding (IS3) and b) 1300˚C, 4 min (IS4).

The porosity distribution through the cross section of sintered Series 2 samples was more even and there was no evidence of pore segregation at the inner regions or along the surface areas (Figure 3.8).
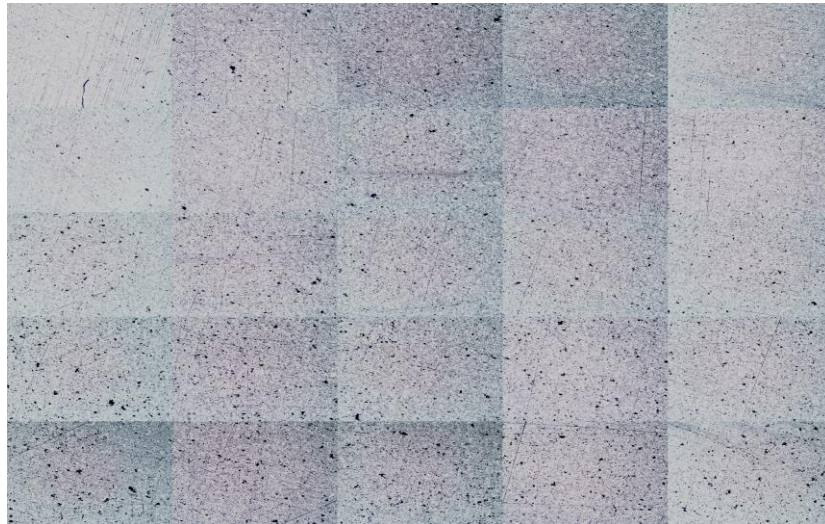
Figure 3.8 Porosity distribution in the cross section of Series 2 sample induction sintered at 1300˚C with no holding (IS3).

Figure 3.9 shows images of the porosity in the areas close to the surface. Those samples sintered at 1200˚C and 1300˚C without using a holding time showed significantly greater porosity, mostly close pores but with a large size (Figure 3.9 a) and c).
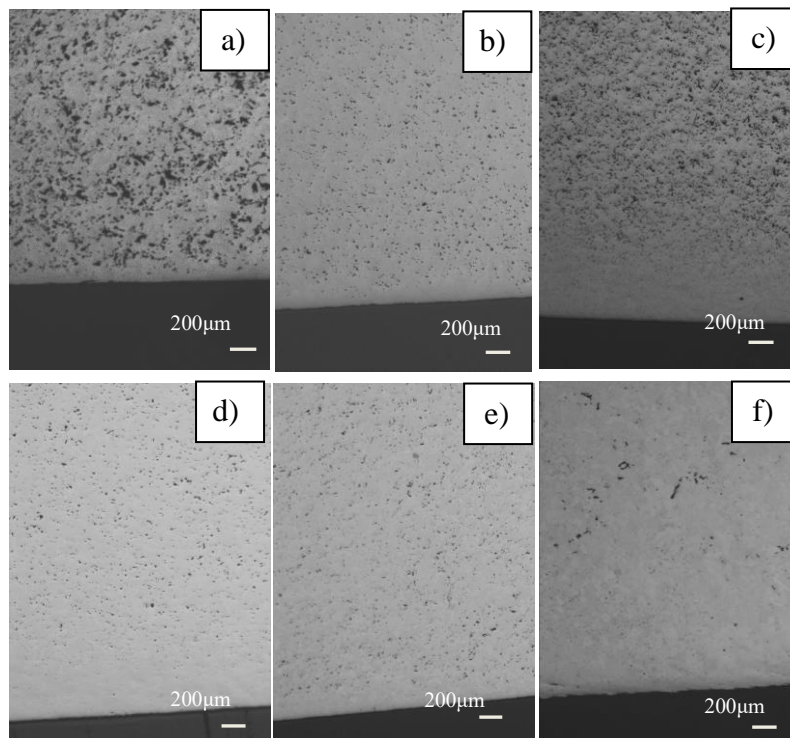
Figure 3.9 Optical micrographs showing the porosity near the surface of Ti Series 2 samples induction sintered at a) and b) 1200˚C, c) and d) 1300˚C and e) and f) 1400˚C, respectively without holding and holding for 4min.

Sintering at 1400°C without holding at temperature resulted in a significant reduction in the pores area, with only closed pores with considerably smaller size (Figure 3.9 e). Introducing a 4 min holding led to significant densification at all three sintering temperatures, evident by the large solid areas with uniformly distributed fine pores, which number gradually decreased with increasing the sintering temperature (Figure 3.9 b, d and f).

SEM was used to image the porosity in the middle sections of the as-sintered samples more closely and observe the development of the interparticle bridging, formation and growth of the diffusion necking and pore closure. This observation was limited to a single section cut from the center of each of the sintered samples. The results may vary, particularly for the Series 1 samples where the porosity distribution was not uniform along the cross section. Figure 3.10 and Figure 3.11 show images of the cross section of samples from Series 1 and Series 2 respectively, induction sintered using different conditions.
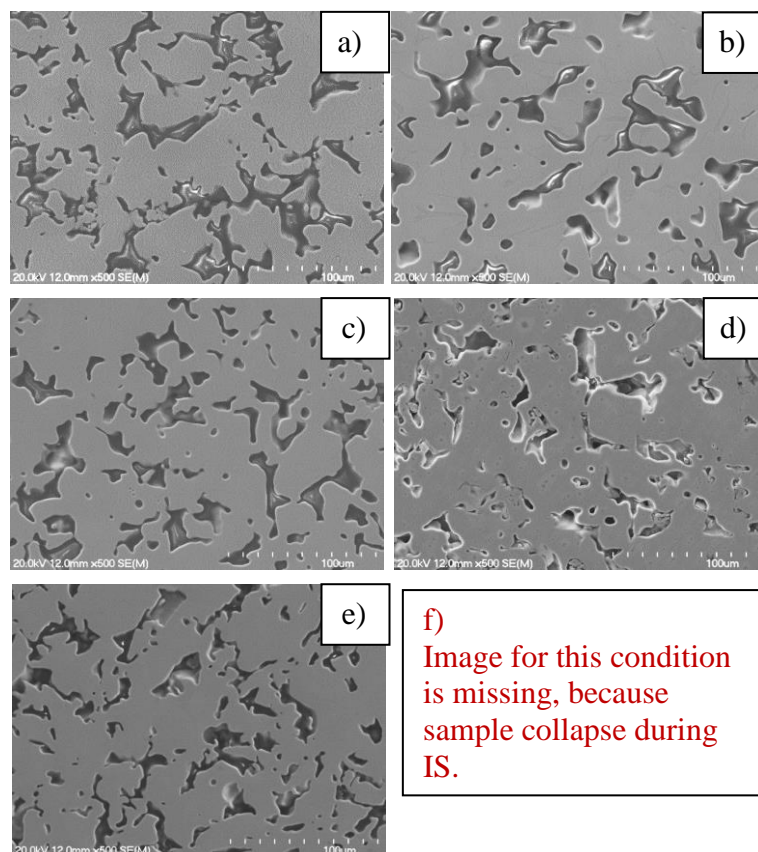
Figure 3.10 SEM images showing the porosity at the middle of the cross section of Series 1 Ti powder compacts induction heated at a) and b) 1200°C, c) and d) 1300°C and e) and f) 1400°C, respectively without holding and holding for 4min.

The appearance of the porosity in Ti- Series 1 samples at all three temperatures (IS-1, IS-3 and IS-5) (Figure 3.10 a, c and e) is fairly similar. There was evidence of neck formation, even in the very early stage of IS at 1200˚C with no holding time (Figure 3.10 a), showing that the first stage of sintering was initiated [6]. The number of diffusion necks increased with increase of the sintering temperature to 1300˚C and 1400˚C without holding at temperature (Figure 3.10 c and e), but the pore network was still evident with easily distinguishable powder particle boundaries. Holding time of 4 min led to closure of some of the inter- particle gaps and reduction in the length of the pore network was observed (Figure 3.10 b and Figure 3.10 d). A number of closed pores were formed showing that the second stage of sintering started along with the progression of stage one [6]. With the increase of the temperature, the size of interconnected pores gradually decreased and the powder particle boundaries became less visible (Figure 3.10 d). In samples with a higher green density (Figure 3.11), the first stage of sintering where the formation of diffusion necks and neck growth take place, was evident at lower temperatures of 1200˚C, even when there was no holding time at the sintering temperature (Figure 3.11 a). There were also a number of closed pores observed in this sintering condition, showing that the second stage of sintering was also started [6].
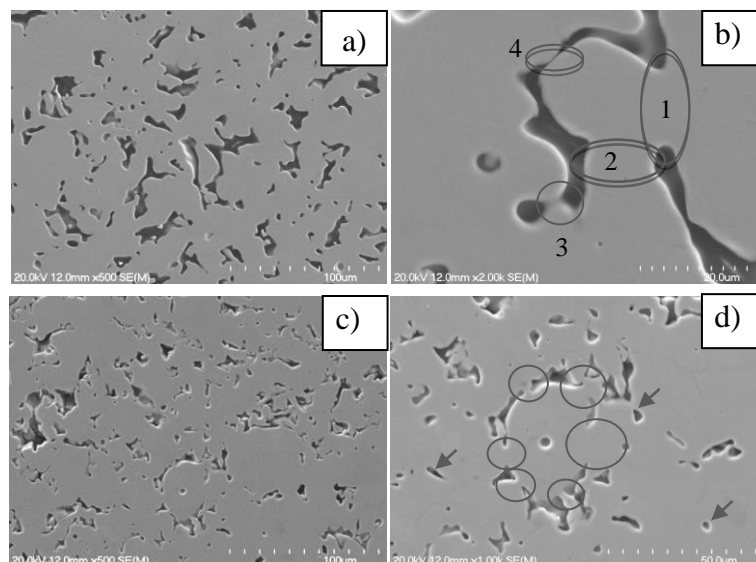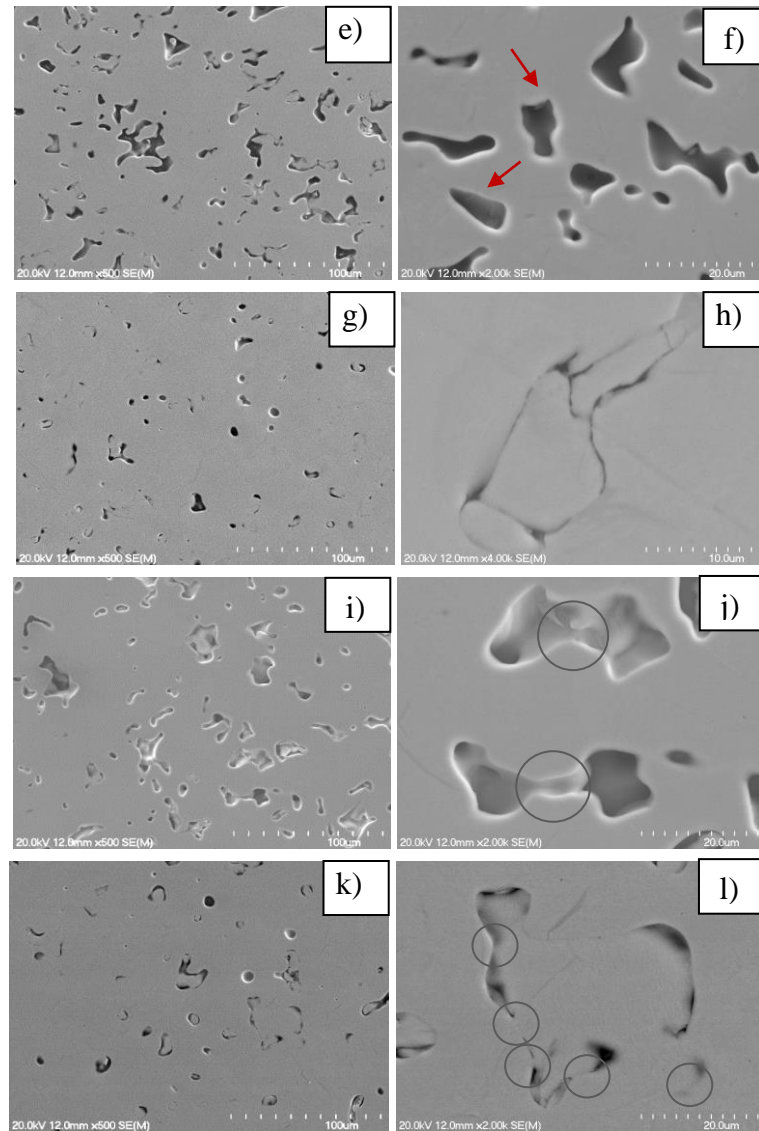
Figure 3.11 SEM images showing the porosity at the middle of the cross section of Series 2 Ti powder compacts induction heated at a) and b) 1200°C no holding c) and d) 1200°C 4min, e) and f) 1300°C no holding, g) and h) 1300°C, 4min, i) and j) 1400°C no holding and k) and l) 1400°C 4min.

With increase of sintering temperature, the areas of the pore network gradually decreased, the powder particle boundaries almost disappeared and large number of closed pores was well evident (Figure 3.11 c) and e). Holding for 4min at 1200°C led to closure of some of the interparticle gaps which led to reduction of the size of the pore network and the total porosity area (Figure 3.11 d). At higher sintering temperature and 4 min holding time, there were almost only closed pores with mostly rounded appearance and size in the range of 5-10 microns (Figure 3.11 g) and k). The amount of the total solid areas increased. This is evidence that the

sintering process was in its final stage where the closed pores started to seal. But fully sintered material was not yet formed.

Figure 3.11 (the higher magnification images) shows the development of interparticle diffusion during IS of Ti-Series 2 samples. Figure 3.11 b) shows the uneven development of interparticle necking, where two of the necks are well developed, while the third one is just formed. A forth neck is about to form. Figure 3.11 d) shows the two different stages of sintering. The first stage is evident by the multiple necking developed along a larger powder particle (circled areas). Each neck has a different surface area showing again the unbalanced neck formation. There were also areas where the sintering was in its second stage evident by appearance of closed porosity (shown by the arrows). Figure 3.11 f) shows areas with significant amount of closed porosity, which is evidence of extended interparticle diffusion during sintering at 1300°C without holding. The first stage of sintering was almost competed and the second stage of formation of closed porosity just started, evident by the uneven size of the pores.

 Figure 3.11 h) shows very closely packed powder particles as a result of the rotation and repacking caused by the unbalanced neck formation and growth. There were still no diffusion bridges observed at this cross section of the particle. Figure 3.11 j) shows the closure of the last section in a pore network. Figure 3.11 l) shows a closely packed powder particle, where formation of multiple necking is closing the last gaps (circled areas). In this sintering condition, all three stages of sintering were evident- neck formation and growth, formation of closed porosity and pore coalescence and the last stage of sealing the closed rounded pores to form solid material [6]

In general, the sintering progress in Ti-Series 2 samples was more evident and more influenced by the sintering conditions. The reason for this was the higher initial powder compact density. The higher green density resulted in smaller gaps and a bigger area of physical contact between the powder particles. Both of these aspects improved the overall conductivity of the powder compact which increased the efficacy of induction sintering by Eddy currents during sintering. Moreover, the increased number of interparticle contact points increased the chances of forming a large number of diffusion bonds. Less time was needed for pore closure because of the initially smaller gaps between the powder particles and the increased number of diffusion bridges.

3.3.3 Effect of the induction sintered conditions on tensile properties and fracture surfaces

Tensile test pieces were taken from each of the Series 1 and 2 induction sintered compacts, as shown in Figure 3.5 e), and their tensile behaviour was evaluated. Some of the stress-strain curves are shown in Figure 3.12. The actual values of the tensile test results of the green sample and the induction sintered samples are given in Table 3.5. Data for the tensile test is not available for Ti-IS6 from Series 1 sample. This sample collapsed during the IS and tensile test pieces were not able to cut. The stress-strain curve for sample Ti-IS3-Series 1 is not visible in the graph (Figure 3.5 a) because is overlapped with the curve of Ti-IS5-Series 1.
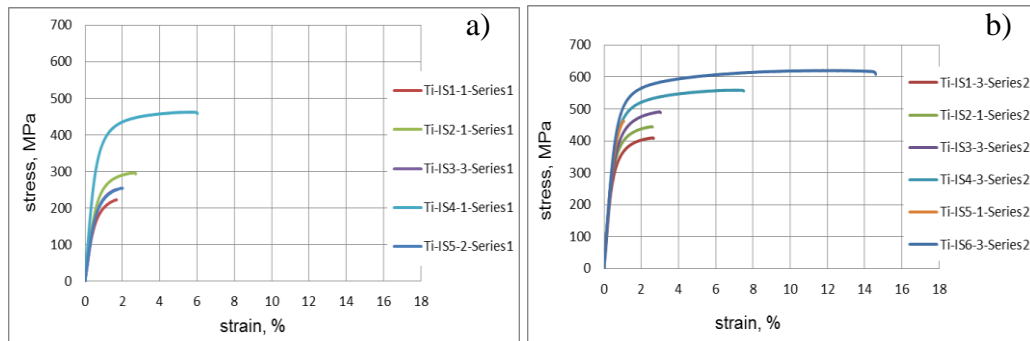
Figure 3.12 Stress-strain curves of Ti induction sintered samples: a) Series 1 and b) Series 2.

Table 3.5 Tensile properties of Ti-Series 1 and Ti-Series 2 samples induction sintered at different temperatures and holding times.

Temperature, °C	Ti-Series 1						Ti-Series 2					
	IS holding time						IS holding time					
	no hold			4 min			no hold			4min		
	YS, MPa	UTS MPa	ε, %	YS, MPa	UTS MPa	ε, %	YS, MPa	UTS MPa	ε, %	YS, MPa	UTS MPa	ε, %
1200	169 ±9	214 ±7	1.5 ±2.0	242 ±5	287 ±5	2.4 ±2.0	320 ±2	405 ±4	2.5 ±1.5	387 ±7	412 ±12	2.3 ±2.0
1300	190 ±13	242 ±7	1.7 ±0.5	**367** ±29	**438** ±24	**5.8** ±0.5	398 ±5	486 ±9	2.8 ±3.0	**506** ±9	**557** ±11	**5.8** ±2.2
1400	215 ±5	248 ±5	1.6 ±0.4	-	-	-	420 ±5	455 ±23	0.9 ±0.2	**550** ±9	**618** ±3	**13.2** ±1.2
Green compact samples - Ti-Series 2: Max Tensile Strength: 67±8 MPa No yield and ductility was observed												

Unlike the tensile behaviour of green samples, after induction sintering tensile test pieces yielded before fracture. There was a significant increase in yield and tensile strength after induction sintering, particularly for Series 2 test-pieces, and the stress-stain curves showed increasing amounts of plastic flow (Figure 3.12) as the sintering temperature increased. For Ti-Series 1 sintered without holding at the sintering temperature, the maximum tensile strength increased from 214MPa to 248MPa with increasing sintering temperature from 1200˚C to 1400˚C. Introducing a holding time of 4 min was not very effective when sintering at 1200˚C, but when the sintering temperature was increased to 1300˚C there was nearly twice the increase in yield strength and the UTS, reaching 367MPa and 438MPa respectively. There was also a large improvement in ductility to 5.8% elongation to fracture. This is more than three times the ductility values given by the other sintering conditions.

The tensile properties for Series 2 samples were much higher. For sintering without holding at the sintering temperature, the values of the YS and UTS varied between 320MPa to 420 MPa and 400MPa and 486MPa respectively with a maximum elongation to fracture of 2.8%. Similarly to Series 1, a 4 min hold at 1200˚ C did not significantly improve the tensile properties. However, 4 minute hold at higher temperatures of 1300˚C and 1400˚C (Figure 3.12 b) significantly increased the YS, UTS and elongation to fracture. For the sample sintered for 4min at 1400˚C the average tensile properties were YS of 550MPa, UTS of 618MPa and 13.2% elongation to fracture. The properties of all three samples tested were consistent with UTS within 3MPa and elongation to fracture within 1.2%.

The fracture surfaces of the tensile specimens were analysed by SEM.

A fracture surface of a green powder compact from Series 2 (Figure 3.13) shows closely packed powder particles. Fracture occurred along powder particle boundaries because powder cohesion was largely by powder particle interlocking achieved during powder compaction. There were no features in the fracture surface to indicate that a solid material had been tested and this explains the very low tensile strength obtained.
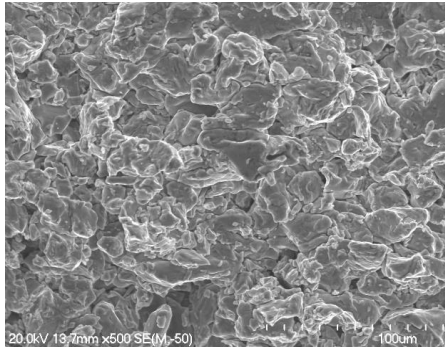
Figure 3.13 SEM image of the fracture surface of a green sample from Series 2.

The fracture surfaces of the tested tensile specimens contain two distinct features: smooth surfaces (indicated by black arrows) in Figure 3.14 and Figure 3.15 and uneven dimpled surfaces (indicated by white arrows) in Figure 3.14.
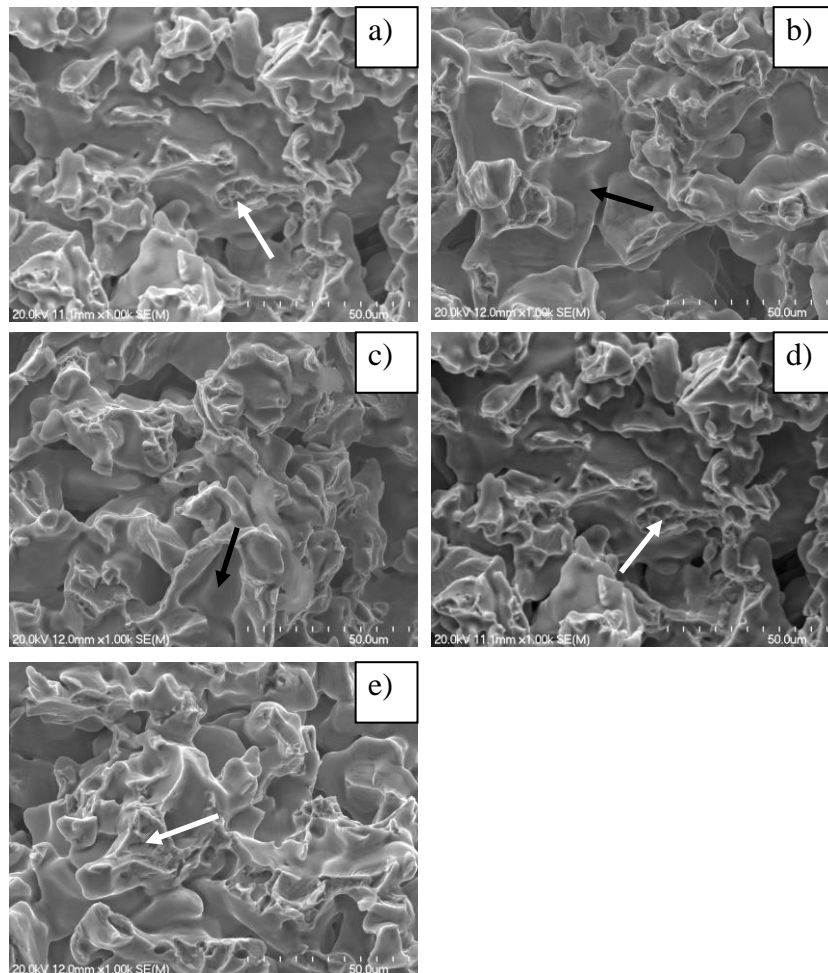
Figure 3.14 SEM images of fracture surface of tensile tested samples cut from Ti Series 1 samples induction sintered at a) and b) 1200˚C, c) and d)1300˚C and e) 1400˚C, respectively without hold and 4 min hold.
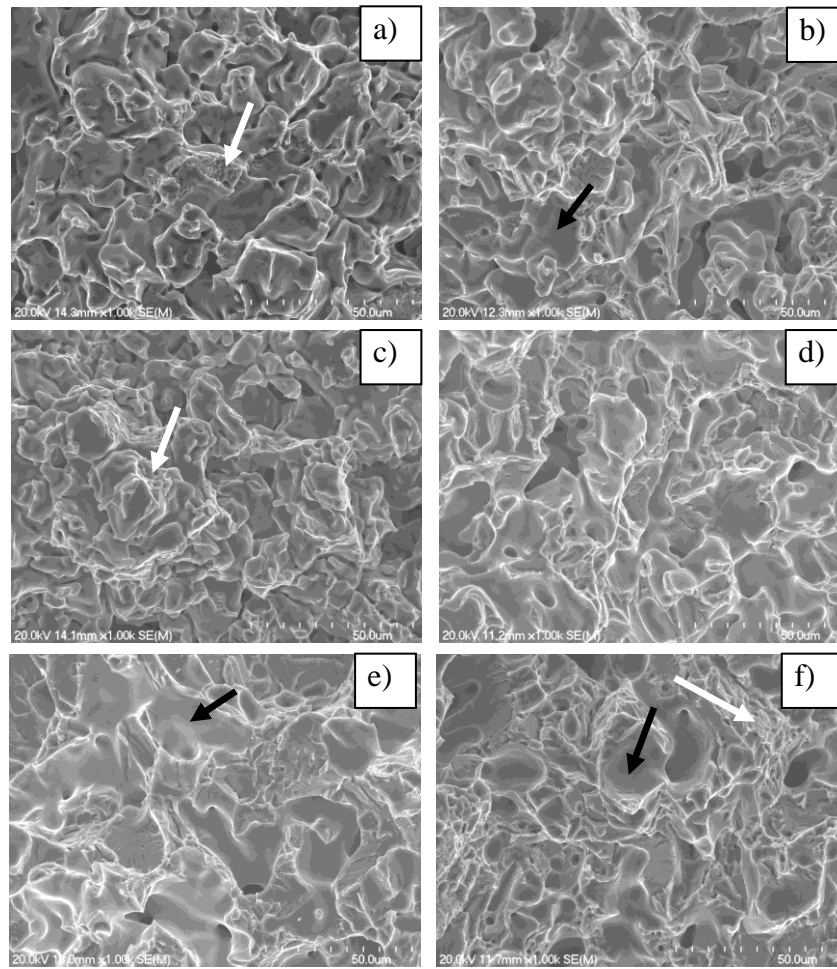
Figure 3.15 SEM images of fracture surface of tensile tested samples cut from Ti Series 2 samples induction sintered at a) and b) 1200˚ C, c) and d)1300˚ C and e) and f) 1400˚ C, respectively without hold and 4 min hold.

The smooth surfaces are powder particle surfaces where interparticle diffusion did not occur. These are the regions with porosity. The surfaces shown by the white arrows are places where diffusin occurred and necking between the powder particles formed. The fracture features in these regions were formed by fracturing at the necks between the powder particles and have a typical solid fracture appearance. This is further evidence that sintering occured during the short heating time which explains the increase in tensile strength, even for those samples induction heated to a comparatively low temperature of 1200°C without holding at temperature. The total area of the regions showing typical solid fracture features varies depend on the initial green density, and the induction sintering conditions.

The fractographs in Figure 3.14 a) and Figure 3.15 a) for Series 1 and Serie 2 respectively, show that after induction sintering at lower temperatures of 1200°C and 1300°C without holding at the sintering temperature, only a few isolated areas of solid fracture can be seen. This indicates the initial stages of necking between the powder particles. For Series 1 samples the number of areas showing solid fracture increased when sintering at 1300˚C with a 4min hold at temperature and at 1400˚C (Figure 3.14d and e) respectively. There are more isolated regions with larger amounts of dimpled fracture. For Series 2 samples, holding for 4 min at temperatures of 1300°C (Figure 3.15 d) and 1400˚C (Figure 3.15 e and f) resulted in a significant increase in the total solid fracture area. These areas had formed an extended network and this is particularly evident in the sample sintered for 4 min at 1400˚C. The solid fracture surface has a dimpled appearance, which explains the much improved ductility in all of the tested samples.

In summary, the results for sintered density, degree of porosity, fracture surface appearance and tensile properties show that the degree of consolidation of Ti powders by induction sintering is closely dependent on three factors: the initial green densilty of the powder compacts, the induction sintering temperature and the amount of time a compact remains at the sintering temperature. A higher green density increases the surface contact area between the particles. More closely packed powder particles have a greater chance of forming large numbers of diffusion bridges and this in turn increases the consolidated area in those samples. A higher sintering temperature increases the diffusion rate and holding at the sintering temperature allows for prolonged sintering and more overall diffusion. It was evident that at temperature of 1200˚C the difusion rate was low and not much progression in the consolidation was observed with increase of the sintering time. The results show that a higher green density of 85% in a combination of induction sintering temperature of 1300˚C and 1400˚C and sintering time of 4 min resulted in improved consolidation and tensile properties.

3.3.4   Oxygen analysis of induction sintered Ti compacts

Table 3.6 shows the results of oxygen analyses for the induction sintered samples from both Series1 and Series 2. The data show an increase in oxygen content after

induction sintering in the samples for all temperature and time conditions, compared to the original oxygen content (0.33wt%).

Table 3.6 Oxygen content of Ti samples induction sintered under different conditions.

Series 1	Oxygen content, wt%	Series 2	Oxygen content, wt%
Ti-IS1	0.80	Ti-IS1	0.53
Ti-IS2	0.67	Ti-IS2	0.60
Ti-IS3	0.67	Ti-IS3	0.48
Ti-IS4	0.78	Ti-IS4	0.50
Ti-IS5	0.69	Ti-IS5	0.56
Ti-IS6	-	Ti-IS6	0.51

The samples with a higher green compact density (Series 2) seemed to pick up considerably less oxygen during processing. The induction sintering conditions, such as temperature or holding time, did not have a significant effect on the amount of oxygen pick up. Holding for 4 min at the induction sintering temperature did not lead to increased oxygen contamination. The degree of oxygen pick-up was very high for the amount of time the titanium powders were exposed to high tempertaures. This confirmed the extreme sensitivity of the titanium to oxygen pick up especially when processing using pure Ti powders.

3.3.5 Factors affecting the tensile properties

The tensile properties were affected mainly by three factors: the sintered density, porosity distribution and the oxygen content after sintering. It was observed that the porosity and density played, to some extent, independent role in the mechanical properties of the sintered samples. This was evident from the results, where two samples with similar density (Series 1 samples, with IS profile 1300°C 4min and 1400°C no hold) have significantly different tensile properties (Table 3.5). This is because the sample hold for 4min shows larger number of closed pores (Figure 3.10 d), while the other sample shows more uniformly distributed but mostly open porosity (Figure 3.10 e).

In Series 2 samples, the effect of the sintered density is more evident. The YS and UTS gradually increase with the density increase. As the density increase the gaps between the particles become smaller. In those samples with higher density and

smaller pores (Figure 3.10 d) and Figure 3.11 d) and f), the tensile strength was significantly higher (Table 3.5, the results in bold). This is in relation to the concept of fracture mechanics where the strength of the material is related to the size and geometry of the crack (or the pore in the case of PM) given by equation 5.1 [7]:

$$K_{Ic}=Y\sigma\sqrt{\pi a} \qquad (5.1)$$

K_{Ic}- critical stress intensity (fracture toughness), Y- crack geometry factor, σ- stress, a- half-crack length

In the samples having mostly closed pores, the increase of the density led not only to improvement in YS and UTS but also significant increase in the elongation to fracture. Increase of the density from 90% to 91.7% led to increase in elongation to fracture more than twice, reaching value of 13.2%.

The oxygen content also played significant role in the tensile properties. It was noted that the oxygen content after induction sintering (Table 3.6) is higher than the one specified in the ASTM standard of PM Ti structural components [6], where the oxygen content vary between 0.18 to 0.4wt% depending on the Ti Grade. It is well known that oxygen can have a strengthening effect in Ti [1]. It was also noted that the YS and UTS of IS samples, particularly the ones with relative densities over 90%, are significantly higher compared to those in the ASTM standard. These high values of YS and UTS were clearly related to the increased oxygen content.

The effect of the oxygen on the plastic deformation was difficult to evaluate even though from the literature, increase of the oxygen content clearly leads to reduction of the ductility [1]. The values of elongation to fracture in most cases were fairly low but the main reason was found to be the presence of open porosity. In a sample with closed porosity and relative density of 92.7%, the elongation to fracture reached 13.2%. Even though this value is comparatively high, it is within 5% lower than the standard values of elongation to fracture of Ti Grade 4. So the reason for the lower plastic flow might be the high oxygen content but also the lower sintered density should be taken in consideration.

3.3.6 Comparison of the properties of induction sintered Ti with thouse obtained by other sintering methods

The induction sintered Ti specimens from both Series 1 and Series 2 showed improved physical and mechanical properties after induction sintering at temperatures above the β-transus. The results of the effect of induction sintering temperature and holding time are in agreement with the research results found in other studies on IS of other than titanium metallic materials [8-10], where a sintering effect was also evident only after heating for 0.5 to 5 min at the required sintering temperature. Similarly, the mechanical properties increased with sintering temperature and sintering time.

The comparison of the physical and mechanical properties of Ti powders consolidated by other sintering methods is shown in Table 3.7.

Table 3.7 Properties of Ti powders sintered by different methods.

Sintering method	Type of Ti and oxygen content:	Powder compact green density, %	Sintering parameters:	Sintered Density, %	YS, MPa	UTS, MPa	ε,%	Reference
Induction sintering	HDH (0.33wt% O)	72	1300°C, 4 min	87.8	367	438	5.8	This study
		85	1300°C, 4 min	90.2	506	557	5.8	This study
		85	1400°C, 4min	91.8	550	618	13.2	This study
		83.8	1350°C, 3min	91.0	470	575	7.5	[11]
Vacuum sintering	HDH (0.33wt% O)	72	1350°C, 120 min	92.5	Not reported	576	7.0	[12]
	HDH (0.27wt% O)	85	1250°C, 120min	96.0	≈500	≈570	10.0	[13]

			1300°C, 120min	96.4	Not reported	≈565	9.2	
			1350°C, 120min	96.8	Not reported	≈590	12.0	
	HDH (<0.4wt%O)	Not reported	1100°C, 120 min	92	Not reported	Not reported	Not reported	[14]
			1300°C, 120 min	96.2	Not reported	Not reported	Not reported	
	GA (0.15wt% O)	Not reported	Not reported	95.5	324	414	15	[15]
	HDH	63 / 73 / 85	1200°C, 120 min	78 / 86 / 92	Not reported	Not reported	Not reported	[16]
	HDH	76 / 80 / 85 / 92	1300°C, 120 min	91 / 92 / 94 / 97	Not reported	Not reported	Not reported	[17]
Microwave sintering	HDH	63 / 73 / 85	1200°C, 120 min	76 / 88 / 93	Not reported	Not reported	Not reported	[16]

When the properties obtained using different sintering methods, such as induction sintering (IS), vacuum sintering (VS), and microwave sintering (MWS), are compared some general conclusions can be made about sintered densities and tensile properties achieved by different sintering methods:

(i) The green powder compact density strongly influences the sintered density.

(ii) Pure Ti HDH powders are difficult to sinter to full or near full density. Even VS powder compacts with a relative green density 92% for 2h at 1300°C achieved only 97 % relative sintered density [17].

(iii) Induction sintering, having a considerably shorter sintering time of up to only 4 min, gives a good combination of sintered density and mechanical properties comparable to those obtained from vacuum sintered Ti HDH powders.

(iv) The initial oxygen content of the Ti powders has a strong influence on the tensile properties. When low oxygen Ti GA powders were used, the UTS of the

consolidated material were with approximately 200MPa lower compared to that obtained with Ti HDH powders. The oxygen content of the powders had less effect on the elongation to fracture. The elongation to fracture of material made with GA powders is 15% compare to 10 to 13% when HDH powders were used.

3.4 Induction sintering of Ti6Al4V powder compacts

3.4.1 Effect of powder compact density and the induction sintered conditions on the sintered density of Ti6Al4V powder compacts

The Ti6Al4V samples were induction sintered using similar conditions to those for the Ti samples (Table 3.3). The relative density of the green powder compacts was on average 61% for Series1 and 69% for Series 2 (Table 3.2). Digital images of some of the induction sintered samples are shown in Figure 3.16 and Figure 3.17.
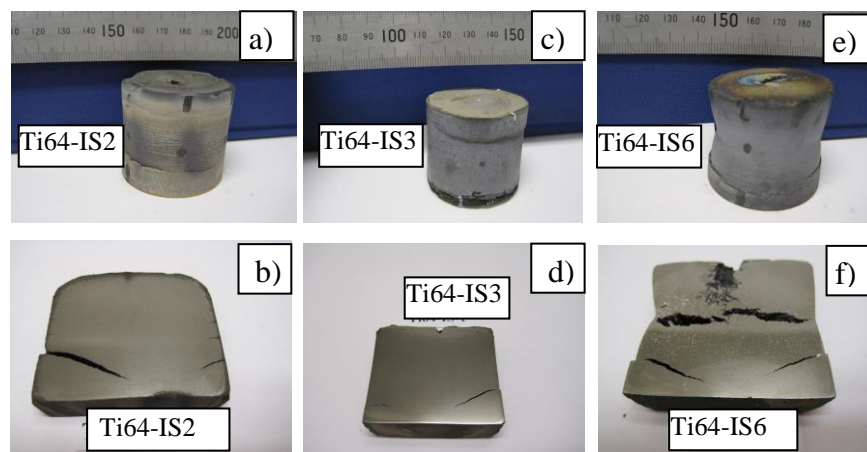
Figure 3.16 Images of Ti6Al4V- Series 1 samples and their polished cross sections induction sintered at: a) and b)1200˚C 4min (IS2), c) and d) 1300˚C without holding (IS3), e) and f) 1400˚C for 4min (IS6).

The samples from Series 1, with lower green density, kept their outer shape when sintered up to 1300˚C. However, a large crack in the bottom half of each sample, running through the cross section was observed. Heating to 1400˚C caused a distortion of the cylindrical shape, observed mainly at the middle section along the perimeter (Figure 3.16 e). Big cracks formed in the bottom half as well as in the middle of the cross section (Figure 3.16 f).

113

Series 2 samples had a better outer appearance after induction sintering for all sintering conditions. There was no observable shape distortion after sintering and compacts also had a smoother surface. Some internal cracking can be seen in the cross section shown in Figure 3.17.
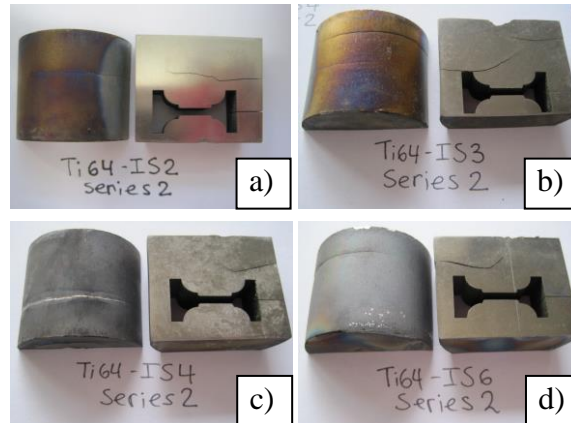
Figure 3.17 Images of Ti6Al4V- Series 2 samples and their polished cross section, induction sintered at a) 1200°C for 4min, b) 1300°C no hold, c) 1300°C 4min and d) 1400°C 4min.

The results of density measurements of Ti6Al4V powder compacts, with different initial green densities, after induction sintering are shown in Figure 3.18. There was an increase in density in all of the induction sintered samples compared with their green density. Series1 samples achieved densities ranging from 64.8% to 86.8% depending on the induction sintering conditions. For similar induction sintering conditions, the samples from Series 2 achieved sintering densities from 74.4% to 85.4%.
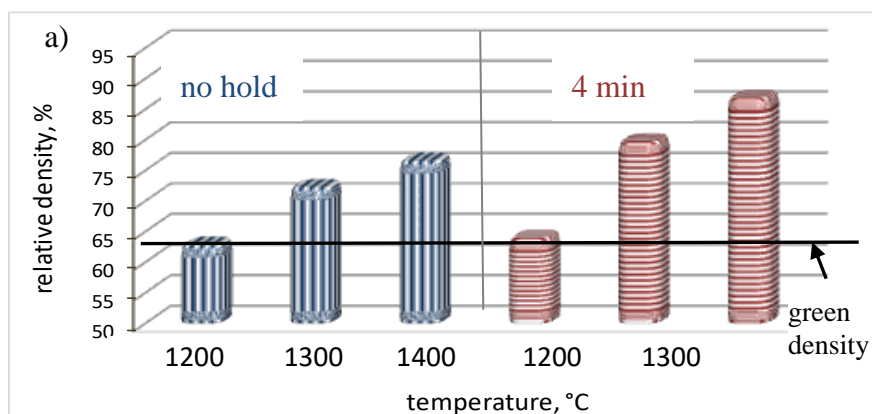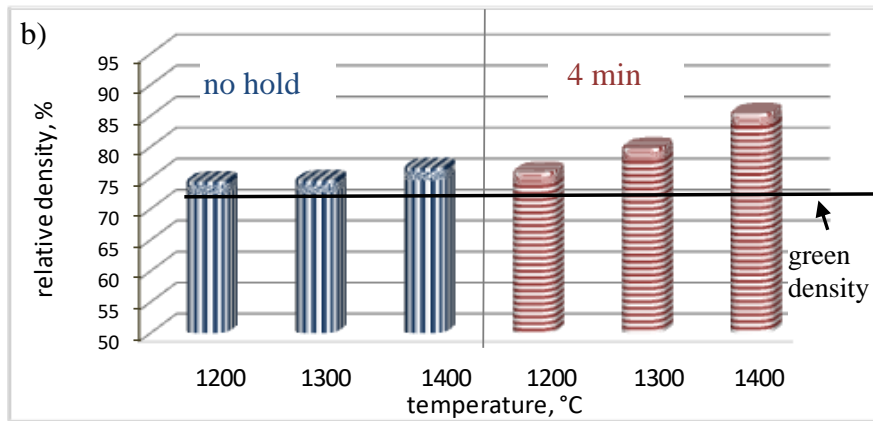
Figure 3.18 Relative densities of Ti6Al4V powder compacts before and after induction sintering at different time- temperature conditions: a) Ti64-Series 1 and b) Ti64-Series 2, samples.

The beneficial effect of a 4 min holding time on the sintered density was much more evident at higher sintering temperatures of 1300˚C and 1400˚C, where the density increase was approximately 25% and 13% for Series1 and Series 2 respectively.

The final densities at the later sintering conditions were similar for both series. The increased densification of the powder compacts with lower green density is related to the sintering theory and it was explained previously in this chapter (Section 3.3.1). At a sintering temperature of 1200˚C, increase of the holding time to 4 min did not have a significant effect on the sintered density, explained with the lower diffusion rate of Ti at this temperature conditions.

3.4.2 Effect of the induction sintering parameters on the porosity of sintered Ti6Al4V powder compacts

Similarly to the induction sintered Ti samples, all Ti6Al4V induction sintered samples were cut along the longitudinal axis and polished for metallographic examination. Optical microscopy was used to develop a map of porosity distribution along the longitudinal cross section of each sample. Some of the maps are shown in Figure 3.19 and Figure 3.20 for Series1 and Series 2 respectively. The pore distribution in the Ti64-Series 1 samples is very uneven. A large number of small pores were observed along the top and bottom section, while the central regions appeared denser with a significantly reduced number of pores of larger size. There was cracking in the samples from both series, but the cracks were

much larger in samples sintered at higher temperature with a 4 min hold. Cracks formed in samples from Series 2 were considerably smaller than those found in Series 1 samples and were mainly distributed in the areas close to the outer surface. The size of the cracks and the pores are in a close relation to the green density and the level of densification.
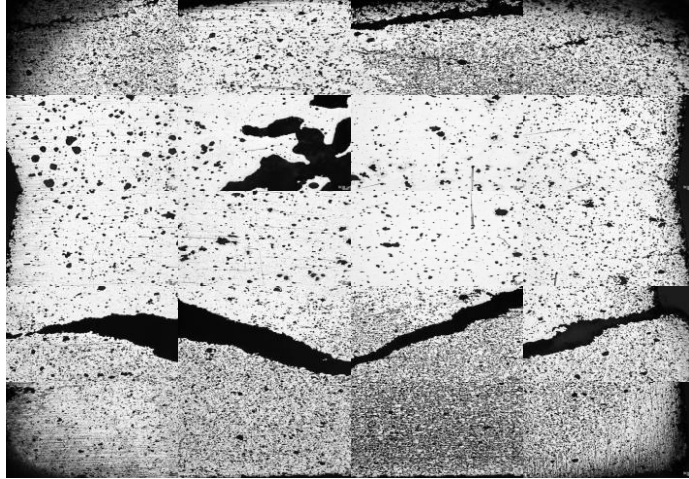
Figure 3.19 Optical micrograph map of the porosity distribution in the cross section of Ti6Al4V sample from Series 1 induction sintered at 1400˚C with no holding at sintering temperature.
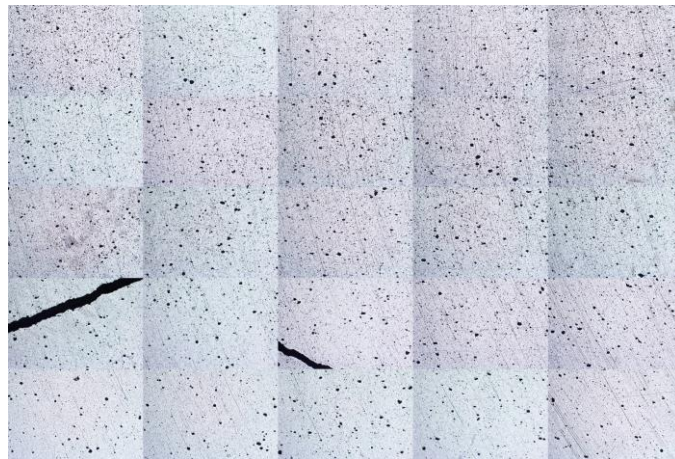
Figure 3.20 Optical micrograph map of the porosity distribution in a cross section of Ti6Al4V sample from Series 2 induction sintered at 1400˚C with no holding at sintering temperature.

The presence of cracks and uneven porosity showed that the green densities were low but also showed uncompleted densification. The uneven formation of diffusion necks in a combination of large amount of space between particles caused preferential rotation, rearrangement and repacking of the powder particles. Because of the large gaps between the particles, they have chance for significant

movement which led to formation of large gaps. The sintering time from other hand was not enough to complete the diffusion and close these gaps.

SEM was used for a closer and more selective examination of the porosity. A sample was taken from the centre of each of the sintered compacts. The SEM images of the polished surface of those samples are shown in Figure 3.21 and Figure 3.22 respectively for Series1 and Series 2 samples.
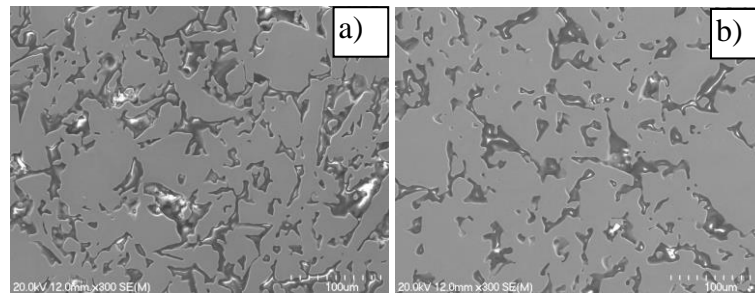
Figure 3.21 SEM images showing the porosity at the middle of the cross section of induction sintered Ti-6Al-4V Series 1 samples a) 1200˚C 4min and b) 1400˚C 4min holding.
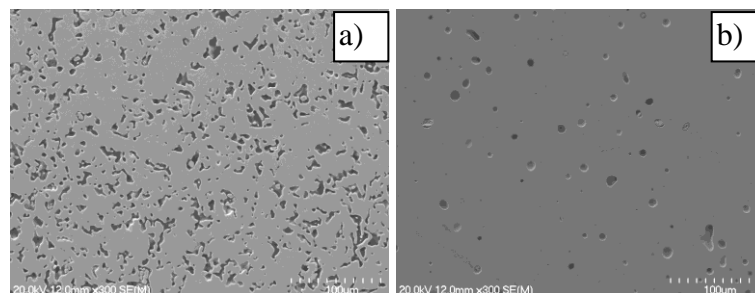
Figure 3.22 SEM images showing the porosity at the middle of the cross section of induction sintered Ti-6Al-4V Series 2 samples a) 1200˚C 4min and b) 1400˚C 4min.

There was a significant difference in the porosity observed in Series 1 and Series 2 sintered samples. The pores formed in Series 1 samples were elongated and clearly situated along the powder particles boundaries. After sintering at a lower temperature of 1200˚C the pores were still interconnected (Figure 3.21 a). Only in a few places, powder particle necking start to develop. The powder particle necking significantly increased with increasing sintering temperature and holding at temperature for 4min (Figure 3.21 b) but interconnected porosity was still present. For the same sintering conditions, the specimens from Series 2 showed significantly reduced porosity with much smaller pores (Figure 3.22). The pores

were mostly closed but still had an irregular shape when sintering was at 1200°C for 4 min (Figure 3.22 a). Increasing the sintering temperature to 1400°C with holding for 4 min led to closure of the majority of the pores. A few larger pores with a rounded appearance were still observed in this sample (Figure 3.22 b).

3.4.3 Tensile properties and fracture behaviour of induction sintered Ti6Al4V samples

Three tensile test pieces, taken from the middle section of each of the induction sintered samples, were prepared and tested. Typical stress-strain curves from both Series 1 and Series 2 samples are shown in Figure 3.23. The average values for the maximum tensile strength are given in Table 3.8.
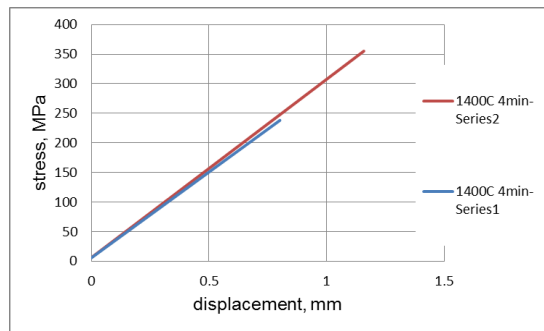
Figure 3.23 Typical tensile stress strain curves of Ti6Al4V induction sintered samples from Series 1 and Series 2, after sintering at 1400° C with a 4 min. hold.

Table 3.8 Maximum tensile strength of Ti64-Series 1 and Ti64-Series 2 samples induction sintered at different temperatures and holding times.

IS Conditions		Maximum Tensile Strength, MPa	
		Series 1	**Series 2**
Green compact		-	15±2
1200° C	no hold	65±5	245±70
	4min	60±2	280±56
1300° C	no hold	140±18	266±53
	4min	248±56	331±11
1400° C	no hold	261±37	353±17
	4min	274±43	357±12

An extensometer was not available to obtain the tensile strain in the test pieces. Instead, values of the displacement of the tensile test machine cross head are plotted in Figure 3.23. All sintered samples showed an increase in tensile strength

compared to the powder compacts. The maximum tensile strength gradually increased with increasing sintering temperature, but the effect of holding time at temperature is inconclusive. For some samples the tensile strength was improved when holding for 4 min at the sintering temperature, while for others the effect of holding time was insignificant. The Series 2 tensile specimens achieved a comparatively higher maximum tensile strength. Nevertheless, all the induction sintered samples had a much lower tensile strength compared to that for press and vacuum sintered Ti6Al4V alloy [18, 19]. Also there was no yielding or observable plastic deformation in any of the tensile specimens.

Fracture surface analysis confirmed the results of the porosity observation and tensile tests (Figure 3.24 and Figure 3.25).
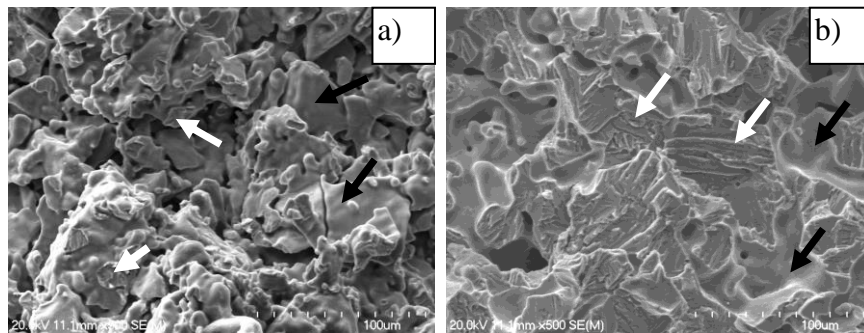
Figure 3.24 SEM images of fracture surface of tensile tested samples cut from Ti6Al4V specimens- Series 1, induction sintered at a) 1200˚C, without holding and (IS1) and b) 1400˚C, 4min holding (IS6).
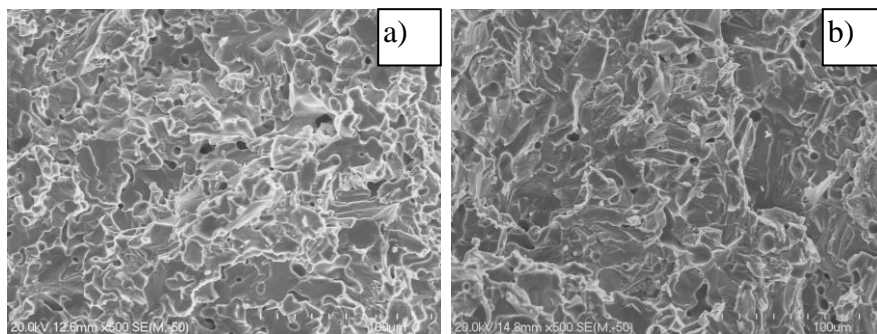
Figure 3.25 SEM images of fracture surface of tensile tested samples cut from Ti-6Al-4V specimens- Series 2, induction sintered at a) 1200˚C without holding (IS1) and b) 1400˚C 4min holding (IS6).

Similarly to the pure Ti induction sintered samples, the fracture surface of the tensile tested Ti6Al4V specimens consisted of two features: smooth non-sintered surfaces where the pores were situated (indicated by black arrows) and surfaces

119

with typical solid fracture characteristics (indicated by white arrows). At a lower sintering temperature of 1200˚C only a few areas with a typical solid fracture appearance were observed for both Series1 and Series2, which explains the improvement in tensile strength compared to that of a green powder compact (Table 3.8). There were large areas with a solid fracture appearance in the specimens sintered at 1400˚C. Accordingly these samples exhibited a much higher maximum tensile strength. The solid fractured areas had a flat appearance which is an indication of brittle fracture. This is consistent with the tensile test results, where there was no evidence of yielding in the stress strain curves.

Even though the Series 2 samples sintered at 1300˚C and 1400˚C for 4 min had significantly lower porosity and the fracture surface showed large amounts of solid fracture, the maximum tensile stress was still very low. The poor strength is due to the high level of oxygen (≈ 0.8wt %) of the starting powders. The hypothesis is that with such high oxygen content, the oxygen is present as a thick TiO layer surrounding each particle. During the short induction sintering time the TiO was only partially broken up due to the thermal expansion of Ti. The high concentration of an oxygen containing compound (most likely TiO) was not easily sinterable because of the relatively low sintering temperatures. The decomposition of the TiO, according to the Ti-O phase diagram, is over 1850˚C[20]. So the excessive amount of titanium oxide compound, situated at the diffusion bonded interfaces, weakens the strength of the solid inter-particle bridges causing the brittleness of the sintered material.

3.5   Summary and Conclusions

Induction sintering was studied as an alternative to traditional vacuum sintering, because induction sintering permits very fast heating rates and hence much faster sintering. The setup for induction sintering is simple and considerably cheaper than using a high vacuum furnace. All of the above reasons are in line with the purpose of this project which is to reduce the cost of titanium powder metallurgy products. Furthermore, the induction sintering setup allows the as-sintered samples to go directly to the next stage of processing by thermomechanical treatment without the need of reheating, as in the case of the vacuum sintering. Pure Ti and pre-alloyed (PA) Ti6Al4V powder compacts were induction sintered

using different temperature and time conditions. Three variables were analysed: the green compact density, the induction sintering temperature and the induction sintering time. The conclusions derived from this study are as follow:

(i)   The powder compact density has a crucial effect and it is one of the most important factors to guarantee successful induction sintering. Specifically, a relative green density over 80% is required for allowing sufficient coupling between the powder particles and, in this way, keeping the induction heating rates stable and comparatively high during the whole heating process. Moreover, the initial powder compact density affects the final integrity and the quality of the final shape of the sintered sample. Even though it was found that the green density does not greatly affect the final induction sintered density, the green density affected the porosity distribution after sintering. Green densities below 80 % caused preferential orientation and segregation of the powder particles in the initial stage of sintering when the first diffusion necking occurs. This resulted in non-uniform porosity along the sintered billet and formation of internal cracks and large pores. Another significant impact of the green compact density is on the tensile properties after induction sintering. Generally, the samples with green density of 85% achieved twice the YS and UTS compared with samples with a green density of 72%. The elongation to fracture was also considerably higher for the samples with a higher green density. Finally a higher green density is beneficial for reducing oxygen contamination during induction sintering.

(ii)   Considering the effect of the induction sintering temperature, all three temperatures investigated in this study were effective in developing sintered structures with sufficient tensile strength (for pure Ti samples). Increasing the induction sintering temperature led to increased sintered densities because of greater interparticle diffusion. This was confirmed from the observations on the porosity and fracture surface. Consequently, an increase in the IS temperature led to better tensile strength.

(iii)   Regarding the effect of the induction sintering time, increasing the sintering time from no holding at maximum temperature to 4 min holding significantly improved the sintered density. The sintered microstructure showed comparatively fewer pores and the fracture surface had larger areas of solid fracture. The tensile strength and ductility of these samples was also higher,

particularly for sintering temperatures of 1300°C and 1400°C. Increase of the holding time at 1200°C did not improve significantly the sintered properties of the samples with higher initial powder compact density, attributed to the slower diffusion rate.

(iv)   The type of porosity developed during sintering, in some cases independent of the density, has significant effect on the tensile plastic deformation. To ensure sufficient plastic flow before fracture only closed porosity with fine pore size in the range bellow 10 microns is required.

(v)   Titanium samples had much better sinterability evident from the sintered densities, porosity distribution and tensile test results. All three stages of sintering were evident for the Ti samples, where mostly fine closed porosity and large areas with solid material were seen. For the same sintering conditions, extended pore network was still evident in the Ti6Al4V samples. Ti induction sintered specimens achieved sintered density up to 91.7%, a YS up to 550MPa and UTS up to 618MPa. For the same sintering conditions the Ti6Al4V specimens achieved density of 85.5% but the maximum tensile strength was only 357MPa. There is clear evidence of yield and in some cases reasonable elongation before fracture in the Ti samples, evident also from the dimples in the fracture surface. In comparison, Ti6Al4V fracture surfaces were flat and had typical features of brittle fracture. This is in agreement with the Ti6Al4V tensile curves which are a straight line with no evidence of yield. The reason for the poor sinterability of Ti6Al4V powder compacts is a combination of the lower green density and the higher oxygen impurities in the starting powders. Both factors increased the degree of insulation which reduced the overall conductivity of the powders and consequently slowed down the induction sintering process.

(vi)   In terms of oxygen contamination, induction sintering at temperatures between 1200°C and 1400°C in a protective argon atmosphere caused an increase in the oxygen content of all pure titanium sintered samples. The oxygen pick up was greater for the samples with a lower green density where, on average, the oxygen content increased with 0.38wt%, compare to 0.20wt% for the samples with higher green density. The degree of oxygen contamination was not affected by increasing the induction sintering temperature and sintering time up to 4min.

(vii)   The increased oxygen content of the sintered Ti samples did have a beneficial effect on the tensile strength, where the values of YS and UTS in some

of the sintered samples exceeded those of the Ti Grade 4. Oxygen content in an addition to the comparatively lower sintered density was the reason for the lower elongation to fracture.

The oxygen content of the starting powders is crucial for success in IS. Powders with oxygen content of 0.8wt% at the studied temperature- time conditions were not able to achieve sufficient sintering. These was attributed to significant thickness of the oxide layer on the powder particle surface, which was not able to fully brake and allow sufficient metal to metal contact and consequent inter diffusion.

Concluding, this study demonstrated that a rapid consolidation of pure HDH Ti powders using fast induction sintering is a viable process. The sintering effect is evident at low sintering temperatures, such as 1200°C, where after only a few minutes of induction heating, the development of interparticle diffusion bridges occurs. The diffusion bridges are evident from SEM observations on cross sections of sintered samples. The fracture surfaces of broken tensile test pieces also show evidence of solid fracture. The maximum tensile strength at the very early stages of induction sintering showed values close to those for solid material. There was also an evidence of yielding before fracture. With the right combination of green powder compact density, induction sintering temperature and a short sintering time of 4 min sintered densities in the range of 90.0% to 91.7% can be achieved with a microstructures showing predominately closed porosity with fine rounded pores. This gives a combination of tensile properties with a tensile strength of over 600MPa and an elongation to fracture of over 13%. These values are comparable with those achieved by high vacuum sintering of similar Ti HDH powders at 1350° C for 2h.

References

1. Boyer, R., G. Welsch, and E.W. Collings, *Titanium data sheets*, in *Materials properties handbook : titanium alloys*. 2007, ASM International. p. 230-231.
2. Bulatova, L.S., *Kinetics of heating of constructional parts of ferromagnetic powders in induction furnaces.* Soviet Powder Metallurgy and Metal Ceramics, 1988. **27**(7): p. 547-550.
3. Pfaffmann, G.D. and W.E. Templeton, *Induction high temperature sintering process and equipment.* Advances in Powder Metallurgy, 1990: p. 399-408.

4. Eddy Current Mehtod compiled by Eddy Current Technology, C.T.M. *Conductivity and Resistivity Values for Titanium & Alloys*. [cited 2016; Available from: https://www.nde-ed.org/GeneralResources/MaterialProperties/ET/Conductivity Ti.pdf.

5. German, R.M., *Solid-state sintering fundamentals*, in *Sintering Theory and Practice*. 1996, John Wiley & Sons, Inc. p. 95-96.

6. German, R.M., *Sintering Theory and Practice*. 1996.

7. Anderson, T.L., *Fracture Mechanics Fundamentals and Applications, Third Edition*. 3rd ed.. ed. Fracture Mechanics, ed. T.L. Anderson. 2005, Hoboken: Hoboken : CRC Press.

8. Nikishov, N.A., I.V. Bogolyubova, and N.V. Nikitina, *Effect of methods of heating during sintering on the properties of iron-base powder materials.* Metal Science and Heat Treatment, 1991. **33**(1-2): p. 61-64.

9. Cavdar, U. and E. Atik, *Induction sintering of 3wt% Cu contented iron based powder metal parts.* Modern Applied Science, 2010. **4**(3): p. 63-70.

10. Salak, A., G. Leitner, and W. Hermel, *Properties of induction-sintered Fe-Mn-C and Fe-Mn-Cu-C steel in the sintered and forged states.* Powder Metallurgy International, 1981. **13**(1): p. 21-24.

11. Jia, M., *The Effect of Powder Characteristics and Processing Conditions on the Microstructure and Mechanical Properties of Titanium Alloys Made by Powder Forging, PhD* in *Engineering*. 2013, The University of Waikato http://researchcommons.waikato.ac.nz/handle/10289/8017: http://researchcommons.waikato.ac.nz/. p. p.238.

12. Lou, J. *Effects of powder conditioning on the quality, microstructure and mechanical properties of sintered titanium alloys*. Engineering 2015 October 2015]; Chapter 6, p 128-160]. Available from: http://researchcommons.waikato.ac.nz/handle/10289/9231.

13. Bolzoni, L., E.M. Ruiz-Navas, and E. Gordo, *Powder metallurgy CP-Ti performances: Hydride–dehydride vs. sponge.* Materials & Design, 2014. **60**.

14. Bolzoni, L., E.M. Ruiz-Navas, and E. Gordo, *Processing of Elemental Titanium by Powder Metallurgy Techniques* Materials Science Forum, 2013. **765**: p. 383-387.

15. German, R.M., *Powder Metal Technologies and Application*, in *ASM Metals Handbook Vol. 7*. 2007, ASM International. p. 1171.

16. Luo, S.D., et al., *Sintering of Titanium in Vacuum by Microwave Radiation.* Metallurgical and Materials Transactions, 2011. **42**(8): p. 2466-2474.

17. Luo, S.D., et al., *Warm die compaction and sintering of titanium and titanium alloy powders.* Journal of Materials Processing Technology, 2014. **214**(3): p. 660-666.

18. ASTM, *Standard Specification for Powder Metallurgy (PM) Titanium and Titanium Alloy Structural Components*, in

19. Bolzoni, L., E.M. Ruiz-Navas, and E. Gordo, *Feasibility study of the production of biomedical Ti–6Al–4V alloy by powder metallurgy.* Materials science and Engineering C, 2015. **49**: p. 400-407.

20. Murray, L.S., *Binary alloy phase diagrams*, in *ASM Metals Handbook Vol.3*. 1992, ASM International. p. 869-870.

Chapter 4

Application of Induction Sintering in Thermomechanical Processing by Open Die Forging of Pre-alloyed Ti6Al4V powder

4.1   Introduction

Powder compact forging is an advanced powder consolidation technique which uses a thermo-mechanical treatment of metal powders to manufacture shapes with intermediate complexity. An application of force during the consolidation of a powder compact at high temperature causes rupture of the oxide layer surrounding each particle and allows the formation of strong bonds between the powder particles. This study focusses on the consolidation of pre-alloyed (PA) Ti6Al4V powder compacts, with oxygen content of 0.5wt%, significantly higher than the standard [1]. The powders are produced by hydrogenated dehydrogenated (HDH) method and significantly lower cost than the traditionally used gas atomized powders. Additional benefit of the HDH powders is their irregular shape which is proven to be easy for compacting. The thermomechanical processing (TMP) will involve induction sintering (IS) followed directly by open die forging (ODF). This study is based on previous research where Ti6Al4V powders with a higher oxygen content of 0.8wt% were used for similar TMP [2, 3]. The novelty of this research derives from using induction heating, instead the traditional high vacuum sintering (HVS), for sintering the powder compacts directly before forging. The advantage is mainly through savings in sintering time and energy cost. Another advantage is the elimination of additional reheating of the sintered compact before ODF. This investigation focusses on a study of induction sintering parameters which allow for sufficient consolidation during subsequent forging to obtain a good combination of tensile strength and ductility. Five different induction sintering temperatures, all above the β-phase transus, in combination with two sintering times, were used. The effect of the IS conditions on the as forged porosity, microstructure, tensile properties and fracture characteristics was studied and the relationship between these was established. Some of the as-forged samples were further heat treated using recrystallization annealing. The effect of

heat treatment on the microstructure, tensile strength and fracture characteristics was studied. The degree of contamination pick-up, such as increases in oxygen, nitrogen and hydrogen content, as a result of the thermomechanical processing are reported.

4.2 Characterisation of the processing parameters

Optical images of the etched cross section of the as received pre-alloyed Ti6Al4V powders used in the experiments are shown in Figure 4.1.
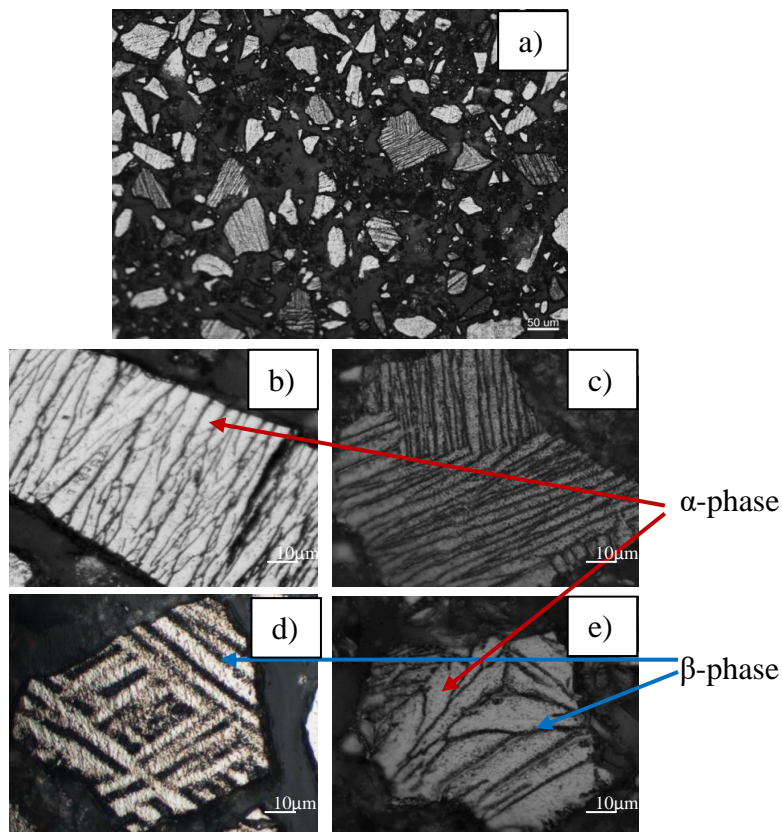
Figure 4.1 Optical micrographs of etched cross sections of pre-alloyed Ti6Al4V powders a) low magnification, b), c), d) and e) higher magnification images.

The powders are irregularly shaped with various sizes below 75 microns. The microstructure of the powders consists of colonies of unidirectionally orientated α+β lamellae. The thickness and the length of α phase (bright phase) vary from particle to particle, as well as the thickness of the β phase (dark phase) on the boundaries of each α phase lamellae. This makes the microstructure of the powders inhomogeneous.

Images of some of the compacted powder samples are shown in Figure 4.2. The average relative green density of the powder compacts was 78.8%.

Figure 4.2 Images of Ti6Al4V alloy powder compacts.

The induction sintering temperature-time conditions are marked F1 to F10. The corresponding parameters are listed in Table 2.3 in Chapter 2 and in Table 4.2. Time-temperature curves showing the heating rates during induction heating and sintering of green compacts, prior to ODF, are shown in Figure 4.3.
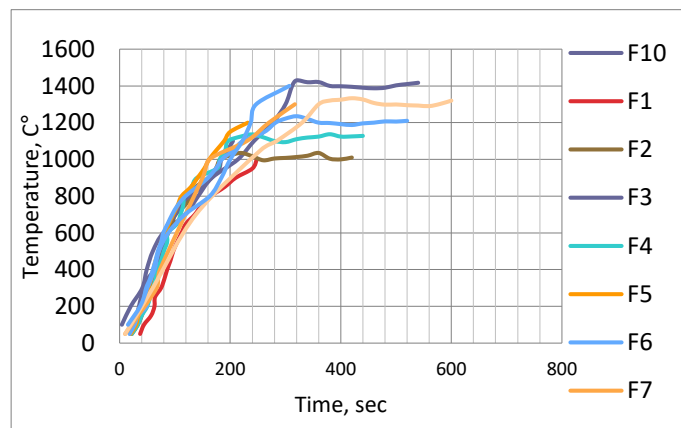
Figure 4.3 Time-temperature curves for induction sintering of Ti6Al4V powder compacts before open die forging.

The average heating time to required temperatures of 1000°C to 1400°C was between 3 and 5 min. The average heating rate was 280°C/min.

4.3   Assessment of the Ti6Al4V forged discs

The forged samples kept their integrity during forging into circular discs. Figure 4.4 shows images of two of the forged surfaces of some of the forged disc. The reduction in height as a result of ODF was 62% to 65%. A relationship between the height reduction and the induction heating parameters is not very consistent.

Top forged surface:	Bottom forged surface:
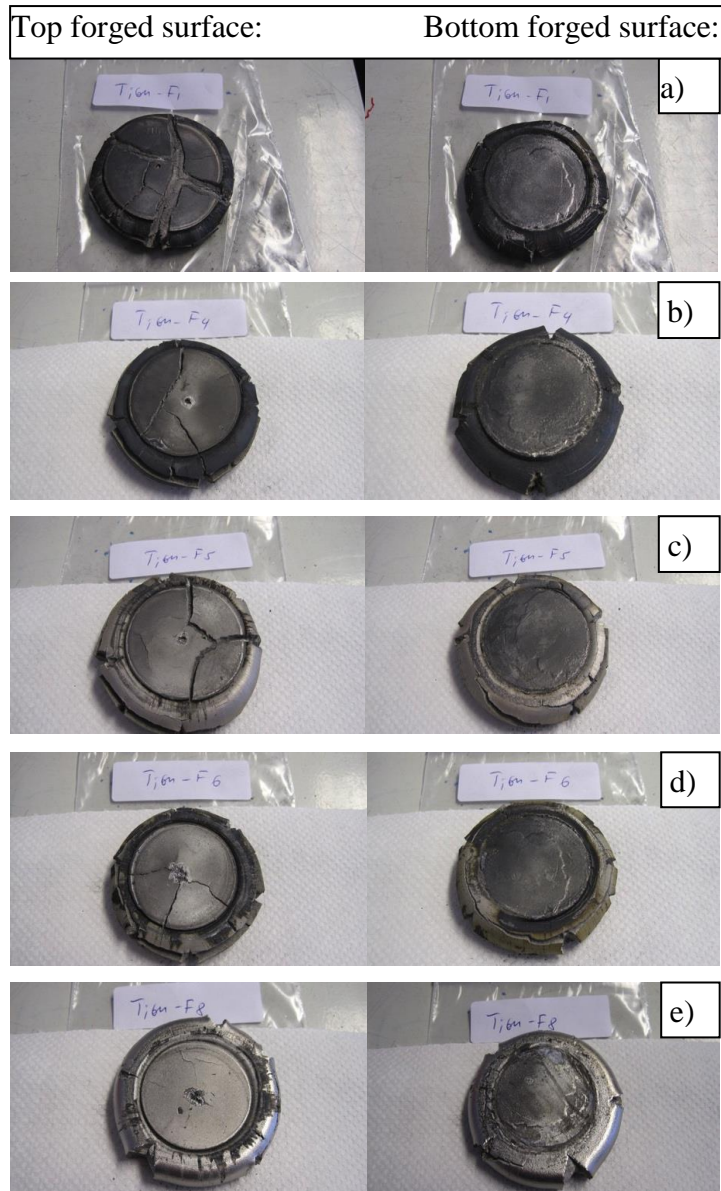
Figure 4.4 Images of some of the Ti6Al4V forged discs prepared under different time/temperature conditions a) 1000˚C no hold (condition F1); b) 1100˚C 4min (condition F4); c) 1200˚C no hold (condition F5); d) 1200˚C 4min (condition F6); e)1300˚C 4min (condition F8).

There are some cracks observed in the perimeter of each disc as well as on the flat surfaces. The cracks are related to the insufficient temperature during forging, caused by the delayed forging and the chilling effect of the forging die surfaces. The reasons for the forging delay were the delay of approximately 5sec to transfer the heated powder compact from the induction coil to the forging die and the slow speed of the hydraulic press ram. Delays prior to forging lead to a drop in temperature, which in some cases may fall below α /β phase transformation temperature. When forging takes place from temperatures below 960˚C, in the α-phase field, material flow is restricted because of the lower formability of the

h.c.p. α- phase, related to its hcp crystal structure. Contact between the heated powder compact with the cold die surfaces would cause a further drop in temperature at the contact surface. This, combined with the friction between the die and the compact would have led to restricted material flow and surface cracking [4].

4.4 Contamination as a result of the thermomechanical processing

The oxygen, nitrogen and hydrogen content of the starting powders and the as-forged discs are shown in Table 4.1.

Table 4.1 Oxygen, nitrogen and hydrogen content of Ti6Al4V samplers before and after open die forging at different conditions.

	Oxygen, wt%	Nitrogen, wt%	Hydrogen ,wt%
Ti6Al4V- as received	0.53	0.01	0.05
F1- 1000˚C, no hold	0.59	0.05	0.05
F2- 1000˚C 4min	0.54	0.05	0.03
F3- 1100˚C, no hold	0.60	0.05	0.04
F4- 1100˚C 4min	0.53	0.06	0.03
F5- 1200˚C, no hold	0.59	0.07	0.03
F6-1200˚C 4min	0.54	0.05	0.03
F7- 1300˚C, no hold	0.50	0.05	0.03
F8- 1300˚C 4min	0.58	0.05	0.02
F9- 1400˚C, no hold	0.56	0.05	0.03
F10-1400˚C 4min	0.50	0.05	0.02

The thermomechanical processing caused a change in the amount of contamination. Most noticeably the nitrogen content increased almost five times. Most forged samples have nitrogen of 0.05wt%, which is the range of the upper limit for PM Ti6Al4V alloy [5]. The hydrogen content decreased gradually from 0.05 to 0.02wt% with increasing induction sintering temperature and holding time and it is within the limits of the standard. Most of the samples showed an increase in oxygen content of between 0.01wt% to 0.07wt%. Some samples showed a slight decrease in the oxygen content. Similarly, to the results in Chapter 3, the oxygen pick up is not dependent on the temperature or the sintering time.

The oxygen content of the as-forged samples varies between 0.5wt% and 0.6wt% and it is well above the limits of the ASTM standard for this PM alloy [5].

4.5 Deformation behaviour

The deformation behaviour of the as forged discs in direction parallel to forging was observed using low magnification optical microscopy. The analysis of the cross section of a forged sample, which covers a region from the forging surface to near the centre of the forged disc (Figure 4.5) showed a non-uniform macrostructure.
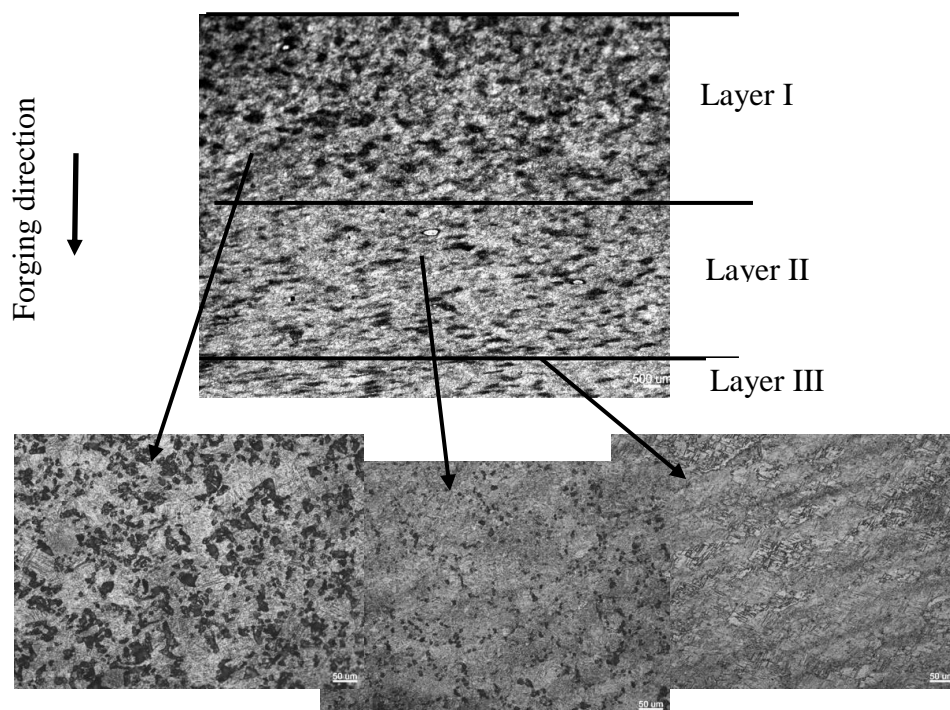
Figure 4.5 Optical micrographs of the cross section of a forged sample prepared using condition F2, showing its deformation behaviour.

The cross section can be divided in three layers. The layers are differentiated by the amount of porosity and the level of grain deformation. In Layer I, the area close to the forging surface, the powder particles were hardly deformed and a large number of pores were observed. This is the layer where the material flow and deformation was most affected by the chilling and the friction effect of the forging die surfaces. In Layer II the powder particles were partially deformed with a significantly reduced amount of porosity. Layer III shows a fully deformed and consolidated area, with no macro size pores observed.

4.6 Porosity distribution along the cross section of the forged discs

The porosity along the forged surfaces was further studied by SEM. Figure 4.6 shows the pore distribution in samples processed using conditions F4, F6 and F10.

a)

Forging direction

b)

c)
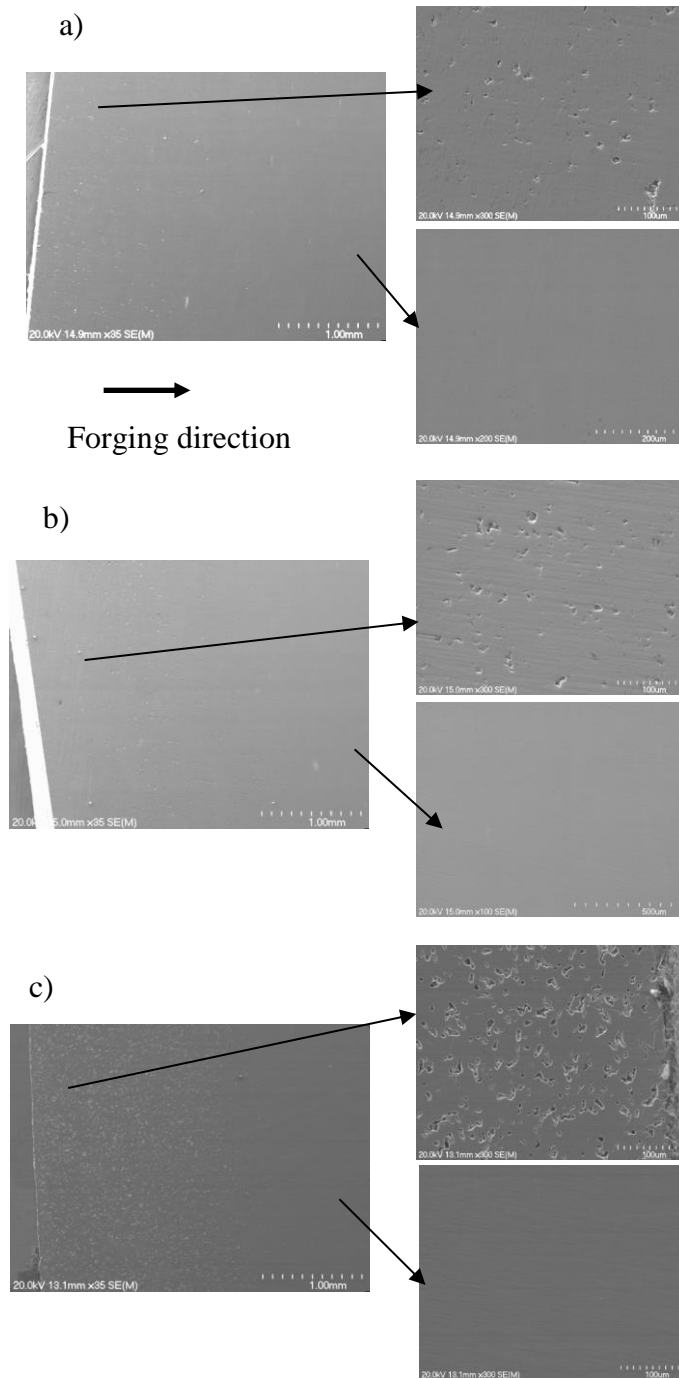
Figure 4.6 SEM images showing porosity distribution in a cross section of samples forged from a) 1100˚C, b) 1200˚C and c) 1400˚C all with 4 min holding.

The thickness of the porous layer is approximately similar, in the range of 0.4 mm for forging conditions F1 to F8 and the pores size is comparatively small. Forging

from higher temperature of 1400℃ (conditions F9a and F10) for both holding times, showed higher thickness of the porous layer of over 1mm, with significantly larger pores (Figure 4.6 c). Induction sintering at this comparatively higher temperature led to increase in the diffusion rate, causing a greater amount of material migration and resulting in a decreased number of pores with large size. The relatively short sintering time was not long enough to obtain closure of the pores. During subsequent forging, the pores were too large to collapse [4]. The pores migrated towards the edges of the billet. The limited material flow in these regions did not allow further deformation and closure of the pores. Underneath the well-defined porous layer, the number of pores gradually decreased, with a few small pores remaining in the inner part of the forged discs.

4.7 Microstructure analysis

The microstructure of as-forged samples was characterized by SEM and optical microscopy. A sample from the cross section of each of the forged compacts was cut as shown in Figure 4.7 and metallographically polished and etched.
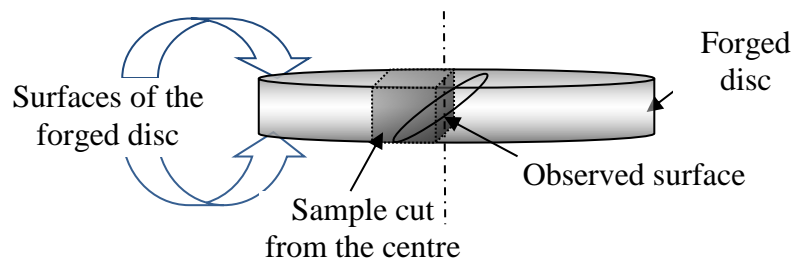
Figure 4.7 A schematic of the sample used for microstructural analysis, cut from a cross section of the forged discs.

In this section, only the microstructure at the centre of a cross section, where full consolidation and plastic deformation occurred, of each forged disc was studied. The microstructure of as-forged discs is influenced by the IS conditions-temperature and time. Induction sintering at temperatures of 1000˚C, in the region close to β phase transformation in both sintering times (conditions F1 and F2) followed by ODF developed an inhomogeneous microstructure (Figure. 4.8a) and d).
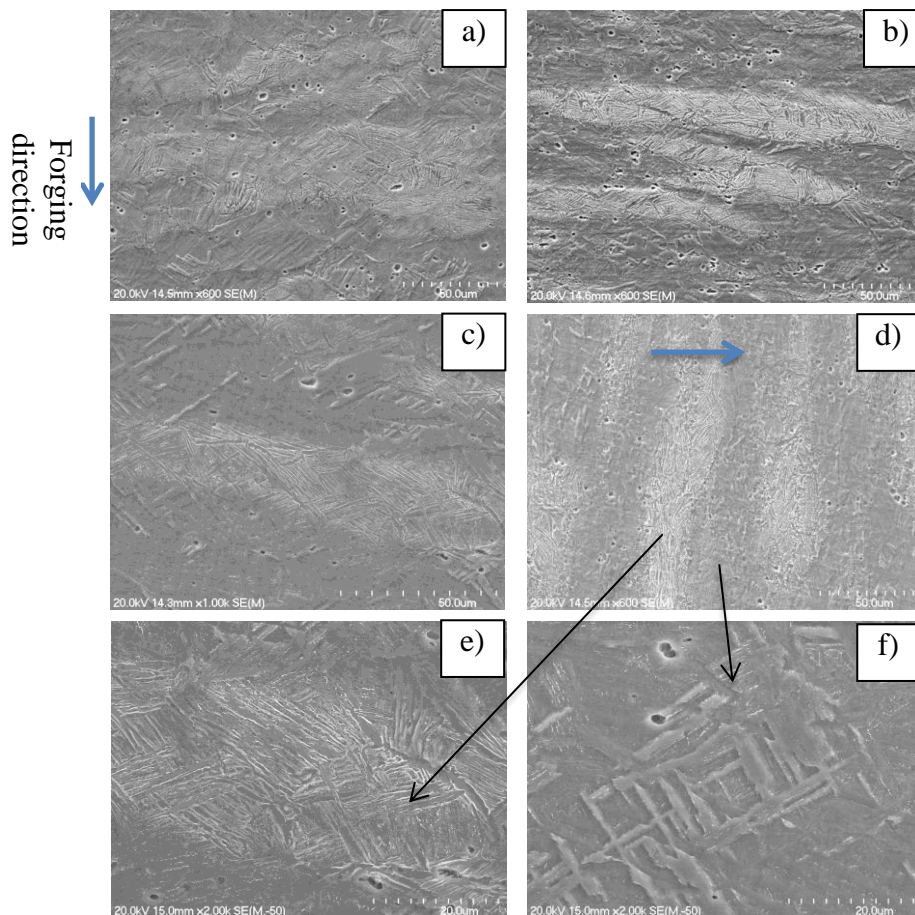
Figure 4.8 SEM images of cross sections of Ti6Al4V alloy discs forged at a) 1000˚C (condition F1), b) 1100˚C (condition F3), c) 1200˚ C (condition F5) without holding at temperature and d), e) and f) 1000˚C with 4min holding (condition F2) showing low and high magnification images respectively.

The primary reason for an inhomogeneous microstructure is the inhomogeneity of the original powders (Figure 4.1). The induction sintering temperature and holding time of 4min at this temperature did not permit full phase transformation and homogenization. Similar, inhomogeneous microstructure was developed at higher sintering temperatures 1100˚C and 1200˚C (conditions, F3 and F5) without holding time (Figure 4.8 b) and c). There are regions with a fine lamellar microstructure (Figure 4.8 e) and regions with a coarser microstructure (Figure 4.8 f). Nevertheless, the powder particles were well deformed.

The microstructure developed after forging from 1100˚C (F4) and 1200˚C (F6) with 4min hold is more homogenous (Figure 4.9). The material was heated to a sufficiently high enough temperature to form a β solid solution, suggesting that full phase transformation and homogenisation had occurred during sintering. The microstructure has very fine lamellae morphology. Forging from these

temperatures did not lead to formation of noticeable amount of martensitic phase, showing that the cooling rates were below the martensitic transformation. The microstructure is finer for the higher temperature (F6) processing condition. It also shows a texture in transvers to the forging force direction.
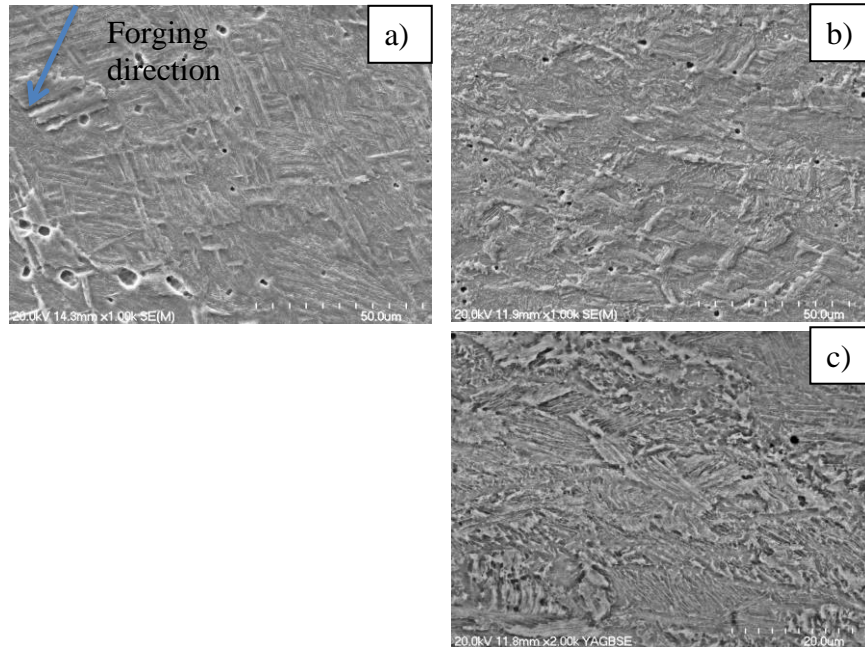
Figure 4.9 SEM images of cross section of Ti6Al4V alloy discs forged at a) 1100˚C 4min (condition F4) and b) and c) 1200˚C 4min (condition F6) at different magnifications.

The microstructure developed during induction sintering at 1300˚C and 1400˚C and subsequent forging is homogeneous, confirming that a full phase transformation and homogenisation during sintering had taken place (Figure 4.10). The microstructure is much coarser than that found after TMP at lower temperatures.

Basketwave structure
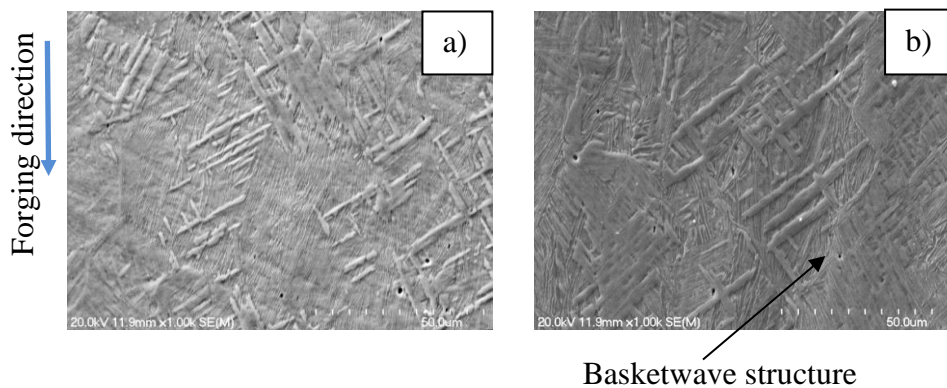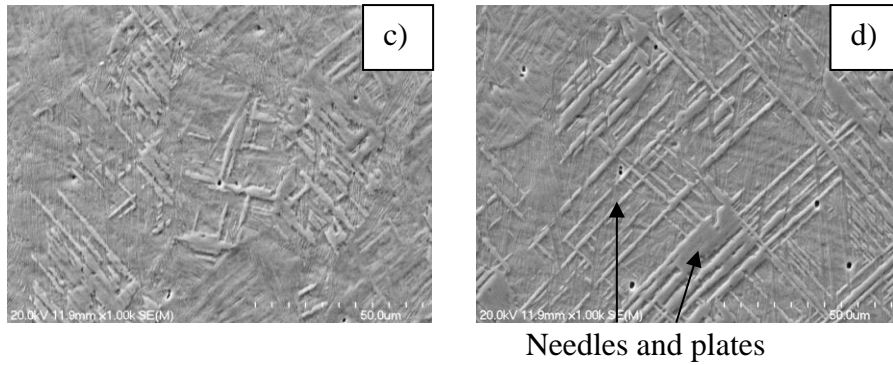
Needles and plates

Figure 4.10 SEM images of the cross section of forged samples from condition a) and b) 1300˚C respectively without holding (condition F7) and 4min holding (condition F8) and c) and d) 1400˚C respectively without holding (condition F9) and 4min holding (condition F10).

Forging from these high temperatures involved a comparatively faster cooling rate, which led to formation of a significant amount of a coarse non-equilibrium martensitic phase. This phase appears as large needles and coarse plates (Figure 4.10d). The martensitic phase is most likely to be hcp α′ phase. From the literature, α′ phase forms during fast cooling from temperatures greater than 900˚C [6]. A fine basket-wave structure is observed between the coarse martensitic needles and plates.

Optical micrographs give a better representation of the α/β phase distribution (Figure 4.11). The forged samples processed at intermediate temperatures in (F4 to F6) showed fine α+β phase lamellae structure known as basketweave or Widmanstäten microstructure. In this case the basketweave appearance is textured due to the plastic deformation caused by forging (Figure 4.11a).

Forging direction

Basketwave α-β phase

Coarser martensitic α′ phase (bright phase) defined with retained β phase (dark phase)
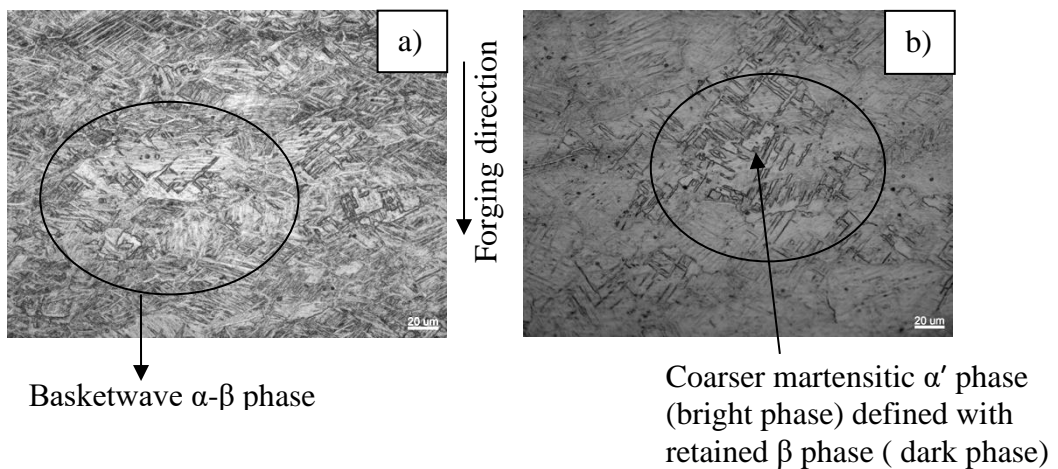
Figure 4.11 Optical microscope image of etched cross section of ODF samples a) F6- 1200˚C 4min and b) F10-1400˚C 4min.

135

The coarse martensitic plates and needles formed after ODF at 1300˚C and 1400˚C (conditions F7 to F10) are also observed in optical micrographs (Figure 4.11b), confirming the SEM observations (Figure 4.10). In addition, optical micrographs showed that the martensitic phase is associated with β-phase (the darker line around the plates and needles).

4.8 Tensile properties

The results from tensile testing are shown in Table 4.2 and the tensile stress-strain curves are in Figure 4.12. Three tensile samples from each of the forged discs were tested. The samples with suffix 1 and 3 were cut from sections close to the forged surfaces and the samples with suffix 2 were taken from the centre of the forged cross section.

Table 4.2 Tensile properties of Ti6Al4V alloy forged after induction sintering with different temperature and time conditions.

IS conditions prior ODF	YS, MPa	UTS, MPa	ε , %
F1-1	-	984	0.7
F1-2 (1000˚C, no hold)	1050	1193	4.8
F1-3	1049	1155	2.2
F2-1	1177	1217	1.5
F2-2 (1000˚C, 4min)	1185	1278	3.5
F3-3	1158	1262	5.3
F3-1	995	1001	1.2
F3-2 (1100˚C, no hold)	1120	1187	1.7
F3-3	1069	1195	5.0
F4-1	1165	1258	3.9
F4-2 (1100˚C, 4min)	1158	1251	8.2
F4-3	1168	1270	9.2
F5-1	1124	1206	2.1
F5-2 (1200˚C, no hold)	1069	1205	2.1
F5-3	1051	1178	3.1
F6-1	1103	1156	1.5
F6-2 (1200˚C, 4min)	1127	1236	10.3
F6-3	1149	1270	7.3
F7-1	1074	1242	2.8
F7-2 (1300˚C, no hold)	1206	1214	5.6
F7-3	1101	1227	6.3
F8-1	1121	1231	4.0
F8-2 (1300˚C, 4min)	1113	1252	5.8
F8-3	1115	1230	6.2
F9-1	1085	1205	2.3
F9-2 (1400˚C, no hold)	1090	1226	3.1
F9-3	1081	1110	1.4

F10-1		1064	1252	2.0
F10-2	(1400˚C, 4min)	1050	1227	1.6
F10-3		-	908	0.8
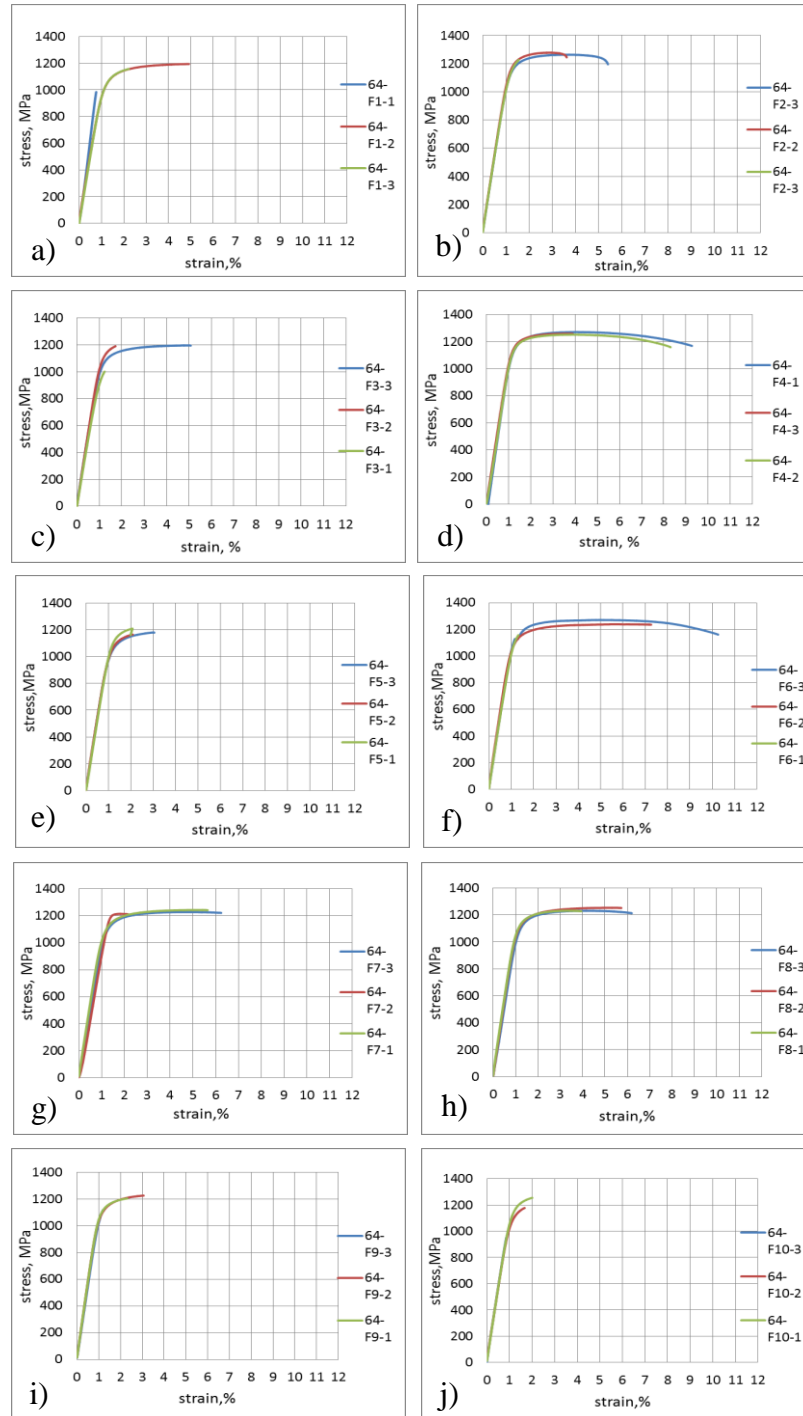
Figure 4.12 Tensile stress-strain curves of Ti6Al4V alloy forged after induction sintering at different conditions a) and b)1000˚C, c) and d) 1100˚C, e) and f) 1200˚C, g) and h) 1300˚C, i) and j) 1400˚ C, respectively no hold and 4min hold at temperature.

At forging temperatures between 1000˚C and 1200˚C (forging conditions F1, F3 and F5), where the powder compacts were not held at the sintering temperature, the tensile properties varied between 1050MPa and 1120MPa YS and 1115MPa and 1200MPa UTS. The elongation to fracture varied from 1.5% to 5%. The sample prepared using forging condition F2 (1000˚C, 4min sintering) showed increased and more consistent YS and UTS compared with conditions F1, F3 and F5, but the ductility did not increase significantly. The most balanced combination of stress and strain was achieved for forging conditions F4 and F6 where the green powder compacts were induction sintered for 4min at 1100°C and 1200°C and then forged. The average YS for these conditions were 1164MPa and 1126MPa and the average UTS were 1260MPa and 1210MPa respectively, for F4 and F6 conditions. Some of the tensile test specimens cut from these forged discs achieved comparatively higher elongation to fracture of 9.1% for forging condition F4 and 10.3% for forging condition F6. Forging from 1300°C (F7 and F8) gave more consistency in tensile properties. All samples had a maximum tensile strength over 1200MPa and an average elongation to fracture around 5%. The samples forged from 1400°C without holding time, showed YS in the region of 1085 MPa and UTS of 1200MPa but it was not consistent. The elongation to fracture in these samples was low and on average only 2%. A holding time of 4 minutes at 1400˚C showed inconsistency of the tensile properties. In the areas close to the forged surface, there was no yield and ductility, while the other areas showed high UTS of over 1200MPa, but low yield and ductility.

4.8.1 Scatter of the tensile properties along the forged cross section

The ductility of test-pieces taken from different positions in a cross-section was not consistent, with test specimens taken close to the surface showing considerably lower ductility compared with those taken from the centre. There are two factors contributing to these results: (a) the degree of porosity observed in the regions close to the forging surface (Figure 4.6) and (b) the deformation gradient along a forged cross section (Figure 4.5). The porosity derives from incomplete consolidation during the short induction sintering times, as well as from incomplete deformation. The gradient in the deformation was due to the temperature gradient through the forged cross section caused by the chilling effect of the die surfaces. Consider the graph in Figure 1. 30 [7] which shows that the forging force for a Ti6Al4V alloy is very sensitive to the temperature gradient. A

temperature drop from 980°C to 900°C leads to a threefold increase in the forging pressure. This is related to the α and β phase ratio in this temperature range. A similar effect on the scatter of tensile properties was observed in other studies [4, 8], where the authors related the scatter in the tensile properties with the difference in the deformation rate due to the thickness gradient in a forged sample.

4.8.2 The effect of induction sintering conditions on the tensile properties of the as-forged alloys.

The role of consolidation prior to forging is to increase the strength of a powder compact by initiating some degree of particle inter-diffusion and reduction in total area of the porosity to ensure pore closure and increase of the cohesion of powder particles during forging. There are two factors affecting consolidation, the IS temperature and the IS time. Exposure of powder compacts to high temperature contributes to a reduction in the surface energy of powder particles, allowing material movement at an atomic scale and powder particle inter-diffusion. Exposure to increased temperature for a period of time also weakens the oxide layer surrounding each powder particle. Considering the lower coefficient of thermal expansion of titanium oxide compared with that of Ti metal [6, 9], the oxide layer fractures and permits contact between oxide free metal surfaces of neighbouring powder particles. Furthermore, the applied forging force contributes to the rupture of the oxide layer, extensive material flow and strong interparticle particle cohesion. This results in disappearance of the existing powder particle boundaries and formation of new microstructure. The degree of plastic deformation and powder particle cohesion during forging reflects on the tensile properties and particularly on the UTS. The microstructural development is also temperature and time dependent. So optimisation of sintering temperature and time is needed to achieve sufficient consolidation during forging and a microstructure conducive to good tensile properties. The effect of IS temperature on tensile strength is shown in Figure 4.13.
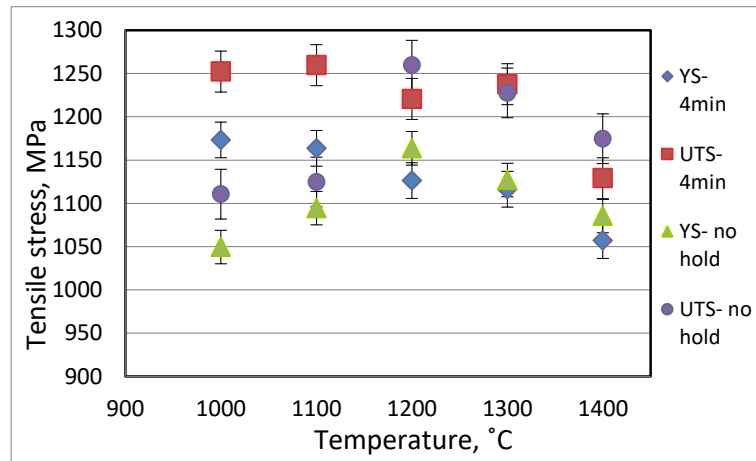
Figure 4.13 Effect of induction sintering conditions on yield and tensile strength after forging.

The increase in YS and UTS with increase in the IS temperature from 1000˚C to up to 1200˚C, when IS was carried out without holding at temperature, is related to increased consolidation as a result of more effective sintering prior forging. 1200˚C is the optimum temperature for this holding time condition. Above this temperature, the YS and UTS begin to fall, which is related to the coarse martensitic microstructure developed during heating and subsequent cooling from this high temperatures (Figure 4.10 a) and c).

The forgings made with conditions when holding of 4min was used, showed high UTS in all temperatures, accept 1400˚C. This leads to the conclusion that 4 min of IS in all temperatures introduced sufficient pre-consolidation to achieve satisfactory plastic deformation and powder particle cohesion during forging, even at the lowest temperature of 1000˚C. Nonetheless, the YS, in this holding time condition gradually decreased with temperature increment, which is related to increased grain size and the formation of coarse martensitically transformed phases in temperatures above 1200˚C (Figure 4.10).

The temperature of a sintered compact directly before forging affects the cooling rate during forging, which consequently influences the α/β phase transformation process and in particular the formation of non-equilibrium phases. This therefore controls the forged microstructure, which influences fracture behaviour and mostly ductility.

The effect of forging temperature on ductility is not so evident in those compacts which have been induction sintered and forged without holding at the IS temperature (Figure 4.14).
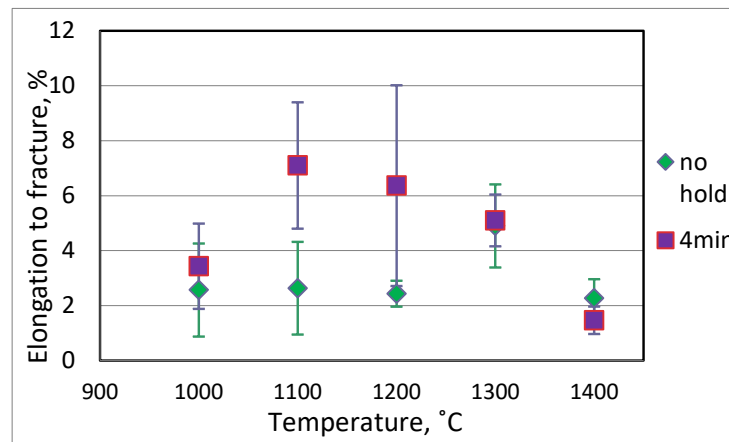
Figure 4.14 Effect of the induction sintering conditions on the elongation to fracture after forging.

The ductility is very low in all temperature conditions. The reason for the low ductility in the lower temperature range of 1000°C and 1100°C is the insufficient consolidation evident by the comparatively low values of YS and UTS and the uncompleted homogenisation evident by the microstructure analyses (Figure 4.8). At temperatures above 1200°C, the low ductility is due to the coarser martensitic phase formed due to the fast cooling rates (Figure 4.10 a) and c).

For the samples held for 4 min at temperature before forging, there is a lot of scatter in elongation to fracture depending on the temperature. The lower ductility when forging from 1000°C or in the α/β phase field was because there was insufficient homogenisation during sintering (Figure 4.8 d).

Forging from intermediate temperatures of 1100°C and 1200°C, which is in the lower β-phase region enabled full phase transformation and homogenization during the 4 minutes holding time (Figure 4.9). The comparatively slow grain growth during the short 4 min holding time at these temperatures, combined with a comparatively slow cooling rate, resulted in a fine and mostly equilibrium microstructure favourable for good elongation. The good tensile properties for these two samples are related to the microstructure which shows features of a basketweave microstructure with fine α-phase lamellae surrounded by fine β-phase (Figure 4.11). The microstructure in sample F6 is similar to that described

141

in the reference study [10] (Figure 1.37 d) and e)), where the authors describe the microstructure as having broken α-phase grain boundaries and refined α-phase lamellae, caused by the deformation during forging. Typically the basketwave structure in Ti alloys is achieved by heat treatment after hot working. In this work the basketweave microstructure was formed during the forging process and it was assumed that a 4 min hold at temperatures of 1100˚C and 1200˚C was enough for all the primary α-phase to transform to β-phase. The cooling rates during forging were slow enough to allow α-phase to precipitate from β phase and form fine lamellae. Fine lines of retained β-phase were found on the boundaries of the α-lamellae, forming a basketwave structure.

The cooling rates during forging at 1300˚C and 1400˚C were above that of the martensitic transformation evident by the microstructure developed at these conditions (Figure 4.10 b) and d) and Figure 4.11 c). The large amount of the martensitic phase resulted in high residual stress which when combined with a coarser microstructure led to very low ductility.

4.8.3 Factors influencing the tensile strength of the as-forged alloys

The values of YS and UTS of Ti6Al4V forged discs produced by short time IS followed by ODF are significantly higher than that found in standard wrought Ti6Al4V alloy [11] and powder metallurgy Ti6Al4V alloy made with gas atomized powders [1]. Firstly, the high tensile strength is evidence that there was sufficient powder particle bonding and effective powder consolidation.

There are another three main reasons for the high tensile strength:

  (1)   First, is the high initial oxygen content of the starting powders. The interstitial oxygen acts as a strengthening element [12] and for pure Ti the maximum tensile strength doubles from 300MPa to 850MPa when the oxygen content increases from 0.1 to 0.5wt%.

   (2) The second factor is the mechanism by which powder particles bond during the application of a forging stress at temperatures above the α/ β-phase transformation. Powder particle bonding relies partially on the inter-particle diffusion during IS. As mentioned in Chapter 2 and from other research [13], even at lower IS temperatures without any holding time at the sintering temperature, some inter-particle necking was observed. The induction sintering only initiates the consolidation process. The forging stress applied directly after IS causes

material flow directed in lateral plane in regards to the forging direction. Material experiences large amounts of plastic deformation. In a difference from the forging of solid materials where the plastic deformation causes mostly texture in the grains, the PM forging is more complex. It involves, collapsing and closure of the pores, deformation in the powder particles, formation of new grain boundaries and at last grain texture [4]. The shear stress experienced by the powder particles, during the plastic deformation, enables the oxide layer surrounding the powder particles to fracture causing the powder particle boundaries to disappear. This allows metal to metal contact and the formation of new grain boundaries resulting in strong inter-particle bonding [14].

(3) The third factor is the residual stress due to the plastic deformation and the high cooling rates. The effect of plastic deformation is evident by the texture observed in the microstructure. The effect of the cooling rates is evident by the presence of the martensitic phase in the microstructure of the discs forged from temperatures above 1200˚C.

4.9 Fracture surface analyses

Fracture surfaces of broken tensile test pieces were complex. Within a single sample, there was a mixture of both intergranular and transgranular fracture, showing both ductile and brittle features.

The tensile test pieces taken from regions close to the forged surface showed different fracture surface features compare to these taken from the middle sections (Figure 4.15).
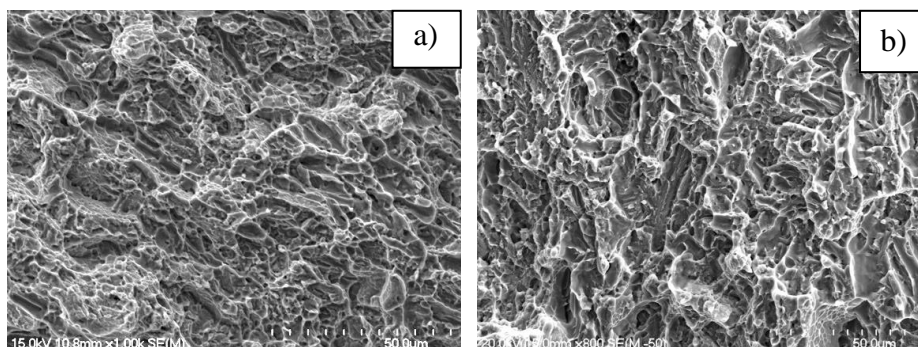
Figure 4.15 SEM images of fracture surface of tensile tested pieces cut from a) middle section and b) section close to the surface, of a forged disc prepared using condition F6.

The tensile sample cut from the middle section with a ductility of 10.3 % showed a fracture surface with very fine dimples (Figure 4.15a), while the other sample taken from a section close to the forged surface, which had an elongation to fracture of 1.2% has typical brittle characteristics (Figure 4.15b). The observed scatter the fracture behaviour reflects the scatter in the tensile properties along the cross section of the forged discs. This confirms that there is an insufficient consolidation at the surface areas, which affects the tensile properties.

The fractographs in Figure 4.16 are from fractured tensile test-pieces of samples forged with different conditions. The tensile test pieces are taken from middle sections of each forged discs where full deformation was undertaken.
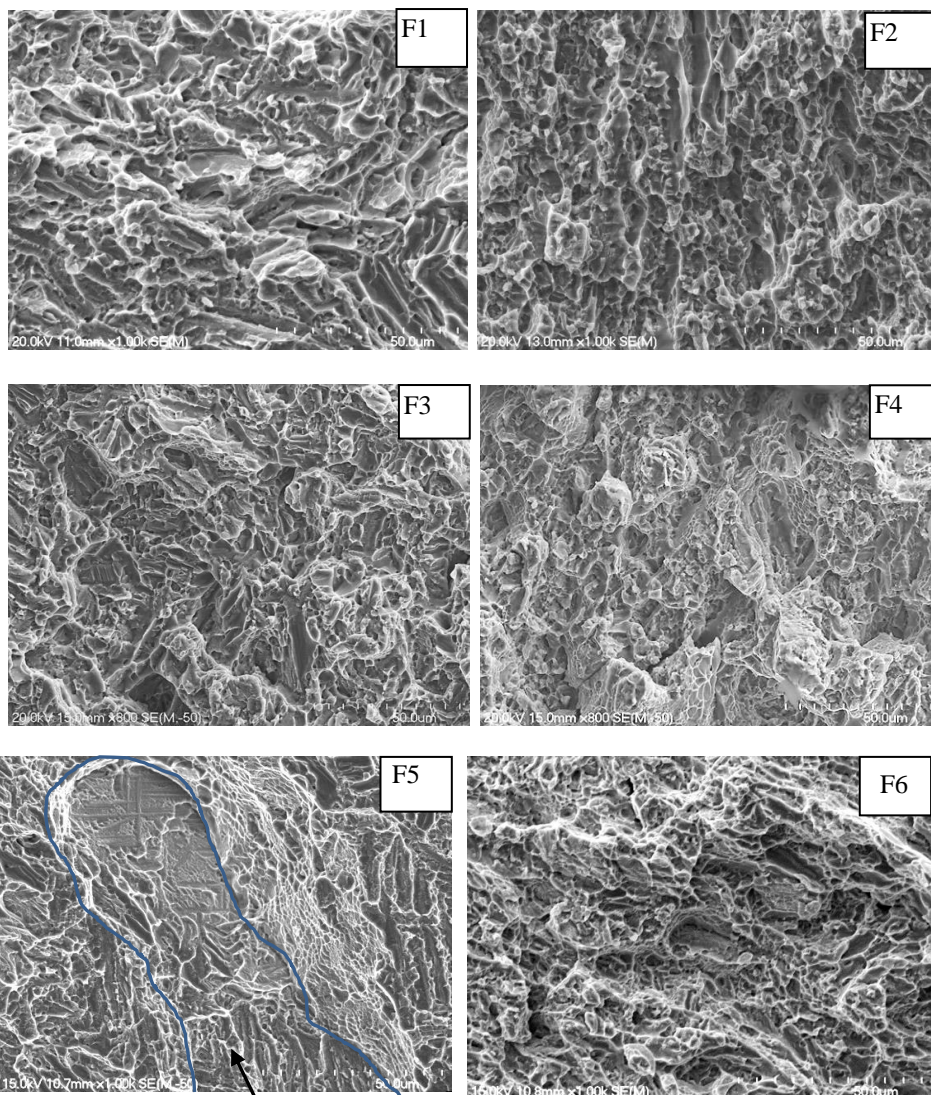
Fracture occurred at the boundary of a flattened powder particle.
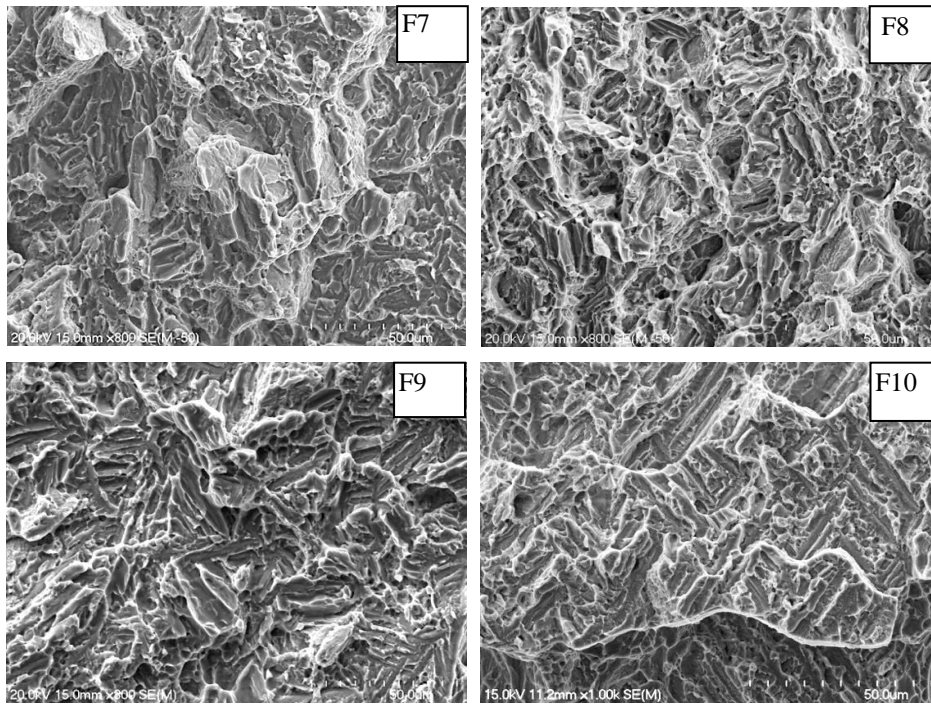
Figure 4.16 SEM images of fracture surface from tensile tested samples forged using different conditions F1 to F10.

The fracture surfaces of all samples showed characteristics of typical fracture of solid material with mixture of intergranular and transgranular fracture. Samples forged from a lower IS temperature, between 1000°C to 1200°C and without holding at temperature (F1, F3 and F5), showed large amount of fracture at the grain boundaries and some shallow dimples, which gave overall brittle fracture with a predominantly flat appearance. Image F5 in Figure 4.16 shows an example of intergranular fracture at grain boundary of flattened grain or former powder particle detached from the solid structure when under tension during testing. This suggested that the temperature and holding time for this ODF condition were not sufficient full powder consolidation to form strong inter-particle bonding and grain boundary of solid material. Increasing the holding time to 4 minutes at 1100°C and 1200°C resulted in a significant increase in the areas with transgranular fracture (Figure 4.16 F4 and F6), with large amount of fine dimples confirming the ductile tensile properties. Fracture by cleavage was also observed in these samples. When the temperature was increased to 1300°C for both time conditions the ductile features started to disappear. There is large amount of fracture by transgranular cleavage in these samples, confirming the high tensile strength but limited ductility. The fracture surfaces of the samples forged from

1400°C have coarse fracture lines showing that fracture happened at the coarse martensitic phase (Figure 4.16 F9 and F10).

4.10 The effect of recrystallization annealing heat treatment on the mechanical properties and microstructure

Two of the discs forged using conditions F8 and F10 were recrystallization annealed. These discs were selected, because they were forged using temperature conditions well above α/β transformation, which led to high consolidation level but also high residual stresses and the formation of a coarse martensitic microstructure, which caused embrittlement and very low ductility. Stress-strain curves from tensile test-pieces taken from forged discs after RA are shown in Figure 4. 17.
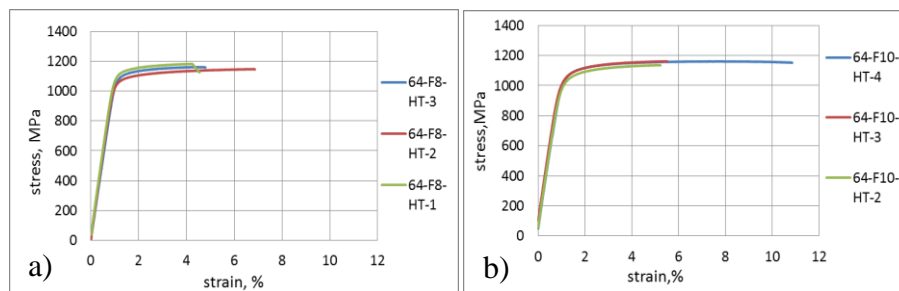
Figure 4.17 Tensile stress-strain curves after recrystallization annealing of Ti6Al4V forged with a) condition F8 and b) condition F10.

Recrystallization annealing caused a reduction in YS and UTS. The YS dropped by approximately 50MPa and the UTS by 100MPa for both conditions, compared with the as-forged condition. The elongation to fracture did not improve significantly for the Ti64-F8 specimen, but it did increase for sample Ti64-F10, where one of the heat treated tensile samples achieved elongation to fracture of 10.9%, while the others reached 5.6% and 5.7%. The average ductility of this sample had increased by approximately three times.

For both conditions the appearance of the microstructure changed significantly. The coarse martensitic α′- phase disappeared, which explains the increase in the ductility. The microstructure was transformed to a fine, homogenous basketweave structure (Figure 4.18), confirming the high values of YS and UTS.
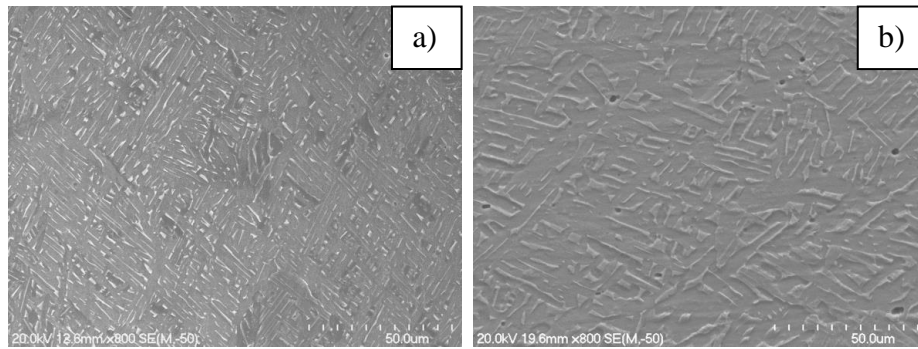
Figure 4.18 SEM images of etched cross section after recrystallization annealing of Ti6Al4V forged with a) condition F8 and b) condition F10.

The fracture surface after recrystallization annealing is also much finer compare to that of the as-forged samples (Figure 4.14 F8 and F10), showing features of transgranular fracture by formation of dimples (Figure 4.19) similarly to those obtained in as-forged Ti64-F4 and Ti64-F6 samples (Figure 4.14, F4 and F6).
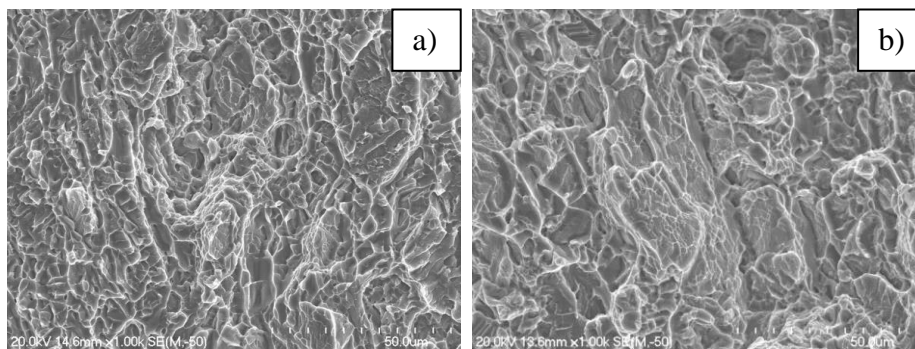
Figure 4.19 SEM images of fracture surface after recrystallization annealing of Ti6Al4V forged with a) condition F8 and b) condition F10.

The results from the post forging recrystallization annealing heat treatment show that the microstructure can be tailored to give a preferred α/β phase size and α/β phase distribution to achieve the required tensile properties. A wide range of forging parameters, such as temperature and sintering time could be used if needed for achieving improved material deformation, pore elimination and full consolidation.

Over all the values of the YS and UTS after HT are significantly higher than that of the standard wrought and PM Ti6Al4V alloy, showing the effect of the high oxygen content. The improvement of the ductility was not consistent. Even though the HT microstructure of Ti64-F8 sample showed no presence of martensitic phase and fully basketweave microstructure was developed, the

ductility has not been increased. The reason is the high oxygen content of 0.58wt% (Table 1).

In contrast, in the heat treated Ti64-F10 sample with comparatively lower oxygen of 0.50wt%, the elongation to fracture increased significantly reaching values comparable to that of the standard Ti6Al4V alloy.

The heat treatment did not eliminate the effect of the porous layer on the ductility, evident from the scatter of the elongation to fracture along the forged cross section.

4.11 Comparison of tensile properties of Ti6Al4V alloy made by open die forging with other methods

The tensile properties of the Ti6Al4V forged discs described in this study were compared to other wrought or forged Ti6Al4V alloys (Table 4.3).

Table 4.3 Comparison of tensile properties of forged Ti6Al4V alloy researched in this study with those from referenced sources.

Ti6A4V alloy	YS, MPa	UTS, MPa	ε, %	Reference
HDH PA Ti6Al4V → Press and IS-4min→ Forged from 1100˚C and 1200˚C (F4 and F6)	1168	1270	9.1	this study
	1127	1270	10.3	
HDH PA Ti6Al4V → Press and IS→ Forged from 1300˚C→ RA	1050	1175	10.9	this study
HDH PA Ti6Al4V→Press and IS→ Forged from 1350˚C	1180	1303	7.1	[13]
GA PA Ti6Al4V→Press and IS→Forged	970	1120	12.0	[2, 3]
GA PA Ti6Al4V –Press and VS→ Forged →HT	≈960	≈980	≈18.0	[15, 16]
PM BE Ti6Al4V – VS and Press→ α/β Forged	951	1027	9.0	[17]
Wrought Ti6Al4V -Forged →annealed	938	979	15.0	[7]
Wrought Ti6Al4V -Forged →RA	860- 965	930-1015	10.0-14.0	[12]
Wrought Ti6Al4V- (α+β) Forged→ mill annealed (MA)	827-862	896-931	10.0	[6]

A comparison of YS and UTS shows that the tensile results achieved in this study are considerably higher compared to those from a reference study (Table 1.10) [2, 3], where similar forging conditions were used but the Ti6Al4V HDH powders used in this work had a higher oxygen content of 0.8wt% (Table 1.10). The as-forged tensile properties from condition F4 and F6 are similar to those obtained for a forged rocker-arm [13], where similar powders and processing conditions were used. The YS and UTS are considerably higher at the expense of ductility compared to reference [2, 3] using similar processing conditions but where GA powders were used instead HDH powders. Similarly, the YS and UTS in this study are significantly higher than those in studies [15, 16], where traditional VS of GA powders was used for consolidation prior to forging. The great difference in ductility is due to the extra heat treatment processing step. Compared with reference [12], the YS and UTS in this work were over 250MPa higher for a comparable ductility.

Overall, some of the conditions in this study show that open die forging combined with induction heating to preheat and sinter the powder compacts is a good way of hot consolidating Ti alloys and in particular for Ti6Al4V alloy with a higher oxygen content of up to 0.5wt%. If the forging conditions are chosen carefully, the as-forged product can achieve acceptable levels of tensile strength and ductility and there is no need for a post forging heat treatment.

In comparison to the tensile properties of PM Ti6Al4V alloy, consolidated using other PM techniques, such as VS, HIP and MIM (Table 4.4), the forged discs in this work achieved considerably higher YS and UTS as well as comparable ductility.

Table 4.4 Tensile properties of Ti6Al4V alloy made by other powder metallurgy methods.

Consolidation method:	YS, MPa	UTS, MPa	ε, %	Reference:
ASTM standard- PM Grade 5	829	895	10	[1]
Metal Injection Moulding (MIM)	-	700	10	[18]
MIM	-	860	2	[19]
Hot Isostatic Pressing (HIP)	-	880	6	[20]
HIP	890	940	15	[21]
VS	860	940	4	[22]

The main reasons for the higher UTS are the comparatively high oxygen content of over 0.5wt%, compared with 0.33wt% in study [22] and 0.2wt% in studies [18-21]. Nevertheless, the fact that forging facilitates large amounts of material lateral flow, causes rupture of the oxide layer surrounding the powder particles and promotes the formation of new strong inter-particle bonds, has contributed to the high tensile strength.

4.12 Summary and Conclusions

- Irregularly shaped Ti6Al4V powders, with a powder particle size below 75 microns produced by the HDH method and having an oxygen content of 0.5wt%, were consolidated by open die forging.
- Induction heating, instead of the more traditionally used high vacuum sintering, was used for heating and pre-sintering powder compacts prior to forging.
- Induction heating rates were, on average, 280˚C/min. The time taken to reach maximum temperature during pre-sintering prior to forging was a maximum of 8 minutes. This is considerably faster when compared with vacuum sintering, where the total processing time can be more than 8 hours.
- The oxygen pick up during induction heating and holding for a maximum of 4 minutes at temperatures up to 1400˚C, was on average 0.06wt%.
- Thermomechanical consolidation resulted in a reduction in height of up to 65%.
- Optical microscopy showed that there was non-uniform deformation through the cross section and a porous layer was observed in the upper and lower surfaces of the forged discs.
- The porous layer and deformation gradient were result of insufficient consolidation due to a restriction in material flow close to the forging surfaces. The insufficient material flow is related to an increase in material resistance to flow because of heat loss. This occurs when transporting a compact from the heating zone to the forging zone and also there is the chilling effect of the forging die surfaces during the forging process. As a result, in some cases forging took place in the α-phase or the α+β phase region rather than in the β phase, which is more favourable for thermomechanical processing.

- The porous layer influenced the tensile properties along forged cross section, causing a scatter in data. Tensile test-pieces cut from the porous regions show a comparatively lower YS and UTS and significantly lower ductility.

- The selected IS parameters, with temperatures between 1000°C and 1400°C and with a sintering time of up to 4 min prior to forging, resulted in high values of YS and UTS. These results are what would be expected from sufficiently well consolidated powders.

- The induction heating parameters are essential for achieving sufficient elongation to fracture in the as-forged condition. The experimental conditions F4 and F6, i.e. heating to 1100°C and 1200°C and holding the samples at these temperatures for 4 min led to a good combination of strength and ductility, with elongations to fracture of 9.1% and 10.3% respectively and with corresponding UTS values of 1270MPa and 1236MPa in those samples cut from the center of a cross section. The good combination of strength and ductility is associated with the microstructure developed during forging. A typical microstructure found in these samples is a basketwave structure in the form of fine α-phase colonies consisting of unidirectionally orientated fine lamellae, with an outline of fine β-phase.

- The fracture surfaces of all the broken tensile tested samples showed evidence of fracture in fully consolidated material. Various type of fracture was observed depending on the ODF conditions and depending on the area of the cross section where the tensile piece was taken from. The fracture surface features are a consequence of the different microstructures and are in agreement with the tensile properties obtained.

- A recrystallization annealing heat treatment changes the microstructure from a coarse martensitic α′- phase to finer and more uniformly distributed colonies of α- phase lamellae outlined with β- phase, forming basketweave structure. The heat treatment did not affect the YS significantly. It resulted in a reduction in UTS, but still kept comparatively high values over 1150MPa. The elongation to fracture increased more significantly, from 2% to 11% after recrystallization annealing a compact forged using condition F10.

- The tensile properties such as YS and UTS achieved in this work are significantly higher compare to those of a wrought forged and annealed Ti6Al4V alloy and a PM Ti6Al4V alloy produced using low oxygen GA powders.

151

- The tensile strength of a PA Ti6Al4V forged disc exceeds that of the same alloy consolidated by other methods such as VS, HIP or MIM.

- The ductility of the forged Ti6Al4V alloy in most of the forging conditions is lower than the standard or it is in the lower range of the standard requirements.

- The reason for the high YS and UTS but lower ductility is the combination of: (1) the high oxygen content, (2) the residual stress caused by the TMP and (3) the mechanism of forging allowing additional cohesion between the powder particles.

- Overall, low cost PA HDH Ti6Al4V powders, with an oxygen content of 0.5wt%, can be used for powder consolidation by ODF.

- The results have shown that thermomechanical consolidation by induction sintering followed by direct forging of low cost PA HDH Ti6Al4V powders has the potential to be employed in the titanium powder metallurgy industry, where high tensile strength and intermediate ductility are required.

References

1.   ASTM, *Standard Specification for Powder Metallurgy (PM) Titanium and Titanium Alloy Structural Components*, in

2.   Zhang, D., et al., *Consolidation of titanium, and Ti-6Al-4V alloy powders by powder compact forging.* Materials Science Forum, 2009. **618-619**: p. 513-516.

3.   Nadakuduru, V.N., et al., *Mechanical Behaviour of Titanium, Ti-6Al-4V (wt %) Alloy and Ti-47Al-2Cr (at %) Alloy Produced using Powder Compact Forging.* Advanced Materials Research Vol. 275 (2011) 2011. **275**: p. 186-101.

4.   Kuhn, H.A. and L.B. Ferguson, *Powder Forging Mechanics*, in *Powder Forging*. 1990, Metal Powder Industry Federation,. p. 70-78.

5.   ASTM, *ASTM B988− 13 Standard Specification for Powder Metallurgy (PM) Titanium and Titanium Alloy Structural Components*.

6.   Boyer, R., G. Welsch, and E.W. Collings, *Alpha-Beta Alloys- Ti6Al4V*, in *Materials Properties Handbook- Titanium Alloys*. 2007. p. 488-597.

7.   Kuhlman, G.W., *Forging of Titanium Alloys*, in *ASM Metals Handbook Vol. 14*. 1993, ASM International. p. 269-601.

8.   Qiu, J.W., et al., *Microstructures and mechanical properties of titanium alloy connecting rod made by powder forging process.* Materials & Design, 2012. **33**: p. 213-219.

9.   Materials, A. *Tanium oxyde*. 2015; Available from: http://www.azom.com/properties.aspx?ArticleID=1179.

10.   Guo, H., et al., *The powder sintering and Isothermal Forging of Ti-10-2Fe-3Al.* JOM, 2008. **60**(11): p. 47-49.

11.   ASTM, *ASTM B348-13 Standard Specification for Titanium and Titanium Alloy Bars and Billets*.

12.   Lampan, G., *Wrought titanium and titanium alloys*, in *ASM Matals Handbook Vol.2*. 1990, ASM International. p. 1782-1886.

13.   Jia, M., *The Effect of Powder Characteristics and Processing Conditions on the Microstructure and Mechanical Properties of Titanium Alloys Made by Powder Forging, PhD* in *Engineering*. 2013, The University of Waikato http://researchcommons.waikato.ac.nz/handle/10289/8017: http://researchcommons.waikato.ac.nz/. p. p.238.

14.   Kuhn, H.A., *Forging and Hot pressing*, in *ASM Metals Handbook*. 1991. p. 1489.

15.   Smarsly, W. and W. Bunk, *Microstructure and texture of Combined Die Forging (CDF) Prealloyd Ti-6Al-4V Powder Compacts*. Powder Metallurgy International, 1985. **17**(26): p. 63-67.

16.   Smarsly, W. and W. Bunk, *Influence of Combined Die Forging (CDF) of Prealloyd Ti-6Al-4V Powder on Microstructure abd Mechanical Properties*. Metal Powder Report, 1986. **41**(10): p. 753-760.

17.   Eylon, D., *Titanium Powder Metallurgy Products*, in *ASM Handbook*. 1991. p. 1915-1925.

18.   Ergül, E., H.Ö. Gütsoy, and V. Günay, *Effect of sintering parameters on mechanical properties of injection moulded Ti-6Al-4V alloys*. Powder Metallurgy, 2009. **52**(1): p. 65-71.

19.   Horke, K., B. Ruderer, and R. Singer, *Influence of sintering conditions on tensile and high cycle fatigue behaviour of powder injection moulded Ti–6Al–4V at ambient and elevated temperatures*. Powder Metallurgy, 2014. **57**(4): p. 283-290.

20.   Liu, N., et al., *Powder metallurgical processing of Ti6Al4V alloy*. 2011 1st International Conference on High Performance Structures and Materials Engineering, ICHPSM 2011, May 5, 2011 - May 6, 2011, 2011. **217-218**: p. 1336-1342.

21.   Kim, Y., Y.-B. Song, and S.H. Lee, *Microstructure and intermediate-temperature mechanical properties of powder metallurgy Ti–6Al–4V alloy prepared by the prealloyed approach*. Journal of Alloys and Compounds, 2015. **637**: p. 234-241.

22.   Bolzoni, L., E.M. Ruiz-Navas, and E. Gordo, *Feasibility study of the production of biomedical Ti–6Al–4V alloy by powder metallurgy*. Materials science and Engineering C, 2015. **49**: p. 400-407.

Chapter 5

Development of Cost Effective Powder Metallurgy Ti Alloys by Thermomechanical Treatment

5.1 Introduction

The study discussed in this chapter originated from and was planned based on the results and the conclusions drawn from the previous two chapters. It was found that the tensile properties of forged PM Ti6Al4V alloy, made with pre-alloyed HDH powders, are not comparable to those of the corresponding wrought alloy. In particular, the YS and UTS were very high at the expense of ductility. The main reason for the difference in the properties was the higher oxygen content of the pre-alloyed powders used.

The main aim of this study was to develop cost effective PM Ti alloys with tensile properties comparable with those of wrought Ti6Al4V alloy and PM Ti6Al4V alloy with lower oxygen content. Instead of using pre-alloyed Ti HDH powders, which were difficult to source with acceptable oxygen content below 0.3wt%, a blended elemental (BE) approach was used to make the alloy compositions. Specifically, a blended elemental approach was chosen because it also allows for an alteration in the ratio of alloying elements or making non-standard alloy compositions, giving an opportunity to make alloys with variable mechanical properties, depending on the requirements for specific applications.

Apart from the α+β Ti6Al4V alloy composition, other cost effective alloy compositions were considered: a near α Ti3Al2V, and two novelty α+β alloys Ti5Fe and Ti3Fe1Cr0.6Ni0.2Mo called Ti5SS. The reasons for investigating these alloys are as follows:

(1) BE Ti6Al4V alloy was studied as a basis for comparing the structure and mechanical properties of the alternative alloy compositions.

 (2) Ti3Al2V alloy was studied because is a relatively new PM alloy which has not been extensively studied. The expectation was to develop a PM alloy with higher YS and UTS compared to the corresponding wrought alloy, due to the higher oxygen content of the starting HDH powder. In particular, the aim was to achieve properties comparable with those of wrought Ti6Al4V alloy to achieve the following benefits: a reduction in the cost of alloying elements; improved

workability of the alloy by a reduction in the amount of the α-phase stabilising element and consequently a reduction in the α to β phase transformation temperature; and improved ductility as a result of the reduced amount of alloying elements.

(3) Instances of alloying Ti with Fe using ingot practice are limited, because of the big difference in the density of the two elements. This causes segregation of Fe and formation of Ti-Fe intermetallic compounds, which are brittle at room temperature and lead to overall embrittlement of Ti. Using Fe as alloying element in PM is more appealing because it does not involve melting. Alloying Ti with Fe has some advantages: Fe and Fe master alloy powders are cheap and readily available; Fe is a β-phase stabiliser, which will improve the hot workability of the alloy. Fe has excellent diffusivity in the Ti crystal structure, which may improve sinterability. In this research, three types of Fe containing additions were used. Pure Fe powders with two different particle sizes were used, where alloy named Ti5Fe-c was made with Fe-carbonyl powders with smaller powder particles and the alloy named Ti5Fe-f was made with coarser powder particles; the third alloy named Ti5SS was made with 316LSS powders. The total alloying addition was set to 5wt%, similar to that in Ti3Al2V alloy.

There were two routes used for consolidation of the powder blends: consolidation by induction sintering (IS) followed by open die forging (ODF) or powder compact extrusion (PCE); and consolidation by vacuum sintering (VS), followed by ODF or PCE. Some of the extruded and forged samples were given a recrystallization annealing heat treatment. The parameters used in the experimental work are described in Chapter 2. Sintering by either IS or VS was done in two steps. Firstly, compacts were heated and held at a temperature lower than the sintering temperature to allow diffusion and homogenisation of the alloying elements in the Ti crystal structure. Secondly, compacts were heated and held at the actual sintering temperature. Slightly lower sintering temperatures were considered for the Ti-Fe based alloys to limit the kinetics of the eutectic reaction and the formation of intermetallic phases. For the thermomechanical treatment, the IS samples were directly transferred to the forging or extrusion die, while the VS samples were reheated using induction heating and then forged or extruded.

Different aspects of the processing method and resulting mechanical properties of the proposed cost effective PM alloy were studied. These included the effect of

sintering method (section 5.2), thermomechanical processing (section 5.3) and recrystallization annealing (section 5.4) on microstructure, tensile properties and fracture characteristics. Those factors affecting powder consolidation and tensile properties are discussed in section 5.5. The last section 5.6 gives a summary and conclusions of the findings in this study.

5.2 Consolidation of Ti6Al4V, Ti3Al2V, Ti5FeSS, Ti5Fe-c and Ti5Fe-f powder blends using vacuum sintering and induction sintering

5.2.1 Density and porosity distribution

For the different compositions investigated, the relative green densities and the densities after induction and vacuum sintering are shown in Figure 5.1.
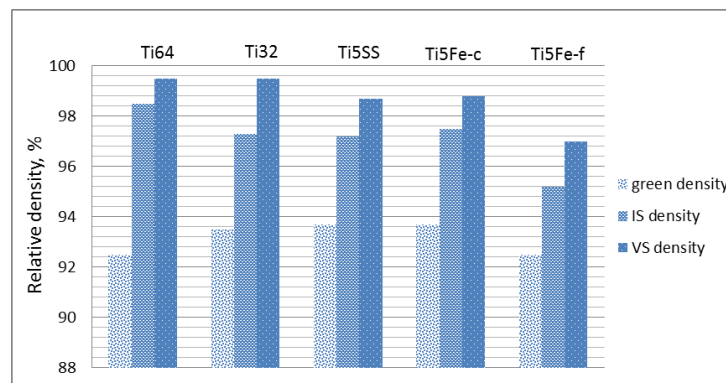
Figure 5.1 Relative green densities and densities as result of IS and VS of Ti6Al4V, Ti3Al2V, Ti5SS and Ti5Fe-c and Ti5Fe-f alloys.

The green densities of the pressed powder compacts varied between 92.5% and 93.7%. The lower green density observed in the Ti6Al4V powder mixture was related to the larger amount of the 60Al40V master alloy constituent which has a higher hardness than the Ti constituent. In the Ti5Fe-f powder compact the lower green density was attributed to the larger powder particle size of the Fe powders. Using either induction heating or a vacuum furnace for sintering resulted in a significant increase in density. The IS samples had densities between 95.2% and 98.5%. Ti6Al4V sample showed a higher IS density of 98.5% and the highest density increase of 6%. The reason for the increased sinterability in Ti6Al4V compared to Ti3Al2V was related to the increased amount of alloying elements in

157

Ti6Al4V. From the literature, there are two theories to account for this. The first is related to the higher diffusivity of Al and V in Ti, compared with Ti self-diffusion [1]. Hence, in the Ti6Al4V alloy with a higher amount of Al and V the amount of diffusion will be greater during the relatively short IS time. In the second theory, the improved sinterability is related to a reaction between Ti and the MA during heating in the temperature range of 850–1050°C, which leads to the formation of a Ti-Al intermetallic compound. This phenomenon was detected by differential scanning calorimetry (DSC) analyses in research studies on sintering mechanism of Ti6Al4V when 60Al40V master alloy powders were used for alloying [2, 3] . In study [3], comparative sintering of PA and BE Ti6Al4V powders showed that BE alloy has greater sinterability, which was related to the a quasi-peritectoid reaction in the Ti/60Al40V system. From here, it was concluded that reaction in the Ti6Al4V in this study would have been more intensive compared to Ti3Al2V because of the higher alloying content and consequently this resulted in greater sintering.

Ti5SS and Ti5Fe-c achieved an average density of 97.3% after IS and an average density increase of 4%, which is similar to that observed for Ti3Al2V. This is in spite of the fact that the IS temperature used for the Ti-Fe based samples was 50°C lower. This is evidence, as stated in the literature, that Fe has faster diffusivity in Ti compared with Al and V.

The lowest IS density of 95.2% was found in the Ti5Fe-f sample giving less than 3% density increase. This lower degree of densification was most likely related to the larger Fe powder particles used.

The vacuum sintered densities were higher compared to the induction sintered densities of the corresponding alloys. Ti6Al4V and Ti3Al2V were almost fully consolidated with a relative density of 99.5%. Clearly, the prolonged sintering time eliminated the effect of the increased sinterability of the Ti6Al4V alloy and gives the same end density for both alloys. The VS density of Ti5SS and Ti5Fe-c was 98.7% and this slightly lower value was probably due to the lower sintering temperature. Similar to the IS Ti5Fe-f alloy, the VS Ti5Fe-f alloy showed the lowest density of 97% and this was attributed to the larger 150µm diameter Fe powder particles used in this alloy composition [4, 5].

Micrographs indicating porosity levels in the as-sintered alloys are shown in Figure 5.2. For both sintering conditions, a significant amount of consolidation was evident. In all cases, only closed porosity with pores having a mostly rounded
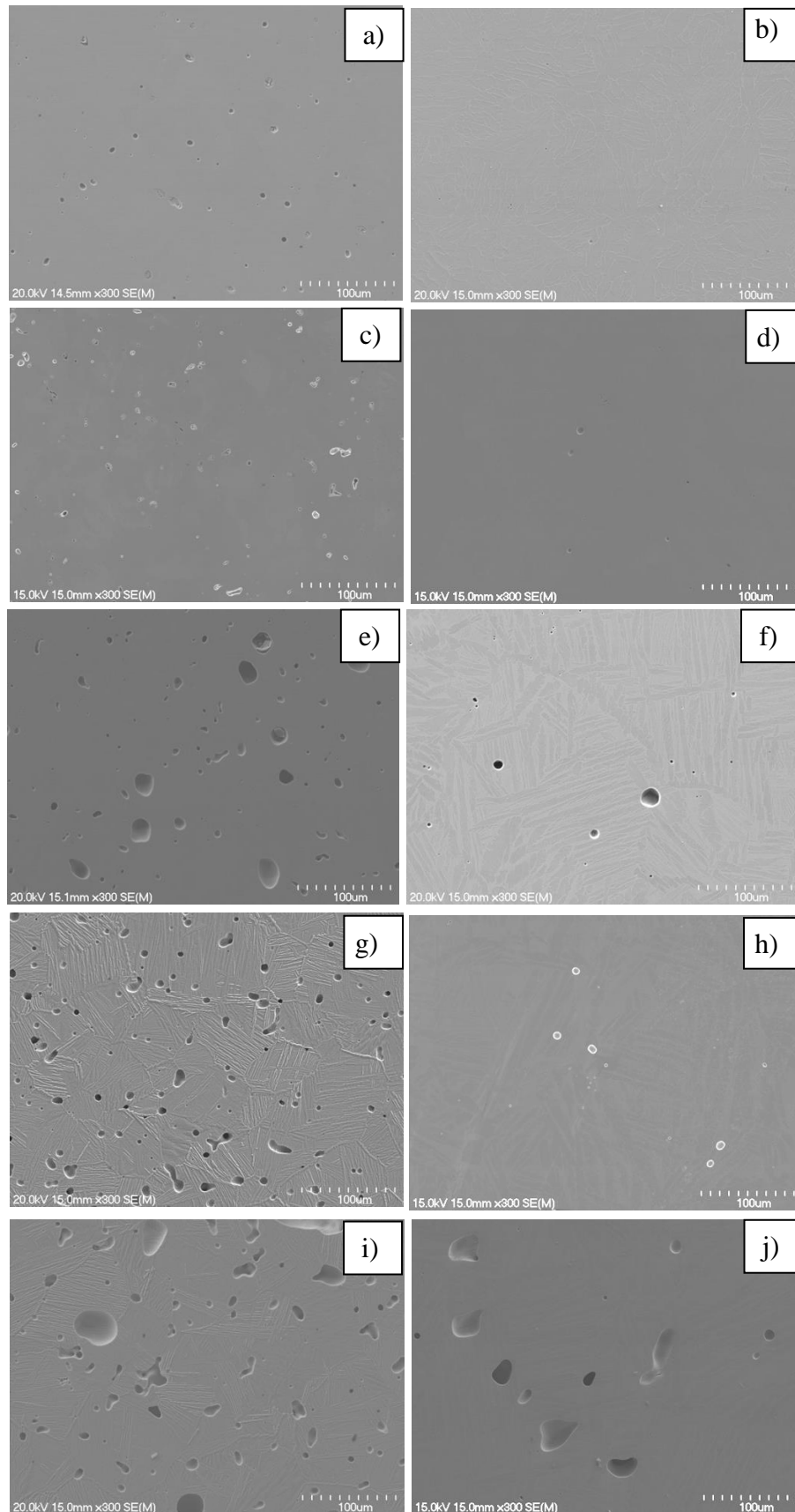
Figure 5.2 SEM images showing the porosity of: a) and b) Ti6Al4V, c) and d) Ti3Al2V, e) and f) Ti5SS, g) and h) Ti5Fe-c, and i) and j) Ti5Fe-f alloys respectively after IS and VS.

159

shape was observed, showing that the first two stages of sintering were completed i.e. material diffusion had occurred across the powder particle boundaries which led to the development of interparticle necking and neck growth to a stage where closed pores were formed.

Due to the much longer sintering time and higher sintering temperature the vacuum sintered samples had less porosity with only a few isolated small pores visible in the cross section (Figure 5.2 b), d), f), h) and j). The third stage of sintering, where the pores became well rounded and mostly closed, was almost completed. The VS densities for the Ti6Al4V, Ti3Al2V and Ti5Fe-c alloys in this work are higher than those reported in the literature [6-9]. The main reason for these results is attributed to the higher initial green density.

The observation of a significant number of well-rounded pores indicates that samples consolidated using IS had reached stage three of sintering (Figure 5.2 a), c), e), g) and i). In the Ti6Al4V and Ti3Al2V IS alloys the pores were much smaller and more uniformly distributed through the cross section. The average pore size in Ti6Al4V and Ti3Al2V alloys was in the range of few microns. The pores in the Ti-Fe based IS samples had wide-ranging sizes with a mixture of smaller pores with few pores bigger than 20-30 microns diameter. The pore size was influenced by the size of the Fe powder particles used for alloying, which is similar to the reported findings in other research on Ti-Fe PM alloys [4, 5]. The pores remaining in the Ti5Fe-f samples, prepared with comparatively larger Fe particles, were much bigger. It seems that the Fe particles diffused into the Ti matrix leaving voids related to the size of the Fe powder particles. This is known as the Kirkendall effect. For the Ti5Fe-f sample, because of the larger Fe particles, the sintering time was not long enough to ensure sufficient self-diffusion of Ti to enable closure of the voids (Figure 5.2 i).

5.2.2 Microstructural analyses

The various microstructures developed during sintering were influenced by the alloying elements as well as the sintering method (Figure 5.3 to Figure 5.7). The grain size (white circled areas) of all alloys was fairly similar. It was noticeable that the grain size was similar to the original Ti powder particle size of 75 microns and below. The mechanism of sintering is as follow: during sintering, Ti self-diffusion occurred at the Ti powder particle boundaries, where new grain

boundaries of the solid material were formed. During cooling, α phase nucleated and formed a layer of α-phase at the newly formed grain boundaries. Formation of this α-phase layer and the grain boundaries was observed in most of the as-sintered samples, excluding the IS Ti-Fe based alloys (Figure 5.5 to Figure 5.7 a) and a1).

During cooling, α-phase also nucleated from β phase inside each grain to form a lenticular or as called lamellar phase. The microstructure consisted of clusters of unidirectionally orientated α-lamellae, interspersed with β-phase. This type of microstructure is common for Ti α+β alloy and it is called basketweave microstructure [10].

The length and thickness of the α lamellae depends on the alloy composition and sintering condition. In the vacuum sintered microstructures, the thickness of the α-lamellae was noticeably bigger and the surrounding β-phase was coarser (Figures 5.3 to 5.7 (b) and (b1)) compared with those found in the IS microstructures (Figures 5. 3 to 5.7 (a) and (a1)). This was attributed to the significantly slower cooling rates in VS.
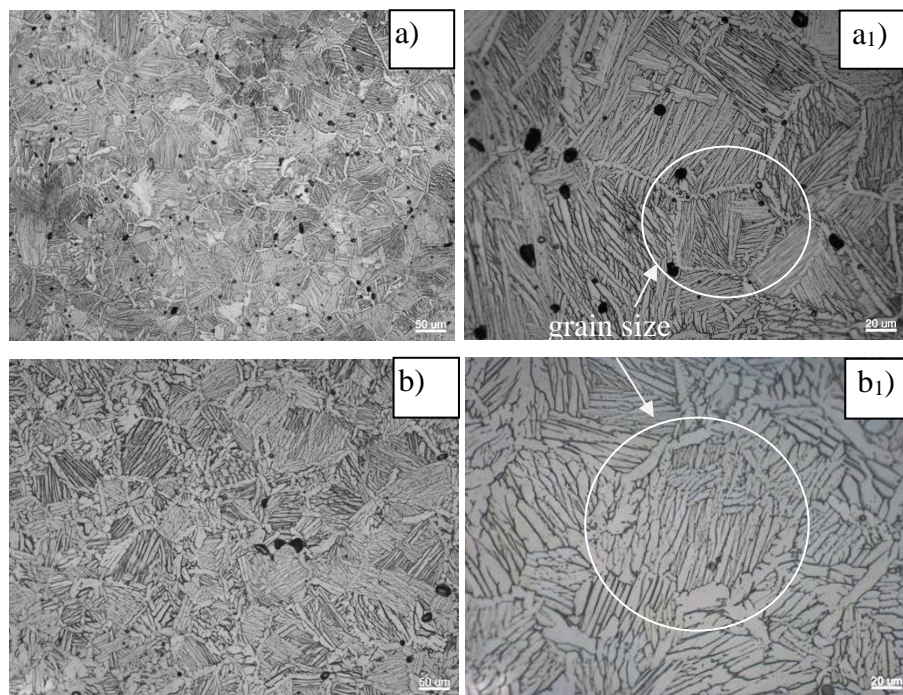
Figure 5.3 Optical microscope images showing the phase distributions in Ti64 alloy after IS (a) and (a1), and VS (b) and (b1).
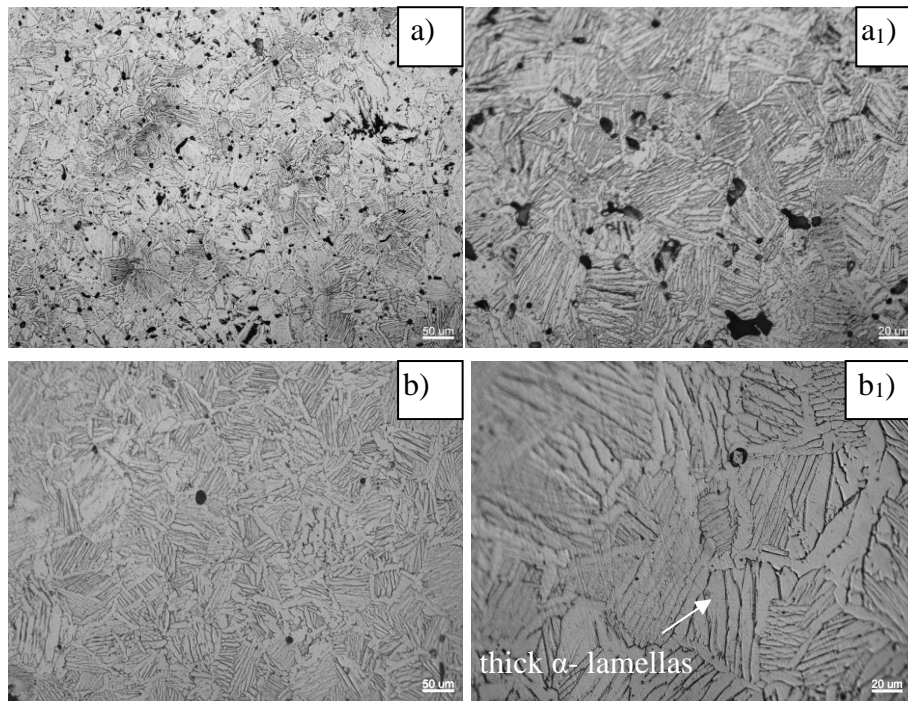
Figure 5.4 Optical microscope images showing the phase distributions in Ti32 alloy after IS (a) and (a1), and VS (b) and (b1).
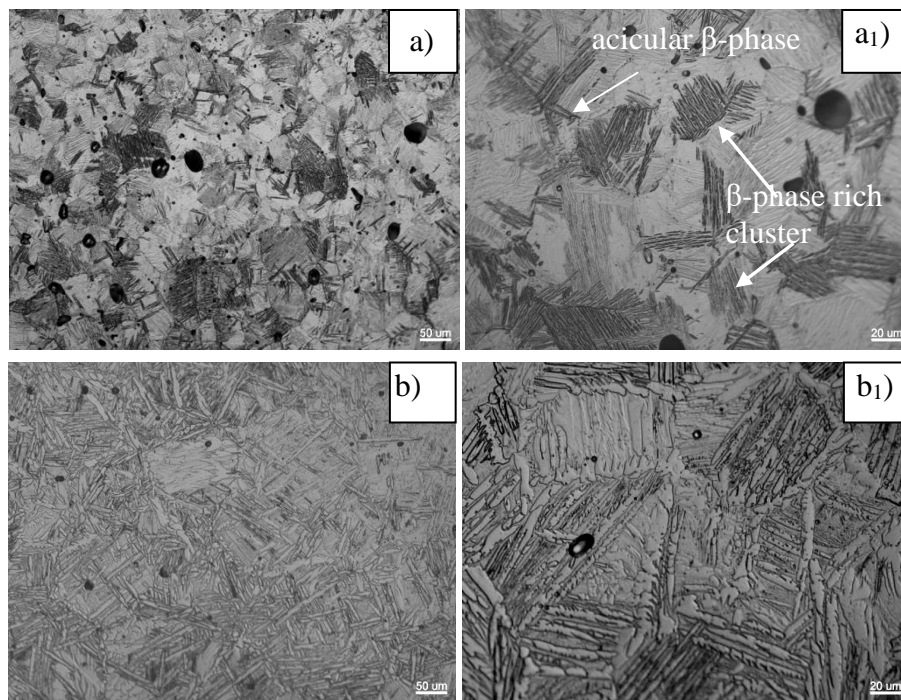
Figure 5.5 Optical microscope images of Ti5SS alloy showing the phase distributions after IS (a) and (a1), and VS (b) and (b1).
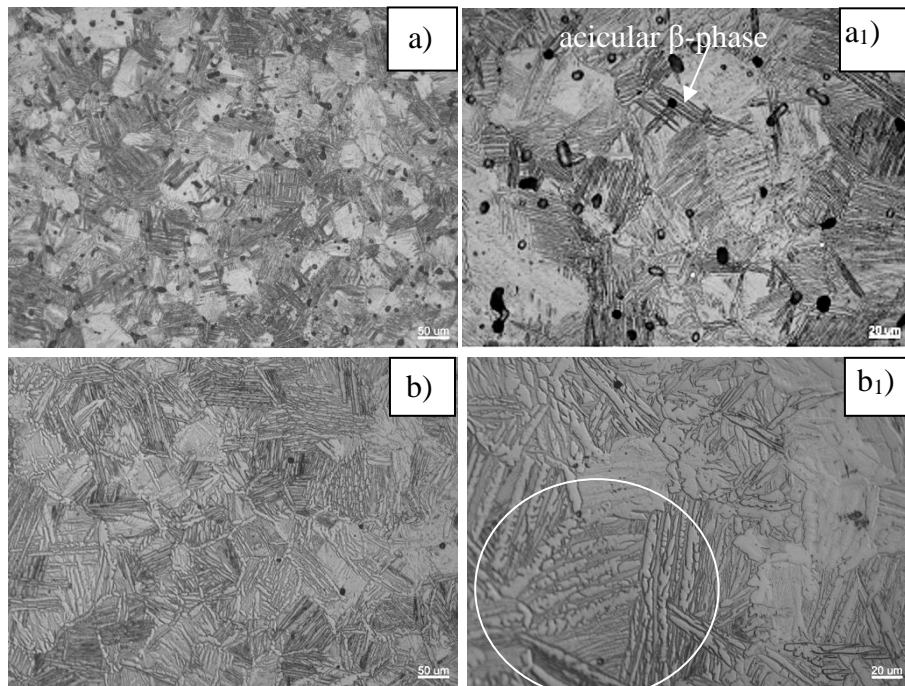
Figure 5.6 Optical microscope images of Ti5Fe-c alloy showing the phase distributions after IS (a) and (a1), and VS (b) and (b1).
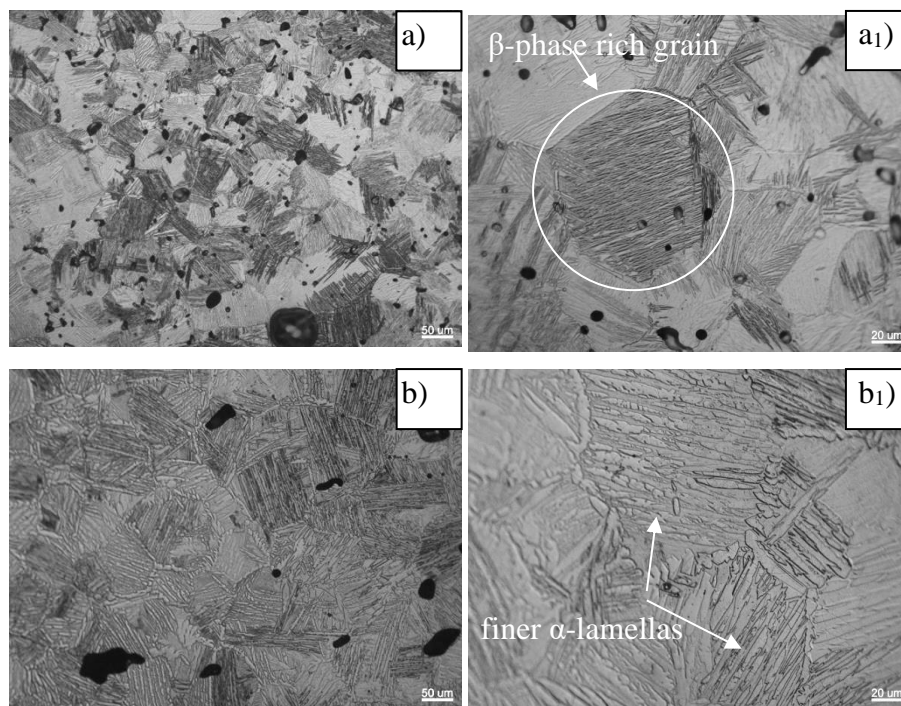
Figure 5.7 Optical microscope image of BE Ti5Fe-f alloy showing the phase distributions after IS (a) and (a1), and VS (b) and (b1).

The microstructures of both IS and VS Ti6Al4V alloy (Figure 5.3) were fairly homogeneous and similar to those reported in the literature [8, 11]. This confirmed that the shorter induction sintering time was able to achieve

microstructures that were similar to vacuum sintered microstructures, with the advantage of finer α phase lamellae in the IS alloy.

For all three IS Ti-Fe based samples, the microstructure was noticeably inhomogeneous (Figures 5.5 to 5.7 a) and a1). A predominately lamellar basketweave structure was still observed, but β-phase was not uniformly distributed. There were some β-reach clusters and grains distinguished by the darker contrast. In some regions, a coarser acicular β-phase was also observed. It was noticeable that the newly formed grain boundaries situated at the former powder particle boundaries were not outlined with α-phase, as observed in the rest of the samples. These might be because of uncompleted self-diffusion of Ti and might be an indication of insufficient consolidation, considering the comparatively lower sintering temperature of these samples.

The microstructures of the VS Ti-Fe based samples were homogeneous (Figures 5.5 to 5.7 b) and b1) with features similar to those of the Ti6Al4V and Ti3Al2V alloys, but the lamellae were finer in length and thickness. This was attributed to the larger amount of retained β phase, which gave more sides of nucleation of α phase and consequently has restricted the growth of the lamellae.

5.2.3 Oxygen contamination during sintering

The results of oxygen analyses of as-mixed powder blends and the sintered alloys are shown in Table 5.1. The oxygen content of the as-mixed powder blends was calculated using the rule of mixtures, based on the oxygen content of the elemental powders and the master alloy powders.

Table 5.1 Oxygen content of as mixed powder blends and after sintering.

Sintering method	Oxygen content, wt%				
	Ti6Al4V	Ti3Al2V	Ti5SS	Ti5Fe-c	Ti5Fe-f
As mixed	0.27	0.25	0.23	0.23	0.25
IS	0.44	0.34	0.32	0.34	0.34
VS	0.45	0.36	0.38	0.38	0.38

Ti6Al4V alloy showed the greater oxygen content after sintering of 0.44 and 0.45wt% respectively for IS- and VS-route. The oxygen increase was 0.17wt% and 0.18wt%, almost double of this recorded for the other alloys. A possible reason could be the comparatively lower green density of the Ti6Al4V powder

compact (Figure 5.1), as it was found out in the study in Chapter 3 (Table 3.6). Another reason could be the increased amount of Al in this alloy, knowing that Al has high affinity to oxygen.

The rest of the alloy compositions showed oxygen increases of 0.09wt% to 0.15wt%, with the induction sintered samples showing a slightly lower amount of oxygen pick-up compared with the vacuum sintered samples. This was expected and it relates to the significantly shorter induction sintering time. Nevertheless, the oxygen contamination after induction sintering was still significant, consider the much shorter sintering time. This was a result of the experimental setup, where the protective gas argon was used instead of high vacuum. The argon gas was flowing during the experiments, which might cause a contamination of the protective atmosphere with air. Reconsideration of the experimental setup might be needed to reduce the contamination during IS. The oxygen content of the as-sintered alloys exceeded that given in the ASTM standard for the corresponding alloys [12]. Overall, the degree of oxygen contamination was typical of that found after PM processing of Ti HDH powders [6, 13].

5.2.4 EDS study

EDS analyses were carried out for the following reasons: (1) to check if any undissolved powder particles of the alloying elements were present; (2) to verify if TiFe intermetallics formed during sintering; (3) to determine whether the alloying elements were evenly distributed in the Ti matrix and (4) to quantify the composition of the two phases observed in the microstructure.

There was concern that short time induction sintering may have left some undissolved Fe, 316SS or Al40V particles in the sintered structures. Some of the SEM images suggested that there might be some undissolved particles (Figure 5.8) and therefore confirmation was sought using EDS compositional analysis. This analysis did not show any compositional anomalies to suggest that there were Fe, Al or V rich regions, which led to the conclusion that short time IS was enough for the dissolution of alloying elements in the Ti matrix.

(a)Ti5Fe-f-IS	Ti, wt%	Fe, wt%
area 1	95.86	4.14
area 2	96.74	3.26
area 3	90.23	9.77
(b)Ti5Fe-c-IS		
area 1	95.96	4.04
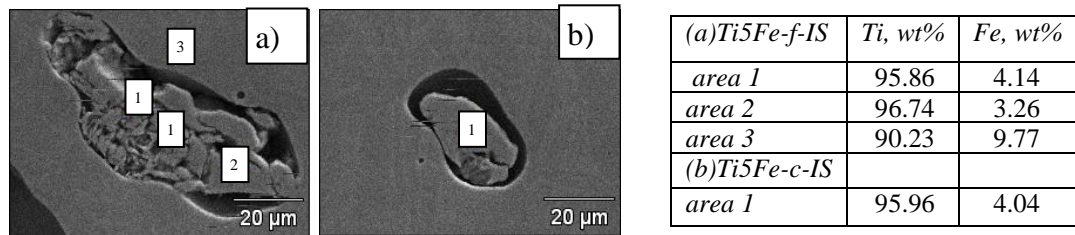
Figure 5.8 EDS elemental analysis of induction sintered a) Ti5Fe-f and b) Ti5Fe-c alloys.

Further elemental analysis were carried out on the cross sections of the Ti5Fe sintered samples to find out how homogeneously the Fe was distributed in the Ti matrix. The results showed a fairly uniform distribution of Fe for both IS and VS Ti5Fe-c alloy (Figure 5.9 a1 and b1), but in the Ti5Fe-f alloy the Fe concentration in the examined cross-section was not as uniform (Figure 5.9 a2 and b2).

	(a1)Ti5Fe-c-VS	(a2)Ti5Fe-f-VS	
	1	1	2
Ti, wt%	95.50	92.92	96.13
Fe, wt%	4.50	7.08	3.87

(b1)Ti5Fe-c-IS			(b2)Ti5Fe-f-IS			(b3)Ti5Fe-f-IS	
	Ti,wt%	Fe,wt%		Ti, wt%	Fe,wt%		Ti, wt%	Fe,wt%
1	94.51	5.49	1	97.15	2.85	1	97.61	2.39
			2	96.24	3.76	2	88.08	11.92
			3	96.00	4.00	3	87.68	12.32
			4	98.14	1.86	4	91.62	8.38
			5	95,27	4.73			
			6	91.96	8.04			
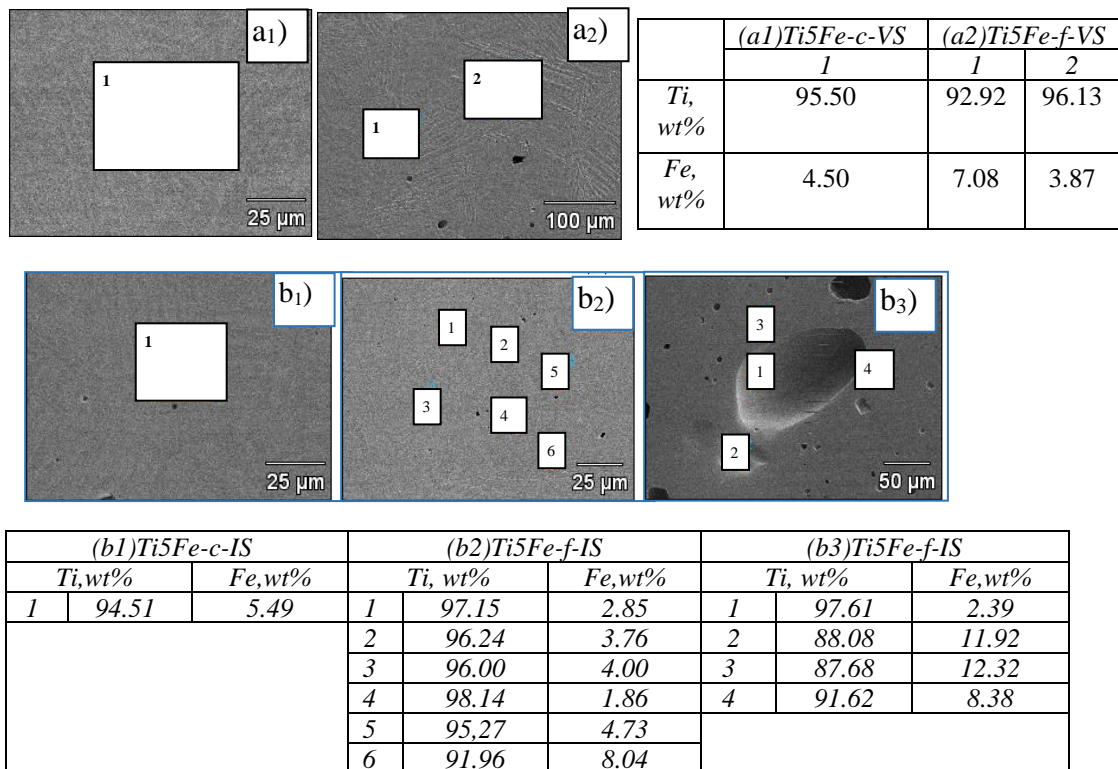
Figure 5.9 EDS elemental analysis of vacuum sintered a$_1$) Ti5Fe-c and a$_2$) Ti5Fe-f and induction sintered b$_1$) Ti5Fe-c, b$_2$) and b$_3$) Ti5Fe-f alloys.

The concentration of Fe associated with the large pores in the Ti5Fe-f sample was two to three times higher than the intended compositional value of 5wt% (Figure 5.9 b$_3$). These results suggested that an IS time of 10min was long enough to dissolve the larger Fe particles, but not long enough to complete the diffusion to obtain a homogeneous distribution of Fe in the Ti matrix. Even VS of Ti-5Fe-f

alloy for 2h at 1300˚C was not long enough to homogenise the microstructure (Figure 5.9 a$_2$). Although the Fe distribution was not uniform, the level of Fe concentration was not consistent with TiFe intermetallic formation. This observation led to the conclusion that there was no eutectic reaction in the Ti5Fe alloys during sintering.

Spot elemental analysis and elemental mapping were carried out to identify the composition of the phases. The results showed that in the Ti-Fe based alloy compositions for both IS and VS conditions, the Fe was mostly situated in the brighter phase (Figure 5.10), while the darker phase was almost entirely pure Ti. Knowing that Fe is a β-phase stabilizer, it was concluded that the bright phase was the β-phase. The amount of the brighter phase in all of the Ti-Fe based sintered samples was comparatively high, suggesting that a significant amount of β-phase had been retained in both IS and VS samples.

a)

5Fe-c-VS	Ti, wt%	Fe, wt%
1	91.82	8.18
2	99.60	0.40

b)
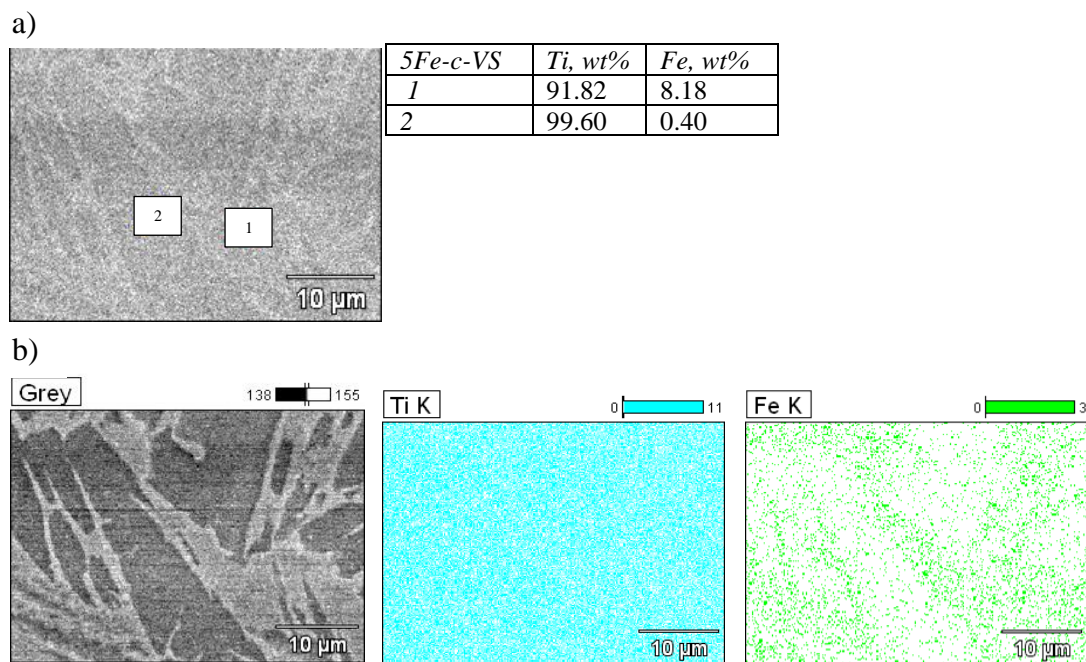
Figure 5.10 EDS elemental a), and b) spectral imaging analysis of Ti5Fe-c alloy consolidated by vacuum sintering.

In the alloys Ti6Al4V and Ti3Al2V, the darker phase was the most dominant. The spot EDS analyses showed that most of the aluminium was concentrated in the darker phases (Figure 5.11, Pt.3 to Pt.7).

Ti6Al4V-VS	Ti, wt%	Al, wt%	V, wt%
1	83.79	2. 03	14.18
2	82.30	1.97	15.74
3	94.23	3.95	1.82
4	92.86	5.64	1.50
5	91.25	6.61	2.14
6	90.11	5.61	4.28
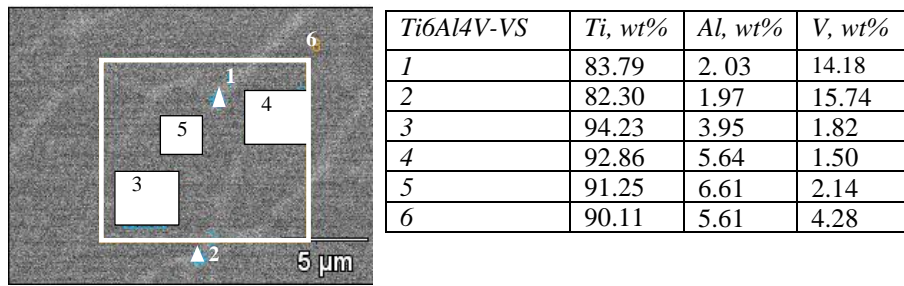
Figure 5.11 EDS elemental analysis of Ti6Al4V alloy consolidated by vacuum sintering.

Aluminium had less tendency to be present in the brighter phase. On the other hand, vanadium was found preferentially in the brighter phase, reaching concentrations of over 15wt% for the Ti6Al4V alloy (Figure 5.11 Pt1 and Pt.2). Overall, the area analyses showed a uniform distribution of the two alloying elements (Figure 5.11 area 8). The results of the EDS analyses suggested that the darker, aluminium rich phase was α-Ti and the brighter, vanadium rich areas were β-phase. Compared to the Ti-Fe based samples, the amount of retained β-phase was significantly less.

5.2.5   XRD study

Further XRD analysis were done to identify the effect of sintering on the constituent phases.

When the XRD patterns of the sintered alloys were compared with those from the as-mixed powders, the peaks of the alloying constituent 60Al40V and Fe, present in the powders, had disappeared after both VS and IS. This confirms the EDS results that all of the powder particles of the alloying elements had dissolved during sintering (Figure 5.12). In Ti3Al2V alloy only α-Ti peaks were noticeable, while in Ti6Al4V there was a β-Ti peak with a very low intensity (Figure 5.12 a). This suggests that the amount of retained β-phase in Ti3Al2V alloy was very small and it was slightly higher in the Ti6Al4V alloy. It was noted that in all sintered XRD patterns of Ti6Al4Vand Ti3Al2V, the α-Ti peaks were slightly shifted from their reference positions in the as-mixed powder, indicating that the lattice parameters were changed due to the incorporation of Al atoms into the Ti crystal structure. The positions of the peaks for VS Ti6Al4V were shifted further to the right than observed in the other alloys. This could be because of the larger Al content in Ti6Al4V. However, this effect was not seen in the IS Ti6Al4V

sample. A possible reason is the shorter heating time, which did not allow sufficient movement of the Al atoms to cause change in the Ti lattice parameters.
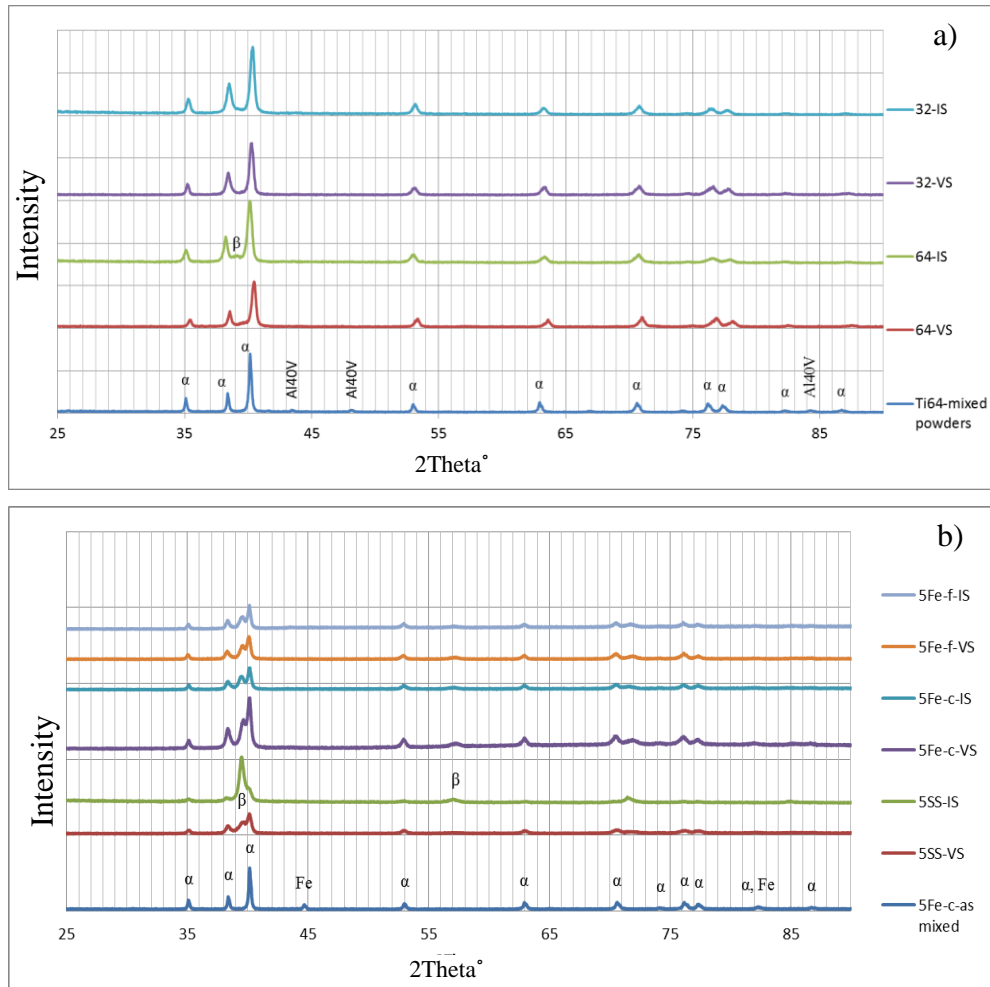
Figure 5.12 X-Ray diffraction patterns of as-sintered a) Ti3Al2V and Ti6Al4V and b) Ti5SS, Ti5Fe-c and Ti5Fe-f alloys.

After both IS and VS, there were no TiFe intermetallic peaks in the XRD patterns from Ti-Fe based alloys, confirming the EDS observation that no liquid phase was formed during sintering.

Peaks of β-Ti were observed in all three Ti-Fe alloys, indicating that a significant amount of β-phase was retained in both IS and VS samples. Similar observations were made in other studies on VS of Ti-Fe alloys [7, 14]. It was noticed that in all Ti-Fe based sintered samples the β-Ti peaks had shifted to the right compared to the positions of the reference peaks, suggesting that the Fe atoms incorporated in the Ti lattice might cause change in the lattice parameters. This was also confirmed from EDS analysis where it was shown that elemental Fe was mostly

associated with the brighter β-phase shown in the elemental maps (Figure 5.10). The Ti peaks in IS Ti5SS were identified as mostly β-Ti peaks. This was explained by the significantly faster room temperature cooling after IS compared to the furnace cooling after VS. This feature of the XRD analysis was only observed in the Ti5SS alloy possibly because phase transformation in this alloy is more sensitive to cooling rate, consider the presence of additional β stabilising elements Cr and Ni.

5.2.6 The effect of sintering method on the tensile properties of sintered alloys

Figure 5.13 shows a comparison of the tensile properties of the sintered alloys.
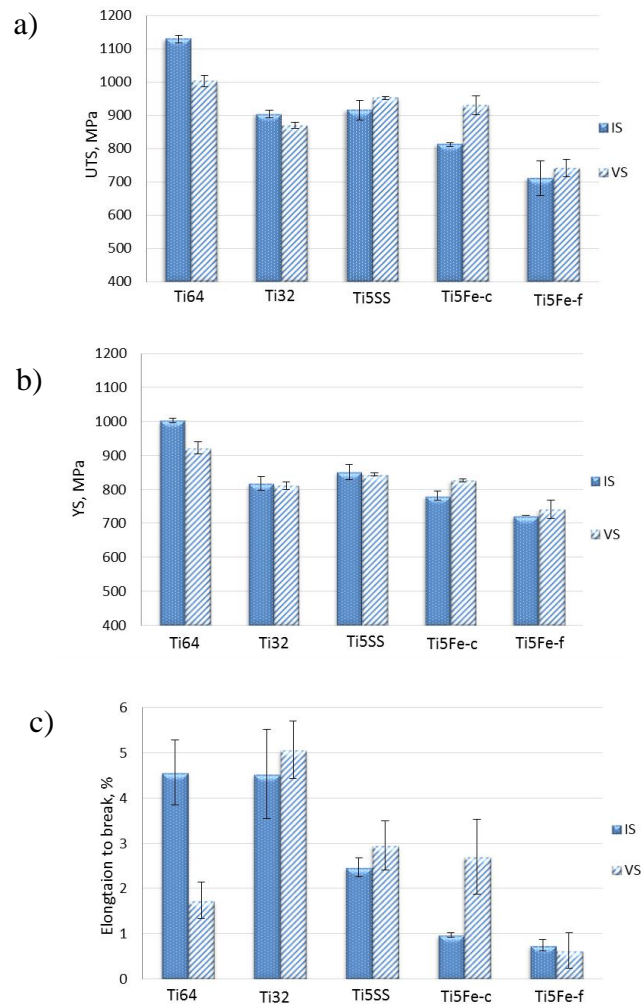
Figure 5.13 Effect of sintering method on the tensile properties: a) YS b) UTS and c) elongation to fracture, of as-sintered Ti6Al4V, Ti3Al2V, Ti5SS, Ti5Fe-c and Ti5Fe-f alloys.

170

As expected, the Ti6Al4V alloy has the highest values of YS and UTS for both sintering conditions, largely because of the higher alloying content which would have contributed to increased strengthening. In spite of its lower density the IS Ti6Al4V alloy was stronger than the VS material with YS and UTS of 1000MPa and over 1130MPa respectively and ductility of 4.5 %. The yield strength and tensile strength of the VS material were 920MPa and 1000MPa respectively with only 1.8% elongation to fracture. The main reason for the higher strength of IS material was the finer α-phase lamellar structure after significantly shorter IS (Figure 5.3).

In spite of the higher level of porosity after IS of the Ti3Al2V alloy, the tensile properties of the IS Ti3Al2V alloy were similar to those of the VS Ti3Al2V alloy. The YS was just over 800MPa for both sintering methods, but the UTS varied slightly and was 880MPa after IS and 900MPa for VS material. Both sintering methods produced a similar elongation to fracture of 4.5% and 5% respectively for IS and VS material. It appears that the finer IS microstructure compensated for its lower density.

Overall, it was noticeable that the YS and UTS of Ti6Al4V and Ti3Al2V sintered alloys were greater than the ASTM specification and the elongation to fracture was much lower. The main reason for this difference was the high oxygen content (Table 5.1) of the processed material.

Similar to the Ti3Al2V, the sintering method did not have a significant effect on the tensile properties of the alloy Ti5SS. In spite of the comparatively lower VS sintering density, the YS and UTS of Ti5SS alloy were slightly higher than that of alloy Ti3Al2V, but the ductility was lower (2.5 to 3%). The higher YS and UTS in the VS Ti5SS alloy were mainly because of the finer α-lamellae in the sintered microstructures. On the other hand, the lower ductility in this sample was related to a coarser acicular morphology of the β-phase found in the microstructure of this alloy (Figure 5.5).

The sintering method had a significant effect on the tensile properties of Ti5Fe-c alloy. This alloy showed a good response to VS with YS and UTS comparable to those for Ti3Al2V and Ti5SS and an elongation to fracture of 3%. This is similar to that for Ti5SS alloy. Unexpectedly the IS UTS was lower reaching a value of only 800MPa, with a low YS and no ductility. The reasons behind the low IS tensile properties could be: the courser morphology of the β-phase (Figure 5.6); and insufficient sintering due to the lower sintering temperature as evidenced by a

lack of α-phase on the newly formed grain boundaries of the sintered material. Another reason for the low tensile properties might be an inhomogeneous α+β distribution, as seen in the optical metallography of these alloys (Figure 5.6 a) and a1).

The Ti5Fe-f alloy showed low tensile properties after both sintering conditions, with a UTS just above 700MPa and with no yielding and ductility. The reasons were the lower sintered densities, the large pores observed in the microstructure (Figure 5.2 i) and j) and an inhomogeneous distribution of Fe as observed from the EDS examination (Figure 5.9 a2) and b2).

5.2.7 Fractography

Fracture analysis of broken tensile pieces from sintered alloys showed that fracture occurred by mixture of intergranular fracture, transgranular cleavage and ductile fracture as evidenced by the ductile dimples. In general, the low magnification images show that in the IS samples (Figure 5.14 a) and c) there is large amount of intergranular fractures, evident by the comparatively large number of long fracture paths along the fracture surface. The amount of similar fracture paths is much less in the VS samples, showing that much stronger interparticle bonding occurred during VS (Figure 5 b) and d).

More details of the fracture behaviour are seen in the higher magnification images in Figure 5.14 e) to h). In the IS Ti3Al2V alloy (Figure 5.14 e), intergranular fracture is evident from the large fracture paths going through a large number of grain boundaries. Large amount of shallow transgranular dimples were also formed during fracture inside the grains. There are also fragments with transgranular cleavage with secondary fracture at the α+β lamellae phase. The fracture surface of the IS samples also shows large amount of voids originating from the porosity of the sintered structures. The fracture at the voids did not have a significant effect on the tensile strength, as seen from the relatively high YS and UTS and presence of ductility in this sample.

In the fracture surface of the VS Ti32 alloy (Figure 5.14 f), the intergranular fracture is significantly less evident. There is a large amount of transgranular dimples. The dimples have a rounded appearance when the fracture is associated with α phase, and have an elongated appearance when the fracture is through the α+β lamellae phase. Compare to the IS samples, there are not many voids in the

fracture surface of the VS material, but the fracture paths at the α+β lamellae are coarser, corresponding to the comparatively larger size of the α+β lamellae. The fracture surface of Ti6Al4V sintered alloy is not shown in this work, but it has similar features to the Ti3Al2V alloy, showing more intergranular fracture and voids in the IS conditions and predominately transgranular cleavage and dimples in the VS conditions.

a)

b)

c)

d)

e)

Fracture at the pores

Intergranular fracture path

Shallow dimples at α grain

Transgranular cleavage and secondary fracture at the α+β lamellae phase

f)

dimples

transgranular fracture at the α+β lamellae

Intergranular fracture path

Kirkendall pores

g)

h)

Dimples formed by fracture at β phase

Fracture at the grain boundaries

Fracture at α+β lamellae phase

Dimples formed by fracture at β phase

Figure 5.14 Fracture surface of a) and b) Ti3Al2V; c) and d) Ti5Fe-c low magnification images and e) and f) Ti3Al2V and g) and h) Ti-5Fe-c high magnification images respectively of induction sintered and vacuum sintered alloys.

Similar to the IS Ti-Al-V alloys, the fracture surface of the IS Ti-5Fe-c alloy contains a large number of voids originating from the pores remaining after IS. Some of the pores are probably Kirkendall pores remaining from the dissolved Fe particles. The significant amount of intergranular fracture in the IS Ti5Fe-c alloy suggests that the inter-particle bonding was not fully developed during the relatively short holding time at maximum temperature during IS. This observation confirms the results from the microstructural analysis, where very small amount of α phase was nucleated at the new grain boundaries. This indicates that there was insufficient diffusion bonding between the Ti powder particles. These results were also confirmed by the low tensile strength and poor ductility of the IS Ti5Fe-c based sample. Ductile dimples were also observed at the fracture surface, indicating that fracture also occurred within the retained β-phase. Nevertheless, that had little effect on the ductility of this alloy.

The amount of intergranular fracture in the VS Ti5Fe-c samples is significantly less. No Kirkendall pores were observed, confirming the high level of sintering in this sample (Figure 5.14 h). A predominantly transgranular fracture with flat elongated segments was observed, where the fracture occurred in the α+β lamellae phase. Ductility in this alloy was confirmed by a significant amount of ductile dimpling associated with the β-phase, which is well present in this alloy.

The fracture behaviour of Ti5SS and Ti5Fe-f sintered alloys is not discussed in details in this work. It was similar to Ti5Fe-c alloy, showing a large amount of voids and intergranular fracture in the IS alloys, and predominately transgranular fracture in the VS structures, evident by the dimples formed during fracture at α+β lamellae or β-phase. The fracture surface of the vacuum sintered Ti5Fe-f alloy showed large amount of porosity remaining from sintering, confirming the insufficient vacuum sintering, due to the large Fe powder particles, and the low tensile properties.

5.3   Thermomechanical treatment of the sintered Ti6Al4V, Ti3Al2V, Ti5SS, Ti5Fe-c and Ti5Fe-f alloys

The sintered billets of all alloy compositions and both sintering methods were further thermomechanically processed (TMP) using open die forging and extrusion. The experiments where the powder compacts were directly forged or extruded after induction sintering is referred as induction sintering route (IS-route). The experiments where the compacts were vacuum sintered and then reheated and forged or extruded is referred as vacuum sintered route (VS-route). Some of the TMT samples were heat treated by annealing. The forged and extruded samples were analysed to identify their formability. The effect of the thermomechanical processing on the microstructure, phase distribution, tensile properties and fracture behaviour were studied. The effect of the heat treatment on the microstructure, mechanical properties and fracture surface were also considered.

5.3.1   Assessment of the formability of the thermomechanically treated alloys

Images of samples after thermomechanical treatment following the IS- and VS-route are shown in Figures 5.15 and Figure 5.16 respectively. After open die forging (ODF) the sintered billets were deformed into discs. There were circular marks on both surfaces of the forged samples, which were similar to those observed in the Ti6Al4V forged samples in Chapter 4. The circular marks were due to a chilling effect causing a restriction in the material flow due to contact with the die surfaces.

Figure 5.15 Images of a) Ti6Al4V, b) Ti3Al2V, c) Ti5SS, d) Ti5Fe-c, e) Ti5Fe-f alloys consolidated by forging or extrusion following IS-route.

Figure 5.16 Images of Ti6Al4V, Ti3Al2V, Ti5SS, Ti5Fe-c and Ti5Fe-f alloys consolidated by forging or extrusion following VS-route.

The reduction in height after forging was 65.6% for the Ti6Al4V forged disc, 68.4% for Ti3Al2V and 69.3% for Ti5Fe-f, Ti5Fe-c and Ti5SS. The smaller reduction in

height for Ti6Al4V during forging is due to the larger amount of Al, which is an α-phase stabilising element. During forging, because of contact with the forging die the temperature of the forged billet fell quickly. Since the α- to β-phase transformation starts comparatively earlier for Ti6Al4V alloy [15], there is less forging time whilst the billet temperature is in the β-phase field and this leads to less deformation.

Ti-Fe based samples were thermomechanical treated at a slightly lower temperature of 1150°C to avoid the eutectic reaction and formation of the intermetallic TiFe compound, which is brittle at room temperature (Figure 5.17).
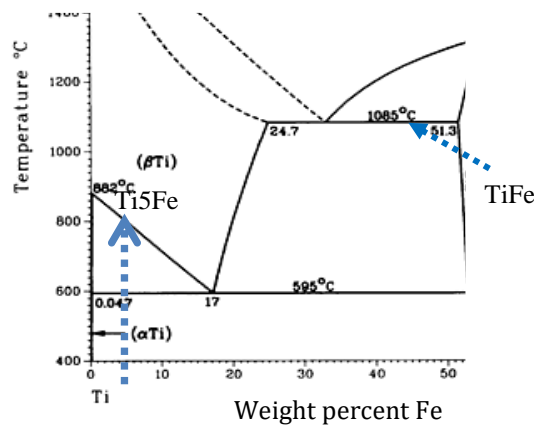
Figure 5.17 Part of Ti-Fe phase diagram [16].

In spite of the lower forging temperature, these samples achieved a reduction in height slightly greater than that of the Ti3Al2V sample. This is, because Fe is a β-phase stabilizing element which lowers the α- to β- phase transformation temperature (Figure 5.17). This allows for a longer forging time whilst in the β-phase region. For the similar reason the Ti-Fe based extruded bars were significantly longer- 220mm compared to 120mm and 100mm for Ti3Al2V and Ti6Al4V respectively.

The sintering method did not have a significant effect on the formability of the thermomechanically treated alloys.

5.3.2   Thermomechanical processing by open die forging

Further thermomechanical treatment by open die forging (ODF) after sintering resulted in significant changes in the microstructure. The high temperature plastic

deformation caused a redistribution in the porosity and changes in the grain structure and phase distribution, which significantly affected the tensile properties.

5.3.2.1 Porosity distribution

An analysis of the cross sections of forged samples revealed differences in the shape, size and the number of the pores. In the middle sections away from the forging surface, most of the pores were collapsed and closed (Figure 5.18).
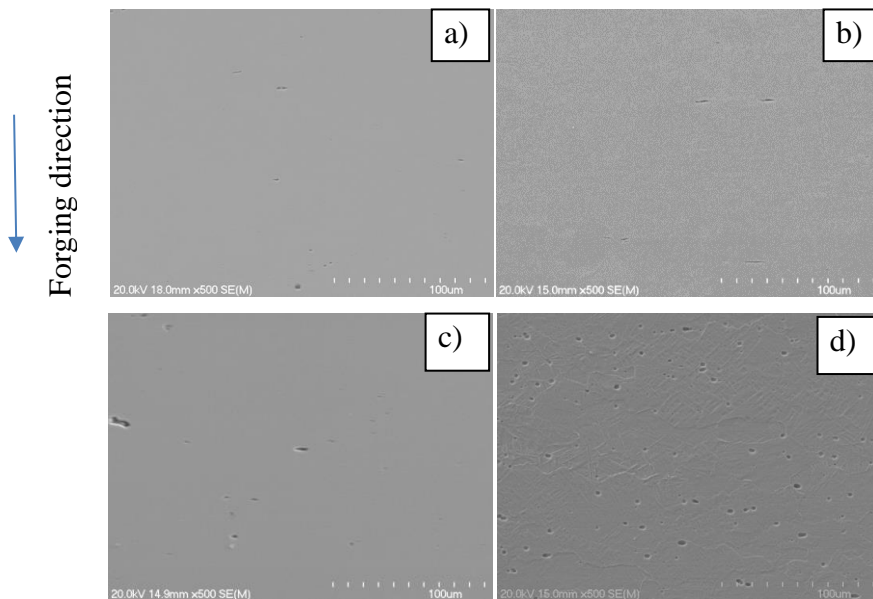
Figure 5.18 SEM images of porosity in the middle section of the forged a) Ti6Al4V, b) Ti3Al2V, c) Ti5Fe-c and d) Ti5Fe-f alloys followed IS-route.

Only a small number of isolated pores with a flattened appearance were observed in most samples (Figure 5.18 a) to c). An exception was for the Ti5SS and Ti5Fe-f samples forged following the IS route, where there were still a large number of smaller pores in the middle sections (Figure 5.18 d).

There was a pore rich layer observed along the forged surfaces (Figure 5.19). The porous layer was about 500μm thick irrespective of the composition and the sintering history of the alloys. The size and number of pores depended on the sintering route. The samples produced by the IS-route showed a greater number of pores (Figure 5.19 a) to e), related to their comparatively low sintered densities. In contrast to the flattened pores in the middle of a forged disc, the pores close to the surface were hardly deformed. This showed that there had been little material flow and consequently little deformation occurring in the areas near to the die surfaces during forging.
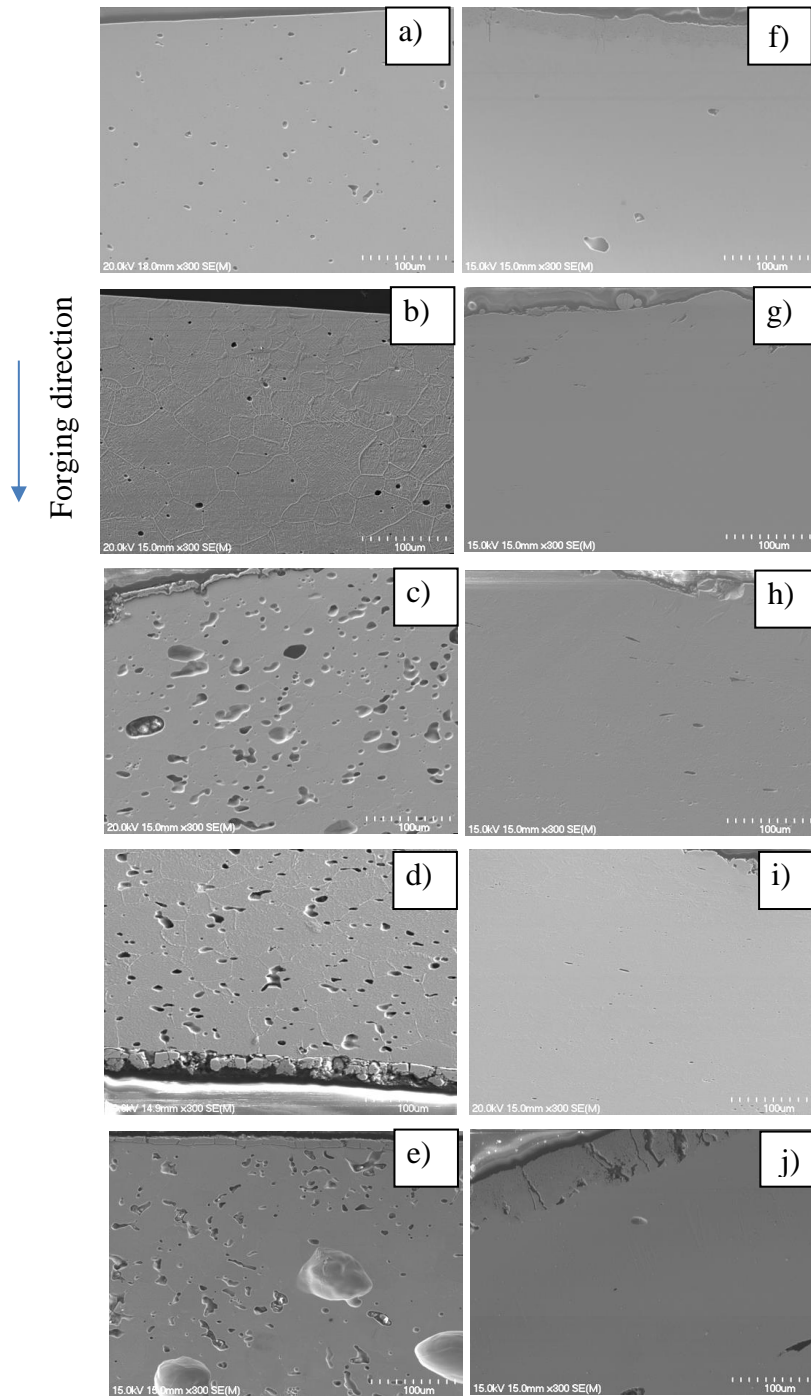
Figure 5.19 Porosity distribution in areas near the forging surface of a) and f) Ti6Al4V, b) and g) Ti3Al2V, c) and h) Ti5SS, d) and i) Ti5Fe-c, and e) and j) Ti5Fe-f followed respectively IS- and VS-route.

In the forged samples processed via the VS route the number of pores in the porous layer was significantly lower, with smaller sized pores with a more flattened appearance (Figure 5.19 f) to j).

After etching the forged cross sections, a gradient of the amount of grain deformation (Figure 5.20) was revealed, similar to that found in the forged Ti6Al4V samples in Chapter 4.
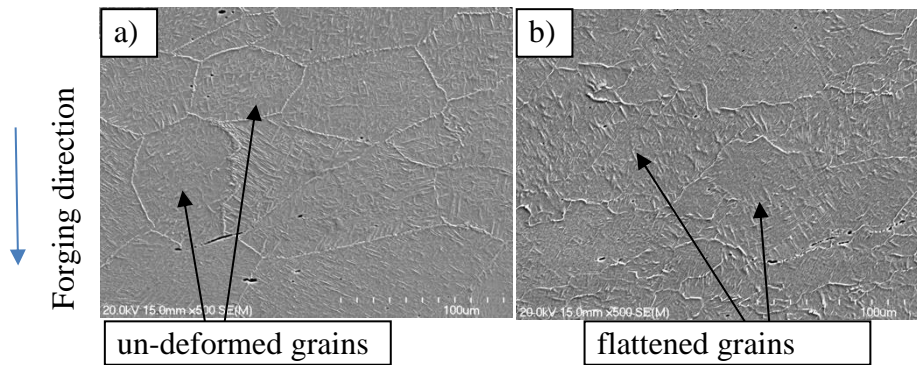
Figure 5.20 Grain morphology of the forged followed IS-route Ti-5Fe-c alloy a) close to the forged surface b) middle section.

The grains close to the forged surface were almost un-deformed, whereas textured and flattened grains were observed in the middle sections. This behaviour was found in all samples, which was due to the nature of the plastic deformation by forging, where the stress state varies throughout the workpiece. The friction at the workpiece/die interface causes a compressive stress along the surface of the sample, which when combined with the chilling effect of the die surfaces lead to limited deformation in these areas [17]. For this reason, it is common to find a limited deformation and porosity layer in forged powder preforms. From the results in this section, the volume fraction of pores was closely dependent on the sintered density. Hence, the sintered density is a key factor for controlling the porosity and densification during hot forging.

5.3.2.2 Microstructural analysis

The middle sections of each forged disc, where full deformation occurred, were used for microstructural analysis.

The microstructures of forged Ti6Al4V and Ti3Al2V alloys had similar features. (Figure 5.21). The α phase grain boundaries and the lamellar α+β structure observed in the as-sintered structures are not present in the as-forged structures. Instead, a coarse acicular phase, referred to as martensitic α phase was observed [18-20], showing that the cooling rates during forging were faster than the critical rate needed for martensitic formation [21, 22]. The dark phase observed in the etched microstructure is retained β-phase. This phase was present in larger amounts in the Ti6Al4V alloy, which is related to the larger amount of β phase stabilizing V.

180
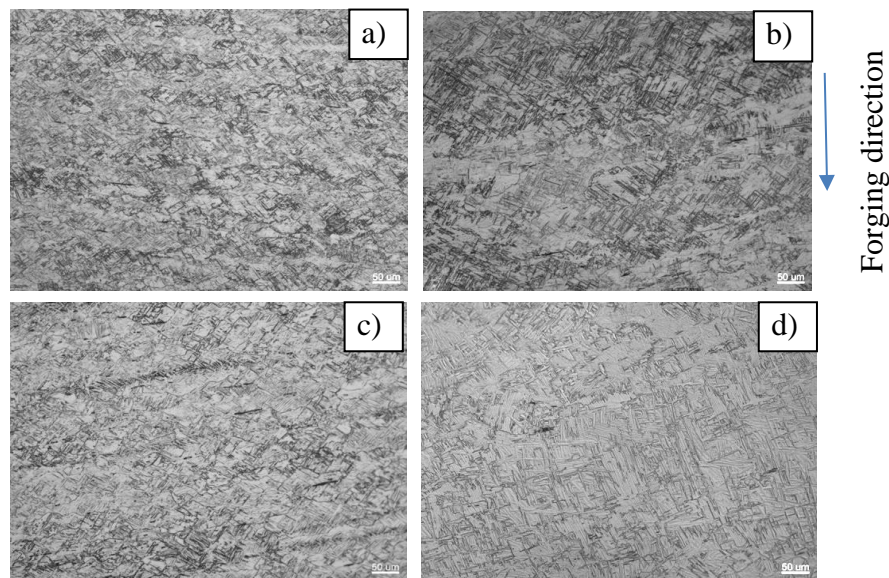
Figure 5.21 Optical micrographs of etched cross sections of forged discs: a) and b) Ti6Al4 and c) and d) Ti3Al2V alloy made respectively by IS- and VS-route.

The SEM images in Figure 5.22 showed that the martensitic phase is finer in the samples made by the IS route. This is related to the significantly shorter IS time, where during sintering finer β grains were formed. This consequently gave larger areas of β phase grain boundaries, which during cooling gave more sides for nucleation of the martensitic phase and limited its growth.
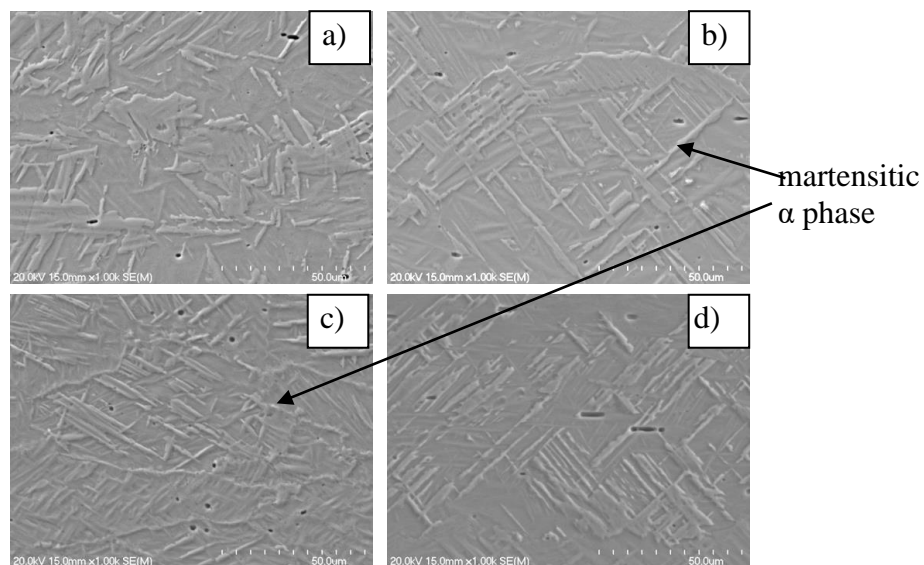
Figure 5.22 SEM images of forged a) and b) Ti3Al2V alloy and c) and d) Ti6Al4V alloy made respectively by IS- and VS-route.

The microstructures found in Ti-Fe based alloys had different features compared to those observed in the Ti-Al-V alloys (Figure 5.23). The microstructure

181

observed with optical microscopy consisted of large deformed grains, flattened in the direction parallel to the forging force. Each grain was outlined with a darker most possibly β phase. The sintering method did not have a significant effect on the grain size. The microstructure inside the grains could not be observed with optical microscope. Except in the IS and forged Ti5Fe-f alloy, where some of the grains had a lamellae structure.
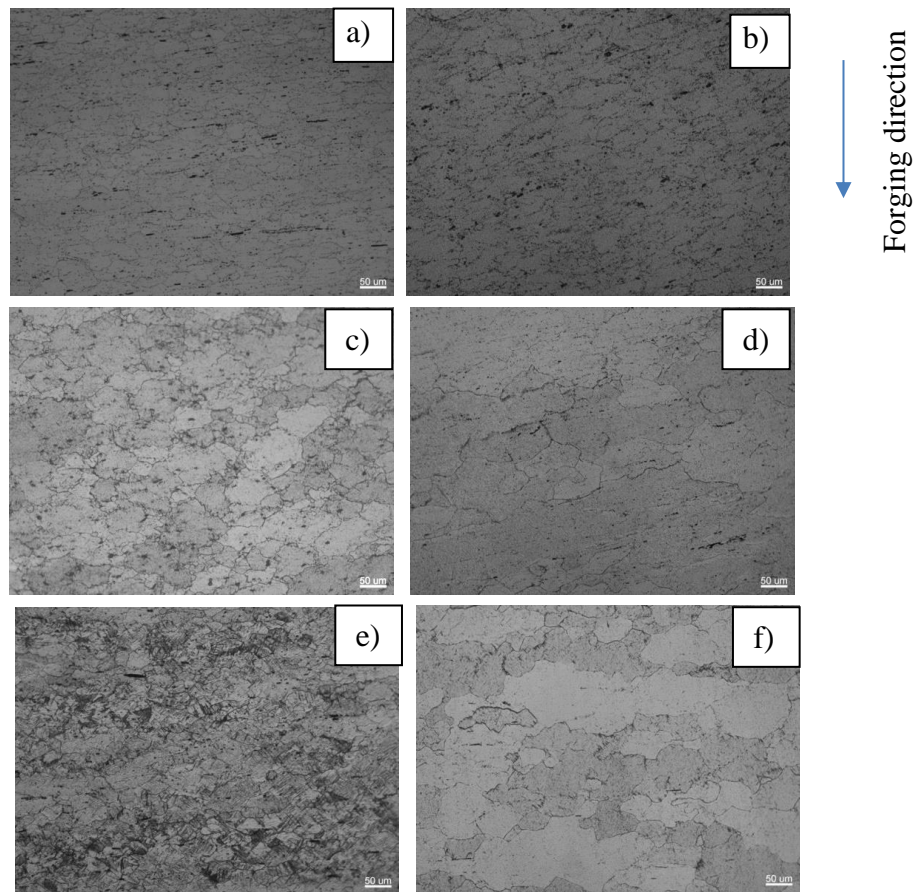
Figure 5.23 Optical micrographs of etched cross section of forged a) and b) Ti5SS alloy; c) and d) Ti5Fe-c alloy; and e) and f) Ti5Fe-f alloy followed respectively IS- and VS-route.

Further analyses of Ti-Fe based samples using SEM showed that the microstructure in each grain consists of a very fine acicular phase with a size in the range of few microns (Figure 5.24). From the microstructural images, the constitution of the acicular phase is not clear. Based on the XRD results where both diffraction peaks of α- and β- Ti are present, the acicular phase is most likely to be α or martensitic α phase nucleated from β phase. The acicular phase is very fine because with reference to the Ti-Fe phase diagram, the nucleation started at a

lower temperature and hence had less time to grow. In addition, the larger amount of retained β phase restricted the growth of the nucleated α phase.
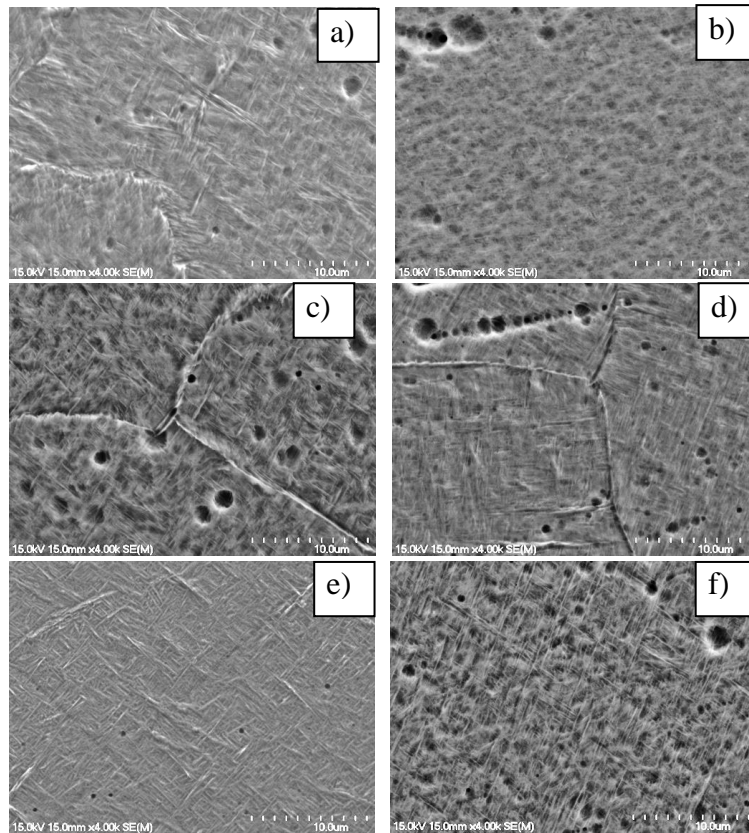
Figure 5.24 SEM images of etched cross section of forged a) and b) Ti5SS c) and d) Ti5Fe-c, and e) and f) Ti5Fe-f alloys followed respectively IS- and VS-route.

The acicular phase appears to be slightly coarser in the forged Ti5Fe-f-IS-F samples. In the rest of the samples, there was not a significant difference in the morphology of the acicular phase. The EDS elemental analysis showed a uniform distribution of iron within the Ti matrix in all forged Ti-Fe alloys, with approximate values between 4wt% to 6 wt%. An exception is the forged Ti5Fe-f alloy processed by the IS route, where some areas have only 2wt% and other up to 10wt% iron. There were no areas, observed using EDS, with Fe concentration in a range to enable formation of the intermetallic phase.

5.3.2.3 Oxygen analyses

5.3.2.4
Further processing by ODF after sintering did not result significant oxygen contamination (Table 5.2) compared to the as-sintered samples (Table 5.1), except

for the Ti3Al2V alloy. Compared to the sintered samples, the oxygen of the forged discs increased with 0.06wt% and 0.04wt% respectively for the samples from IS and VS route.

Table 5.2 Oxygen content of the forged discs

Processing route	Oxygen content, wt%				
	Ti6Al4V	Ti3Al2V	Ti5SS	Ti5Fe-c	Ti5Fe-f
IS-F	0.45	0.40	0.34	0.33	0.34
VS-F	0.47	0.40	0.37	0.38	0.38

The samples made by the VS-route have slightly higher oxygen content. The Ti6Al4V alloy showed higher oxygen contamination compared Ti3Al2V alloy, related to the increased amount of Al, known for its high affinity to oxygen. The oxygen pickup in Ti-Fe based samples is lower, which is most likely because of the lower processing temperature. Overall, all the alloys exceeded the maximum oxygen level of 0.3wt% required by the ASTM standard for PM Ti alloys.

5.3.2.5 Tensile properties
Due to the non-uniform consolidation of the forged alloys, as shown by the variation in porosity in the cross section of the forged material (Figure 5.19), there was variability in tensile properties at different positions in a cross section parallel to the forging direction (Figure 5.25). The presence of a porous layer particularly affected the ductility. Those samples cut from regions close to the surface had a lower elongation to fracture compared to those taken from the middle (Figure 5.25 c). The difference in ductility was greater in samples taken from forged material, which was induction sintered prior to forging. This is related to the lower density after induction sintering and consequently, larger number of pores retained in the porous layer after forging.

 For the Ti6Al4V and Ti3Al2V alloy, the YS and UTS of the forged material (Figure 5.25) increased by more than 100MPa compared with the corresponding sintered material (Figure 5.13). The strength and elongation to fracture of the samples made by the IS-route were higher than those of the samples made by the VS-route. The fine martensitic structure formed during forging following the IS-route, resulted in significantly higher UTS and elongation to fracture for both Ti6Al4V and Ti3Al2V alloys.

Forging directly after IS resulted in an average YS of 990MPa and a UTS of 1040MPa for the Ti3Al2V, and 1130MPa YS and 1220MPa UTS for the Ti6Al4V

alloy. The values of the UTS of the forged samples followed the VS-route were with more than 120MPa lower.
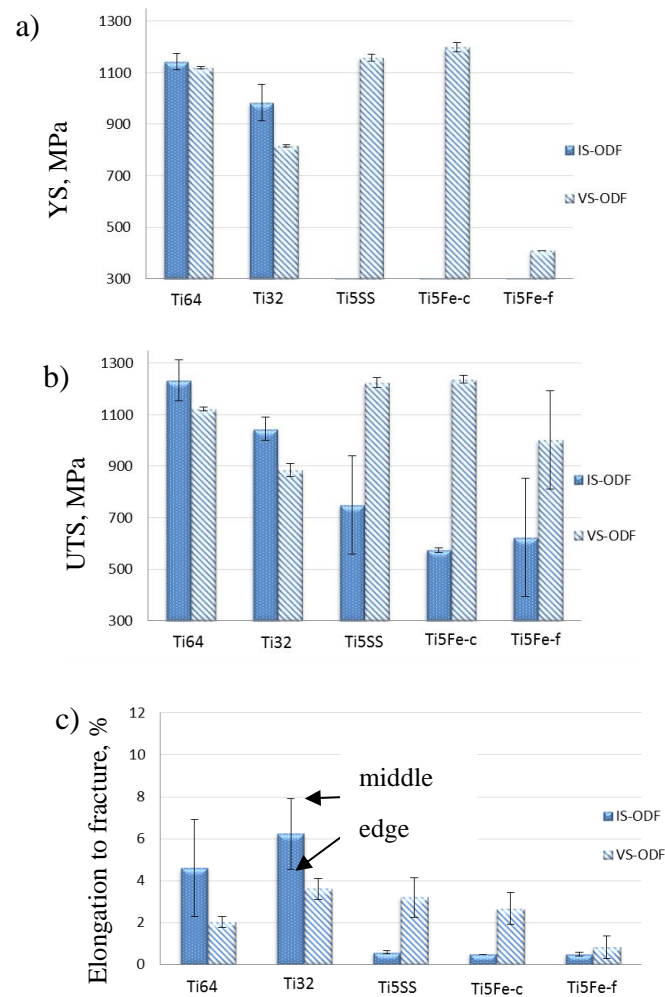
Figure 5. 25 Effect of the pre-consolidation method on the tensile properties of the as-forged Ti6Al4V, Ti3Al2V, Ti5SS, Ti5Fe-c and Ti5Fe-f alloys a) YS, b) UTS and c) elongation to fracture.

As expected, the Ti3Al2V alloy had a lower YS and UTS compared to that of the Ti6Al4V alloy because of the lower amount of alloying in the former.

An improvement in the ductility of as-forged Ti6Al4V and Ti3Al2V, compared to the as-sintered alloys was also observed, particularly when compacts were forged after induction sintering. Maximum values of elongation to fracture of 7% and 8% respectively were obtained for Ti6Al4V and Ti3Al2V.

Compared to the tensile properties of forged Ti6Al4V made with PA powders and processed using a similar route (Table 4.2), the BE Ti6Al4V forged alloy in this study achieved similar tensile properties. This is an indication that induction

185

sintering prior to thermomechanical processing is a feasible initial consolidation method for making Ti6Al4V alloy using BE synthesis. The difference in oxygen content, approximately 0.55wt% in the PA Ti6Al4V and 0.45wt% in the BE Ti6Al4V, did not have much influence on the tensile properties.

The Ti-Fe based alloys, which were forged after vacuum sintering, have very high tensile strength, which exceeds that found in the Ti6Al4V forged alloy. The average YS and UTS were approximately 1160MPa and 1200MPa respectively for Ti5SS and 1200MPa and 1230MPa respectively for Ti5Fe-c alloy. The maximum elongation to fracture was 4.2% and this exceeded that found in Ti6Al4V processed using vacuum sintering route and similar to that in the material forged after induction sintering. As result of forging from the β-phase field the high tensile YS and UTS were most likely related to the fine acicular microstructure combined with the relatively fast cooling which resulted in retention of large amount of β-phase and fine martensitic phase.

The Ti5Fe-f sample had lower tensile strength but this was related to the excessive porosity and inhomogeneous microstructure, which was caused by the larger Fe powder particles used to prepare this alloy.

Nevertheless, the tensile properties of the forged Ti-Fe based alloys followed the IS-route, were lower than those in as-sintered material. The UTS was in the range of 600MPa to 720MPa and the material showed no yield strength and ductility (Figure 5.25 a) and b) blue bars). As the microstructure of the forged alloys made using each of the sintering routes were similar (Figure 5.23 and Figure 5.24), the reason for the lower tensile properties of forgings made by the IS route cannot be attributed to differences in microstructure. The EDS study did not detect any intermetallic TiFe compound in the microstructure, which could cause an embrittlement (Figure 5.8 and Figure 5.9). A possible reason might have been insufficient consolidation during IS. Even though the sintered density of these samples were comparatively high and similar to those for Ti3Al2V, the lower sintering temperature of 1150˚C combined with a short sintering time might not have been enough to achieve sufficient Ti self-diffusion which was evident by a lack of α-phase at the grain boundaries in these samples (Figure 5.5a) and a1) to Figure 5.7 a) and a1) [10, 23]. Additional forging did not have the expected result of causing a further consolidation of the Ti powder particles.

Overall, the values of YS and UTS of the forged alloys, except for the Ti-Fe alloy forged followed IS-route, are higher compared with the corresponding forged

wrought alloys or the PM alloys made with Ti GA powders. The reason for the high YS and UTS in the as forged Ti-Al-V alloys is the formation of non-equilibrium α martensite caused by the fast cooling rates. In the Ti-Fe based forged alloys, the main reason for the high YS and UTS was the large amount of fine acicular α or martensitic phase formed in the microstructures.

The other factor, which would have affected the tensile properties, is the excessive amount of the oxygen in the forged alloys as evidenced by the results from oxygen analysis.

5.3.3 Thermomechanical processing by PCE

Thermomechanical consolidation by extrusion using a reduction in cross-section area ratio of 11:1 was carried out for all five alloys made by both IS- or VS-route. Porosity, microstructure and tensile properties are discussed in this section.

5.3.3.1 Porosity

The nature of extrusion involves extensive flow of the material in direction parallel to the extrusion force and this allows collapsing and closing of most of the pores remaining from sintering. Unlike the forged samples, a porous layer along the extruded surface was not observed (Figure 5.26).
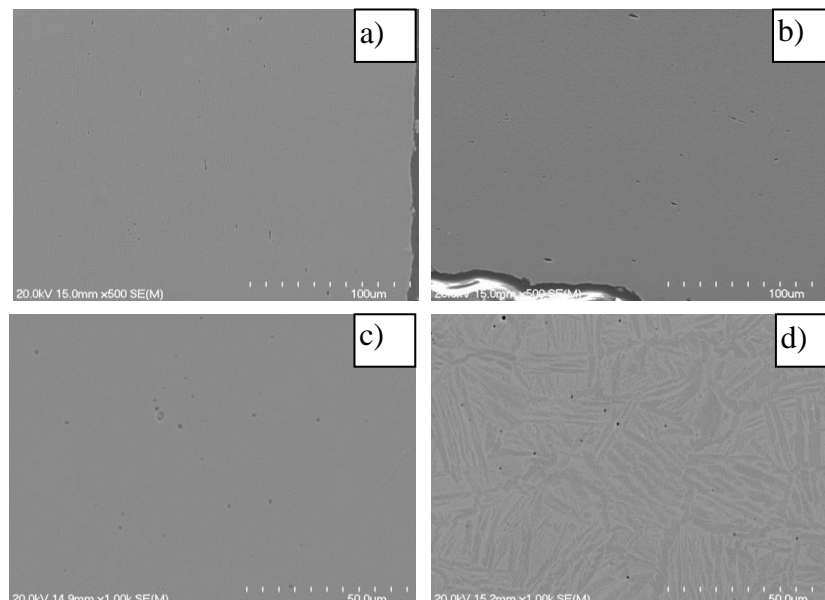
Figure 5.26 SEM images of representative examples showing the porosity of the extruded Ti3Al2V and Ti5Fe-f IS alloys respectively a) and b) near the surface, and c) and d) inside the material.

Only a few small pores, randomly distributed were observed through the cross section. These observations were similar in all samples irrespective of the sintering method or composition.

5.3.3.2 Microstructural analysis

The microstructures from a cross-section of extruded bars, perpendicular to the extrusion direction were studied.

For the extruded Ti6Al4V and Ti3Al2V material, followed the IS-route, the microstructural features were similar to the sintered microstructures, consisting of grains outlined by α phase and α+β lamellar structure within the grains (Figure 5.27 a) and c). The lamellae of the Ti6Al4V alloy are finer than this of the Ti3Al2V alloy.

The microstructures found in the extruded Ti6Al4V and Ti3Al2V alloys, processed by the VS-route, have significantly finer appearance, where the Ti6Al4V alloy has significantly more retained β-phase (Figure 5.27 b) and d).
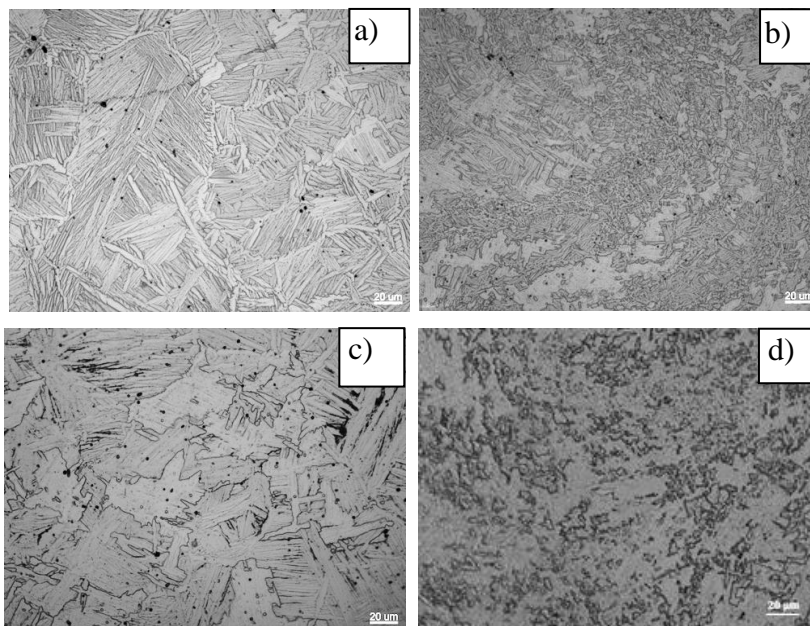
Figure 5.27 Optical micrographs of etched cross sections of extruded a) and b) Ti6Al4V, and c) and d) Ti3Al2V alloys followed respectively IS- and VS-route .

The difference in the grain morphology in the Ti6Al4V and Ti3Al2V extruded structures can be clearly seen in the higher magnification SEM images shown in Figure 5.28. In both alloys, there were two distinct phases. The matrix consists mostly of a lamellar α+β phase. The lamellae are coarser for the Ti3Al2V alloy made by the IS-route, corresponding to the lower amount of alloying elements,

which normally act as grain refiners. In the extruded Ti3Al2V alloy processed by the VS route, the matrix contains mostly equiaxed α-phase grains, typical of pure titanium and reflecting a lower amount of alloying additions (Figure 5.28 d). The second phase had a lenticular or plate like shape, typical of martensitic α phase [24], showing that the cooling rate during extrusion was high enough to form a non-equilibrium martensitic phase. This phase is much finer in the alloys processed by the VS route.
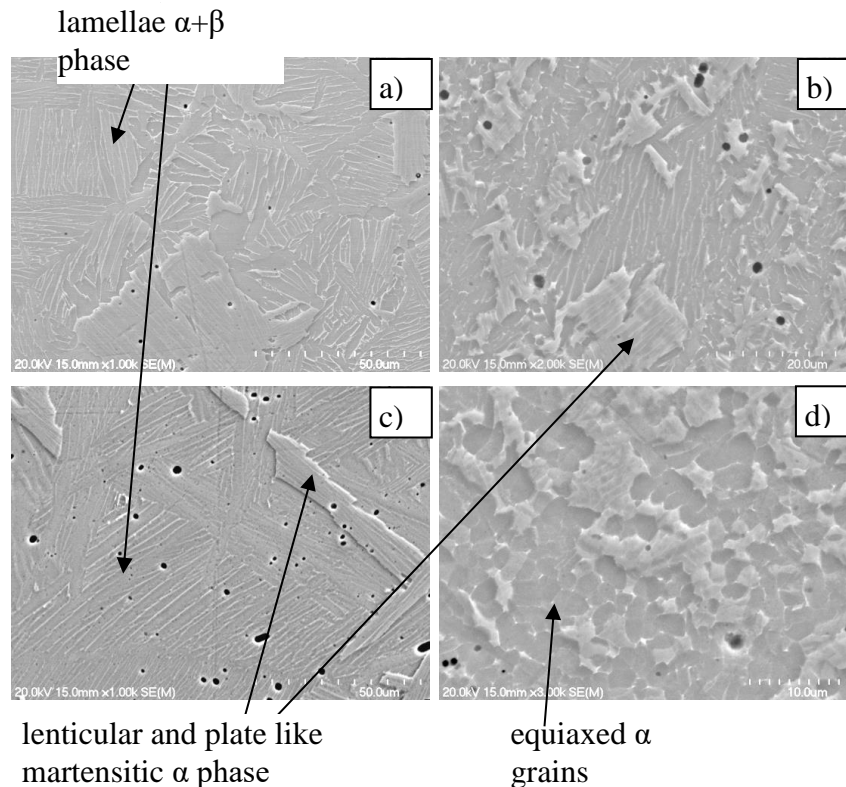
Figure 5.28 SEM images of extruded a) and b) Ti6Al4V, and c) and d) Ti3Al2V alloys followed respectively IS- and VS-route.

The microstructures of the extruded Ti-Fe alloys have similar featured (Figure 5.29 a), b), e) and f), consisting of clusters of unidirectionally orientated lamellae. The microstructure in most samples is not homogeneous, showing regions with β phase rich clusters (darker contrast) and some comparatively coarse acicular β phase. The lamellae of the samples processed by IS- route (Figure 5.29 a) and e) are finer compare with those processed by a VS-route (Figure 5.29 b) and f). The microstructure of the extruded Ti5Fe-c alloy (Figure 5.29 c) and d) is distinctive with fine uniformly sized lamellae dispersed in the matrix phase. In the Ti5Fe-c alloy processed by the VS-route the phase distribution is

189

homogeneous (Figure 5.29 d), while those processed by the IS-route have areas with coarse β reach acicular phase (Figure 5.29 c).
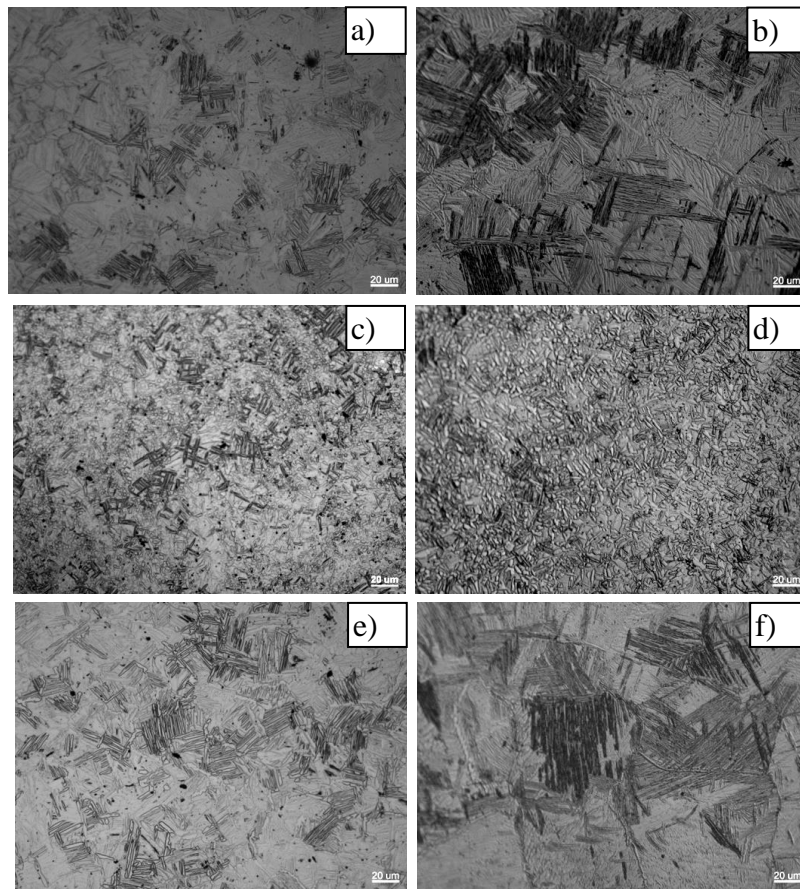
Figure 5.29 Optical micrographs of etched cross sections of extruded a) and b) Ti5SS, c) and d) Ti5Fe-c; and e) and f) Ti5Fe-f alloys followed respectively IS- and VS-route.

A clearer analysis of the microstructure in extruded Ti5Fe-c was obtained by SEM imaging (Figure 5.30 a) and b). The microstructure consisted of a mixture of fine equiaxed grains and short lamellas distributed throughout the matrix.

α-phase lamellae   equiexed α-phase

β-phase matrix

	Ti, wt%	Fe, wt%
area 1	99.28	0.72
area 2	91.73	8.27
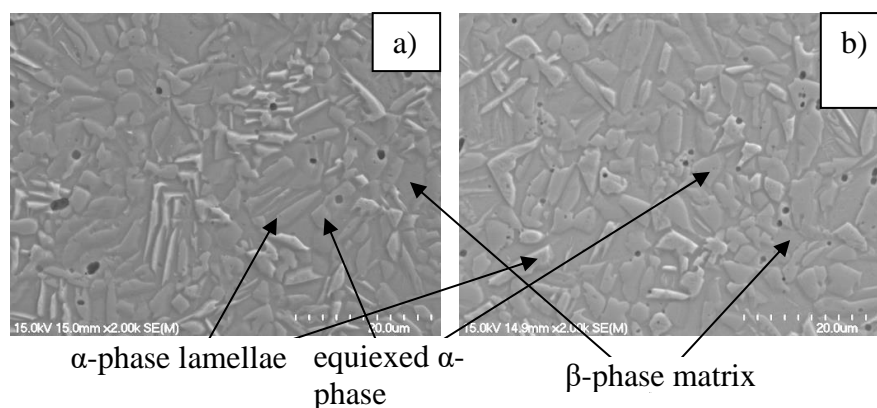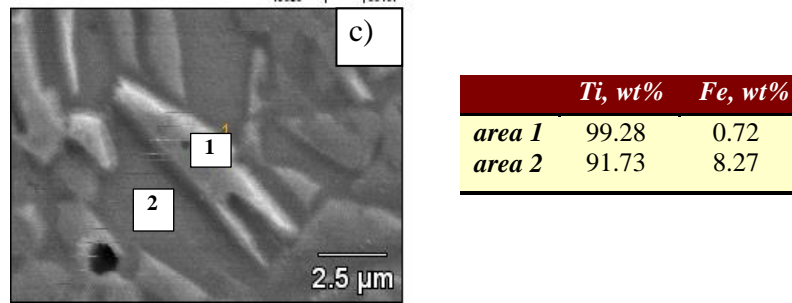
Figure 5.30 SEM images of extruded Ti5Fe-c alloy followed a) IS-route and b) VS-route, and c) EDS elemental analysis.

The EDS elemental analysis showed that the matrix composition was 9 to 10 wt% Fe and Ti was the balance (Figure 5.30 c). The lamellae and the equiaxed grains were mostly composed of Ti with very small amount of Fe up to 1wt%. A similar observation was made for the other two extruded Ti-Fe alloys, where the SEM and EDS elemental analysis suggests that the microstructure of the extruded Ti-Fe based samples consisted of α-phase lamellae dispersed in a β-phase matrix.

5.3.3.3 Oxygen contamination during extrusion

Further processing by extrusion did not cause changes in the oxygen content for the Ti6Al4V and Ti5Fe-f alloys (Table 5.3). For the rest of the alloy compositions, direct extrusion after IS showed an increased amount of oxygen pickup between 0.04 and 0.06wt%. Extrusion of the VS samples did not show a significant change in the oxygen content. Over all the oxygen content of the extruded alloys exceeded the maximum of 0.3 wt% for oxygen content in the ASTM standard for PM Ti alloys.

Table 5.3 Oxygen content of the extruded alloys.

Sintering method	Oxygen content, wt%				
	Ti6Al4V	Ti3Al2V	Ti5SS	Ti5Fe-c	Ti5Fe-f
IS-E	0.44	0.40	0.39	0.38	0.33
VS-E	0.45	0.39	0.37	0.33	0.33

5.3.3.4 Tensile properties

The trend in the tensile properties of the extruded alloys was similar to that for the forged samples. The yield stress, tensile strength and elongation to fracture were higher than those found in sintered samples.

The as-extruded tensile testing results for material pre-consolidated by IS or VS are shown in the bar graphs in Figure 5.31.
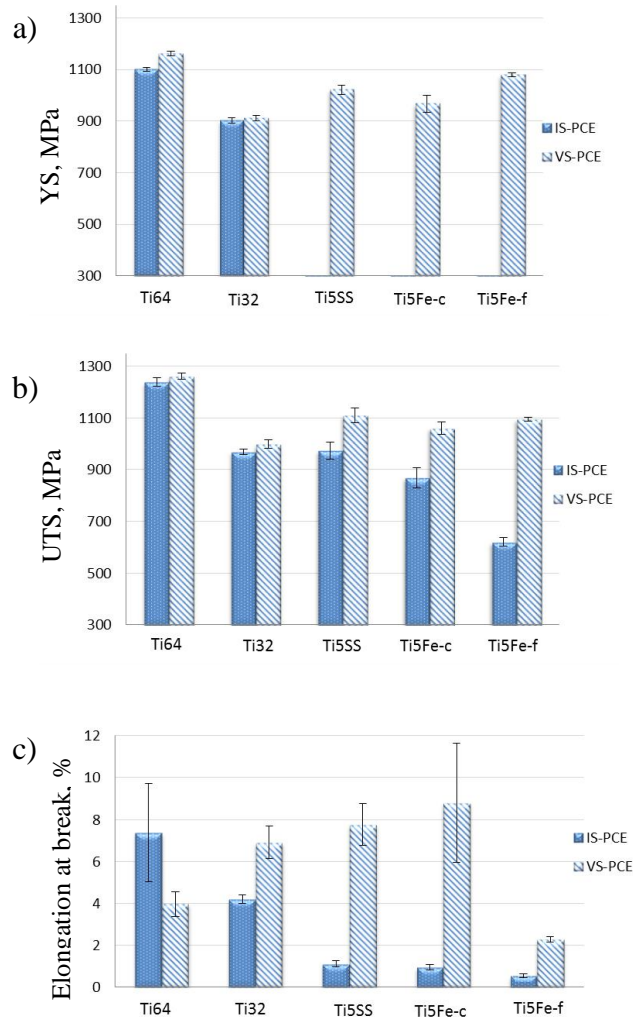
Figure 5.31 Effect of the pre-consolidation method on the tensile properties of the extruded Ti6Al4V, Ti3Al2V, Ti5SS, Ti5Fe-c and Ti5Fe-f alloys, a) YS, b) UTS and c) elongation to fracture.

Extrusion was beneficial for improving the tensile properties of Ti6Al4V alloy, giving high YS of over 1100MPa, a UTS of approximately 1270MPa and an elongation to fracture reaching a maximum of 9.8% in the case of material pre-consolidated using IS followed by extrusion. The elongation to fracture of the alloy made by VS was considerably lower. Similar results were found in the

literature when Ti6Al4V powder blends, with similar oxygen content, were pre-consolidated using VS before extrusion [25, 26]. The high tensile properties in the Ti6Al4V alloy derive from a higher alloying content in Ti6Al4V which leads to retention of β phase and the formation of an α+β lamellar microstructure favourable for high strength. The high oxygen content and formation of non-equilibrium martensitic phase as seen from the microstructural analysis (Figure 5.29) also contributed for the high tensile strength.

The extruded Ti3Al2V alloy, with a lower amount of alloying constituents, had lower YS and UTS, compared with that of extruded Ti6Al4V alloy. Nevertheless, the YS and UTS are higher than those in the corresponding wrought alloy. The reason is similar to that described earlier in this section for the Ti6Al4V alloy. The elongation to fracture did not show the expected increase. The main reason for this was the coarser extruded microstructure, particularly for the IS alloy. The sintering route did not have any significant effect on the extruded YS and UTS of this alloy, but the elongation to fracture of the alloy made by the VS route was higher.

Similar to processing by forging, all the Ti-Fe alloys, which were extruded after induction sintering, had poor tensile properties. Since optical micrographs and analysis by EDS and XRD did not show evidence of a eutectic phase, the reason for the lower tensile properties was attributed to insufficient consolidation during IS of limited Ti self-diffusion because of the lower sintering temperature and short dwell time during IS.

The extruded Ti-Fe based alloys pre-consolidated by VS showed a good combination of YS, UTS and elongation to fracture. The YS and UTS were higher than the values for extruded Ti3Al2V alloy. The Ti5SS alloy had the highest all round tensile properties with YS of 1010MPa and UTS of 1100MPa. The alloys Ti-5Fe-c and Ti5Fe-f had slightly lower UTS. The Ti-Fe alloys investigated also had good ductility reaching a maximum of 11.8% elongation to fracture for the Ti5Fe-c alloy. However, the Ti5Fe-f alloy had low ductility, influenced mainly by residual porosity as a result of the large Fe powder particle size used in this alloy composition. The high values of tensile properties were related to the large amount of β phase retained after TMP, which gave more sites for nucleation of the α-phase and consequently promoted formation of a fine lamellar phase, giving the high strength. The β phase forming the matrix contributed to the elevated ductility.

The relatively high oxygen content would have also contributed to the higher YS and UTS in a similar manner to that found in the other alloys.

5.3.4 Fracture behaviour of the thermomechanically treated alloys

The fracture behaviour of Ti3Al2V and Ti5Fe-c alloys are described using representative examples. The fracture behaviour of Ti6Al4V is similar to that of Ti3Al2V. The same is valid for Ti5Fe-f and Ti5SS in regards to Ti5Fe-c alloy. The fracture surface of the as-forged and as-extruded Ti3Al2V samples for both sintering routes showed fracture typical of fully consolidated material (Figure 5.32 a) and b). The porosity, evident in the fracture surface of IS material (Figure 5.14), had disappeared as a result of the plastic deformation during forging or extrusion. The fractures have predominately transgranular features. In the as-forged alloy there is a significant amount of cleavage fracture (Figure 5.32 a) and b) and also, there are ductile dimples at some of the cleavage surfaces.
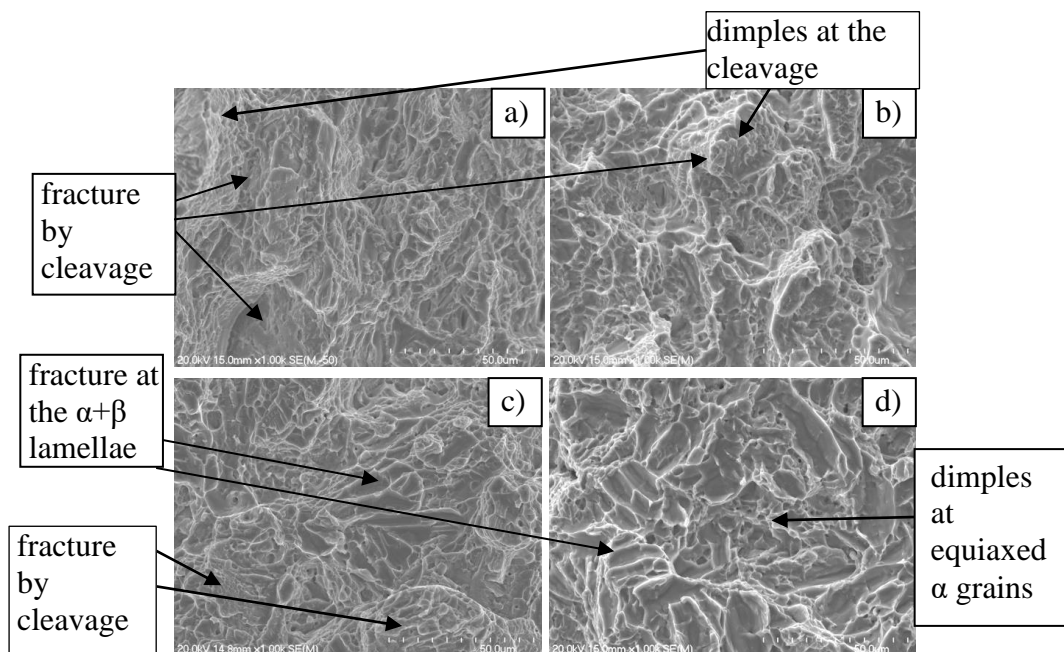
Figure 5.32 Fracture surface of Ti3Al2V alloy a) and b) forged, and c) and d) extruded followed respectively IS- and VS-route.

There is also a large amount of shallow dimples in the fracture surface of the as-forged samples. The fracture fragments are finer, which corresponds to the finer lamellae formed during forging.

In the extruded Ti3Al2V fractured test pieces from both IS- and VS-route, the fracture surface has typically transgranular features, with fracture occurred mostly

within the α+β lamellae phase. In the samples made by the IS-route, the fracture at the lamellae phase is mixed with cleavage fracture and secondary dimples at the cleavage surface (Figure 5.32 c). While in the samples made by the VS-route, the fracture also occurred at the equiaxed α grains, evident by the fine dimples (Figure 5.32 d).

The fracture surface in the as-forged Ti-Fe-c alloy (Figure 5.33 a) and b) consists of very fine shallow dimples and intergranular fracture paths.
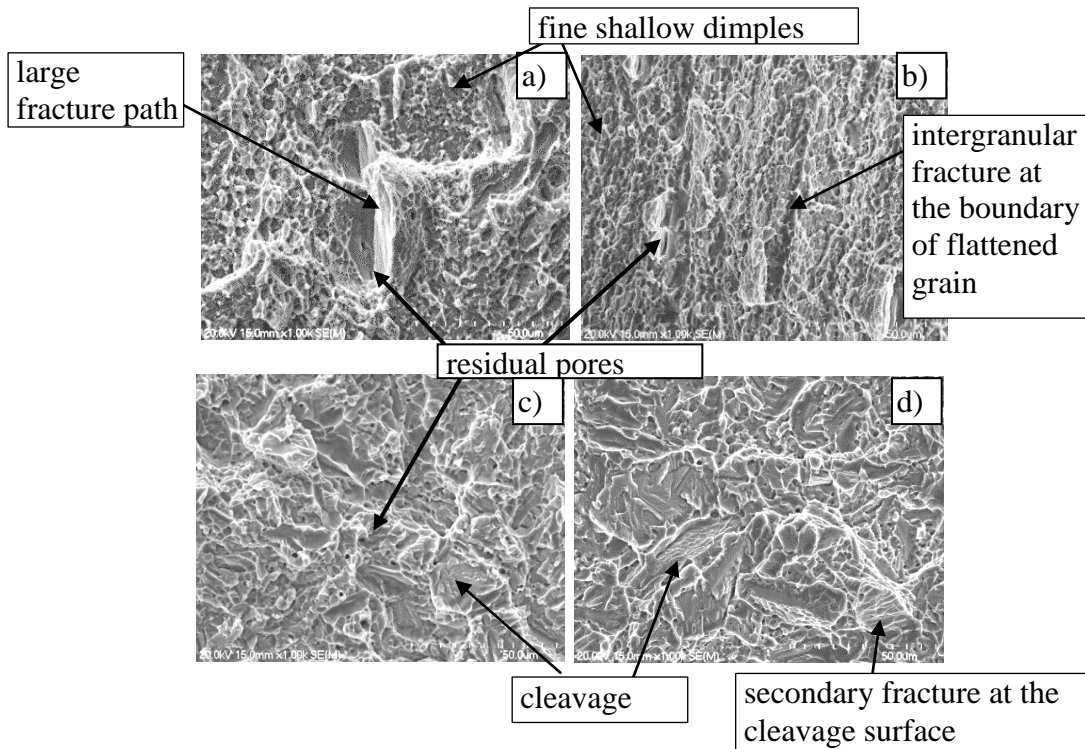
Figure 5.33 Fracture surface of Ti5Fe-c alloy a) and b) forged, and c) and d) extruded followed respectively IS- and VS-route.

In the sample made by the IS-route, there are large flattened voids, where profound intergranular fracture paths are observed (Figure 5.33 a). The fracture paths spread along large area of the fracture surface, showing a big influence on the fracture behaviour and consequently on the tensile strength of this alloy. From the lower magnification image of forged Ti5Fe-c alloy made by IS-route (Figure 5.34 a), it was clear that the pores were sites of fracture initiation. This porosity was not observed in polished samples of the corresponding material (Figure 5.19 c). It seems these pores are a result of incomplete consolidation during forging. The pores would have collapsed due to the plastic deformation, but in some cases the welding and formation of fully solid material was not completed. The

localised stresses during tensile testing would have most likely led to a reopening of these pores making these locations sites of stress concentration and crack propagation, as seen in the image in Figure 5.34b. These observations might be the reason for the significantly lower tensile properties of the induction sintered and forged Ti-Fe samples. The effect of residual porosity on the fracture behaviour of the extruded Ti5Fe-c alloy made by the IS-route was not so obvious (Figure 5.33 c), but because of its lower tensile properties it seems the fracture mechanism was similar to that of the forged samples made by similar sintering route.

pores

a crack initiated from the edge of a collapsed pore
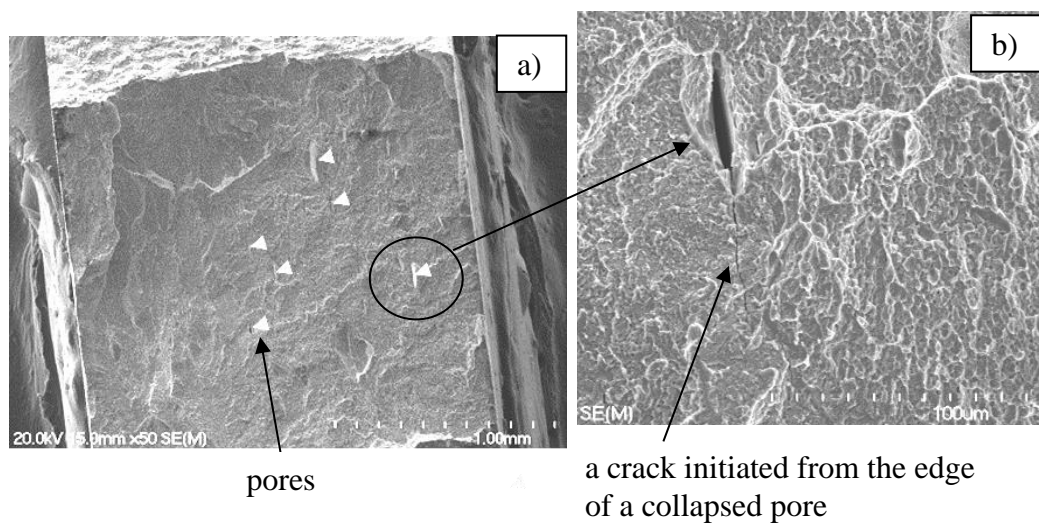
Figure 5.34 Fracture surface of forged Ti5Fe-c alloy followed IS-route showing a) large numbers of pores and b) a crack formed at collapsed pore during tensile test.

In the forged Ti5Fe-c alloy made by the VS-route (Figure 5.33b), intergranular fracture at the boundaries of flattened grains was also found but the fracture paths are much smaller and shallow and well blended with the fine shallow dimples. The high tensile strength of this alloy showed that the intergranular fracture did not have much influence on the strength but might be the reason for the insufficient ductility.

The fracture surface of the extruded Ti5Fe-c alloy followed the VS-route shows a transgranular fracture consisting of large amount of cleavage with secondary dimpling at the cleavage surface, and fine ductile dimples at the retained β-phase. (Figure 5.33 d). This combination of cleavage and dimpling fracture shows well consolidated structures, which is evident by the high tensile strength and sufficient ductility.

196

5.4 Heat treatment of the thermomechanically treated alloys

Some of the forged and extruded alloys were further heat treated.
The thermomechanically treated Ti3Al2V alloy was given a standard recrystallization annealing heat treatment [27]. This involved heating and holding in the α+β field aiming to promote the transformation of the martensitic α phase to α phase and partial transformation of α to β-phase. The dwell time was followed by slow cooling to allow precipitation of fine α-phase on the β phase grain boundaries and to form an α+β basket weave microstructure. A standard solution treatment (ST) commonly used for strengthening Ti-Fe based alloys [27] was not applied for the Ti5Fe and Ti5SS because the as-forged and extruded UTS was very high and the ductility was low. This showed that a ST effect was already undergone during the relatively high cooling rates during ODF and extrusion [28]. Only annealing, by heating and holding at temperature in the upper regions of the α+β phase field followed by slow cooling to allow precipitation of a fine α-phase was used to balance the strength and ductility.
In the case of Ti3Al2V, SEM imaging showed that the former martensitic plates and needles had transformed into α+β lamellae arranged in colonies to form a typical basketweave microstructure (Figure 5.35).
The α+β lamellae in forged and heat treated Ti3Al2V alloy were about 20-50μm in length and 2-5μm wide. The colonies of α+β lamellae were mixed with equiaxed α-phase with a diameter of 20-50 μm. This combination of two different phase morphologies gave a good combination of tensile properties with a YS of 950MPa, a UTS of 995MPa and 15.8% elongation to fracture in the Ti3Al2V IS, forged and heat treated alloy (Figure 5.36). In the case of the extruded and heat treated Ti3Al2V alloy, the α-lamellas were slightly coarser and rounded leading to a comparatively lower YS of 920MPa but a higher UTS of 1100MPa and 17.5% elongation to fracture. The fracture surface of these two alloys showed predominantly transgranular fracture with mixture of ductile and brittle features. Fine dimples formed by fracture at β-phase along the α-lamellae, mixed with cleavage at the equiaxed α-grains (Figure 5.35 c) and f).
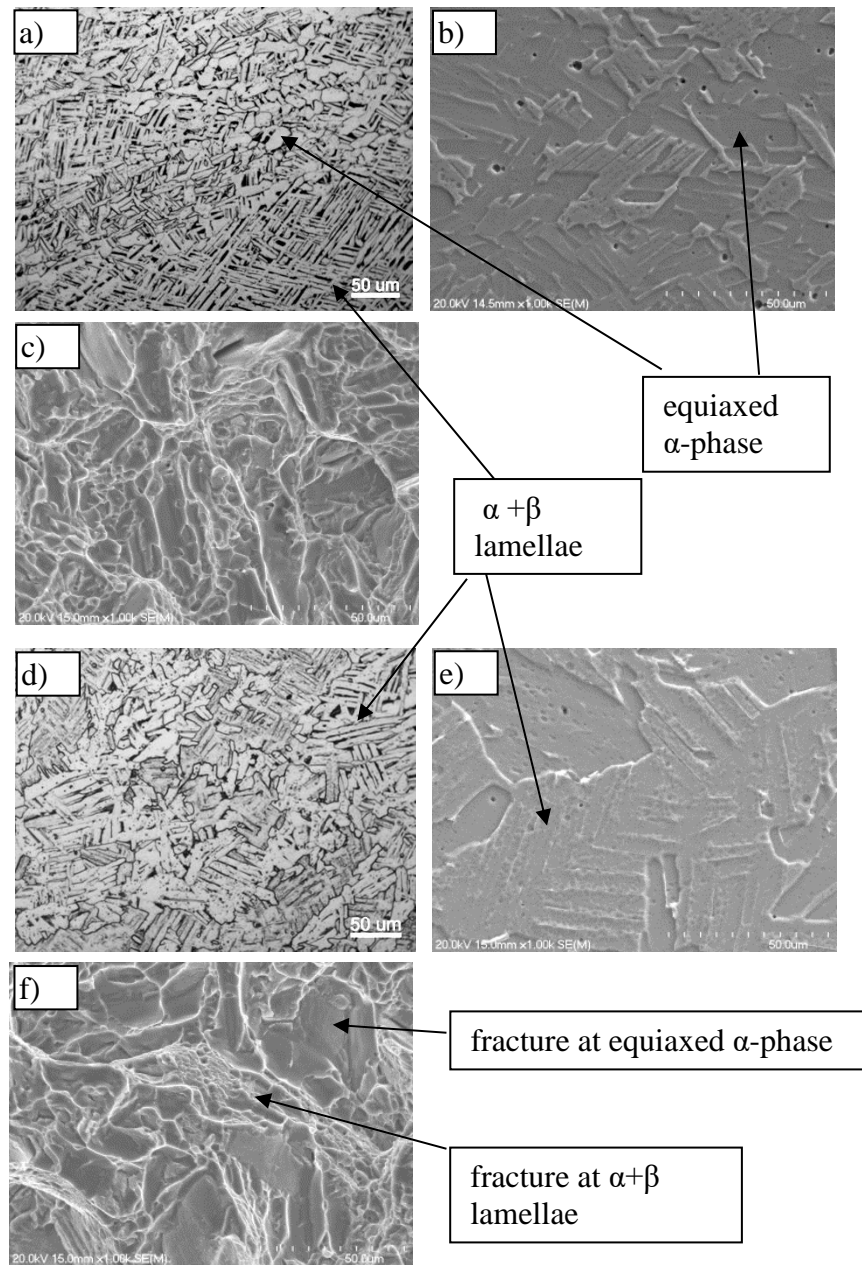
Figure 5.35 Effect of recrystallization annealing on the: microstructure a) and d) optical microscopy, b) and e) SEM; and fracture surface c) and f) respectively for forged followed IS-route Ti3Al2V and extruded followed VS-route Ti3Al2V alloys.
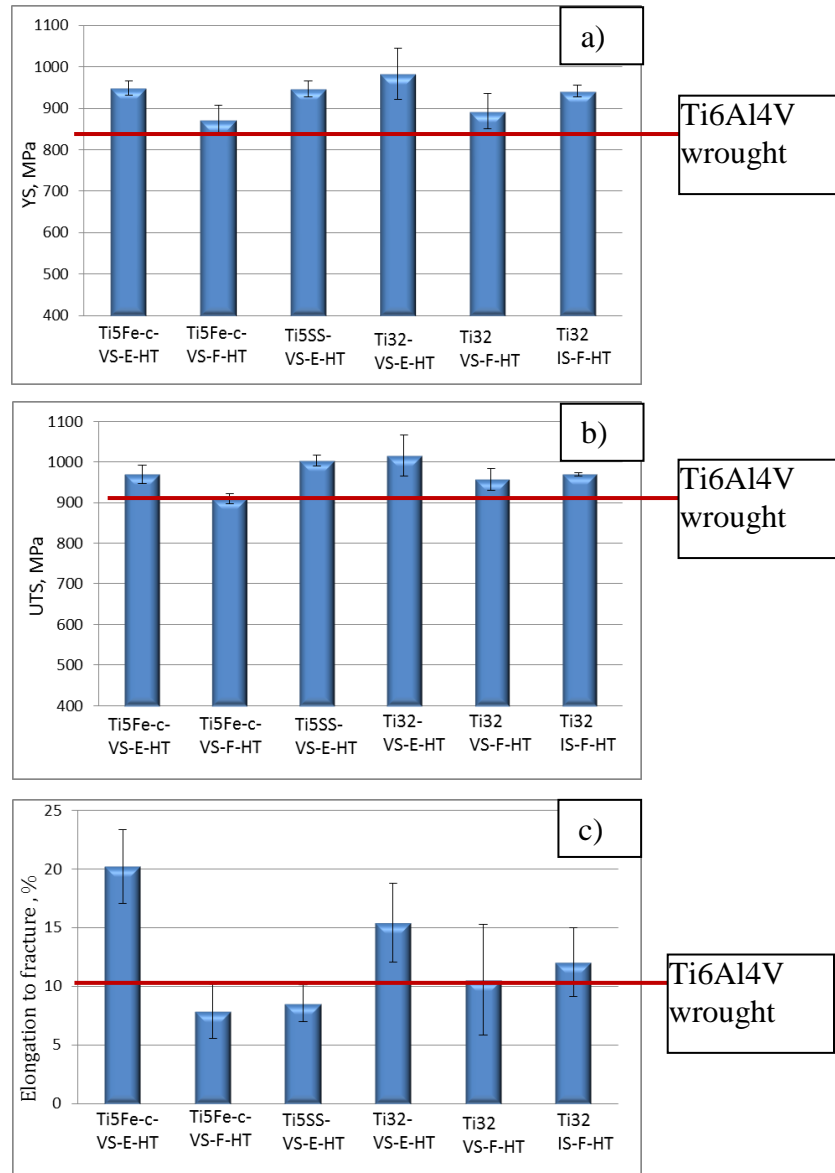
Figure 5.36 Tensile properties of heat treated Ti3Al2V, Ti5Fe-c and Ti5SS alloys produced by open die forging or extrusion: a) YS, b) UTS and c) elongation to fracture.

The microstructure of the heat treated Ti5Fe-c alloys showed different features depending on the thermomechanical treatment (Figure 5.37). In the as-forged alloy, the microstructure consisted of micron size acicular phase (Figure 5.24), after a heat treatment where the alloy was held at temperatures in the upper region of the α+β phase field, some of the acicular phase had remained and had grown into rod like phase with an average length of 10μm (Figure 5.37 a). It was confirmed by EDS analysis that these phase is 99.5wt% α-Ti (Figure 5.37 b) point 1, the bright phase). The matrix showed two phase structure: Ti-rich lamellas with 2-3 wt% Fe (Figure 5.37 b), darker grey contrast, Point 2) and Fe-rich phase with

Fe content up to 14wt% (Figure 5.37 b), Point 3- darkest grey contrast). The matrix microstructure, with a fine lamellar α-phase dispersed in the β-phase matrix resulted in a significant reduction in yield and tensile strength, with values of 860 MPa and 890MPa respectively, but with a significant improvement in elongation to fracture with maximum value of 11% (Figure 5.36).
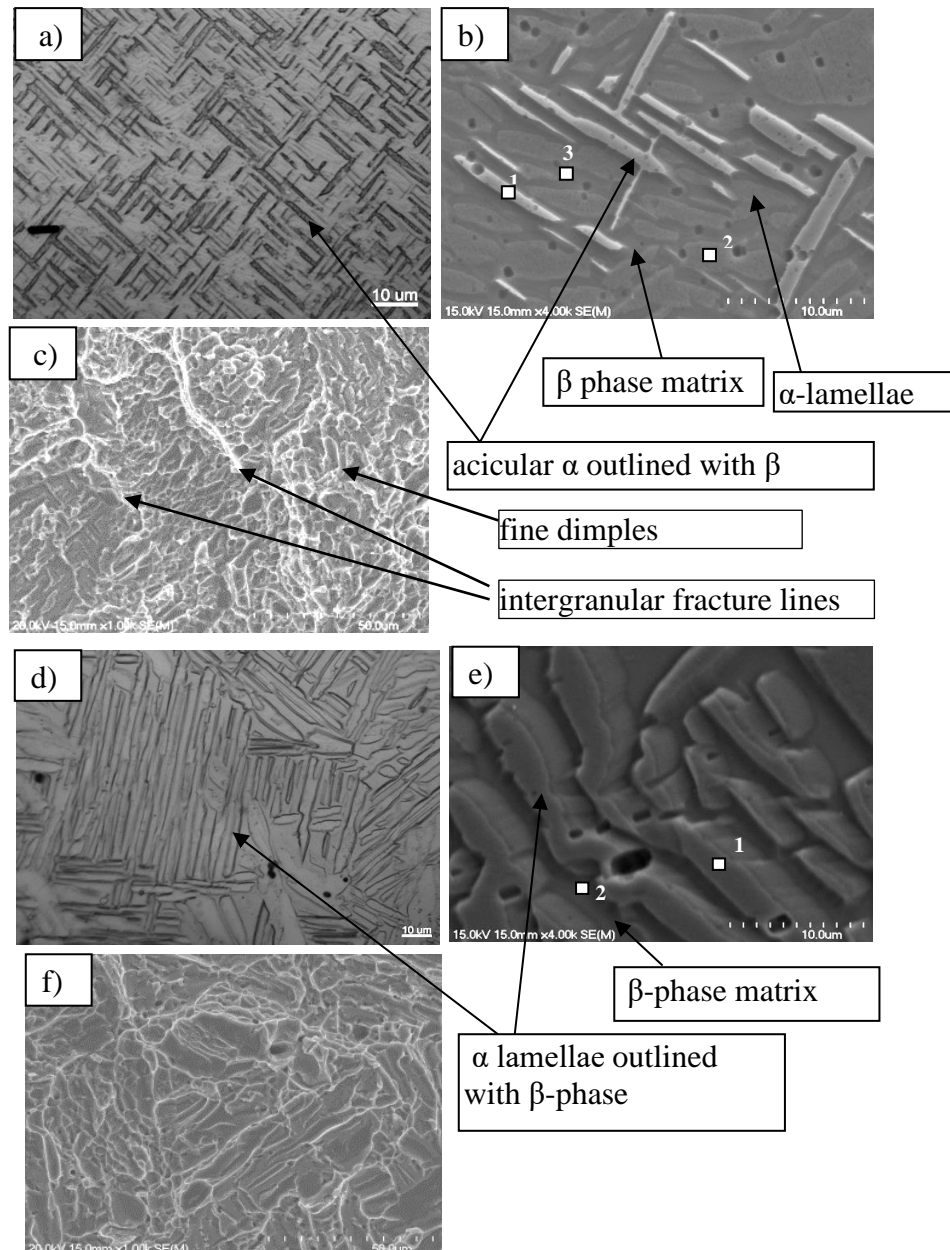
Figure 5.37 Effect of recrystallization annealing on the: microstructure a) and d) optical microscope, b) and e) SEM and EDS elemental analyses, and c) and f) fracture surface, respectively for forged and extruded Ti5Fe-c alloy followed VS-route.

Nevertheless, the ductility was affected by the presence of α-phase with an acicular morphology. The presence of a porous layer along the forged surface also

200

affected ductility, where the tensile test pieces had ductility of only 4.5% elongation to fracture. The fracture surface of the heat-treated forged Ti5Fe-c alloy shows predominately transgranular fracture with ductile appearance evident by fine shallow dimples (Figure 5.37 c). Some intergranular fracture at the boundaries of flattened due to forging grains are also found.

The arrangement of the α-lamellae in the heat treated Ti5Fe-c-VS-E (Figure 5.37 d) and e) alloy was similar to that of the heat treated Ti3Al2V alloy (Figure 5.35) forming a basketweave structure, but the α lamellae were finer, with a length in the range of 10-15 microns and a thickness of approximately 2 microns. The β-phase was also better defined in the extruded and heat treated Ti5Fe-c alloy (Figure 5.37 d). EDS analysis showed that the matrix phase was Fe-rich with up to 14wt% Fe, suggesting that it was retained β-phase (point 2 Figure 5.37 e). The lamellae were Ti-rich with almost no Fe (point 1 Figure 5.37 e). The YS of 860 MPa was comparatively low but UTS of 980 MPa was quite good and this material had excellent ductility reaching 23% elongation to fracture (Figure 5.36). This was due to a large amount of β-phase present in the matrix and along the α-lamellae. The fractured tensile surface showed predominantly transgranular fracture, occurred at the α+β lamellae phase and fine dimples at β-phase matrix, and having ductile appearance.

The heat treated microstructure of extruded Ti5SS alloy showed two types of α-lamellae (Figure 5.38 a) and b): coarser α+β lamellae with a length 20-60μm and approximately 2 microns thickness, having almost acicular shape; and finer slightly rounded α lamellae, similar to those observed in the heat treated Ti5Fe-c and Ti3Al2V alloy processed under similar thermomechanical conditions (Figure 5.37 d) and 5.35 d).

The heat treated Ti5SS alloy showed high values of YS of 940MPa and UTS of over 1000MPa, but because of coarser α-lamellae in the microstructure has lower elongation to fracture of 8% on average (Figure 5.36). The fracture surface showed ductile transgranular fracture along the elongated α-lamellae and fine dimples at the retained β-phase matrix (Figure 5.38 c).

colonies of coarse α+β lamellae in β matrix

colonies of rounded α lamellae in β matrix

fracture at the β-phase matrix

fracture at the coarse α+β lamellae
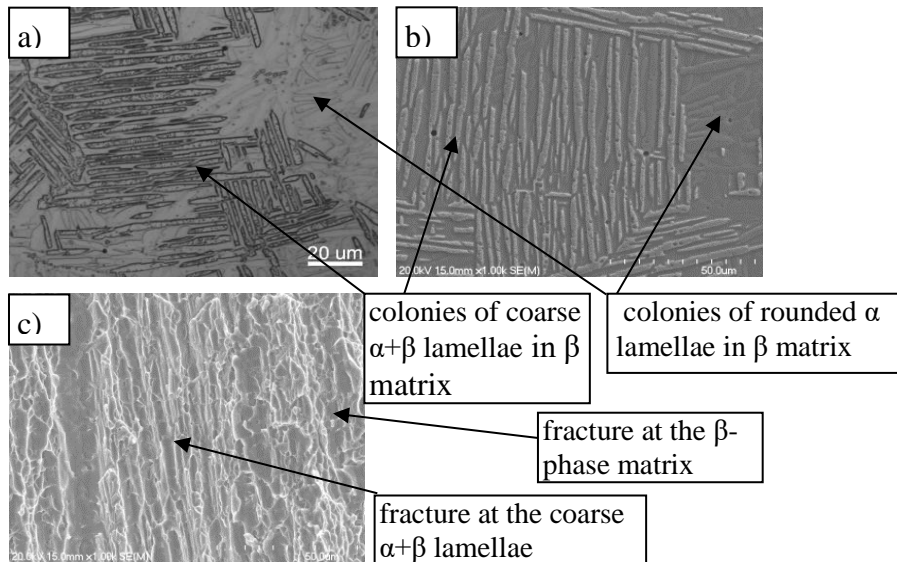
Figure 5.38 Effect of recrystallization annealing on the: microstructure a) optical microscopy, b) SEM, and c) fracture surface of extruded Ti5SS alloy followed VS-route.

Relating the tensile results to the corresponding microstructures it can be concluded that the tensile properties are strongly influenced by the α-phase morphology such as the shape, length and the width of the α lamellae as well as the amount of retained β-phase [24]. Microstructures such as those found in heat treated Ti32-IS-F, Ti32-VS-E and Ti5Fe-c-VS-E samples, where the α phase formed lamellae less than 50 microns long, 2-5 microns wide and arranged in a basketweave structure resulted in a good balance of strength and ductility. When the lamellar microstructures is situated in a β-phase matrix, as in the Ti5Fe-c samples, this was particularly beneficial to ductility.

Some of engineering tensile stress-strain curves from the heat treated alloys are shown in Figure 5.39.
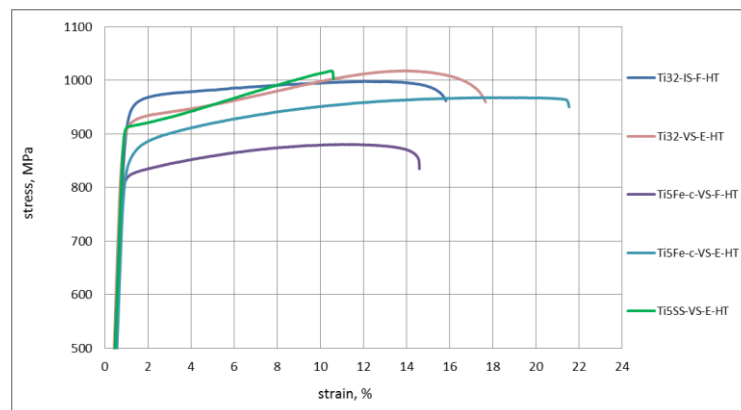
Figure 5.39 Representative stress strain curves of some of the heat treated alloys.

To further determine the amount of strain hardening during tensile testing, the work hardening exponent for each of the HT alloys was found using the Hollomon equation (5.1) [29]:

$$\sigma = K.\varepsilon^{n} \qquad (5.1)$$

where: σ-true stress, ε- true strain, K- a material constant, n- the work hardening exponent

It was found that the log(σ-)log(ε) for the HT alloys is not a linear relation. Hence the n-value is not a constant as expected from the Hollomon equation. This phenomena is not unusual, it is reported in the literature [29, 30] and is most commonly seen when a slow strain rate below 10^{-3}sec^{-1} or a very fast strain rate is used during tensile testing.

The log(σ)-log(ε) graphs for a Ti5Fe-c alloy in the VS, forged, extruded and heat treated conditions is shown in Figure 5.40.
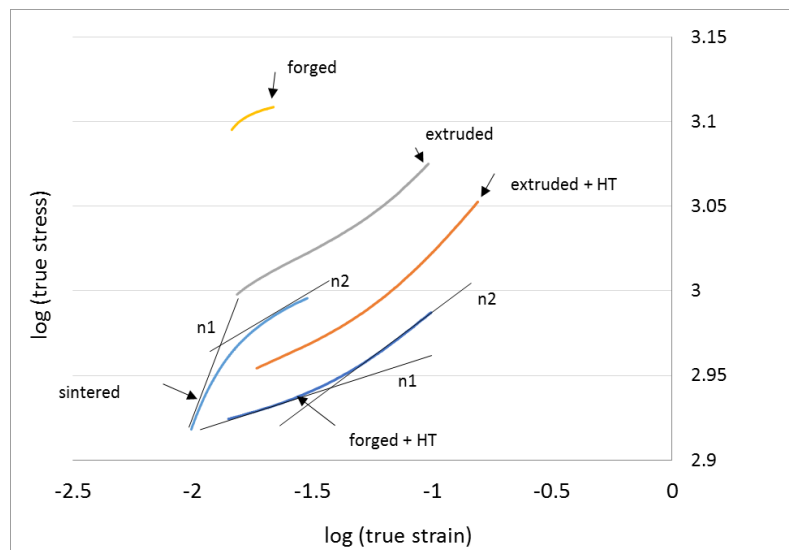
Figure 5.40 Log (true stress)-Log (true strain) curves for Ti5Fe-c alloy processed using different methods and tensile tested with a strain rate of $8.33.10^{-5}\text{s}^{-1}$.

It is noticeable that the log(σ)-log(ε) curves evolved differently depending on the processing conditions. If the curves are divided in two sections and straight lines (named n1 and n2) are plotted in each section, as shown in Figure 5.40 for the sintered and forged + HT sample, it is seen that the n-value for n2-line in the sintered alloy is smaller than that of n1-line. The forged sample curve shows similar behaviour. In the curve for forged + HT material, the trend for n-value is opposite. Similarly, n-value of n2-line is higher than that of n1-line in the as-

203

extruded and extruded + HT alloys (Figure 5.40). A study of the other two alloys Ti3Al2V and Ti5SS showed similar results. Since the degree of strain hardening is related to the dislocation density, in the extruded and in the HT samples, the dislocation density increases faster with increasing strain. The reason for this is related to the grain structure and the influence of grain texture, grain size, the presence of precipitates and solutes in the microstructure and how the dislocation are formed and interact with the grain boundaries and with each other. From the results in this study, it is difficult to find a particular reason for differences in the strain hardening mechanism within a single alloy composition processed by different routes. Further study is needed for a comprehensive understanding. The n-values for each alloy were approximated by building a straight trend line on each of the $\log(\sigma)$- $\log(\varepsilon)$ curves, and calculating the n-value from the corresponding line. The results for the n-values of as-thermomechanically treated and corresponding heat treated alloys are shown in Figure 5.41.
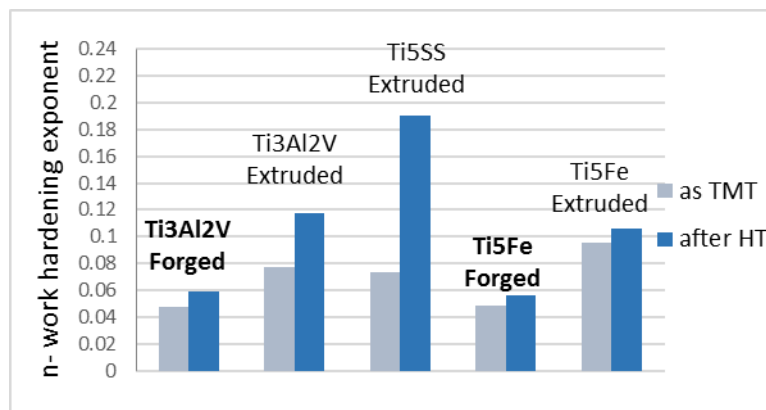
Figure 5.41 Strain hardening exponent obtain by tensile test with strain rate of $8.33.10^{-5}s^{-1}$ of Ti3Al2V, Ti5Fe-c and Ti5SS alloys at as-thermomechanically treated and heat treated conditions.

n-value of the HT samples is higher compare to this of the TMT samples. The main reason for these is that after recrystallization annealing, the grain size of the HT samples was finer. Another reason could be significantly higher number of precipitates generated during the slow cooling during HT, which according to the literature also have an effect on the dislocation density [31].

The lower n-value for forged material compared with those for extruded material, indicates that the forged samples had undergone more plastic deformation at temperatures below the recrystallization temperature during the thermomechanical processing, which in the literature is referred to as a cold working effect causing

strain hardening [32]. Further, during tensile testing, these samples only had a limited ability for further plastic deformation and strain hardening. The greater strain hardening in the as-forged Ti5Fe-c sample is also evident from the higher tensile strength recorded (Figure 5.25). A similar decrease in n-value with increasing plastic deformation during initial cold working is reported for a Ti6Al4V wrought alloy [33].

Values for the strain hardening exponent for Ti3Al2V and Ti5Fe alloys were not found in the literature. However, the measured n-values for these alloys were compared to those for a Ti6Al4V wrought alloy found in the literature [33]. Values of strain hardening exponent `n` of 0.04 to 0.06 for Ti3Al2V and Ti5Fe-c alloys in the as forged condition and after HT, are comparable with values for a Ti6Al4V alloy sheet in un-deformed annealed and solution treated condition, tested with similar strain rate. The strain hardening exponents for extruded and heat treated Ti3Al2V and Ti5Fe-c alloys are 0.08 to 0.12 respectively and are similar to values for Ti6Al4V sheet material which has been 10% deformed and then annealed or solution treated. The extruded and heat treated Ti5SS alloy shows the highest n-value of over 0.18 and is comparable to a Ti6Al4V alloy in solution treated condition and tested at a higher strain rate of $0.1.10^{-2}\,s^{-1}$.

Since n-values are an important characteristic for structural metallic materials and their value varies a lot depending on many factors such as microstructure, processing parameters, strain rate etc., further study on the effect of these variables on the n-value is needed for these newly developed PM alloys.

Overall, the tensile properties of all HT alloys had decreased YS and UTS compared with the corresponding forged or extruded alloys. Conversely, there was a significant improvement in ductility.

The tensile properties achieved in most of the HT alloys were comparable or slightly higher than the minimum requirements of wrought and PM Ti6Al4V alloy as specified by the ASTM standard (the red lines in Figure 5.38) [12, 34]. The alloys with the most comparable tensile properties to wrought Ti6Al4V alloy were:

- Ti3Al2V processed by induction sintering and forging and subsequently heat treated;

- Ti3Al2V processed by vacuum sintering and extrusion and subsequently heat treated;

- Ti5Fe-c processed by vacuum sintering and extrusion and subsequently heat treated;

Microstructure and related tensile properties showed that the chosen heat treatments were not the optimum. Specifically, a prolonged holding at the recrystallization annealing temperature led to a coarsening of the acicular α-phase, limiting improvement in ductility. Moreover, a decrease in YS and UTS after heat treatment of Ti-Fe alloys was affected by large amounts of β-phase retained in the microstructure. Considering that Ti-Fe alloys are new alloys and are not available in the cast and wrought form, there is only a limited amount of information available on PM Ti-Fe alloys. An extensive further study is needed on the heat treatment of Ti-Fe alloys processed by thermomechanical treatment.

5.5 Factors affecting consolidation and mechanical properties

From the results analyses in previous sections in this chapter, it was found that there are several factors affecting the degree of consolidation, the microstructure and the tensile properties. These are sintering method, thermomechanical processing conditions, the alloy composition, powder particle size of the alloying elements, type of heat treatment and oxygen content.

5.5.1 Effect of sintering method

(1) Induction sintering was an effective way of sintering the two Ti-Al-V alloys. The IS density of Ti6Al4V and Ti3Al2V made using a BE approach was comparable to those achieved by VS reported by other workers [8, 35]. IS alloys showed features of solid material, with newly developed grain boundaries at the former powder particle boundaries and a comparatively finer lamellar structure within the grains, typical of the corresponding PM alloys. In spite of the generally lower IS densities compared with those of the corresponding VS alloys (Figure 5.1), the IS tensile properties were as good as and even exceeded the properties of corresponding VS alloys (Figure 5.13). The main reason for the enhanced IS tensile properties was their finer α-phase lamellae (Figure 5.3) which were found to be the controlling factor for the mechanical properties in Ti alloys.
(2) The sintering method also had an effect on the microstructure and tensile properties of the alloys after TMP. Pre-consolidation by induction sintering was particularly beneficial for forged samples, where the UTS was over 100MPa greater than equivalent vacuum sintered samples for both Ti6Al4V and Ti3Al2V. The elongation to fracture using induction sintering for pre-consolidation and

forging was double that found in corresponding samples that had been vacuum sintered and forged.

(3) Using induction sintering for pre-consolidation was not as beneficial for the Ti-Fe based alloys. Even though the induction sintered densities of Ti5Fe-c and Ti5SS alloys were similar to those of Ti3Al2V (Figure 5.1) and the microstructures suggested significant consolidation, with largely closed porosity (Figure 5.2), the tensile properties even after hot deformation were very low (Figure 5.25 and Figure 5.31). The reason for the low tensile properties in the as sintered conditions were mainly attributed to the lower induction sintering temperature of 1150°C and a shorter sintering time chosen for these samples. This affected the degree of sintering between the Ti powder particles, because of the lower diffusion rate of Ti at this temperature [10, 36]. The insufficient consolidation was evident by a lack of grain boundary α-phase in induction sintered Ti-Fe structures, compared with the other sintered alloys. Large flattened pores were observed in the fracture surface after forging, showing incomplete elimination of the porosity. Premature fracture was initiated from these pores (Figure 5.34b) which resulted in low tensile strength (Figure 5.25).

(4) Vacuum sintering on the other hand gave high relative densities of 98.2% for Ti5Fe-c and Ti5SS alloys with tensile YS and UTS similar to those for Ti3Al2V, but with lower ductility. The reason for the lower ductility is because of the lower sintered density of the Ti5Fe-c and Ti5SS alloys, resulting in a comparatively high residual porosity [37]. Thermomechanical consolidation after vacuum sintering gave very high values of YS and UTS, which were comparable to those of Ti3Al2V. Using vacuum sintering and open die forging, the tensile properties were close to those for Ti6Al4V alloy following similar TMP.

5.5.2 Effect of thermomechanical processing

Figure 5.42 summarizes the tensile properties of samples consolidated by the three different consolidation methods following the VS-route.
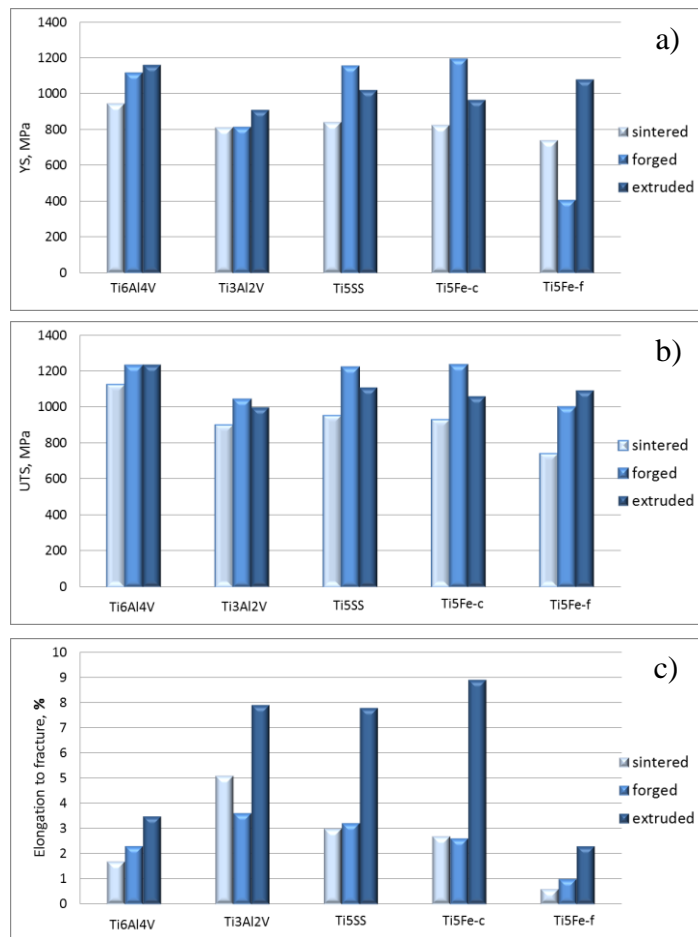
Figure 5.42 Effect of the consolidation method on the a) YS, b) UTS and c) elongation to break of the studied alloys.

As expected, the additional high temperature plastic deformation by forging or extrusion after sintering led to a significant improvement in tensile properties. The main reason was the significant material flow during hot plastic deformation resulting in: a reduction or elimination of residual porosity left over from sintering; elimination of any powder particle boundaries remaining after sintering and the formation of a grain structure which creates additional coherence between the powder particles [38]. The increase in the tensile YS and UTS after thermomechanical processing was also the result of formation non-equilibrium martensitic phase due to the fast cooling during processing.

The plastic deformation during forging was particularly beneficial for creating a fine grain structure (Figure 5.24). This in turn gave the highest values of YS and UTS in most alloy compositions, as seen from Figure 5.42 a) and b). The problem associated with forging was related to the un-deformed areas along the surface (Figure 5.20) which resulted in formation of a pore rich layer close to the surface

areas (Figure 5.19) and inconsistent ductility within the forged cross section (Figure 5.26c)

The increase in YS and UTS in the extrusion direction was mainly related to elimination of residual porosity and the formation of non-equilibrium phases during fast cooling (Figure 5.29). An important characteristic of the extruded alloys is the high ductility, which is two to three times higher than that found in the corresponding sintered and forged alloys. The high ductility was mainly associated with the shape of the residual pores which, appeared to be much smaller and rounded in the fracture surfaces of the extruded alloys (Figure 5.35).

5.5.3 Effect of the alloying composition

Two aspects of alloy composition were studied: the effect of a reduction in the amount of alloying elements by carrying out a comparative study on Ti6Al4V and Ti3Al2V alloys; the effect of the nature of the alloying element and its effect on phase stabilisation. The alloys investigated used a combination of α and β phase stabilizers (Al and V) and a β-phase stabilizer (Fe).

A reduction in the amount of Al and V showed:

(1)   A clear improvement in the formability as reflected in a higher reduction ratio in forged samples and an increase in the length of extruded bar compared with a Ti6Al4V alloy (Figure 5.16).

(2)   Clear decreases in YS and UTS for all processing conditions, but these values were close to those for wrought Ti6Al4V.

(3)   An increase in ductility was evident when pre-consolidation was by vacuum sintering. The elongation to fracture of Ti3Al2V alloy was almost three times higher than that for Ti6Al4V (Figure 5.42c).

(4)   The sinterability of Ti3Al2V powder alloy was not as good as that of TI6Al4V-IS and this was evident from the lower sintered density after induction sintering (Figure 5.1). The lower sinterability was related to the lower amount of Al which reacts with Ti during sintering and accelerates the process.

Using Fe instead of a mixture of Al and V for alloying with Ti showed:

(1)   A significant improvement in formability with more than twice the length of extruded bar compared to Ti3Al2V and three to four times the length of Ti6Al4V extruded bar (Figure 5.15 and Figure 5.16).

(2)   Finer microstructures, with smaller α-lamellae in the as-sintered microstructures (Figure 5.5 to Figure 5.7), a very fine forged microstructure (Figure 5.24) and a fine α-phase in extruded alloys (Figure 5.30).

(3)   The refined α-phase microstructures led to improved YS and UTS with values exceeding those for Ti3Al2V and similar to those for Ti6Al4V alloys produced using a similar TMP.

(4)   A significant improvement in ductility after RA. Ti5Fe-c alloy showed a ductility reaching 23% elongation to fracture, which was 25% higher than that achieved for a Ti3Al2V alloy with similar oxygen content and similarly processed.

5.5.4   Effect of the power particle size of the alloying elements

Using two different sizes of Fe powders to prepare Ti5Fe-c and Ti5Fe-f alloys showed that the powder particle size of the alloying element had an effect on all the properties of the processed powder mixtures, starting from the green density, to the sintered density and the mechanical properties. The EDS elemental analysis on as-sintered alloys confirmed the results from other studies [4, 5] which showed that the powder particle size of the alloying elements plays an important role in the homogenization of the alloying elements. The main problems caused by the large Fe powder particles were associated with an inhomogeneous distribution of Fe in the Ti matrix and the large residual pores after sintering. Further thermomechanical processing could not fully eliminate these larger pores, which led to lower yield and tensile strength and poor ductility.

5.5.5   Effect of heat treatment

Recrystallization annealing significantly changed the microstructure of the forged and extruded alloys. Even though the annealed microstructures could be differentiated according to the alloy composition and the type of hot deformation, there was a common feature. All annealed microstructures showed a lamellar structure, consisting of α-phase with β-phase grain boundaries. From the tensile testing results, it was found that the size and shape of the α+β lamellas controls the tensile strength. In Ti3Al2V the two-phase structure, consisting of a mixture of lamellar and equiaxed grains, gave an acceptable combination of tensile strength and ductility (Figure 5.35 d) and e). In the Ti5Fe-c alloy, the good tensile

properties were achieved by a microstructure showing a lamellar structure in a matrix of retained β-phase (Figure 5.37 d) and e).

5.5.6 Effect of oxygen content on the tensile properties

The relatively high oxygen content in the alloys studied was a result of the higher oxygen content of the Ti HDH powders used. Further contamination with oxygen was caused by the high temperature processing and mostly during sintering. The oxygen content of the alloys studied was higher than quoted for standard Ti wrought and PM alloys in the ASTM standards [12].

From the tensile testing results it was clear that the high oxygen content, falling in the range between 0.32wt% to 0.47wt%, had effect on YS and UTS and elongation to fracture, with significantly higher values of YS and UTS compared to the corresponding alloys processed under similar conditions but with a lower oxygen content (Table 5.4).

Table 5.4 Effect of oxygen content on the tensile properties

alloy	This study					Reference					Ref.
	processing	oxygen wt%	YS, MPa	UTS, MPa	ε, %	processing	oxygen wt%	YS MPa	UTS MPa	ε, %	.
Ti6Al4V	IS	0.44	1005	1128	4.6	IS	-	-	-	-	-
	VS	0.45	949	1007	1.7	VS	0.30	828	895	10	[12]
	IS-F	0.45	1153	1289	6.2	WA-F	<0.20	896	931	6-8	[15]
	IS-E	0.44	1103	1238	7.4	WA-E-A	<0.20	827-861	896-830	10	[15]
	VS-E	0.45	1162	1264	4.0						
Ti3Al2V	IS	0.44	825	903	4.5	IS	-	-	-	-	-
	VS	0.36	815	870	5.1	VS	0.30	483	620	15	[12]
	IS-F-RA	0.40	930	980	12.5	WA- F- A	<0.20	480-515	585-620	15-20	[15]
	VS-F-RA	0.40	890	960	10.0						
	VS-E-RA	0.39	980	1100	15.0	WA- E- A	<0.20	480-515	585-620	15-20	[15]
Ti5Fe-c	VS	0.38	827	930	2.7	VS-A	0.14	-	760	17	[7]
	VS-F-RA	0.38	860	910	7.5	-	-	-	-	-	-
	VS-E-RA	0.33	940	980	20	--	-	-	-	-	-

Note: IS- induction sintered; VS-vacuum sintered; F-forged; E-extruded; RA-recrystallization annealed; A- annealed; WA-wrought alloy;

It was noticeable that the oxygen content had an effect on tensile properties in both the as-sintered and TMP conditions. An increase in oxygen content by up to approximately 0.2wt% led to increased YS and tensile UTS by 100MPa to 350MPa and decreased elongation to fracture by 2 to 8%.

In the annealed condition, the high oxygen content had a significantly less adverse effect on ductility. The elongation to fracture values for annealed Ti3Al2V and

Ti5Fe-c alloy, with oxygen in the range of 0.33 to 0.39wt%, are comparable to those for corresponding alloys with low oxygen. Additionally, a significantly higher YS and UTS, combined with good ductility, can be achieved with these higher oxygen levels.

From the tensile properties of the alloys studied, a high tensile strength and low ductility were caused by a combination of two factors: the formation of the non-equilibrium martensitic α phase due to the fast cooling rates and secondly, the high oxygen content acting as an extra strengthening element. After HT, which eliminated the non-equilibrium phases and reformed the microstructure by changing the grain shape and the phase distribution, the YS and UTS were reduced but were still higher than the values for corresponding alloys with a lower oxygen content. The yield and tensile strength of RA Ti3Al2Vand Ti5Fe alloys showed values comparable to those for wrought Ti6Al4V and PM Ti6Al4V given in the ASTM standard [12, 34]. The ductility was significantly improved with values of elongation to fracture within the requirements given in ASTM standards for corresponding alloys and comparable to the ductility of wrought and PM Ti6Al4V in the ASTM standards.

The results have shown that, the increased oxygen content of the Ti alloys produced by the consolidation methods used in this work, could be beneficial for increasing yield and tensile strength without being detrimental to ductility.

5.6   Summary and Conclusions

5.6.1   Summary

The reason for this investigation was to show that: induction sintering can be used as part of the processing for making Ti alloys using a blended elemental approach, whilst achieving tensile properties comparable with those that can be achieved using vacuum sintering; processing costs can be reduced by using lower cost HDH Ti powder in Ti powder metallurgy without significantly affecting the tensile properties; good tensile properties with acceptable ductility, equal to those found in wrought and PM Grade 5 Ti6Al4V, can be achieved in Ti3Al2V and Ti5Fe based alloys with high oxygen.

It was found that induction heating could be successfully used for consolidation of Ti6Al4V and Ti3Al2V powder mixtures. The density after induction sintering was lower than that after vacuum sintering but overall the values were comparable

with those found in other research. A high level of consolidation was evident after induction sintering as shown by the mostly closed porosity and pores with a rounded appearance. EDS elemental analyses showed that the alloying elements were uniformly distributed and formed homogeneous microstructures. A shorter sintering time combined with comparatively fast room temperature cooling, resulted in microstructures with fine α lamellae, which led to enhanced tensile properties compared with vacuum sintered microstructures.

Consolidation by induction sintering was not successful for Ti-Fe powder alloys. The main reason was insufficient consolidation due to the lower Ti inter-diffusion at the chosen induction sintering temperatures, and the high residual porosity after thermomechanical processing. Ti-Fe based powder blends could be effectively consolidated when Fe and 316SS powders with a finer powder particle size were used and vacuum sintering used for pre-consolidation.

Compared with sintered alloys, the tensile properties of forged and extruded alloys were significantly improved due to a reduction in residual porosity, additional cohesion between the powder particles caused by increased powder particle deformation.

The oxygen content of all alloy compositions was higher than that in the standard for Ti wrought alloys. The high oxygen content was because of the originally high oxygen content Ti powders used and the oxygen contamination during processing, particularly during sintering. The high oxygen content was also a reason for the high strength of the alloys, compared with corresponding wrought alloys.

Using induction sintering for pre-consolidation before open die forging of Ti3Al2V and Ti6Al4V powder blends caused a higher residual porosity and the formation of porous layers in the regions close to the surface. This led to non-uniform ductility within a cross section of the forged discs.

The tensile results achieved after induction sintering and extrusion of Ti3Al2V and Ti6Al4V powder blends, were comparable to those obtained using vacuum sintering and extrusion.

An expectation that alloying with Fe would improve sinterability was not very clear. Fe with a smaller powder particle size dissolved well and became homogeneous during prolonged vacuum sintering to achieve a good sintered density. The behaviour of Fe additions during induction sintering did not meet expectations. The sintered densities were similar to those for Ti3Al2V alloy but

the low tensile properties, particularly thermomechanical processing showed that there had been incomplete consolidation.

Using Fe as an alloying element instead of Al and V led to a considerable improvement in formability, a refined microstructure after sintering, forging and extrusion. This resulted in high values of yield and tensile strength after thermomechanical processing in general and after forging in particular.

Heat treatment was an essential step after thermomechanical processing, since it eliminated non-equilibrium phases and changed the α and β phase morphology. The yield and tensile strength decreased but the ductility of all alloys increased and reached values of 10% to 23% elongation to fracture.

5.6.2   Conclusions

- Induction heating can be used for making Ti alloys using a blended elemental approach.

- The density, microstructure and tensile properties of BE Ti6Al4V and Ti3A2V alloys consolidated by induction sintering are comparable to those when vacuum sintering is used for consolidation.

- The induction sintering temperature used for sintering Ti-Fe based powder blends was too low to achieve sufficient consolidation and the tensile strength was lower after sintering, open die forging and extrusion.

- Short time induction sintering combined with direct forging or extrusion was successfully applied in the thermomechanical processing of Ti6Al4V and Ti3Al2V alloy, resulting in a finer microstructure and good tensile properties compared with vacuum sintered material.

 - Thermomechanical processing by open die forging or extrusion after sintering improved the consolidation and resulted in significantly higher tensile properties compared with the sintered properties.

- After thermomechanical processing, all alloy compositions showed yield and tensile strengths significantly higher than those in the corresponding wrought alloys or PM alloys with oxygen content satisfying the ASTM standard. The main reason for the higher tensile properties was the high oxygen content of the HDH Ti powders and the non-equilibrium phase formed during plastic deformation.

- An annealing heat treatment after thermomechanical processing resulted in a reduction in YS and UTS and a significant improvement in ductility. The YS and

UTS of the Ti3Al2V and Ti5Fe alloys were higher than those for the corresponding wrought alloys but with comparable ductility.

- The tensile properties of thermomechanically treated and annealed Ti3Al2V, Ti5SSa and Ti5Fe alloys were comparable to those of wrought Ti6Al4V and PM Grade 5 Ti6Al4V alloy.

Processing of PM Ti3Al2V and Ti5Fe alloys using HDH Ti powders to achieve tensile properties similar to those of Ti6Al4V as specified in the ASTM standard is viable. The results showed that halving the alloying constituents in Ti6Al4V alloy compensated for the detrimental effect of high oxygen on tensile strength and ductility. The alloys Ti3Al2V and Ti5Fe achieved tensile properties comparable to those of wrought Ti6Al4V. A combination of thermomechanical processing followed by an annealing heat treatment was necessary to achieve these results.

- The alloy Ti3Al2V showed better formability compared with Ti6Al4V alloy.

- The alloy Ti5Fe showed better formability compared with Ti3Al2V and Ti6Al4V alloys.

Reference

1.   Chen, W., et al., *The investigation of die-pressing and sintering behavior of ITP CP-Ti and Ti-6Al-4V powders.* Journal of Alloys and Compounds, 2012. **541**(0): p. 440-447.
2.   Steedman, G. and S.F. Corbin, *Determining sintering mechanisms and rate of in situ homogenisation during master alloy sintering of Ti6Al4V.* Powder Metallurgy, 2014. **58**(2015, No1): p. 67-80.
3.   Xu, X., G. Nash, and P. Nash, *Sintering mechanisms of blended Ti6Al4V powder from diffusion path analysis.* J Mater Sci 2013. **46**(2014): p. 994–1008.
4.   Esteban, P.G., E.M. Ruiz-Navas, and E. Gordo, *Influence of Fe content and particle size the on the processing and mechanical properties of low-cost Ti-xFe alloys.* Materials Science and Engineering: A 2010. **527**(21-22): p. 5664-5669.
5.   O'Flynn, J. and S.F. Corbin, *The influence of iron powder size on pore formation, densification and homogenization during blended elemental sintering of Ti–2.5Fe.* Journal of Alloys and Compounds, 2015. **618**: p. 437-448.
6.   Bolzoni, L., E.M. Ruiz-Navas, and E. Gordo, *Investigation of the factors influencing the tensile behaviour of PM Ti–3Al–2.5V alloy.* Materials Science and Engineering: A, 2014. **609**: p. 266-272.

7.   Chen, B.-Y., K.-S. Hwang, and K.-L. Ng, *Effect of cooling process on the α phase formation and mechanical properties of sintered Ti–Fe alloys.* Materials Science and Engineering: A, 2011. **528**(13–14): p. 4556-4563.

8.   Bolzoni, L., E.M. Ruiz-Navas, and E. Gordo, *Influence of sintering parameters on the properties of powder metallurgy Ti-3Al-2.5V alloy.* Materials Characterization, 2013. **84**: p. 48-57.

9.   Esteban, P.G., et al., *PM processing and characterisation of Ti-7Fe low cost titanium alloys.* Powder Metallurgy, 2011. **54**(3): p. 242-252.

10.   Pereloma, E., et al., *Microstructure development and alloying elements diffusion during sintering of near-alpha titanium alloys.* Key Engineering Materials, 2012. **520**: p. 49-56.

11.   Kim, Y., Y.-B. Song, and S.H. Lee, *Microstructure and intermediate-temperature mechanical properties of powder metallurgy Ti–6Al–4V alloy prepared by the prealloyed approach.* Journal of Alloys and Compounds, 2015. **637**: p. 234-241.

12.   ASTM, *ASTM B988− 13 Standard Specification for Powder Metallurgy (PM) Titanium and Titanium Alloy Structural Components.*

13.   Singh, A.P., et al., *Effect of Pre-Consolidation Methods and Oxygen on the Mechanical Properties of As-Extruded Ti-6Al-4V Alloy Rod.* Conference proceedings:The 13th World Conference on Titanium 2015, 2015.

14.   Siqueira, R.P., et al., *Microstructural evolution during sintering of the blended elemental Ti-5Al-2.5Fe alloy.* Journal of Alloys and Compounds, 2009. **476**(1-2): p. 130-137.

15.   Boyer, R., G. Welsch, and E.W. Collings, *Materials Properties Handbook Titanium Alloys.* ASM International ed, ed. A. International. 2007.

16.   Murray, L.S., *Ti phase diagrams.* ASM Metal Handbook Vol.3. Vol. 3. 1992.

17.   Kuhn, H.A. and L.B. Ferguson, *Powder Forging Mechanics*, in *Powder Forging*. 1990, Metal Powder Industry Federation,. p. 70-78.

18.   Jovanović, M.T., et al., *The effect of annealing temperatures and cooling rates on microstructure and mechanical properties of investment cast Ti–6Al–4V alloy.* Materials & Design, 2006. **27**(3): p. 192-199.

19.   Pinke, P., M. Reger, and T. Kovacs, *Heat Treatment of the casted Ti6Al4V titanium alloy*, in *12th International Scientific Conference, Bratislava 2004*. 2004. p. 1042-1046.

20.   Yan, M. *Microstructure characterization of as -sintered titanium and titanium alloys.* Titanium Powder Metallurgy 2015 [cited 2016 13/04/16].

21.   Donachie, M.J., *Introduction to selection of Ti alloys*, in *Titanium : A Technical Guide* 2000, ASM International: Materials Park, OH, USA. p. 5-15.

22.   Polmear, I.J., *Titanium alloys*, in *Light alloys: metallurgy of the light metals*. 1995, John Wiley & Sons. p. 249-254.

23.   Peterson, N.L., *Diffusion in refractory metals.* Advanced Metals Research Corporation, 1961. **May, 1961**(Technical report): p. 123-156.

24.   Yan, M., *Microstructural characterization of as-sintered titanium and titanium alloys* in *Titanium Powder Metallurgy*. 2015, Butterworth-Heinemann. p. 555-578.

25.   Yang, F., et al., *Microstructural evolution during extrusion of a Ti/Al/Al35V65 (Ti–6Al–4V) powder compact and the mechanical properties of the extruded rod.* Materials Science and Engineering: A, 2014. **598**(0): p. 360-367.

26. Yang, F., et al., *Preparation, Microstructure and Properties of Ti-6Al-4V Rods by Powder Compact Extrusion of Powder Mixture.* Key Engineering Materials, 2012. **520**: p. 70-75.
27. Gillbert, R. and R. Shannon, *Heat treating of Titanium and Titanium alloys*, in *ASM Metals Handbook Vol.4*. 1998, ASM International. p. 2043-2060.
28. Nyakana, S.L., J.C. Fanning, and R. Boyer, *Quick reference guide for beta titanium alloys in the 00s.* Journal of Materials Engineering and Performance, 2005. **14**(6): p. 799-811.
29. Dieter, G., *Matematical Expression for the flow curve*, in *ASM Metal Handbook Vol. 8*. 1998. p. p.247-248.
30. Bergström, Y. *The Hollomon n – value, and the strain to necking in steel* [http://www.plastic-deformation.com/paper8.pdf] 2011 [cited 2016; Available from: http://www.plastic-deformation.com/paper8.pdf.
31. Callister, W., *Materials science and engineering an introduction*. 2003: John Wiley &Sons.
32. Anderson, J., et al., *Strengthening mechanisms*, in *Material Science 4th Edition*
C.a. Hall, Editor. 1990. p. 194-204.
33. Gupta, R.K., et al., *Strain hardening of Titanium alloy Ti6Al4V sheets with prior heat treatment and cold working.* Materials Science and Engineering: A, 2016. **662**: p. 537-550.
34. ASTM, *ASTM B348-13 Standard Specification for Titanium and Titanium Alloy Bars and Billets*.
35. Bolzoni, L., E.M. Ruiz-Navas, and E. Gordo, *Feasibility study of the production of biomedical Ti–6Al–4V alloy by powder metallurgy.* Materials science and Engineering C, 2015. **49**: p. 400-407.
36. Wei, W., et al., *Effect of Fe addition on sintering behaviour of titanium powder.* Powder Metallurgy, 2003. **46**(3): p. 246-250.
37. Fujita, T., et al., *Microstructure and properties of titanium alloy produced in the newly developed blended elemental powder metallurgy process.* Materials Science and Engineering A, 1996. **213**: p. 148-153.
38. Zhang, D.L., C.C. Koch, and R.O. Scattergood, *The role of new particle surfaces in synthesizing bulk nanostructured metallic materials by powder metallurgy.* Materials Science and Engineering: A, 2009. **516**(1–2): p. 270-275.

Chapter 6

Conclusions and Recommendations for further work

6.1 Conclusions

The aim of this work was to research possibilities of cost effective consolidation of Ti and Ti alloy powders to make materials with intermediate tensile properties suitable for application in everyday life. The approach was to use induction heating as an alternative for sintering, the main aim being to reduce the sintering time, and the use of low cost Ti powders produced by the HDH method. This study had three main directions: (1) investigating the effect of the induction sintering (IS) process parameters on the properties of Ti and Ti6Al4V powders, (2) using IS in thermomechanical processing (TMP) by open die forging (ODF) and extrusion, with a target of eliminating additional reheating after sintering and (3) synthesis of low alloy composition Ti alloys such as Ti3Al2V and the use of cheaper alloying elements such as Fe and 316SS master alloy powders. Both IS or vacuum sintering (VS) were investigated as single consolidation methods or in combination with thermomechanical processing.

The effect of heat treatment on the properties of the TMP alloys was also studied. The main conclusions derived from the results of this study are:

- Induction heating can be used as an alternative to electric heating to sinter and consolidate Ti and Ti prealloyed (PA) or blended elemental (BE) alloy powders.

- In addition IS can be used for pre-consolidation of Ti and Ti alloy powder billets in TMP. An advantage of using IS is eliminating an additional reheating step when VS is used for pre-consolidation.

- Successful synthesis of Ti low cost alloys using Ti HDH powders, with lower alloying constituent of 5% Fe, 316SS or Al40V master alloy. These were processed by sintering, followed by ODF or extrusion and an additional heat treated by recrystallization annealing (RA) gave tensile properties comparable with those obtainable in wrought or low oxygen powder metallurgy (PM) Ti6Al4V alloy.

The main conclusions support the hypothesis proposed at the beginning of this thesis.

More detailed conclusions from the investigations carried out to test the hypothesis are described in the following subsections.

6.1.1 Conclusions from the investigations on the application of induction heating for sintering of Ti and Ti alloy powders

The main reason for using induction sintering was its potential for faster powder sintering. Various powder compositions with different amounts of oxygen were used to consolidate pure Ti, pre-alloyed Ti6Al4V powders, Ti3Al2V and Ti-Fe based blended elemental powder mixtures.

For Ti and Ti alloy powder compacts it was found that 4 to 10min of induction sintering was enough to significantly improve the density of the powder compacts and cause enough interparticle diffusion to achieve properties comparable with those achievable after prolonged vacuum sintering. There are various factors, such as the green density of powder compacts, the temperature and time for sintering, the alloy composition and the oxygen content of the starting powders which affect the sintered properties:

(a) The effect of green density:

The green density of the powder compacts and the induction sintering conditions play a significant role on the IS heating rate, porosity distribution, tensile properties and oxygen pick up in the sintered structures.

Samples with low green density showed lower conductivity and this was evident from the heating curves, where an incubation period in the initial stage of induction heating was detected. This incubation period slowed down the overall heating rate.

In the case of IS of pure Ti powders, an increase in the relative green density from 70% to 82% resulted in a significant improvement in the porosity distribution. Samples with higher green density showed evenly distributed pores and for some sintering conditions only closed porosity was observed showing evidence of solid structures. An increase in green density significantly affected the tensile properties and those samples sintered under similar conditions, but with higher green density, had considerably higher YS, UTS and ductility. Green density also had an effect on the degree of oxygen contamination during IS. The oxygen

increase as a result of IS varied from 0.1wt% to 0.4wt%, depending on the relative green density. The amount of oxygen pickup was significantly lower for relative green densities of over 80%.

(b) The effect of IS temperature and sintering time:

Induction sintering of pure Ti HDH powders at temperatures between 1300°C and 1400°C and for a minimum sintering time of 4min is required to achieve sufficient powder consolidation with large amounts of closed porosity. These conditions lead to tensile properties comparable with those of fully solid material with yield strength above 500MPa, UTS above 550MPa and an elongation to fracture between 5% and 14%. Below this temperature range and holding time, there was a lower degree of consolidation and the higher porosity levels influenced the tensile properties and there were not as good as those found in solid material.

(c) Induction sintering of Ti blended elemental alloy powders:

IS was successfully used for synthesising Ti alloys from elemental powder mixtures. Ti HDH powders and 60Al40V master alloy powders were mixed in the correct ratios to produce Ti6Al4V and Ti3Al2V alloys. The mixtures were blended and subsequently compacted and then IS. Induction sintering was done in two stages, homogenization at 1000°C for 8min and a further IS at 1200°C for 2min. Both of the IS alloys showed properties typical of solid material. Sintered relative densities of over 97% with some small rounded pores were comparable with those of the corresponding vacuum sintered alloys. EDS and XRD results showed that the alloying elements were fully dissolved and uniformly distributed in the Ti matrix. The microstructure of the IS alloys was the typical for these alloys lamellar structure. The microstructure showed a finer $\alpha+\beta$ phase distribution compared to that of the corresponding VS alloys. The tensile properties of the IS Ti6Al4V and Ti3Al2V alloys were comparable and in some cases exceeded those of the corresponding VS alloys.

(d) Induction sintering of non-standard Ti alloys:

IS was also used for synthesis of non-standard Ti5Fe based alloys using blended elemental mixtures of Ti HDH powders and pure Fe or 316SS master alloy powders. The IS properties of Ti5Fe and Ti5SS material, such as density and porosity distribution were comparable to those of the common vacuum sintered Ti alloys. Nevertheless the microstructure showed an inhomogeneous phase distribution and the tensile properties were lower in respect to the corresponding VS alloys. The main reason was the comparatively lower IS temperature of

1150˚C, where the self-diffusivity of Ti is lower and this led to insufficient solid bonding between the Ti powder particles.

(e) The effect of the oxygen content on sinterability:

The oxygen content of the starting powders had an effect on the sinterability. Ti based powders with an oxygen content above 0.5wt%, in particular Ti6Al4V alloy powders with 0.78wt% oxygen, were difficult to sinter using induction heating. Compared with the Ti samples, Ti6Al4V samples induction sintered with similar conditions had very low tensile properties with a fracture strength of about 300 MPa with no yielding or ductility before fracture. The lack of consolidation was evident by the very few solid bonds between the powder particles and large amount of open porosity. This was related to the high oxygen content of these powders, which limited the consolidation. The IS heating rates of the Ti6Al4V samples were also significantly lower due to the high oxygen content making the powder compact less conductive.

6.1.2 Conclusions on the use of induction sintering as a pre-consolidation method in thermomechanical processing

Using induction sintering as a pre-consolidation method in thermomechanical processing is viable. Six different Ti alloy compositions, pre-alloyed Ti6Al4V and blended elemental Ti6Al4V, Ti3Al2V, Ti5SS and Ti5Fe with two different Fe powder particles, were consolidated using IS followed by direct forging or extrusion.

(a) The detailed investigation on the consolidation of PA Ti6Al4V powders by IS and direct ODF showed that the sintering conditions have a significant effect on the properties of the as forged discs. IS for 4min at temperatures above the α+β region, such as 1100˚C and 1200˚C, followed by forging from these temperatures allows sufficient consolidation and formation of a fine α+β phase basket-weave microstructure. This results in a good combination of YS, UTS and ductility, with values typical of those obtainable in fully solid material.

(b) IS of blended elemental Ti alloys in combination with direct ODF and extrusion was studied and compared with the more traditionally used VS route. In the study where Ti6Al4V and Ti3Al2V BE powders were used, IS route of thermomechanical processing (TMP) achieved tensile properties comparable or

higher than those given by material processed using the VS route. The main reason was the finer IS microstructures, which resulted in a comparatively fine martensitic phase.

 IS route of TMP was not effective for the Ti-Fe based BE alloy powders. The main reason was the insufficient interparticle diffusion during IS of these samples. Further TMP did not improve the level of consolidation, evident from the fracture surface of these alloys, where fracture was initiated at the edges of the not fully closed pores.

(c) It was clear that after sintering, forging or extrusion gave increased tensile properties. The reasons for this were: firstly, the additional coherence between the powder particles due to pores closure; and secondly, the formation of a non-equilibrium martensitic phase during the comparatively fast cooling rates during TMP.

Both ODF and extrusion gave high values of YS and UTS for all studied alloys. An advantage of extrusion is more uniformity in properties along the cross section of the extruded material, particularly in the ductility.

The inconsistency in tensile properties of the forged discs is due to the formation of a porous layer along the two forged surfaces as a result of insufficient consolidation. This is caused by insufficient material flow due to heat losses during transporting the sample from the heating to the forging zone, and the chilling effect of the forging die surfaces. To minimise the effect of the deformation gradient, a high sintered density is required.

(d) The research on consolidation of PA HDH Ti6Al4V powders by ODF showed that the tensile properties such as YS and UTS are much higher than those of the corresponding wrought alloy or alloy made with GA Ti6Al4V powders as specified in the ASTM standard for Ti and Ti alloys. The main reason for this difference was the strengthening effect caused by a higher oxygen content of in the starting HDH powders.

6.1.3   Conclusions on the investigation on synthesis of low cost alloys

 Alloy compositions, with lower amount of alloying elements than found in commercially available alloys and non-conventional alloy compositions, were studied using low cost starting powders to prepare Ti3Al2V, Ti5Fe and Ti5SS

alloys. Knowing that the high oxygen content of the Ti HDH powders used in this study contributes to the strengthening effect of titanium, it was expected that these alloys would have higher tensile strengths compared with their wrought alloy equivalents and those made with lower oxygen GA powders. In particular, tensile properties comparable to those of wrought Ti6Al4V alloy and PM alloy specified by the ASTM standard were targeted.

(a) Ti3Al2V alloy showed good response to both IS and VS. Thermomechanical formability was better than that of the Ti6Al4V alloy studied. The tensile properties in the as-consolidated conditions varied between 800MPa and 950MPa YS, 880MPa and 1020MPa UTS and elongation to fracture between 4.5% and 7%. The YS and UTS were comparable to those of the wrought Ti6Al4V alloy. The recrystallization annealing heat treatment of the alloys after thermomechanical processing caused a slight reduction in YS and UTS but the values were still in the range specified for wrought Ti6Al4Valloy. In return, the ductility increased remarkably, being in the range of 10 to 16% elongation to fracture, fulfilling the requirement for wrought Ti6Al4V alloy (i.e.10%).

(b) Using Fe or 316SS as cheap and available alloying constituents showed good results. The results from XRD and EDS analyses showed that Fe based powder particles were fully dissolved and homogeneously dispersed into the Ti matrix and no intermetallic compounds were formed in both IS and VS alloys. This confirmed the hypothesis that using Fe as a powder metallurgical addition to titanium alloys is viable and does not cause problems with segregation as it does in casting technology.

Nevertheless, the particle size of the Fe powders had a big influence on the properties after consolidation. Using larger size Fe powders in the range of 150 microns led to problems with homogenisation and residual porosity, resulting in lower tensile properties in all consolidation conditions.

Using IS-route for consolidation of Ti-Fe based powder mixtures resulted in microstructures with an inhomogeneous distribution of α and β phases and incomplete consolidation leading to poor tensile properties. The reason for the incomplete consolidation seemed to be the relatively low sintering temperature which resulted in insufficient cohesion between the Ti particles, but further investigation is needed to confirm this.

VS-route for synthesis of Ti-Fe based alloys gave satisfactory results. An addition of Fe, a β-phase stabilizer in the Ti alloy, was shown to give a significant

improvement in hot workability, which was evident by the lower TMP temperature used and the length of the extruded bars being more than twice that obtainable in Ti6Al4V and T3Al2V alloys. The retention of larger amount of β phase in the as-sintered and thermomechanically treated alloys led to a finer microstructure, comparatively high tensile strength and ductility. After TMP Ti5FeSS and Ti5Fe-c alloys showed very fine microstructures which contributed to the high YS and UTS. In the as-forged conditions the YS and UTS reached values similar to those found in Ti6Al4V. As-extruded Ti5Fe-c and Ti5SS bars showed YS and UTS in the range of 1000MPa and 1100MPa respectively with good ductility between 7% and 11.5%.

6.1.4 Conclusions on the effect of oxygen on tensile properties

Both the beneficial and deleterious effects of oxygen is evident from its influence on formability and the level of tensile properties.

The oxygen content derives from both, the oxygen content of the starting Ti or Ti6Al4V HDH powders, which vary between 0.23wt% and 0.78wt%, and the oxygen pick up during processing. The oxygen content of the final consolidated materials was between 0.32wt% and 0.80wt%. Consolidated samples with oxygen above 0.78wt% showed very poor tensile properties, indicating that Ti based materials with such oxygen content are not suitable for use in applications requiring good strength and ductility.

In Ti based materials with an oxygen content between 0.32wt% and 0.54wt% the YS and UTS showed values significantly higher than those found in corresponding wrought or PM Ti and Ti alloys with lower oxygen content (below 0.20wt%). Although relatively low, in some cases the ductility of these materials, in as-consolidated conditions without post heat treatment, falls in the lower range of the requirements in ASTM standard specification for Ti and Ti alloys.

The YS and UTS of Ti6Al4V alloys made by both PA and BE powders showed YS and UTS up to 300MPa higher than values given in the ASTM standard for Ti 6Al4V alloy but with lower ductility in the lower range of the standard requirements.

6.1.5 Conclusions on the effect of the recrystallization annealing heat treatment on the tensile properties

Recrystallization annealing after TMP by forging and extrusion is a viable way of achieving tensile properties with a good combination of YS, UTS and elongation to fracture. Such a combination of tensile properties requires a microstructure with a fine α+β basketweave structure. After recrystallization annealing a high ductility of 12% to 23% elongation to fracture is achievable, showing that any embrittlement caused by high oxygen content in the 0.33wt% and 0.5wt% range can be minimized by suitable heat treatment, to create a fine α+β phase basketweave microstructure.

6.2 Recommendations for further work

- A study on the corrosion resistance of Ti-Fe based alloys.
- A study on the fracture toughness of Ti32, Ti5SS, Ti5Fe alloys made by thermomechanical processing.
- More detailed microstructure analysis including high resolution SEM or TEM, EBSD for analyses of crystal orientation and texture.
- Developing processing maps for TMP- pressure and temperature/microstructure and properties.
- Investigation on effect on IS parameters on the properties of the sintered Ti5Fe-c and Ti5SS alloys.
- Optimization of the IS conditions to improve porosity distribution and mechanical properties along the cross section of Ti and Ti alloys powder compacts consolidated by ODF.
- Effect of the recrystallization annealing temperature and holding time on the microstructure and tensile properties of the Ti5Fe-c and Ti5SS alloys.
- Research on using induction sintering for the development of porous structures and control of porosity by varying the green compact density, induction sintering parameters and by using different powder sizes and morphologies.
- Research on the potential of using induction heating in heat treatment practice such as solution heat treatment.